**Fakultät für Medizin**

**TranslaTUM - Zentralinstitut für Translationale Krebsforschung**

**Klinikum rechts der Isar**

# Generation and Characterization of Genetically Engineered Mouse Models of Pancreatic Ductal Adenocarcinoma

**Chen Zhao**

Vollständiger Abdruck der von der Fakultät für Medizin der Technischen Universität München zur Erlangung des akademischen Grades eines

**Doctor of Philosophy (Ph.D.)**

genehmigten Dissertation.

**Vorsitzender:** Priv.-Doz. Dr. Christian Sorg

**Betreuer:** Prof. Dr. Dieter Saur

**Prüfer der Dissertation:**

1. Prof. Dr. Marc Schmidt-Supprian

2. Prof. Dr. Günter Schneider

Die Dissertation wurde am 05.08.2021 bei der Fakultät für Medizin der Technischen Universität München eingereicht und durch die Fakultät für Medizin am 28.10.2021 angenommen.

# Table of contents

## List of Tables

## List of Figures

# List of Abbreviations

| | |
|---|---|
| °C | degree Celsius |
| 4-OHT | 4-hydroxytamoxifen |
| ADM | acinar-to-ductal metaplasia |
| AFLs | atypical flat lesions |
| AML | acute myeloid leukemia |
| ANOVA | analysis of variance |
| apCAF | antigen-presenting cancer-associated fibroblasts |
| ARID1A | AT-rich interactive domain-containing protein 1A |
| ART | ADP-ribosyltransferase |
| ATF | activating transcription factor |
| ATM | ataxia telangiectasia mutated |
| BMPs | bone morphogenetic proteins |
| bp | base pair |
| BRCA1 | breast cancer type 1 susceptibility protein |
| BSA | bovine serum albumin |
| CAFs | cancer-associated fibroblasts |
| CCL5 | Chemokine (C-C motif) ligand 5 |
| CCND1 | Cyclin D1 |
| CDK | cyclin-dependent kinase |
| CDKN2A | cyclin-dependent kinase (CDK) inhibitor 2A |
| cDNA | complementary deoxyribonucleic acid |
| CIN | chromosomal instability |
| CK19 | cytokeratin 19 |
| CNV | copy number variation |
| CPM | counts per million |
| CSF-1 | colony-stimulating factor-1 |
| CTLA4 | cytotoxic T-lymphocyte-associated protein 4 |
| CXCL12 | C-X-C motif chemokine 12 |
| CXCL5 | C-X-C motif chemokine 5 |
| CXCR4 | C-X-C chemokine receptor 4 |
| Da | Dalton |
| DMEM | Dulbecco´s modified Eagle medium |
| DMSO | dimethylsulfoxide |
| DNA | deoxyribonucleic acid |
| dNTP | deoxynucleoside triphosphate |
| doxy | doxycycline |
| DR | desmoplastic reaction |
| DRS | dual-recombinase system |
| DTT | dithiothreitol |
| ECM | extracellular matrix |
| EDTA | ethylenediaminetetraacetic acid |
| Emp3 | epithelial memrance protein 3 |
| EMT | epithelial-mesenchymal transition |
| ES | embryonic stem |

| | |
|---|---|
| EtOH | ethanol |
| EtOH | ethanol |
| FCS | fetal calf serum |
| FDR | false discovery rate |
| FSF | frt-stop-frt |
| FTI | farnesyltransferase inhibitor |
| FZD | frizzled receptor |
| g | gram |
| GAP | GTPase-activating protein |
| GC | gastric cancer |
| GEMMs | genetically engineered mouse models |
| GNAS | guanine nucleotide binding protein alpha stimulating |
| GO | gene ontology |
| GSEA | gene set enrichment analysis |
| h | hour |
| H&E | hematoxylin and eosin |
| Hnf4α | Hepatocyte nuclear factor 4α |
| H-R | hypoxia-reoxygenation |
| iCAFs | inflammatory cancer-associated fibroblasts |
| ICOS | inducible costimulator |
| ICOS-L | inducible costimulator ligand |
| IDO | 2.3-dioxygenase |
| IFN-γ | interferon γ |
| IHC | immunohistochemistry |
| IL-1 | interleukin-1 |
| IL-6 | interleukin-6 |
| IPMN | intraductal papillary mucinous neoplasm |
| ITPN | intraductal tubulopapillary neoplasm |
| JAK3 | Janus kinase 3 |
| kb | kilo base pair |
| Kras | v-Ki-ras2 Kirsten rat sarcoma viral oncogene homolog |
| L | liter |
| LATS1 | large tumor suppressor kinase 1 |
| LB | Luria Broth Bertani |
| LSL | loxP-stop-loxP |
| M | molar |
| MAPK | mitogen-activated protein kinase |
| MCN | mucinous cystic neoplasm |
| M-CSF | macrophage colony stimulated factor |
| mDCs | myeloid dendritic cells |
| MDM2 | murine double minute 2 |
| MDS | multidimensional scalling |
| MDSCs | myeloid-derived suppressor cells |
| MEFs | mouse embryonic fibroblasts |

| | |
|---|---|
| mg | milligram |
| MIF | migration inhibitory factor |
| min | minute |
| MIP-3α | macrophage inflammatory protein-3α |
| mL | milliliter |
| mm | millimeter |
| mM | millimolar |
| MMF | midazolam, medetomidine, fentanyl |
| MMP 2 | matrix metalloproteinase 2 |
| MMP 3 | matrix metalloproteinase 3 |
| MMP 9 | matrix metalloproteinase-9 |
| mRNA | messenger ribonucleic acid |
| MSI | microsatellite instability |
| MW | molecular weight |
| myCAFs | myofibroblastic cancer-associated fibroblasts |
| ng | nanogram |
| NGS | next-generation sequencing |
| NK | natural killer |
| nm | nanometer |
| nM | nanomolar |
| NNMF | non-negative matrix factorization |
| NSCLC | non small cell lung cancer |
| OD | optical density |
| OS | overall survival |
| PAGE | polyacrylamide gel electrophoresis |
| PALB2 | partner and localizer of BRCA2 |
| PanIN | pancreatic intraepithelial neoplasia |
| PBRM1 | polybromo 1 |
| PBS | phosphate buffered saline |
| PCA | principal component analysis |
| PCR | polymerase chain reaction |
| PDAC | pancreatic ductal adenocarcinoma |
| PDK1 | 3-phosphoinositide-dependent protein kinase 1 |
| PD-L1 | programmed death-ligand 1 |
| Pdx1 | pancreatic and duodenal homeobox 1 |
| PH | pleckstrin homology |
| PI3K | phosphoinositide 3-kinase |
| PI3K | phosphoinositide 3-kinase |
| PIK3CA | phosphatidylinositol-4,5-bisphosphate 3-kinase catalytic subunit alpha |
| PKA | protein-kinase-A |
| PRSS1 | serine protease 1 |
| PSCs | pancreatic stellate cells |
| PTC | papollary thyroid cancer |
| PTEN | phosphatase and tensin homolog |
| Ptf1a | pancreas transcription factor subunit alpha |

| | |
|---|---|
| QM-PDA | quasi-mesenchymal |
| qRT-PCR | quantitative real time PCR |
| RA | retinoid acid |
| RNA | ribonucleic acid |
| RNAi | RNA interference |
| RNA-seq | RNA sequencing |
| RNF43 | ring finger protein 43 |
| ROS | reactive oxygen species |
| rpm | revolutions per minute |
| Rrna | ribosomal RNA |
| rRNA | ribosomal ribonucleic acid |
| RT | room temperature |
| RTK | receptor tyrosine kinase |
| rtTA | reverse tetracycline transactivator |
| SACC | salivary adenoid cystic carcinoma |
| SDF-1α | stromal-derived factor 1α |
| SDS | sodium dodecyl sulphate |
| SEM | standard error of mean |
| SIK | salt-inducible kinases |
| SMAD4 | mothers against decapentaplegic homolog |
| SMARCB1 | SWI/SNF related, matrix associated, actin dependent regulator of chromatin, subfamily b, member 1 |
| SNP | single-nucleotide polymorphism |
| SOX9 | SRY-box transcription factor 9 |
| Sprr2a3 | small proline-rich protein 2A3 |
| STAT3 | signal transducer and activator of transcription 3 |
| STAT3 | signal transducer and activator of transcription 3 |
| STK11 | serine/threonine kinase 11 |
| TAE | tris-acetate-EDTA |
| TAM | tamoxifen |
| TBST | tris-buffered saline tween-20 |
| TE | tris-EDTA buffer |
| TEMED | N,N,N',N'-tetramethylethylenediamine, 1,2-bis(dimethylamino)-ethane |
| TGF-β | transforming growth factor β |
| Tgfβr2 | type II transforming growth factor β receptor |
| Th1 | type 1 T helper |
| Th17 | type 17 T helper |
| Th2 | type 2 T helper |
| TLT | tertiary lymphoid tissue |
| TME | tumor microenvirent |
| Tnc | tenascin C |
| TNF-a | tumor necrosis factor a |
| TP53 / Trp53 | transformation related protein 53 |
| TRAIL | TNF-related apoptosis-inducing ligand |

| | |
|---|---|
| Tregs | regulatory T cells |
| TRP53 | tumor protein p53 |
| tTA | tetracycline transactivator |
| U | unit of enzyme activity |
| Ubr1 | ubiquitin protein ligase E3 component N-recognin 1 |
| UV | ultraviolet |
| V | volt |
| VEGF | vascular endothelial growth factor |
| w/v | weight per volume |
| WB | western blot |
| WHO | world health organization |
| WT | wild type |
| WT | wild type |
| αSMA | α smooth muscle actin |
| µg | microgram |
| µL | microliter |
| µm | micrometer |
| µM | micromolar |

# 1 Abstract

Our understanding of pancreatic cancer has been improved by the studies of genetically engineered mouse models (GEMMs). However, our knowledge of the mechanisms of the pathogenesis of pancreatic ductal adenocarcinoma (PDAC) is still limited. Multi-omics analysis has demonstrated the complex molecular features in pancreatic cancer patients. It is essential to identify the correlation between the pathological and molecular features. Here, GEMMs of PDAC were characterized and a new mouse model was generated, aiming to provide insight into the mechanisms of PDAC progression and maintenance. This study revealed the correlation between the survival time and metastasis formation in PDAC mouse models. Tumor grade, an important prognostic indicator, was shown to be related to the mitotic activity, metastasis, stromal content, and infiltrated immune cells. In addition, tumor grade was also demonstrated to be associated with the classical subtype of PDAC. The molecular signatures of tumor grade and mitosis were identified, and the transcriptomic profiling data corroborated the strong correlation between these two cancer features. Liver metastasis was showed to be related to tumor grade and the transcriptomic signatures leading to this secondary tumor were identified. This thesis also revealed four immune cell subpopulations that have significantly different distributions between low- and high- grade tumors, suggesting a potential role of these immune cells in disease progression. To study KRAS as a target for PDAC therapy, a new mouse model was generated which allows the time specific permanent inactivation of endogenous oncogenic *Kras*$^{G12D}$. This facilitates the investigation of oncogene dependence in future studies.

# 2 Zusammenfassung

Unser Verständnis von Bauchspeicheldrüsenkrebs wurde durch die Untersuchung gentechnisch veränderter Mausmodelle (GEMMs) verbessert. Unser Wissen über die Mechanismen der Pathogenese des Pankreas-Duktal-Adenokarzinoms (PDAC) ist jedoch noch begrenzt. Die Multi-Omics-Analyse hat die komplexen molekularen Merkmale bei Patienten mit Bauchspeicheldrüsenkrebs gezeigt. Es ist wichtig, die Korrelation zwischen den pathologischen und molekularen Merkmalen zu identifizieren. Hier wurden GEMMs von PDAC charakterisiert und ein neues Mausmodell generiert, um Einblicke in die Mechanismen der PDAC-Progression zu erhalten. Diese Studie zeigte die Korrelation zwischen der Überlebenszeit und der Metastasenbildung in PDAC-Mausmodellen. Es wurde gezeigt, dass der Tumorgrad, ein wichtiger prognostischer Indikator, mit der mitotischen Aktivität, Metastasierung, dem Stromagehalt und den infiltrierten Immunzellen zusammenhängt. Darüber hinaus wurde gezeigt, dass der Tumorgrad mit dem klassischen Subtyp von PDAC assoziiert ist. Die molekularen Signaturen von Tumorgrad und Mitose wurden identifiziert, und die transkriptomischen Profildaten bestätigten die starke Korrelation zwischen diesen beiden Krebsmerkmalen. Es wurde gezeigt, dass die Lebermetastasierung mit dem Tumorgrad zusammenhängt, und die transkriptomischen Signaturen, die zu diesem sekundären Tumor führten, wurden identifiziert. Diese Arbeit enthüllte auch vier Immunzell-Subpopulationen, die signifikant unterschiedliche Verteilungen zwischen niedrig- und hochgradigen Tumoren aufweisen, was auf ein Potenzial dieser Immunzellen bei der Tumordifferenzierung hinweist. Es wurde ein neues Mausmodell erstellt, das die Inaktivierung der endogenen onkogenen Mutation des Kirsten-Ratten-Sarkom-Virus (*Kras*) ermöglicht.

# 3 Introduction

## 3.1 The progression of pancreatic ductal adenocarcinoma

Pancreatic neoplasms are classified into a broad range of types, according to their biological behavior in benign, pre-malignant or malignant neoplasms and their cellular differentiation levels. The majority of all the neoplasms of the pancreas is pancreatic ductal adenocarcinoma (PDAC) which accounts for 90 to 95% of all pancreatic neoplasms (Cascinu et al., 2010). Pancreatic cancer is one of the most malignant cancers, which has an overall five-year survival (OS) rates of 9% in United States of America (Siegel et al., 2020).

PDAC develops from precursor lesions, including noncystic and cystic lesions. Pancreatic intraepithelial neoplasia (PanIN) is defined as noncystic lesion. Cystic lesions comprise intraductal papillary mucinous neoplasm (IPMN), intraductal tubulopapillary neoplasm (ITPN), and mucinous cystic neoplasm (MCN). These precursors display distinct clinical characteristcs and molecular features. Through stepwise tumorigenesis involving the accumulation of molecular alterations and phenotype changes, each of these four precursor lesions may result in the progression of invasive pancreatic cancer.

PanIN lesions are the predominant precursors of PDAC (Brat et al., 1998). PanINs are defined as microscopic mucinous lesions in the small pancreatic ducts. In PDAC progression, PanINs are classified as PanIN-1A, PanIN-1B, PanIN-2 and PanIN-3. Furthermore, PanIN-1A and PanIN-1B are defined as low grade. PanIN-2 and PanIN-3 are the intermediate and high grade, respectively (Nagtegaal et al., 2020). PanIN-1A comprises the early stage of PDAC precursor lesions with columnar cells and supranuclear mucin. The cells have small and round to oval shaped nuclei. PanIN-1B is also an epithelial lesion with papillary structures. Compared with PanIN-1A and PanIN-1B lesions, a PanIN-2 lesion has more complex architecture, composed of a flat or papillary mucinous epithelium. Some nuclear abnormalities can be observed in this stage (Hruban et al., 2001). The nuclei of PanIN-2 have various sizes, are overcrowded and lose polarity. Hyperchromatism can also be found. A PanIN-3 lesion is normally papillary, however rarely flat and is characterized by true cribriforming of epithelial cells into luminal necrosis, irregular stratification and mitosis. In addition, this lesion also shows a loss of nuclear polarity (Hruban et al., 2001). Acinar-to-ductal metaplasia (ADM) is identified as the earliest step in PDAC development. Oncogenic *Kisrten rat sarcoma virus* (*KRAS*) mutations initiate the transdifferentiation of pancreatic acinar cells to cells with ductal characteristics. ADM is observed before PanIN formation, indicating ADM is an early stage of pancreatic tumorigenesis. ADM has been shown to be a critical process in the pathogenesis of pancreatic cancer and chronic pancreatitis (Pinho et

al., 2011; Rooman and Real, 2012). Therefore, ADM is considered as an initiating event of pancreatic cancer development (Stanger and Hebrok, 2013). Atypical flat lesions (AFLs) are considered as a precursor to PDAC via ADM in the studies of genetically engineered mouse models (GEMMs) and confirmed to occur also to PDAC patients (Aichler et al., 2012; Franklin et al., 2020; Morita et al., 2018). AFLs have tubular structures and are highly proliferative. Nuclear abnormalities, including enlarged nuclei and hyperchromatism in ADM areas, are the features of AFLs.

The development of PDAC is a process of accumulating molecular alterations that change the phenotypes of cells. These alterations affect the signaling pathways and, as a result, are closely correlated with the phenotypes of the stages in the progression from PanINs, the most common precursors, to PDAC.

The genetic changes of PanIN-1 lesions include telomere shortening, *KRAS* mutations and *cyclin-dependent kinase* (*CDK*) *inhibitor 2A* (*CDKN2A*) loss (Feldmann et al., 2007; Shen et al., 2013). A telomere located at the end of a chromosome is a region of repetitive short DNA sequences, which prevents a chromosome from deterioration and fusing with neighboring chromosomes during cell division. Remarkable telomere shortening has been detected in about 91% of PanIN-1 cases compared to the cells in adjacent normal pancreatic tissues (van Heek et al., 2002). Therefore, shortening of telomeres is suggested as one of the earliest events of the pancreatic cancer progression. As a result of telomere shortening, abnormal chromosome end-to-end fusion, dicentric chromosomes, chromosomal instability (CIN) and translocation are observed during mitosis. Altoghether, these abnormalities eventually promote the progression of PDAC (Koorstra et al., 2008). *KRAS* belongs to the canonical RAS gene family which encodes small GTP-binding proteins and includes *HRAS* and *NRAS*. *KRAS* mutation is considered as one of the earliest driving forces of pancreatic carcinogenesis, detected in over 90% of pancreatic cancers. A previous study has reported that *KRAS* activation is necessary for the early stages of PDAC lesion formation (Morris et al., 2010). *KRAS* oncogenic mutations are involved in inhibiting tissue repair and regulating cell differentiation. Most of the *KRAS* point mutations occur in codon 2 (Goggins, 2007; Jimeno and Hidalgo, 2006; Singh and Maitra, 2007), resulting in the activation of KRAS downstream signaling pathways, including the mitogen-activated protein kinase (MAPK) pathway and the phosphoinositide 3-kinase (PI3K) pathway(Calhoun et al., 2003; Schneider and Schmid, 2003). *KRAS* mutations are commonly found not only in patients but also in healthy individuals, which explains why these mutations are not good biomarkers for diagnosis of PDAC (Yan et al., 2005). *CDKN2A* is among the genes encoding tumor suppressors that have been shown to be inactivated in the development of PanINs. More than 80% of pancreatic cancers possess loss-of-function *CDKN2A* mutations (Chang et al.,

2014; Kleeff et al., 2016). The inactivation mechanisms of *CDKN2A* are the loss of both alleles and intragenic mutation together with hemizygous deletion or hypermethylation in the promoter region in the progression of PDAC (Schutte et al., 1997). *CDKN2A* encodes both tumor suppressor proteins, $p16^{INK4a}$ and $p14^{ARF}$. $p16^{INK4a}$ binds to CDKs, including CDK4 and CDK6, and controls the crucial checkpoint of the G1/S transition in the cell cycle, suggesting its importance in cellular senescence and division (Collado et al., 2007; Gil and Peters, 2006; LaPak and Burd, 2014). $p14^{ARF}$ interacts with murine double minute 2 (MDM2) which is a tumor protein p53 (Trp53) positive regulator (Pomerantz et al., 1998).

As in PanIN-1s, diverse genetic aberrations are identified in PanIN-2 and PanIN-3. *Cyclin D1* (*CCND1*), *TRP53*, and *mothers against decapentaplegic homolog 4* (*SMAD4*) mutations are detected in the intermediate- and late-stage PanINs. Cyclin D1 encoded by *CCND1* gene is a subunit CDK4 and CDK6 and interacts with retinoblastoma (Rb) protein, suggesting its central role in the cell cycle regulation (Nagata et al., 2007). Over 60% pancreatic cancers show the overexpression of *CCND1* which exerts an oncogenic effect in carcinogenesis in about 30% and 60% of PanIN-2 and PanIN-3 cases respectively (Jares et al., 2007). In the last decades, some studies indicate a potential role of CCND1 as a regulator of transcriptional activities in in vitro models. These studies found that CCND1 interacts with several transcriptional factors, such as the estrogen; and proteins associated with chromatin-remodeling and histone-modifying (Casimiro et al., 2014; Horstmann et al., 2000; Pestell, 2013; Reutens et al., 2001). *Trp53* codes for a transcriptional factor protein involved in cell cycle and shows the tumor suppressive function. In average 62.5% of PDAC patients, the *TRP53* gene shows loss of function by the combination of hemizygous deletion of a wild type allele and intragenic mutation (Redston et al., 1994). The demonstrative evidence has revealed that loss-of-function in *Trp53* results in genomic instability of PDAC (Hingorani et al., 2005). The accumulation of *TRP53* gene mutation is detected in advanced PanIN-3 and it is considered to be altered in the late stage of PDAC progression. SMAD4 protein belongs to the SMAD family which consists of transcription factor proteins, and it functions as a tumor suppressor. The combination of intragenic mutation and hemizygous deletion in *SMAD4* locus is observed in over 50% of PDAC (Hahn et al., 1996). The alteration of the *SMAD4* gene is commonly detected in the development of pancreatic cancer, such as in the late stage of PanIN and infiltrating adenocarcinomas (Wilentz et al., 2000). SMAD4 protein is involved in the transforming growth factor-β (TGF-β) pathway. Previous studies reported that the loss of SMAD4 function is related to widespread metastasis and poor prognosis of PDAC (Javle et al., 2014; Jiang et al., 2012).

## 3.2 Histology of pancreatic cancer

Pathological examination is an essential step in the diagnosis of PDAC. Normally, PDAC is solid, white-yellowish ill-defined mass. In the majority of cases, PDAC is found in the proximal part of pancreas, rarely in the body or tail. This subtype of pancreatic cancer can be described histologically as malignant epithelial lesions with differentiated ductal structures. The differentiated ductal structures are defined as dilated tubular glands under the light microscopy and can be validated by stains for markers of ductal differentiation, such as cytokeratin 19 (CK19). PDAC can be divided into the following five groups: tubular adenocarcinoma, adenosquamous carcinoma, colloid carcinoma, medullary carcinoma and undifferentiated carcinoma (Wilentz et al., 2000). Tubular adenocarcinoma is defined as PDAC with well differentiated ductal components and without any predominant components of other carcinoma types (Calhoun et al., 2003; Wu et al., 2011a). Adenosquamous carcinoma includes the PDAC with dominant compartments of both squamous and ductal differentiation (Imaoka et al., 2014). The adenocarcinoma in which more than 80% of the components are neoplastic epithelial cells producing mucins and suspended in extracellular mucin is defined as colloid carcinoma, also known as mucinous non-cystic carcinoma (Gao et al., 2015). Medullary carcinoma is associated with poor differentiation, pushing borders, and necrosis (Kondo et al., 2000; Yamamoto et al., 2001). Finally, the undifferentiated carcinoma does not show any kind of differentiation. The undifferentiated carcinoma with anaplastic giant cells is composed of noncohesive pleomorphic neoplastic mononuclear cells mixed with non-neoplastic multinucleated giant cells (Yang et al., 2020).

PDAC should be histopathologically graded according to World Health Organization (WHO) criteria and it is a critical factor for diagnosis, prognosis and treatment (Hartwig et al., 2011). The grading criteria includes the architecture of neoplasms, the presence of mucin, nuclear morphology and the number of cells undergoing mitosis (Haeberle and Esposito, 2019). Based on these features, PDAC is histopathologically subdivided into Grade 1 (G1, well differentiated carcinomas); Grade 2 (G2, moderately differentiated carcinomas), Grade 3 (G3, poorly differentiated ductal adenocarcinomas) and Grade 4 (G4, undifferentiated carcinomas) (Kloppel et al., 1985; Luttges et al., 2000). G1 consists of well-defined glands, having typical cribriform or tubular patterns. G1 may also have irregular papillary projections in large ductal structures. The neoplastic cells with mucin producing are columnar. The nuclei are basally oriented, and their shapes are round to oval. Loss of polarity is not commonly observed and only a few of cells are undergoing mitosis in G1 grade tumors. G2 shows incomplete gland formation. The ductal structures embedded in stroma are of variable shapes. Nuclei are moderately polymorphous, and their sizes are various compared with those of G1. G2 has larger and more irregular nucleoli. G3 forms small and densely packed

poorly defined glands and solid tumor areas. Typical dilated ductal structures and intraductal components of neoplasms are absent. They show prominent nuclear pleomorphism. The nuclei have abnormal shapes, showing pleomorphism, and nucleoli are more irregular. The cells of G3 produce less mucin than those better differentiated carcinomas. Mitotic activity is common and atypical. G4 shows no specific ductal differentiated structures that indicate the origin sites of the lesions. G4 is commonly considered to be very aggressive, presenting higher levels of apoptosis and higher probability of metastasis formation.

### 3.3 Molecular characteristics of PDAC

PDAC is a cancer caused by genetic abnormality. The identification of the characteristics of genetic alterations in PDAC is critical to understand the biology of its pathogenesis. Large-scale genomic sequencing technologies are powerful tools to gain insights into genetic alteration of pancreatic cancer. In 2008, the first global genomic sequencing identified genetic alterations in pancreatic cancer and these alterations include numerous mutations and copy number alterations in somatic cells (Jones et al., 2008). This study revealed that, on average, each pancreatic cancer sample contains 63 genetic alterations. Most of these alterations are point mutations. All these alterations are associated with the activation of the function of key oncogenes and inactivation of the tumor suppressor genes. With the development of whole genomic sequencing technologies, these findings have been validated by the following whole genome and whole exome sequencing studies. In addition, Witkiewicz and colleagues emphasize the heterogeneity of pancreatic cancer (Witkiewicz et al., 2015). Genomic instability has been observed in PDAC samples. Germline DNA damage repair gene alterations, including *breast cancer type 1 susceptibility protein* (*BRCA1*), *BRCA2*, *ADP-ribosyltransferase* (*ART*) or *partner and localizer of BRCA2* (*PALB2*) mutations, lead to genomic instability and could render pancreatic tumors more sensitive to DNA damage response inhibitors and DNA damaging agents (Golan et al., 2014; Roberts et al., 2016; Sahin et al., 2016; Tutt et al., 2018). Recent whole genome sequencing studies show that complex chromosomal rearrangement is detected in 30% to 60% of PDAC cases, indicating the choromosomal rearrangement as a feature of PDAC (Mueller et al., 2018; Notta et al., 2016). The studies of gene expression have categorized PDAC in several subtypes (Bailey et al., 2016; Chan-Seng-Yue et al., 2020; Collisson et al., 2011; Moffitt et al., 2015). These subtypes have prognostic and biological significance.

Whole exome sequencing studies have identified significant recurrent mutations in *KRAS*, *CDKN2A*, *SMAD4* and *TRP53* (Jones et al., 2008; Numata et al., 2013). Multiple oncogenic *KRAS* mutations, including G12D, G12V and G12R are detected at higher prevalence and other mutations at lower prevalence, such as G12S, G12L and Q61L (Bryant et al., 2014; Kanda et al., 2012). G12D is the predominant mutation in PDAC patients. Some individual

neoplastic cells have multiple *KRAS* mutations and these mutations are usually on different alleles (Cancer Genome Atlas Research Network, 2017). In addition, the mutations in *AT-rich interactive domain-containing protein 1A* (*ARID1A*), *ring finger protein 43* (*RNF43*), *polybromo 1* (*PBRM1*) and *guanine nucleotide binding protein alpha stimulating* (*GNAS*) have also been observed (Bailey et al., 2016; Biankin et al., 2012; Cancer Genome Atlas Research Network, 2017; Jones et al., 2008; Waddell et al., 2015; Witkiewicz et al., 2015). The protein encoded by *ARID1A* is one of DNA-binding subunits of SWI/SNF chromatin-remodeling complex and one of the most commonly mutated components of the SWI/SNF complex (Wang et al., 2019c). A recent study has described that *ARID1A*, as a tumor suppressor gene, restrains IPMN formaton and IPMN-derived PDAC in the presence of *KRAS* mutations (Kimura et al., 2018). *ARID1A* deletion downregulates *SRY-box transcription factor 9 (SOX9)* expression and induces the dedifferentiation of pancreatic cancer cells and the proliferation of the ductal structures. Moreover, *ARID1A* is critical for DNA repair. Cancer cells with loss of function of this gene are highly vulnerable to DNA damage (Watanabe et al., 2014). *RNF43* mutations are frequently detected in IPMN and MCN. RNF43 can reduce membrane expression level of Frizzled receptor (FZD) to restrain Wnt/β-catenin signaling pathway, serving as a regulator of a negative feedback mechanism. This indicates that FZD antibodies can be used for novel targeted cancer therapies in PDAC patients with *RNF43* mutations (Jiang et al., 2013; Steinhart et al., 2017). *PBRM1* encodes a tumor suppressor protein and the upregulated expression of this gene is associated with the reduction of the tumor size. The rate of five-year survival of patients with a high expression *PBRM1* level is higher than that of those with a low expression level (Numata et al., 2013). *GNAS* codes for the α subunit of a stimulatory G-protein. *GNAS* mutations were detected in approximately 66% of IPMNs and identified as one of the recurrent driver alterations of PDAC (Wu et al., 2011b). Furthermore, oncogenic mutations of *GNAS* were detected in the precursors of IPMNs, indicating *GNAS* mutations are the drivers of IPMNs (Matthaei et al., 2014). A new mouse model with inducible overexpression of the $GNAS^{R201C}$ mutation was established to uncover the functional impact of this mutation in IPMN pathogenesis. This GEMM revealed that coexpression of $KRAS^{G12D}$ and $GNAS^{R201C}$ accelerates the progression of IPMNs compared with the setting of single $KRAS^{G12D}$ mutation. Both *in vivo* and *in vitro* evidence shows coexpression of *GNAS* and *KRAS* mutations lead to epithelial differentiation and moderately differentiated pancreatic tumor. This combination increases MAPK activities and decreases the colony forming ability and the invasive potential. The expression of *GNAS* mutations increases the expression levels of *YAP1* suppressors, *large tumor suppressor kinase 1* (*LATS1*) and *α-E-catenin*, indicating their roles in the epithelial differentiation (Ideno et al., 2018). The mouse model harboring $KRAS^{G12D}$ and $GNAS^{R201C}$ recapitulates the

progression of IPMNs to pancreatic cancer observed in humans and is a good tool to investigate the function of mutant *GNAS* in the tumorigenesis. Consistent with the previous study, another study also demonstrated that, together with *KRAS*$^{G12D}$, *GNAS*$^{R201C}$ drives the initiation and progression of IPMNs to pancreatic neoplasms. *GNAS*$^{R201C}$ drives the development of PDAC by inducing protein-kinase-A (PKA)-mediated salt-inducible kinases (SIK) suppression and the remodelling of lipid metabolism (Patra et al., 2018).

About 10% of patients have a family history of pancreatic cancer, and previous studies have identified the germline mutations associated with PDAC (Cancer Genome Atlas Research Network, 2017; Roberts et al., 2016). The results of germline exome sequencing for alterations show mutant *BRCA2*, *PALB2*, *ataxia telangiectasia mutated* (*ATM*) and *serine protease 1* (*PRSS1*) are related to familial pancreatitis and lead to an increased risk of PDAC. Single-nucleotide polymorphism (SNP) microarrays and whole exome sequencing revealed that more than 30% of pancreatic tumors have aberrations on chromosome arms, such as deletions of 8p, 9p, 18p and 18q and amplifications of 1q (Bailey et al., 2016; Cancer Genome Atlas Research Network, 2017; Ideno et al., 2018; Waddell et al., 2015). Some recurrent events have been identified, including deletions of *CDKN2A*, *SMAD4*, *ARID1A* and *phosphatase and tensin homolog* (*PTEN*) and amplifications of *GATA6*, *KRAS*, and *MYC* (Cancer Genome Atlas Research Network, 2017; Waddell et al., 2015).

With the development of next-generation sequencing (NGS), a molecular taxonomy helps to understand the molecular pathology of pancreatic cancer in details. Different molecular characteristics give us an insight into PDAC biology. The classification of these molecular features provides some implications for therapeutic development and clinical decisions. The classification approaches used for other malignancies based on their transcriptomic data were used to identify the subtypes of pancreatic cancer. Previous studies have used mRNA profiling to define the subtypes of lymphoma and breast cancer (Alizadeh et al., 2000; Perou et al., 2000). Even though clinical features and histopathological classification play an important role in clinical decision, they involve specialized subjective interpretation. The classification based on transcriptome profiling is unbiased, robust and reproducible. Nowadays this strategy has been used to classify many tumor entities, such as colorectal cancer (De Sousa et al., 2013; Marisa et al., 2013; Sadanandam et al., 2013). The classification has been accepted in clinical practice and provides the basis for subtype-based targeted interventions (Guinney et al., 2015). Array-based hybridization was firstly used for transcriptomic studies. In the past decade, transcriptomic studies start employing next generation RNA sequencing (RNA-seq). Stratification of PDAC based on the analysis of transcriptomic profiling has been studied by several research groups. Two major subtypes, the classical and the basal-like subtypes, have been identified consistently in these studies.

Input materials, the sources of the tumors and the assumption of the analysis may explain the major variations and differences of the outcomes among these studies. In 2011, the first classification of PDAC subtypes was published by Collisson and colleagues (Collisson et al., 2011). The mRNA expression data from array-based hybridization was used for the classification. The input materials were primary resected PDAC without treatment. Three subtypes were defined, including Classical, Quasi-mesenchymal (QM-PDA) and Exocrine-like (Collisson et al., 2011). Compared to the QM-PDA subtype, the Classical subtype proved to be more dependent on oncogenic *KRAS* mutations and to have a higher expression level of *GATA6*. *GATA6* belongs to the family of GATA transcription factors which are used as markers for the identification of the subtypes of other cancers and related to tissue specific differentiation (Decker et al., 2006; Kouros-Mehr et al., 2006; Kwei et al., 2008; Mehra et al., 2005). The QM-PDA subtype is associated with high tumour grade and the survival of patients with this subtype is poor. In addition, the ones from the QM-PDA subtype were more sensitive to gemcitabine, while the cell lines from the classical subtype showed to be more sensitive to erlotinib.

In 2015, Moffitt and colleagues collected untreated, resected primary and metastatic PDAC tumors for the classification (Moffitt et al., 2015). Hybridization arrays and RNA-seq were performed for the analysis and the validation of their findings respectively. By using non-negative matrix factorization (NNMF) to virtually microdissect the PDAC tumor samples, they successfully defined tumor- and stroma-related subtypes which have the prognosis relevance. Two tumor-specific subtypes were defined, including the classical subtype and the basal-like subtype, and two stroma-specific subtypes were identified, including the normal stromal subtype and the activated stromal subtype.

In 2016, nontreated resected, primary PDAC samples from 266 patients were collected for the study of PDAC subtypes by Bailey and colleagues (Bailey et al., 2016). RNA-seq was performed on 96 tumor samples containing a high epithelial percentage ( $\geqslant$ 40%). Subsequently unsupervised clustering of the sequencing data was used to identify the subtypes of PDAC. Samples from different PDAC pathological subtypes were included in this study. For example, adenosquamous carcinoma, mucinous non-cystic (colloid), undifferentiated (anaplastic) carcinoma, carcinoma associated with IPMN, undifferentiated carcinoma with osteoclast-like giant cells and acinar cell carcinoma were taken into consideration in this study. Based on the expression levels of transcriptional factors and genes associated with lineage specification and cell differentiation in the pancreas development, they defined the following four subtypes: (1) squamous; (2) pancreatic progenitor; (3) immunogenic; and (4) aberrantly differentiated endocrine exocrine (ADEX). These subtypes overlapped with those identified by Collisson and colleagues, except the

novel immunogenic subtype. The QM-PDA subtype identified in 2011 was named after Squamous, as this subtype has the expression of ΔNp63, a p63 isoform, indicating squamous epithelia, and the mRNA profile of this subtype shows a similar pattern to the squamous bladder and lung tumours (Hoadley et al., 2014).

Considering these subtypes show different response to treatments, a clinically relevent molecular taxonomy is a helpful tool in clinical practice. Molecular classification of pancreatic cancer may improve the strategies of current therapeutic approaches and facilitate the development of novel treatments for PDAC patients.

### 3.5 Metastasis of PDAC

Metastasis is the main cause of mortality of pancreatic cancer patients. Liver and lung are the most common sites of metastasis in patients. The process of metastasis involves angiogenesis/lymphangiogenesis, epithelial–mesenchymal transition (EMT), invasion to surrounding tissues and migration, pre-metastatic niche formation and growth at the metastatic site (Ren et al., 2018). Anti-immune cells should recognize and deplete cancer cells to inhibit metastasis. Unfortunately, PDAC cancer cells can escape from immune surveillance and migrate to other organs by interacting with the cells with immunosuppressive effects. PDAC cancer cells and the immunosuppressive cells can induce angiogenesis facilitating the migration of tumor cells to blood, and metastasis by secreting some cytokines and growth factors. Vascular endothelial growth factor (VEGF) is critical for PDAC angiogenesis and signal transducer and activator of transcription 3 (STAT3) is related to *VEGF* expression (Wei et al., 2003). Similar to angiogenesis, lymphangiogenesis plays an important role in the progression of PDAC and the formation of lymph node metastasis. Cancer cells and M2-like macrophages can promote the growth of new lymphatic vessels (Kurahara et al., 2013). EMT is a biological process by which epithelial cells lose cell-cell adhesion capacity and polarity, break through the basement membrane and therefore become mesenchymal cells (Ren et al., 2018). EMT has been shown to be associated with portal vein invasion in pancreatic cancer patients and the metastaisis in lymph nodes (Yamada et al., 2013). Previous studies show that macrophages and stellate cells can facilitate EMT. For example, M2-like macrophages can stimulate EMT by increasing the activities of matrix metalloproteinase 2 (MMP2) and matrix metalloproteinase 3 (MMP3) (Liu et al., 2013). Invasion and migration are the critical step of PDAC metastasis. Tumor cells invade capillaries and enter portal veins for metastasis. The pancreatic cancer microenvironment can promote metastasis. For example, macrophage inflammatory protein-3α (MIP-3α) in the tumor tissues is revealed to be related to pancreatic cancer cell invasion (Kleeff et al., 1999). Palladin, an actin-associated protein, expressed by cancer-associated fibroblasts (CAFs), facilitates the invasion of PDAC cancer cells by remodeling the

extracellular matrix (Goicoechea et al., 2014). The growth of cancer cells at the metastatic sites is influenced by the local microenvironment. The supportive microenvironment for tumor growth in the secondary organ is termed a pre-metastatic niche. It facilitates PDAC metastasis and makes contributions to tumor dormancy for recurrence at the metastatic sites. Several molecular and cellular components are involved in the formation of the pre-metastatic niches for cancer cell colonization in PDAC. For instance, Kupffer cells can take up primary tumor derived-exosomes, which regulate fibronectin production in hepatic stellate cells, to form a fibrotic microenvironment in the liver (Costa-Silva et al., 2015).

### 3.4 Immune landscape of PDAC

As the immune system plays an important role in several cancers, the understanding of the immune landscape in the tumor microenvironment (TME) can provide useful information about the tumorigenesis. It can be valuable in clinical practice regarding the use of immunomodulatory approaches (Mlecnik et al., 2016).

There are multiple ways of immune evasion in PDAC patients, including infiltration of regulatory immune cells, the secretion of chemokines and the expression of membrane proteins, such as cytotoxic T-lymphocyte-associated protein 4 (CTLA4) and programmed death-ligand 1 (PD-L1) (Chen and Flies, 2013; Knudsen et al., 2017; Martinez-Bosch et al., 2018). Since the specific immune compositions of tumor microenvironment (TME) might be associated with tumor progression, the knowledge of the interactions between immune cells and tumor cells may be helpful to elucidate the mechanisms of tumorigenesis of pancreatic cancer.

As mentioned previously, several studies have classified the subtypes of pancreatic cancer based on their genetic and transcriptomic profiles and their microenvironment (Bailey et al., 2016; Collisson et al., 2011; Connor et al., 2017; Moffitt et al., 2015). It seems that the balance of both immune and cancer cell populations can be shifted in the PDAC subgroups, indicating that the immune responses of PDAC are quite diverse. The subgroups of PDAC represent the diversity of TME and give us clues to study the mechanisms for the evasion of the immune responses of the hosts.

There are three immune related phenotypes in PDAC patients. The immune-escape phenotype is detected in the majority of PDAC patients. This phenotype shows immunosuppressive features. It is characterized by a high percentage of regulatory T cells (Tregs) and a low percentage of T and B cells in TME (Facciabene et al., 2012). The immune-escape tumors present an aggressive phenotype which is characterized by high activities of epithelial-mesenchymal transition (EMT) factors and poor prognosis. The average survival of this phenotype is about 10 months. The patients with an immune-escape

phenotype normally bear a high mutational burden of *KRAS*, *phosphatidylinositol-4,5-bisphosphate 3-kinase catalytic subunit alpha* (*PIK3CA*), *TRP53*, *SMAD4* and *CDKN2A*.

The second phenotype is the immune-rich phenotype. More than one third of all PDAC cases display this phenotype, being characterized by high T cells and B cells infiltration and low Tregs infiltration. More precisely, the immune-rich phenotype shows high infiltration of effector $CD4^+$ and $CD8^+$ T cells and M1 macrophages, a high percentage of tertiary lymphoid tissue (TLT) and the absence of M2 macrophages. Compared with those of the immune-escape phenotype, the patients of the immune-rich phenotype have the tumors with low grades and prolonged survival of 19 months. It is worth mentioning that this phenotype represents the subgroup with the most diverse genetical alterations. However, it displays a lower *PIK3CA*, *CDKN2A* and *SMAD4* mutational burden than the immune-escape phenotype. In this group, the mutations of *GNAS* and *isocitrate dehydrogenase 2* (*IDH2*) genes were also observed. The patients with this phenotype also have high mutational frequencies of *ATM*, *serine/threonine kinase 11* (*STK11*) and *SWI/SNF related, matrix associated, actin dependent regulator of chromatin, subfamily b, member 1* (*SMARCB1*) (Tamborero et al., 2018). In addition, one previous study found that about 44% of the patients with the immune-rich phenotype showed the most favourable outcome.

The third subtype is the immune-exhausted group. An average OS of this subtype is 10 months and only 11% of PDAC patients show this phenotype. The immune-exhausted subtype has two subgroups. The first group is featured by a high *PIK3CA* mutational burden, a high expression level of *PD-L1* and a high cell ratio of $CD8^+$/ Treg, whilst the second group is associated with loss of functions of DNA mismatch repair genes, microsatellite instability (MSI) and PD-1/PD-L1 blockade. Besides, this subgroup also displays highest $CD8^+$/ Treg cell ratio and high mutational frequencies of *PIK3CA* and *Janus kinase 3* (*JAK3*) (Wartenberg et al., 2015).

In PDAC, many cell types, including immune cells, pancreatic stellate cells (PSCs), endocrine cells and nerve cells, interact with cancer cells, leading to the dynamic PDAC microenvironment and the disruption of the architecture of the normal pancreas. A recent study suggested that the tissue, other than the pathogen, is important in determining types of immune responses, providing a new perspective of immune responses within the tumors (Matzinger and Kamala, 2011). Based on the immunology studies of immune-privilege sites and oral vaccination, it is well known that the tissue controls the immune response. A better understanding of tissue-specific factors associated with the control of immune functions is important to elucidate the mechanisms of immune responses for both invading pathogens and the development and progression of tumors (Schreiber et al., 2011). The cell types

contribute to the immune environment in pancreatic cancer and cellular composition shapes the features of the pathogenesis of pancreatic cancer.

Chemokine (C-C motif) ligand 5 (CCL5) and C-X-C motif chemokine ligand (CXCL) 5 secreted by cancer cells can recruit immunosuppressive Tregs and neutrophils (Nywening et al., 2018). Cancer cells also secret colony-stimulating factor-1 (CSF-1) to lead to the expansion of macrophages (Candido et al., 2018). Immature myeloid cells can be attracted by tumor-derived exosome (Basso et al., 2017). Alternatively, the exosomes can also lead to the infiltration of M1 macrophages and activated M2 macrophages (Penny et al., 2016). In addition, cancer cells can secret TGF-β to inhibit the functions of cytotoxic T cells, inducing the anergy of cytotoxic T cells (Pu et al., 2018). This creates an immunosuppressive microenvironment which further enhances the inhibitory effects on cytotoxicity against intrinsic tumor cells.

One feature of PDAC is the presence of an intense desmoplastic reaction (DR) which is defined as the growth of host fibrous or connective tissue to response to the tumor formation (Amedei et al., 2014; Clark et al., 2007). It consists of the abnormal accumulation of cancer associated fibroblasts (CAFs), endothelial cells, lymphocytes and extracellular matrix (ECM) components (Erkan et al., 2012; Nielsen et al., 2016; Patel et al., 2014). The stroma often accounts for 50-80% of the volume of PDAC (Chu et al., 2007). The stromal compartment is related to tumor growth, invasive behavior and resistance to therapy (Hasebe et al., 1997). Previous studies have shown that the strong interactions between CAFs and immune cells contribute to the progression of pancreatic cancer. CAFs are derived from PSCs and make contributions to an immunosuppressive microenvironment (Nielsen et al., 2016). Activated PSCs and CAFs stimulate the secretion of vascular endothelial growth factor (VEGF) and take part in neoangiogenesis (Sun et al., 2018). EMT of cancer cells can also be induced by CAFs and PSCs, which promotes PDAC invasion and metastasis (Kadaba et al., 2013; Kikuta et al., 2010; Rucki et al., 2017). TGF-β secreted by CAFs can induce the proliferation of cancer cells and an EMT phenotype simultaneously (Ligorio et al., 2019). A previous study has shown that C-X-C motif chemokine 12 (CXCL12) secreted by activated PSCs can recruit $CD8^+$ T cells. The C-X-C chemokine receptor 4 (CXCR4) activated by CXCL12 enhances angiogenesis and progression of primary tumors, contributing to metastasis formation (Dewan et al., 2006; Domanska et al., 2013; Ene-Obong et al., 2013; Luker and Luker, 2006). After being triggered by cancer cells, CAFs-secreted chemokines can also result in the expansion of myeloid-derived suppressor cells (MDSCs), neutrophils and M2 macrophages (Sano et al., 2019). There are three different types of CAFs identified in PDAC. They are inflammatory CAFs (iCAFs), antigen-presenting CAFs (apCAFs), and myofibroblastic CAFs (myCAFs). The iCAFs secret IL-6 to allow the infiltration of few effector T cells and have a

high expression level of *PD-L1*, therefore stimulating an immunosuppressive environment. The secretion of IL-6 also leads to the activation of *STAT3*, which leads to a more invasive PDAC (Mace et al., 2018; Nagathihalli et al., 2016). Consequently, the interleukin-1 (IL-1)/JAK-STAT3 signaling pathway is activated to promote inflammation (Biffi et al., 2019). Macrophage colony stimulated factor (M-CSF) is secreted by iCAFs and induces the M2 macrophage polarization, promoting the progression and invasiveness of pancreatic tumor (Zhang et al., 2017). The apCAFs, as their name indicates, present antigens to T cells. However, the presence of apCAFs decreases the ratio of $CD8^+$ T cells to Tregs and therefore promotes an immunosuppressive effect in PDAC (Elyada et al., 2019). Similar to iCAF, apCAFs are suggested to support tumor progression (Elyada et al., 2019). Finally, myCAFs show the expression of the markers, such as α smooth muscle actin (αSMA), and are in the regions adjacent to tumor cells. The myCAFs play an essential role in inhibiting tumor growth and invasion. The depletion of myCAFs results in the increase of Tregs numbers and the enhancement of dedifferentiation and invasion of tumors (Ozdemir et al., 2014). The functions of myCAFs appear to conflict with those of iCAFs. Altogether, these findings have proved that different types of immune cells and CAF populations have different effects on dissemination of pancreatic cancer cells and the formation of secondary tumors in distant organs.

Myeloid-derived suppressor cells (MDSCs) have the immunosuppressive effects in pancreatic cancer. They inhibit T cell activities and efficiently promote metastasis (Takeuchi et al., 2015; Trovato et al., 2019). Neutrophils appear to exert mostly the function of promoting tumor progression as matrix metalloproteinase 9 (MMP9) and elastase derived from neutrophils induce EMT and angiogenesis (Bausch et al., 2011; Gaida et al., 2012; Grosse-Steffen et al., 2012). The M1 pro-inflammatory and M2 immunosuppressive macrophages induce neoangiogenesis and metastasis to promote the tumor progression in PDAC (Ozdemir et al., 2014; Penny et al., 2016; Shapouri-Moghaddam et al., 2018; Yin et al., 2019a). M1 macrophages also promote the formation of ADM (Liou et al., 2015; Liou et al., 2013).

Gene alterations were commonly detected in $CD14^+$ monocytes and $CD4^+$ T cells in PDAC. 261 genes were found altered in $CD14^+$ monocytes. These genes are associated with the inflammation, cell cycle, adhesion and development. In $CD4^+$ T cells, the expression levels of 496 genes were significantly different between the PDAC patients and healthy individuals. The genes are mostly associated with cell cycle, DNA damage, apoptosis and inflammation (Komura et al., 2015). PDAC patients have a higher number of PD-$1^+$ $CD4^+$ T cells when compared with the healthy controls. They also have high rates of PD-$1^+$ and FoxP$3^+$ $CD4^+$ T cells infiltration (Komura et al., 2015). It has been reported that both activated $CD4^+$ effector

and regulatory T cells take part in EMT through the release of tumor necrosis factor α (TNF-α) and IL-6. In this case, $CD4^+$ T cells favor tumor progression. However, one study reported the correlation between the high number of infiltrated $CD4^+$ T cells and a better median OS of patients with pancreatic cancer (Wang et al., 2016). Several studies have found the immunsuppressive function of Tregs (Helm et al., 2014; Lim et al., 2019; Shevchenko et al., 2013). The numbers of infiltrated Tregs and M2 immunosuppressive macrophages increase during PDAC progression, while that of infiltrated $CD8^+$ T cells decreases significantly (Bengsch et al., 2017; Wartenberg et al., 2015). One study also reported that Tregs stimulate the liver metastasis in PDAC mice (Kenkel et al., 2017). Collectively, it has been proved that Tregs exert the tumor promoting role in PDAC, whereas the function of $CD4^+$ T cells is still debatable and needs to be investigated further.

Natural killer (NK) cells and $CD8^+$ T cells are two predominant immune cell populations which can suppress the progression of PDAC. Compared with patients with other cancers, PDAC patients have a lower level of infiltrated cytotoxic $CD8^+$ T cells (Sakellariou-Thompson et al., 2017). A lower degree of tumor differentiation (G1 and G2 tumors vs. G3 tumor) was paralleled by an increasing infiltration of $CD8^+$ T cells in PDAC patients (Helm et al., 2014). Furthermore, the infiltrating number of $CD8^+$ T cells negatively correlated with the size of the lesions (Quaranta et al., 2018). It indicates $CD8^+$ T cells either make no contributions to the suppression of tumor progression and differentiation or do not exist in the large and dedifferentiated PDAC tumors. $CD8^+$ T cells are even not detected in the peripheral blood (Basso et al., 2013; Xu et al., 2014). The reduced number of infiltrated $CD8^+$ T cells in the primary tumor and blood is correlated with poor prognosis of pancreatic cancer patients (Xu et al., 2014).

Altogether, characterization of the histological and molecular features of pancreatic tumor is helpful for us to gain insight into the mechanisms of PDAC progression. The infiltrated immune cells and their interactions also play important roles in promoting the development of pancreatic cancer. A better understanding of the immune cell networks may contribute to the development of novel immune therapies for PDAC patients.

## 3.6 Aim of this work

GEMMs have been used as a powerful tool to improve our knowledge of pancreatic cancer. The development of next generation sequencing broadens our understanding of the alterations of molecular structures in PDAC tumors and multi-omics analysis has revealed the complex molecular features in patients with PDAC. In order to elucidate the mechanisms of PDAC pathogenesis, it is essential to find out the correlation between the pathological phenotypes and molecular features. This thesis focuses on the pathological features and transcriptomic profiling data of PDAC GEMMs and characterizes these mouse models to

provide insight into the mechanisms of the progression of pancreatic cancer. This study aims to identify the molecular signatures of tumor grade, mitosis, metastasis, and the immune cell subpopulations involved in PDAC tumorigenesis. In addition, in order to inactivate the endogenous oncogenic *Kras* mutation, we generated a new mouse model.

# 4 Materials

## 4.1 Technical equipment

**Table 1. Technical equipment.**

| Device | Source |
|---|---|
| 96-well magnetic ring-stand | Applied Biosystems, Inc., Carlsbad, CA, USA |
| Analytical balance A 120 S | Sartorius AG, Göttingen, DE |
| Analytical balance BP 610 | Sartorius AG, Göttingen, DE |
| Autoclave 2540 EL | Tuttnauer Europe B.V., Breda, The Netherlands |
| AxioCam HRc | Carl Zeiss AG, Oberkochen, DE |
| AxioCam MRc | Carl Zeiss AG, Oberkochen, DE |
| Bag sealer Folio FS 3602 | Severin Elektrogeräte GmbH, Sundern, DE |
| Centrifuge Avanti® J25 | Beckman Coulter GmbH, Krefeld, DE |
| Centrifuge Rotina 46R | Andreas Hettich GmbH & Co. KG, Tuttlingen, DE |
| ClarioStar MARS microplate reader | BMG Labtech, Ortenberg, DE |
| $CO_2$ incubator HERAcell® | Heraeus Holding GmbH, Hanau, DE |
| $CO_2$ incubator MCO-5AC 17AI | Sanyo Sales & Marketing Europe GmbH, Munich, DE |
| Confocal microscope TCS SP8 | Leica Microsystems GmbH, Wetzlar, DE |
| Dewar carrying flask, type B | KGW-Isotherm, Karlsruhe, DE |
| Electrophoresis power supply Power Pac 200 | Bio-Rad Laboratories GmbH, Munich, DE |
| Electroporation System, Gene Pulser®II | Bio-Rad Laboratories GmbH, Munich, DE |
| Gel Doc™ XR+ system | Bio-Rad Laboratories GmbH, Munich, DE |
| Glass ware, Schott Duran® | Schott AG, Mainz, DE |
| Heated paraffin embedding module EG1150 H | Leica Microsystems GmbH, Wetzlar, DE |
| HERAsafe® biological safety cabinet | Thermo Fisher Scientific, Inc., Waltham, MA, USA |
| Hiseq2000 platform | Illumina, San Diego, CA, USA |
| Hiseq1500 platform | Illumina, San Diego, CA, USA |
| Homogenizer SilentCrusher M with tool 6F | Heidolph Instruments GmbH & Co. KG, Schwabach, DE |
| Horizontal gel electrophoresis system | Biozym Scientific GmbH, Hessisch Oldenburg, DE |
| Horizontal shaker | Titertek Instruments, Inc., Huntsville, AL, USA |
| Incubator shaker Thermoshake | C. Gerhardt GmbH & Co. KG, Königswinter, DE |
| Laminar flow HERAsafe | Heraeus Holding GmbH, Hanau, DE |
| Leica Aperio AT2 scanner | Leica Biosystems Imaging, Inc., CA, USA |
| Magnetic stirrer, Ikamag® RCT | IKA® Werke GmbH & Co. KG, Staufen, DE |
| Microcentrifuge 5415 D | Eppendorf AG, Hamburg, DE |

| | |
|---|---|
| Microcentrifuge 5417 R | Eppendorf AG, Hamburg, DE |
| Microscope Axio Imager.A1 | Carl Zeiss AG, Oberkochen, DE |
| Microscope Axiovert 25 | Carl Zeiss AG, Oberkochen, DE |
| Microscope DM LB | Leica Microsystems GmbH, Wetzlar, DE |
| Microtome Microm HM355S | Thermo Fisher Scientific, Inc., Waltham, MA, USA |
| Microwave | Siemens AG, Munich, DE |
| Mini centrifuge MCF-2360 | LMS Consult GmbH & Co. KG, Brigachtal, DE |
| Mini-PROTEAN® Tetra Cell | Bio-Rad Laboratories GmbH, Munich, DE |
| Multipette® stream | Eppendorf AG, Hamburg, DE |
| Neubauer hemocytometer, improved | LO-Laboroptik GmbH, Bad Homburg, DE |
| Odyssey® infrared imaging system | Li-Cor Biosciences, Lincoln, NE, USA |
| Paraffin tissue floating bath Microm SB80 | Thermo Fisher Scientific, Inc., Waltham, MA, USA |
| pH meter 521 | WTW Wissenschaftlich-Technische Werkstätten GmbH, Weilheim, DE |
| Pipetus® | Hirschmann Laborgeräte GmbH & Co. KG, Eberstadt, DE |
| Power supplies E844, E822, EV243 | Peqlab Biotechnologie GmbH, Erlangen, DE |
| Qubit® 2.0 Fluorometer | Invitrogen GmbH, Karlsruhe, DE |
| Spectrophotometer NanoDrop 1000 | Peqlab Biotechnologie GmbH, Erlangen, DE |
| StepOnePlus™ real time PCR system | Applied Biosystems, Inc., Carlsbad, CA, USA |
| Stereomicroscope Stemi SV 11 | Carl Zeiss AG, Oberkochen, DE |
| Surgical instruments | Thermo Fisher Scientific, Inc., Waltham, MA, USA |
| Thermocycler T1 | Biometra GmbH, Göttingen, DE |
| Thermocycler Tgradient | Biometra GmbH, Göttingen, DE |
| Thermocycler Tpersonal | Biometra GmbH, Göttingen, DE |
| Thermocycler UNO-Thermoblock | Biometra GmbH, Göttingen, DE |
| Thermomixer compact | Eppendorf AG, Hamburg, DE |
| Tissue processor ASP300 | Leica Microsystems GmbH, Wetzlar, DE |
| Tumbling Table WT 17 | Biometra GmbH, Göttingen, DE |
| Vortex Genius 3 | IKA® Werke GmbH & Co. KG, Staufen, DE |
| Water bath 1003 | GFL Gesellschaft für Labortechnik mbH, Burgwedel, DE |

## 4.2 Disposables

**Table 2. Disposables.**

| **Disposable** | **Source** |
|---|---|
| Cell culture plastics | Becton Dickinson GmbH, Franklin Lakes, NJ, USA; Greiner Bio-One GmbH, Frickenhausen; TPP Techno Plastic Products AG, Trasadingen, Switzerland |

| | |
|---|---|
| Cell scrapers | TPP Techno Plastic Products AG, Trasadingen, Switzerland |
| Cell strainer, 100 µm, yellow | BD Biosciences, Franklin Lakes, NJ, USA |
| Chromatography paper, 3 mm | GE Healthcare Europe GmbH, Munich, DE |
| Combitips BioPur® | Eppendorf AG, Hamburg, DE |
| Conical tubes, 15 mL | TPP Techno Plastic Products AG, Trasadingen, Switzerland |
| Conical tubes, 50 mL | Sarstedt AG & Co., Nümbrecht, DE |
| Cover slips | Gerhard Menzel, Glasbearbeitungswerk GmbH & Co. KG, Braunschweig, DE |
| CryoPure tubes | Sarstedt AG & Co., Nümbrecht, DE |
| Disposable scalpels | Feather Safety Razor Co., Ltd., Osaka, Japan |
| Gene Pulser®/MicroPulser™ cuvettes, 0.2 cm gap | Bio-Rad Laboratories GmbH, Munich, DE |
| Filtropur S 0.2 | Sarstedt AG & Co., Nümbrecht, DE |
| Filtropur S 0.45 | Sarstedt AG & Co., Nümbrecht, DE |
| Glass slides Superfrost® Plus | Gerhard Menzel, Glasbearbeitungswerk GmbH & Co. KG, Braunschweig, DE |
| MicroAmp® optical 96-well reaction plate | Applied Biosystems, Inc., Carlsbad, CA, USA |
| Microtome blades S35 and C35 | Feather Safety Razor Co., Ltd., Osaka, Japan |
| Mr. Frosty™ freezing container | Thermo Fisher Scientific, Inc., Waltham, MA, USA |
| Pasteur pipettes | Hirschmann Laborgeräte GmbH & Co. KG, Eberstadt, DE |
| PCR reaction tubes | Brand GmbH + Co. KG, Wertheim; Eppendorf AG, Hamburg, DE |
| Petri dishes | Sarstedt AG & Co., Nümbrecht, DE |
| Pipette tips | Sarstedt AG & Co., Nümbrecht, DE |
| Reaction tubes, 0.5 mL, 1.5 mL and 2 mL | Eppendorf AG, Hamburg, DE |
| Precision wipes | Kimberly-Clark Worldwide Inc., Irving, TX, USA |
| Safe-lock reaction tubes BioPur® | Eppendorf AG, Hamburg, DE |
| Serological pipettes | Sarstedt AG & Co., Nümbrecht, DE |
| Single use needles Sterican® 27 gauge | B. Braun Melsungen AG, Melsungen, DE |
| Single use syringes Omnifix® | B. Braun Melsungen AG, Melsungen, DE |
| Tissue embedding cassette system | Medite GmbH, Burgdorf, DE |
| Transfer membrane Immobilon-P | Millipore GmbH, Schwalbach am Taunus, DE |

## 4.3 Reagents

**Table 3. Reagents.**

| **Reagent** | **Source** |
|---|---|
| 1 kb DNA extension ladder | Invitrogen GmbH, Karlsruhe, DE |

| | |
|---|---|
| 1,4-Dithiothreitol (DTT) | Carl Roth GmbH + Co. KG, Karlsruhe, DE |
| 2-Log DNA ladder (0.1–10.0 kb) | New England Biolabs GmbH, Frankfurt am Main |
| 2-Mercaptoethanol, 98% | Sigma-Aldrich Chemie GmbH, Munich, DE |
| 2-Propanol (isopropanol) | Carl Roth GmbH + Co. KG, Karlsruhe, DE |
| ABsolute qPCR ROX Mix | Thermo Fisher Scientific, Inc., Waltham, MA, USA |
| Agarose | Sigma-Aldrich Chemie GmbH, Munich, DE |
| Agencourt AMPure XP Beads | Beckman Coulter GmbH, Krefeld, DE |
| Ammonium persulfate | Sigma-Aldrich Chemie GmbH, Munich, DE |
| Ampicillin sodium salt | Carl Roth GmbH + Co. KG, Karlsruhe, DE |
| Blotting grade blocker non-fat dry milk | Bio-Rad Laboratories GmbH, Munich, DE |
| Bovine serum albumin, fraction V | Sigma-Aldrich Chemie GmbH, Munich, DE |
| Bradford reagent | Serva Electrophoresis GmbH, Heidelberg, DE |
| Chloramphenicol | AppliChem GmbH, Darmstadt, DE |
| Complete, EDTA-free, protease inhibitor cocktail Tablets | Roche Deutschland Holding GmbH, Grenzach-Wyhlen, DE |
| CreActive TAM400 | LASvendi, Soest, DE |
| Dimethylsulfoxide (DMSO) | Carl Roth GmbH + Co. KG, Karlsruhe, DE |
| dNTP mix, 10mM each | Fermentas GmbH, St. Leon-Rot, DE |
| Dodecylsulfate Na-salt in pellets (SDS) | Serva Electrophoresis GmbH, Heidelberg, DE |
| Dulbecco's phosphate buffered saline, powder | Biochrom AG, Berlin, DE |
| Ethanol (100%) | Merck KGaA, Darmstadt, DE |
| Ethidium bromide | Sigma-Aldrich Chemie GmbH, Munich, DE |
| Ethylenediaminetetraacetic acid (EDTA) | Invitrogen GmbH, Karlsruhe, DE |
| Gel loading dye, blue | New England Biolabs GmbH, Frankfurt am Main, DE |
| Gelatine | Carl Roth GmbH, Karlsruhe, DE |
| GeneRuler™ 100bp DNA ladder | Fermentas GmbH, St. Leon-Rot, DE |
| Glycerol | Sigma-Aldrich Chemie GmbH, Munich, DE |
| HotStarTaq DNA polymerase | Qiagen GmbH, Hilden, DE |
| Hydrochloric acid (HCl) | Merck KGaA, Darmstadt, DE |
| Isotonic sodium chloride solution | Braun Melsungen AG, Melsungen, DE |
| Immersion oil Type F | Leica Microsystems GmbH, Wetzlar, DE |
| LB agar (Luria/Miller) | Carl Roth GmbH + Co. KG, Karlsruhe, DE |
| LB broth (Luria/Miller) | Carl Roth GmbH + Co. KG, Karlsruhe, DE |
| Magnesium chloride | Carl Roth GmbH + Co. KG, Karlsruhe, DE |
| Methanol | Merck KGaA, Darmstadt, DE |
| N, N-dimethylformamide | Sigma-Aldrich Chemie GmbH, Munich, DE |
| Orange G | Carl Roth GmbH + Co. KG, Karlsruhe, DE |
| Peanut oil | Sigma-Aldrich Chemie GmbH, Munich, DE |

| | |
|---|---|
| Phosphatase inhibitor mix I | Serva Electrophoresis GmbH, Heidelberg, DE |
| Polyethylene glycol 4000 | Merck KGaA, Darmstadt, DE |
| Precision Plus Protein™ all blue standard | Bio-Rad Laboratories GmbH, Munich, DE |
| Proteinase K, recombinant, PCR grade | Roche Deutschland Holding GmbH, Grenzach-Wyhlen, DE |
| REDTaq® ReadyMix™ PCR reaction mix | Sigma-Aldrich Chemie GmbH, Steinheim, DE |
| Restriction endonucleases | New England Biolabs GmbH, Frankfurt am Main, DE |
| RNase-free DNase set | Qiagen GmbH, Hilden, DE |
| RnaseA | Fermentas GmbH, St. Leon-Rot, DE |
| Rotiphorese® gel 30 | Carl Roth GmbH + Co. KG, Karlsruhe, DE |
| S.O.C. medium | Invitrogen GmbH, Karlsruhe, DE |
| Sodium acetate buffer solution | Sigma-Aldrich Chemie GmbH, Munich, DE |
| Sodium chloride (NaCl) | Merck KGaA, Darmstadt, DE |
| Sodium hydroxide solution (NaOH) | Merck KGaA, Darmstadt, DE |
| Tamoxifen chow CreActive TAM400 | LASvendi, Soest, DE |
| TE buffer, pH 8.0 | AppliChem GmbH, Darmstadt, DE |
| TEMED | Carl Roth GmbH + Co. KG, Karlsruhe, DE |
| Tissue-Tek® O.C.T.™ compound | Sakura Finetek Europe B.V, Alphen aan den Rijn, Netherlands |
| Tris hydrochloride | J.T. Baker® Chemicals, Phillipsburg, NJ, USA |
| Tris Pufferan® | Carl Roth GmbH + Co. KG, Karlsruhe, DE |
| Triton® X-100 | Merck KGaA, Darmstadt, DE |
| Tween® 20 | Carl Roth GmbH + Co. KG, Karlsruhe, DE |

## 4.4 Antibodies

**Table 4. Antibodies.**

| **Antibody** | **Source** |
|---|---|
| Anti-mouse IgG (H+L) (DyLight® 680 Conjugate), #5470, RRID: AB_696895 | Cell Signaling Technology, Inc., Danvers, MA, USA |
| Anti-rabbit IgG (H+L) (DyLight® 800 Conjugate), #5151, RRID: AB_10697505 | Cell Signaling Technology, Inc., Danvers, MA, USA |
| Cytokeratin 19, P19001, RRID: AB_2133570 | Developmental Studies Hybridoma Bank, Iowa, USA |
| Cre Recombinase, 15036, RRID: AB_2798694 | Cell Signaling Technology, Inc., Danvers, MA, USA |
| Estrogen Receptor alpha (D8H8), 8644S, RRID: AB_2617128 | Cell Signaling Technology, Inc., Danvers, MA, USA |
| Hsp90, sc-13119 (H1704), RRID: AB_675659 | Santa Cruz Biotechnology, Inc., Dallas, TX, USA |

## 4.5 Molecular biology

Bidistilled $H_2O$ is used to prepare the buffers.

**Table 5. Buffers and solutions for molecular biology.**

| Buffer | Component |
|---|---|
| IP buffer, pH 7.9 | 50 mM HEPES<br>150 mM NaCl<br>1 mM EDTA<br>0.5% Nonidet P40<br>10% Glycerol<br>Phosphatase inhibitor (add prior to use)<br>Protease inhibitor (add prior to use) |
| Stacking gel buffer | 0.5 M Tris, adjusted to pH 6.8 with HCl |
| Separating gel buffer | 1.5 M Tris, adjusted to pH 8.8 with HCl |
| Running buffer | 25 mM Tris<br>192 mM Glycine<br>0.1% SDS |
| Transfer buffer, pH 8.3 | 25 mM Tris<br>192 mM Glycine<br>20% Methanol |
| 5x Protein loading buffer (Laemmli), pH 6.8 | 10% SDS<br>50% Glycerol<br>228 mM Tris hydrochloride<br>0.75 mM Bromphenol blue<br>5% 2-Mercaptoethanol |
| 6x Loading buffer orange G | 60% Glycerol<br>60 mM EDTA<br>0.24% Orange G |
| 10x Gitschier's buffer | 670 mM Tris, pH 8.8<br>166 mM (NH4)2SO4<br>67 mM MgCl2 |
| Soriano lysis buffer | 0.5% Triton® X-100<br>1% 2-Mercaptoethanol<br>1x Gitschier's buffer<br>400 µg/mL Proteinase K (add prior to use) |
| SucRot solution (for PCR) | 1.5 mg/mL Cresol red<br>100 mM Tris, pH 9.0<br>30% Saccharose |
| 50x Tris acetate EDTA (TAE) buffer, pH 8.5 | 2 M Tris<br>50 mM EDTA<br>5.71% Acetic acid |

**Table 6. Kits for molecular biology.**

| Kit | Source |
|---|---|
| EndoFree® plasmid maxi kit | Qiagen GmbH, Hilden, DE |

| | |
|---|---|
| QIAamp DNA mini kit | Qiagen GmbH, Hilden, DE |
| QIAfilter plasmid midi kit | Qiagen GmbH, Hilden, DE |
| QIAprep® spin miniprep kit | Qiagen GmbH, Hilden, DE |
| QIAshredder | Qiagen GmbH, Hilden, DE |
| RNeasy mini kit | Qiagen GmbH, Hilden, DE |
| TruSeq® Stranded mRNA sample preparation kit | Illumina, San Diego, CA, USA |

**Table 7. Competent bacteria.**

| **Bacterial strain** | **Source** |
|---|---|
| One Shot® Stbl3™ chemically competent E. coli | Invitrogen GmbH, Karlsruhe, DE |

**Table 8. Plasmids.**

| **Plasmid** | **Source** |
|---|---|
| pBluescript II SK (#212205) | Addgene, Cambridge, MA, USA |

### 4.5.1 Primers

Primers were purchased and produced by Eurofins MWG GmbH (Ebersberg). The concentration of the primers is 10 µM in $H_2O$.

**Table 9. Primers used for genotyping.**

| **PCR name** | **Primer name** | **Sequence (5´ → 3´)** |
|---|---|---|
| *Pdx1-Flp* | Pdx1_Flp Forward | AGAGAGAAAATTGAAACAAGTGCAGGT |
| | Pdx1_Flp Reverse | CGTTGTAAGGGATGATGGTGAACT |
| | Control forward | AACACACACTGGAGGACTGGCTAGG |
| | Gabra reverse (Ctrl) | CAATGGTAGGCTCACTCTGGGAGATGATA |
| *FSF-Kras$^{G12D}$* | FSF-Kras common forward | CACCAGCTTCGGCTTCCTATT |
| | FSF-Kras WT reverse | AGCTAATGGCTCTCAAAGGAATGTA |
| | FSF-Kras mut reverse | GCGAAGAGTTTGTCCTCAACC |
| *FSF-Kras$^{G12D}$* recombination | FSF-Kras del forward | AGAATACCGCAAGGGTAGGTGTTG |
| | FSF-Kras del reverse | TGTAGCAGCTAATGGCTCTCAAA |
| *CreER$^{T2}$* | CreERT2 forward (*Rosa26$^{CAG\text{-}CreERT2}$* line) | GAATGTGCCTGGCTAGAGATC |
| | CreERT2 reverse (*Rosa26$^{CAG\text{-}CreERT2}$* line) | GCAGATTCATCATGCGGA |
| | CreERT2 recombined reverse | CGATCCCTGAACATGTCCATC |
| *Rosa26$^{CAG}$* | R26 common forward | AAAGTCGCTCTGAGTTGTTAT |

| | | |
|---|---|---|
| | R26 WT reverse | GGAGCGGGAGAAATGGATATG |
| | R26CAG-CreERT2 mut reverse | TCAATGGGCGGGGGTCGTT |
| *FSF* | FSF forward | TGAATAGTTAATTGGAGCGGCCGCAATA |
| | FSF reverse | CAGGGTGTTATAAGCAATCCC |
| *FSF* recombination | FSF-Cre stop del forward | GTTCGGCTTCTGGCGTGT |
| | FSF-Cre stop del reverse | CGATCCCTGAACATGTCCATC |
| *Pdk1$^{lox}$* | Pdk1 floxed forward | ATCCCAAGTTACTGAGTTGTGTTGGAAG |
| | Pdk1 floxed reverse | TGTGGACAAACAGCAATGAACATACACGC |
| *Pdk1$^{lox}$* recombination | Pdk1 recombined forward | CTATGCTGTGTTACTTCTTGGAGCACAG |
| | Pdk1 non-recombined forward | CCCTCTAGCAAATGTTCTGTCTGGAATGTCT |
| | Pdk1 floxed reverse | TGTGGACAAACAGCAATGAACATACACGC |
| *Pdk1$^{L155E}$* | Pdk-L155E-P1 | GGAACTTACTCTGTAGACCAGGCTG |
| | Pdk-L155E-P2 | GACGTGTCCTAATACTACCACAAGTGGC |
| *Pdk1$^{L155E}$* recombination | Pdk-L155E-RE-UP1 | CTATGCTGTGTTACTTCTTGGAGCACAG |
| | Pdk-L155E-RE-UP2 | CCCTCTAGCAAATGTTCTGTCTGGAATGTCT |
| | Pdk-L155E-RE-LP | TGTGGACAAACAGCAATGAACATACACGC |
| *Trp53$^{lox}$* | Trp53 LOX Forward | CACAAA AACAGGTTA AACCCAG |
| | Trp53 LOX Forward | AGCACATAGGAGGCAGAGAC |
| *Trp53$^{frt}$* | Trp53 FRT Forward | CAAGAGAACTGTGCCTAAGAG |
| | Trp53 FRT Forward | CTTTCTAACAGCAAAGGCAAGC |
| *Trp53$^{frt}$* recombination | Trp53 FRT Forward | CAAGAGAACTGTGCCTAAGAG |
| | Trp53 recombination | ACTCGTGGAACAGAA ACAGGCAGA |
| *LSL-Trp53$^{R172H}$* | Trp53$^{R172H}$ forward | AGCCTTAGACATAACACACGAACT |
| | Trp53$^{R172H}$ mut forward | GCCACCATGGCTTGAGTAA |
| | Trp53$^{R172H}$ reverse | CTTGGAGACATAGCCACACTG |
| *Ptf1a$^{Cre}$* | Ptf1a-Cre-GT-LP-URP | CCTCGAAGGCGTCGTTGATGGACTGCA |
| | Ptf1a-Cre-GT-wt-UP | CCACGGATCACTCACAAAGCGT |
| | Ptf1a-Cre-GT-mut-UP-neu | GCCACCAGCCAGCTATCAA |
| *LSL-Kras$^{G12D}$* | Kras-WT-UP1 | CACCAGCTTCGGCTTCCTATT |
| | Kras-URP-LP1 | AGCTAATGGCTCTCAAAGGAATGTA |
| | KrasG12Dmut_UP | CCATGGCTTGAGTAAGTCTGC |
| *LSL-Rosa26$^{Snail}$* | pGL3-UP | TGAATAGTTAATTGGAGCGGCCGCAATA |
| | Snail Reverse | ACCAGGAAGGAGCGCGGCAT |
| *LSL-Rosa26$^{Snail}$* | R26-Tva-GT-UP | AAAGTCGCTCTGAGTTGTTAT |

| | | |
|---|---|---|
| recombination | Snail Reverse | ACCAGGAAGGAGCGCGGCAT |
| *Cdkn2a*$^{lox}$ | INK4A-UP | CCAAGTGTGCAAACCCAGGCTCC |
| | INK4A-LP | TTGTTGGCCCAGGATGCCGACATC |
| *Ink4a** | VBC-Ink4a-PM-UP | GCAGTGTTGCAGTTTGAACCC |
| | VBC-Ink4a-PM-LP | TGTGGCAACTGATTCAGTTGG |
| *Pdx1-Cre* | Pdx-UP2 | GCTCATTGGGAGCGGTTTTG |
| | V-Cre-LP2 | ACATCTTCAGGTTCTGCGGG |
| | Pdx-LP1 | CACGTGGTTTACCCTGGAGC |
| *LSL-PIK3CA*$^{H1047R}$ | pGL3-UP | TGAATAGTTAATTGGAGCGGCCGCAATA |
| | PI3K-Rev | AAATAGCCGCAGGTCACAAAGTCTCCG |
| *FSF-Kras*$^{lox-G12D-lox}$ | pGL3- UP | TGAATAGTTAATTGGAGCGGCCGCAATA |
| | Kras-URP-LP1 | AGCTAATGGCTCTCAAAGGAATGTA |
| *Tgfβr2*$^{lox}$ | Tgfbr2 Forward | TAAACAAGGTCCGGAGCCCA |
| | Tgfbr2 Reverse | ACTTCTGCAAGAGGTCCCCT |
| *LSL-Rosa26*$^{Tgfβ1}$ | R26-Tva-GT-UP | AAAGTCGCTCTGAGTTGTTAT |
| | mTGF-b1-LP | GCTGATCCCGTTGATTTCC |
| | pGL3-UP | TGAATAGTTAATTGGAGCGGCCGCAATA |
| *Tnc*$^{ko}$ | Tnc-Forward | AGCCCCTGCCTACCTTTTCCTAATG |
| | Tnc Reverse | CTTCGGGAGTGAGGGCAA ACA |
| *Hnf4a*$^{lox}$ | Hnf4a Forward | AGAATGACCCTGAAGCACCAGG |
| | Hnf4a Reverse | GCCAGAGGTCTGTGA AACAAGG |
| *Rosa26*$^{mT-mG}$ | mTmG-LP1 | GTACTTGGCATATGATACACTTGATGTAC |
| | R26-Tva-GT-UP | AAAGTCGCTCTGAGTTGTTAT |
| | mTmG-LP2 | GGAGCGGGAGAAATGGATATG |
| *Rosa26*$^{mT-mG}$ recombination | mTmG-Re-UP1 | GTTCGGCTTCTGGCGTGT |
| | mTmG-Re-LP1 | CCATGTGATCGCGCTTCTCGT |
| | mTmG-Re-LP2 | GCTTGGTGTCCACGTAGTAGTAGC |

**Table 10. Primers for quantitative real time PCR.**

| Gene | Primer name | Sequence (5´ → 3´) | Origin |
|---|---|---|---|
| *neo* | neo-TM-UP1 | TGGATTGCACGCAGGTTCT | Mus musculus |
| | neo-TM-LP2 | GTGCCCAGTCATAGCCGAAT | |
| | Labelled probe neo | CGGCCGCTTGGGTGGAGAGG | |
| β-actin | Mbact-DANN-taq-FW | TTCAACACCCCAGCCATGTA | Mus musculus |
| | Mbact-DANN-taq-Rev | TGTGGTACGACCAGAGGCATA | |

| | | | |
|---|---|---|---|
| | Labeled probe β-actin | TTTGAGACCTTCAACACCCCAGCCAT | |

**Table 11. Primers for embryonic stem cell clone.**

| Gene | Primer name | Sequence (5´ → 3´) | Origin |
|---|---|---|---|
| ES screen | pGL3-pA-pause-4645-UP | TGAATAGTTAATTGGAGCGGCCGCAATA | Mus musculus |
| | ESkras-co-LP1 | GGCTATAGCCACAGCCCCTCCTTCA | |
| distal loxP | lox-bgl-UP1 | CAGATGCTGCGATTAAAGATGTAC | Mus musculus |
| | lox-bgl-LP1 | CTTCCTGCTAATCTCGGAGGTT | |
| Positive mice PCR1 (Figure 18Ea) | Kras-WT-UP1 | CACCAGCTTCGGCTTCCTATT | Mus musculus |
| | Kras-URP-LP1 | AGCTAATGGCTCTCAAAGGAATGTA | |
| | FSASFneosc-LP2 | ATTGCATCAGCCATGATGGATACTTTCT | |
| Positive mice PCR2 (Figure 18Eb) | Lox-For 2 | AGTTTAGGCTTTCCAAAAGGC | Mus musculus |
| | Lox-Rev2 | GTATTGCTAAGAACTTGTTGC | |
| Positive mice PCR3 (Figure 18Ec) | pGL3-pA-pause-4645-UP | TGAATAGTTAATTGGAGCGGCCGCAATA | Mus musculus |
| | lox-bgl-LP1 | CTTCCTGCTAATCTCGGAGGTT | |

## 4.6 Cell culture

**Table 12. Cell lines.**

| Cell line | Source |
|---|---|
| Gryphon™ Eco retroviral packaging cell line | Allele Biotechnology, San Diego, CA, USA |
| DF-1 fibroblasts | American Type Culture Collection, Manassas, VA, USA |
| W4/129S6 embryonic stem ells | Taconic Farms, Inc., Hudson, NY, USA |

**Table 13. Cell culture medium.**

| Medium | Components |
|---|---|
| MEF medium | D-MEM<br>10% FCS (Biochrom AG)<br>1% Penicillin-streptomycin<br>1% L-Glutamine |
| Embryonic stem cell medium | D-MEM without glutamine<br>15% ES-FCS<br>1% Penicillin-streptomycin<br>1% L-Glutamine<br>1% Sodium pyruvate MEM<br>1% MEM non-essential amino acids<br>0.1% 0.1 M 2-Mercaptoethanol<br>**1000 U/mL LIF** |
| Cancer cell medium | DMEM<br>10% FCS (Biochrom AG) |

| | |
|---|---|
| | 1% Penicillin/Streptomycin |
| Gryphon™ Eco medium | DMEM<br>10% FCS (Biochrom AG)<br>1% Penicillin/Streptomycin<br>1% L-Glutamine |
| Freezing medium | 70% DMEM<br>20% FCS<br>10% DMSO |

**Table 14. Reagents and kits for cell culture.**

| **Reagent / Kit** | **Source** |
|---|---|
| 4-hydroxytamoxifen (≥70% Z isomer) | Sigma-Aldrich Chemie GmbH, Munich, DE |
| Collagenase type 2 | Worthington Biochemical Corporation, Lakewood, NJ, USA |
| Dulbecco's modified eagle medium (DMEM) with L-glutamine | Invitrogen GmbH, Karlsruhe, DE |
| Dulbecco's modified eagle medium (DMEM) without L-glutamine (for ES cell medium) | Invitrogen GmbH, Karlsruhe, DE |
| Dulbecco's phosphate buffered saline (PBS) | Invitrogen GmbH, Karlsruhe, DE |
| Effectene® transfection reagent | Qiagen GmbH, Hilden, DE |
| ESGRO ® (LIF) | Millipore GmbH, Schwalbach am Taunus, DE |
| Fetal calf serum (FCS) | Biochrom AG, Berlin, DE |
| Fungizone® antimycotic | Invitrogen GmbH, Karlsruhe, DE |
| G418, Geneticin® | Invitrogen GmbH, Karlsruhe, DE |
| Gelatin | Sigma-Aldrich Chemie GmbH, Munich, DE |
| L-Glutamine 200 mM | Invitrogen GmbH, Karlsruhe, DE |
| MEM non-essential amino acids | Invitrogen GmbH, Karlsruhe, DE |
| Penicillin (10000 units/mL) / Streptomycin (10000 µg/mL) solution | Invitrogen GmbH, Karlsruhe, DE |
| Puromycin dihydrochloride | Sigma-Aldrich Chemie GmbH, Munich, DE |
| Sodium pyruvate MEM | Invitrogen GmbH, Karlsruhe, DE |
| Trypsin, 0.05% with 0.53 mM EDTA 4Na | Invitrogen GmbH, Karlsruhe, DE |
| Venor® *GeM* mycoplasma detection kit | Minerva Biolabs GmbH, Berlin, DE |

## 4.7 Histology

**Table 15. Reagents and kits for histological analysis.**

| **Reagent / Kit** | **Source** |
|---|---|
| Aluminium sulfate | Honeywell Specialty Chemicals Seelze GmbH, Seelze |
| Antigen unmasking solution, citric acid based | Vector Laboratories, Inc., Burlingame, CA, USA |
| Avidin/biotin blocking kit | Vector Laboratories, Inc., Burlingame, CA, USA |

| | |
|---|---|
| Cytoseal™ XYL mounting medium | Thermo Fisher Scientific, Inc., Waltham, MA, USA |
| DAB peroxidase substrate kit, 3,3'-diaminobenzidine | Vector Laboratories, Inc., Burlingame, CA, USA |
| Donkey serum D9663 | Sigma-Aldrich Chemie GmbH, Munich, DE |
| Eosine | Waldeck GmbH & Co KG, Münster, DE |
| Goat serum G9023 | Sigma-Aldrich Chemie GmbH, Munich, DE |
| Hematoxylin | Merck KGaA, Darmstadt, DE |
| Hydrogen peroxide 30% | Merck KGaA, Darmstadt, DE |
| Rabbit serum R9133 | Sigma-Aldrich Chemie GmbH, Munich, DE |
| Roti® Histofix 4% | Carl Roth GmbH + Co. KG, Karlsruhe, DE, DE |
| Roti® Histol | Carl Roth GmbH + Co. KG, Karlsruhe, DE, DE |
| Sucrose (saccharose) | Merck KGaA, Darmstadt, DE |
| Vectashield® mounting medium with DAPI | Vector Laboratories, Inc., Burlingame, CA, USA |
| Vectastain® elite ABC kit | Vector Laboratories, Inc., Burlingame, CA, USA |

**Table 16. Secondary antibodies for histological analysis.**

| Antibody | Source |
|---|---|
| Biotinylated anti-rat IgG (H+L), BA-4000, RRID:AB_2336206 | Vector Laboratories, Inc., Burlingame, CA, USA |
| Goat anti-mouse DyLight800, SA5-35521, RRID:AB_2556774 | Thermo Fisher Scientific, Inc., Waltham, MA, USA |
| Goat anti-Rabbit IgG (H+L), Alexa Fluor 700, A-21038, RRID:AB_2535709 | Thermo Fisher Scientific, Inc., Waltham, MA, USA |

## 4.8 Software

**Table 17. Software.**

| Software | Source |
|---|---|
| AxioVision 4.8, RRID:SCR_002677 | Carl Zeiss AG, Oberkochen, DE |
| Excel, RRID:SCR_016137 | Microsoft Corporation, Redmont, WA, USA |
| FlowJo v10, RRID:SCR_008520 | FlowJo LLC, Ashland, OR, USA |
| ImageScope v12.3, RRID:SCR_020993 | Leica Biosystems, Wetzlar, DE |
| R v3.1.2, RRID:SCR_001905 | R Core Team |
| GraphPad Prism 8, RRID:SCR_002798 | La Jolla, CA, USA |
| Odyssey® v1.2, RRID:SCR_014579 | Li-Cor Biosciences, Lincoln, NE, USA |
| StepOne™ v2.3, RRID:SCR_014281 | Applied Biosystems, Inc., Carlsbad, CA, USA |

# 5 Methods

## 5.1 Mouse experiments

All animal experiments were performed in accordance with the European guidelines for the care and use of laboratory animals and were approved by the reginal authorities. Mice were on a mixed C57BL6/J;129/S6 background.

### 5.1.1 Mouse strains

This study used the conditional Cre/*loxP* and Flp/*frt* mice. These mice have genes with *loxP*/*frt* flanked or the loxP-stop-loxP (*LSL*)/frt-stop-frt (*FSF*) were interbred with the mice having the expression of Cre/Flp recombinase controlled by a pancreas-specific promoter to conditionally silence the expression of the genes of interest or activate gene expression in pancreas. The combination of the Flp/*frt* recombination system initiating the PDAC progression and the Cre/*loxP* system for the manipulation of the gene of interest allows to inactivate the effectors of Ras in PanIN lesions and pancreatic cancer cells.

***Ptf1a*$^{Cre/+}$** (Nakhai et al., 2007). RRID: BCBC_184. This is a knock-in mouse line kindly provided by Dr. Hassan Nakhai (Klinikum rechts der Isar, Technical University Munich, DE). The Ptf1a is a component of the pancreas transcription factor 1 and is involved in the development of mammalian pancreas. The pancreatic specific *Ptf1a* promoter controls the Cre recombinase expression.

***LSL-Kras*$^{G12D/+}$** (Hingorani et al., 2003; Jackson et al., 2001). RRID: IMSR_JAX:008179. This is a knock-in mouse line kindly provided by Prof. Tyler Jacks (Massachusetts Institute of Technology, Cambridge, MA, USA). The *LSL-Kras*$^{G12D/+}$ mouse strain has the G12D mutation in the exon 2, which is the most common mutation detected human PDAC. The *LSL* cassette deletion mediated by Cre recombinase results in the constitutive activation of Kras signaling pathway.

***LSL-PIK3CA*$^{H1047R/+}$** (Eser et al., 2013). RRID: IMSR_JAX:016977. This is a knock-in mouse strain developed in the lab of Prof. Dieter Saur. The oncogenic *PIK3CA*$^{H1047R}$ is a knockin cassette at the *Rosa26* locus and the *LSL* is used for the silencing of the expression of this mutation. The mice with the *PIK3CA*$^{H1047R}$ allele carry a mutation in codon 1047. The Cre mediated *LSL* deletion allows the *p110α*$^{H1047R}$ expression, activating the PI3K signaling way.(Hayhurst et al., 2001)

***LSL-Rosa26$^{Snail/+}$***. RRID: BCBC_194. This is a knock-in mouse line and was developed in the lab of Prof. Dieter Saur. This construct consists of *LSL* elements and the cDNA of mouse *Snail* gene and was inserted into the *Rosa26* locus. The overexpression of *Snail* is mediated by Cre recombinase. This construct is flanked by two frt cassettes, allowing the removal of this construct with Flp recombinase.

***Pdk1$^{lox/+}$*** (Lawlor et al., 2002). RRID: MGI:5442314. The exons 3 and 4 of the endogenous *Pdk1* locus in this mouse strain are flanked by two *loxP* sites and therefore, crossing with the mouse strain with the expression of Cre recombinase leads to the inactivation of *Pdk1*.

***Pdx1-Flp*** (Schönhuber et al., 2014). RRID: MGI:6154332. This is a transgenic mouse line developed in the lab of Prof. Dieter Saur. Pancreas progenitor cells and adult pancreas show the expression of *Pdx1*. The Flp-O recombinase expression is controlled by the *Pdx1* promotor.

***Pdx1-Cre*** (Schönhuber et al., 2014). RRID: IMSR_JAX:034623. This is a transgenic mouse line and was kindly provided by Prof. David Tuveson (Cold Spring Harbor Laboratory, Princeton, NJ, USA). The progenitor cells of pancreas and adult pancreas express *Pdx1*. This transgenic mouse strain expresses Cre recombinase controlled by *Pdx1* promotor.

***FSF-Kras$^{G12D/+}$*** (Schönhuber et al., 2014). RRID: IMSR_JAX:008179. This is a knock-in mouse line established in the lab of Prof. Dieter Saur. The expression of endogenous *Kras$^{G12D}$* mutation is silenced by the *FSF* cassette and Flp recombinase can activate the expression of the oncogenic *Kras$^{G12D}$* mutation.

***FSF-Rosa26$^{CAG-CreERT2/+}$*** (Schönhuber et al., 2014). RRID: MGI:2176738. This is a knock-in mouse line developed in the lab of Prof. Dieter Saur. The *CreER$^{T2}$* allele controlled by the *CAG* promoter is silenced by the *FSF* and CreER$^{T2}$ can be activated by tamoxifen (TAM). *FSF-Rosa26$^{CAG-CreERT2/+}$* is a knock-in construct at the *Rosa26* locus.

***Trp53$^{frt/+}$*** (Lee et al., 2012). RRID: IMSR_JAX:017767. This mouse line was kindly provided by Dr. David Kirsch (Duke University School of Medicine, Durham, NC, USA). The exons 2 to 6 of the endogenous *Trp53* are flanked by two *frt* cassettes. The expression of the Flp recombinase leads to the inactivation of *Trp53*.

***Trp53$^{lox/+}$*** (Lee et al., 2012). RRID: IMSR_JAX:008462. The exons 2 to 10 of the endogenous *Trp53* are flanked by two *loxP* cassettes. This mouse strain can be interbred with the mouse line with the expression of Cre recombinase leading the conditional inactivation of *Trp53*.

***LSL-Trp53$^{R172H/+}$*** (Hingorani et al., 2005; Olive et al., 2004). RRID: IMSR_JAX:002659. This is a knock-in mouse line and was kindly provided by Prof. Tyler Jacks (Massachusetts Institute of Technology, Cambridge, MA, USA). This *Trp53$^{R172H}$* mutation, a missense mutation, has been found in the patients with spontaneous tumors. The *LSL-Trp53$^{R172H}$* mice have the mutation in the exon 5 at the endogenous *Trp53* locus. The removal of the *LSL* cassette results in the expression of mutated *Trp53* (de Vries et al., 2002; Liu et al., 2000).

***Ink4a$^{*/+}$*** (Krimpenfort et al., 2001). RRID: IMSR_RBRC09236. This is a knock-out mouse line kindly provided by Prof. Anton Berns (The Netherlands Cancer Institute, Amsterdam, The Netherlands). This mouse strain habors a nonsense mutation in the codon 101 in the exon 2 at the *Cdkn2a* locus. This mutation result in the destabilization of the p16$^{INK4A}$ protein. The expression of p19$^{ARF}$ protein is not affected by this mutation.

***Cdkn2a$^{lox/+}$*** (Aguirre et al., 2003). RRID: MGI:3822321. This mouse line was kindly provided by Prof. Nabeel Berdeesy (Harvard Medical School, Boston, MA, USA). In this mouse strain, the exons 2 and 3 at the *Cdkn2a* locus are flanked by two *loxP* sites. Cre expression leads to the deletion of both *p16$^{INK4A}$* and *p19$^{ARF}$* at the same time.

***Tgfβr2$^{lox/+}$*** (Chytil et al., 2002). RRID: MGI:5544817. The exon 2 of the endogenous *Tgfβr2* locus in this mouse strain is flanked by two *loxP* sites. Interbreeding this mouse strain with the mice with Cre expression results in the deletion of *Tgfβr2.*

***LSL-Rosa26$^{Tgfβ1/+}$***. This is a knock-in mouse strain developed in the lab of Prof. Dieter Saur. The *Tgfβ1* cDNA is silenced by the *LSL* cassette and can be activated by Cre recombinase. *LSL-Rosa26$^{Tgfβ1/+}$* is a knock-in construct at the *Rosa26* locus.

***Smad4$^{lox/+}$*** (Bardeesy et al., 2006). RRID: IMSR_JAX:017462. The exons 8 and 9 are flanked by two *loxP* sites in the endogenous *Smad4* locus. Interbreeding this mouse strain with the mouse strain expressing Cre recombinase leads to the deletion of *Smad4*.

***Pdk1$^{L155E/+}$*** (Bayascas et al., 2008). RRID: MGI:5759390. This knock-in mouse line carries a missense point mutation L155E introduced in the exon 4 of the endogenous *Pdk1* locus. A

minigene cassette consists of the exons 3 to 14 of *Pdk1* and is inserted in front of exon4, which is flanked by two *loxP* sites. The removal of the minigene by the Cre recombinase results in the *Pdk1*$^{L155E}$ expression.

***Tnc*$^{-/+}$** (Forsberg et al., 1996). RRID: MGI:6287937. The exon 2 of *Tnc* is replaced by the neomycin cassette, which leads to the silence of the *Tnc* gene.

***Hnf4α*$^{lox/+}$** (Hayhurst et al., 2001). RRID: MGI:3653182. The exons 4 and 5 of *Hnf4α* gene are flanked by two *loxP* sites in this mouse strain. Interbreeding this mouse strain with the mouse strain expressing Cre recombinase result in the deletion of *Hnf4α* gene.

### 5.1.2 Mouse nomenclature

Mouse genotypes were abbreviated as listed in Table 18 to improve readability of this thesis.

**Table 18. Nomenclature of mouse strains.**

| Complete genotypes | Abbreviation |
|---|---|
| *Pdx1-Flp;FSF-Kras*$^{G12D/+}$ | PK |
| *Pdx1-Cre;LSL-Kras*$^{G12D/+}$ | |
| *Ptf1a*$^{cre/+}$*;LSL-Kras*$^{G12D/+}$ | |
| *Pdx1-Flp;FSF-Kras*$^{G12D/+}$*;Trp53*$^{frt/+}$ | PKP_HET |
| *Pdx1-Cre;LSL-Kras*$^{G12D/+}$*;Trp53*$^{lox/+}$ | |
| *Ptf1a*$^{cre/+}$*;LSL-Kras*$^{G12D/+}$*;Trp53*$^{lox/+}$ | |
| *Ptf1a*$^{cre/+}$*;LSL-Kras*$^{G12D/+}$*;Trp53*$^{R172H/+}$ | |
| *Pdx1-Flp;FSF-Kras*$^{G12D/+}$*;Trp53*$^{frt/frt}$ | PKP_HOM |
| *Pdx1-Cre;LSL-Kras*$^{G12D/+}$*;Trp53*$^{lox/lox}$ | |
| *Ptf1a*$^{cre/+}$*;LSL-Kras*$^{G12D/+}$*;Trp53*$^{lox/lox}$ | |
| *Ptf1a*$^{cre/+}$*;LSL-Kras*$^{G12D/+}$*; Trp53*$^{R172H/R172H}$ | |
| *Ptf1a*$^{cre/+}$*;LSL-Kras*$^{G12D/+}$*;Cdkn2a*$^{lox/+}$ | PKC_HET |
| *Ptf1a*$^{cre/+}$*;LSL-Kras*$^{G12D/+}$*;Cdkn2a*$^{lox/lox}$ | PKC_HOM |
| *Ptf1a*$^{cre/+}$*;LSL-Kras*$^{G12D/+}$*;LSL-ROSA26*$^{Snail/+}$ | PKS |
| *Ptf1a*$^{cre/+}$*;LSL-Kras*$^{G12D/+}$*;LSL-ROSA26*$^{Snail/+}$; *Cdkn2a*$^{lox/+}$ | PKS_C _HET |
| *Ptf1a*$^{cre/+}$*;LSL-Kras*$^{G12D/+}$*;LSL-ROSA26*$^{Snail/+}$; *Trp53*$^{lox/+}$ | PKS _P _HET |
| *Ptf1a*$^{cre/+}$*;LSL-Kras*$^{G12D/+}$*;Tgfβr2*$^{lox/+}$ | PKT_HET |
| *Ptf1a*$^{cre/+}$*;LSL-Kras*$^{G12D/+}$*;Tgfβr2*$^{lox/lox}$ | PKT_HOM |
| *Ptf1a*$^{cre/+}$*;LSL-Kras*$^{G12D/+}$*;Tgfβr2*$^{lox/lox;}$*Tp53*$^{lox/+}$ | PKT_HOM_P_HET |
| *Pdx1-Flp;FSF-Kras*$^{G12D/+}$*; FSF-Rosa26*$^{CAG-CreERT2/+}$*; Ink4α*$^{*/+}$*;Smad4*$^{lox/lox}$*;Tp53*$^{lox/+}$ | PKP_HET_C_HET_Smad4_HOM |

| | |
|---|---|
| *Ptf1a$^{cre/+}$;LSL-Kras$^{G12D/+}$; Pdk1$^{lox/+}$; Pdk1$^{L155E/+}$* | PKPdk$^{lox/L155E}$ |
| *Pdx1-Cre;LSL-PIK3CA$^{H1047R/+}$* | PPI3K |
| *Ptf1a$^{cre/+}$;LSL-PIK3CA$^{H1047R/+}$* | |
| *Ptf1a$^{cre/+}$;LSL-PIK3CA$^{H1047R/+;}$ Trp53$^{lox/+}$* | PPI3KP_HET |
| *Ptf1a$^{cre/+}$;LSL-PIK3CA$^{H1047R/+;}$ Trp53$^{lox/lox}$* | PPI3KP_HOM |

### 5.1.3 Genotyping

A small piece of the ear, about 1mm, was taken from a 2-3 weeks old mouse. Each mouse was numbered by the explicit earmarks. Genomic DNA was isolated as described in 5.4.1.

### 5.1.4 Mouse dissection

The mouse was euthanatized by isoflurane inhalation and cervical dislocation before the dissection. After fixiation and disinfection, the abdomen of the mouse was cut open and the dissection of the mouse was performed in sterile conditions. The tissue samples taken from pancreas were homogenized with RLT buffer containing 2-mercaptoethanol (1:100) for RNA isolation. IP buffer supplemented with phosphatase inhibitor and proteinase inhibitor was used for the isolation of protein. A piece of pancreatic sample was snap-frozen for the subsequent isolation of DNA. All these samples were snap-frozen and stored at -80 °C. The weight and the size of the pancreas were measured. 4% Roti® Histofix was used to fix the organs, including pancreas, liver, lung, spleen and heart, for the subsequent analysis.

## 5.2 Histopathological analysis

### 5.2.1 Sections of the paraffin embedded tissues

The tissue samples were fixed in 4% Roti® Histofix for 24 hours (h). Afterwards, the tissue samples were dehydrated in the tissue processor ASP300. Paraffin was used to embed the samples and the tissue blocks were stored at room temperature (RT). For the subsequent stainings, the serial sections were cut at a thickness of 2.5-3 µm in the Microm HM355S.

### 5.2.2 Hematoxylin and eosin (H&E) staining of the paraffin sections

The wax of the tissue sections was dissolved by the incubation of the section two times for 5 min each time in Roti® Histol. Rehydration was performed by passing through a series of ethanol (EtOH) solutions: two times of 99% EtOH for 3 minute (min) each, two times of 96% EtOH for 3 min each and two times of 80% EtOH for 3 min each. Afterwards, the slide was rinsed in distilled water. Then, the slide was stained in hematoxylin for 5 second (s) for nuclear staining and subsequently was blued by being rinsed in tap water for about 5 min.

Afterwards, the section was placed in eosin solution for 20 s and rinsed in distilled water. Slides then were passed through an ascending series of EtOH solutions (two times of 80% EtOH for 3 min each, two times of 96% EtOH for 3 min each and two times of 99% EtOH for 3 min each) to remove water and were incubated two times for 5 min each in Roti® Histol before being covered by Cytoseal™ XYL mounting medium.

### 5.2.3 Immunohistochemistry (IHC) of the paraffin sections

The slides of paraffin-embedded pancreatic tissue went through the paraffin removal and rehydration steps as described in 5.2.2. The slides were heated in a citric acid-based antigen unmasking solution in a microwave oven at 360 W for 10 min for antigen retrieval. Afterwards, the slides were cooled down in the citrate buffer at RT for 20 min and were rinsed three times in water. To block the activity of endogenous peroxidase, the slides were incubated in 3% $H_2O_2$ in the dark for 15 min. Then, the sections were rinsed in PBS. Next, they were blocked in 3-5% serum/Avidin/PBS for 1h at RT to prevent nonspecific background staining. PBS was used to wash the slides three times before the incubation of the first antibody which was diluted in 3-5 % serum/Biotin/PBS and the slides were incubated in the first antibody solution overnight at 4 °C. Afterwards, the sections were washed three times in PBS and were incubated in the biotinylated secondary antibody diluted 1:500 in 3-5 % serum/PBS solution for 1 h at RT. Then, the sections were rinsed three times in PBS. The Vectastain® elite ABC kit and the DAB peroxidase substrate kit were used for the detection according to the protocol provided by the manufacturer. The slides went through the counterstaining with hematoxylin and dehydration and were covered with the mounting medium as described in 5.2.2.

### 5.2.4 Analysis of the histopathological sections

Sections were scaned using the Leica Aperio AT2 scanner for the documentation. The representative images are shown in the results. The pathologist, PD Dr. med. Moritz Jesinghaus (Klinikum rechts der Isar, Technical University of Munich, DE), evaluated the pathological features of the pancreatic tumor tissues, including the tumor grades, mitosis and stromal contents and lymphocytes. Dr. med. vet. Katja Steiger (Klinikum rechts der Isar, Technical University of Munich, DE) also gave her advice on the evaluation.

## 5.3 Cell culture

### 5.3.1 Generation and culture of mouse primary cancer cell lines

The cancer cells from the PDAC mice were isolated in sterile conditions. A piece of the pancreatic tumor was taken and washed with sterile PBS. The tumor tissue was minced with

a scalpel in a biological safety cabinet and digested by collagenase type 2 in 5 mL cancer cell medium at 37 °C for 24-48 h. The tumor cells was spun down at 1200 rpm for 5 min. The medium was discarded. Then the cells were suspended in 5 mL cancer cell medium and transferred to the culture flask and incubated in the culture condition of 37 °C and 5% $CO_2$.

To passage the tumor cells, the cancer cell medium was discarded, and the cancer cells were rinsed in PBS. The cancer cells were incubated with trypsin/EDTA in the cell culture incubator until the cells were detached from the culture flask. Then the culture medium was used to stop the trypsinization. Thereafter, the cells were ready for seeding. The number of the cells was counted with a hemacytometer.

The cryopreservation of the primary tumor cells was perfomed as follows. The tumor cells were suspended in the fresh cancer cell medium after the trypsinization and spun down at 1200 revolutions per minute (rpm) for 5 min. The cells were resuspended in the pre-cooled freezing medium. The aliquots of cell suspension were dispensed into CryoPure. Then the cells were frozen at -80 °C for 24 h. After 24h, the CryoPure tubes were transferred and stored in liquid nitrogen.

### 5.3.2 Treatment of 4-hydroxytamoxifen (4-OHT)

Primary cancer cells were treated with 600 nM 4-hydroxytamoxifen (4-OHT) for 2, 4, 6 and 8 days to activate $CreER^{T2}$ which mediates the deletion of *loxP*-flanked sequences in the *in vitro* expriments. The EtOH treated cells were considered as the control group. Afterwards, cells were harvested or seeded for the further analysis.

### 5.3.3 Retrovirus production

The Gryphon™ Eco Packaging cell line is the engineered HEK293T cells with the expression of gag, pol and envelope proteins which are critical for retrovirus production. The Effectene® transfection reagent was used to transfect the Gryphon™ Eco cells. 1-5 x $10^6$ Gryphon™ Eco cells were seeded in a 10-cm dish. When the cells were 60-80% confluent, they were transfected with the shRNA vectors. 3 µg of the plasmid was diluted with EC buffer to 300 µL. 48 µL enhancer then was added. The solution was vortexed and incubated for 2 min. Then, 30 µL Effectene® reagent was added to the DNA-enhancer solution and the solution was vortexed for 10 s. After 10 min incubation, the formed transfection complexes and the fresh medium were mixed, and the mixture was added dropwise onto the cells. 48 h post-transfection, retrovirus in the medium was harvested and 10 mL fresh medium was added to the cells. After 24 h, retrovirus was harvested again. The viral supernatant went through a 0.45 µm filter and then stored in a storage tube.

### 5.3.4 Retroviral transduction

1 x $10^5$ of the cancer cells per well were seeded in a 12-well plate. The transduction was performed the next day. For retroviral transduction, the fresh medium was added to replace the old medium. 8 µg/mL polybrene and 1 mL of the filtrated virus supernatant were added to each well. 48 h later, the selection of transduced cells was performed by using appropriate antibiotics.

### 5.3.5 Embryonic stem (ES) cell culture

**Culture and cryopreservation.** Mouse embryonic fibroblasts (MEFs) were used for the ES cell culture. They are mitotically inactivated by irradiation in 34 gray and G418 resistant. A 10 cm dish was coated by gelatine. MEFs were seeded in the MEF medium on the dish the day before ES cells were seeded. W4/129S6 ES cells were cultured on a monolayer of MEFs in the ES cell medium. The passaging of the ES cells was performed regularly to prevent the differentiation. For cryopreservation, the ES cells were trypsinized and harvested. Afterwards, the cells were spun down at the speed of 1200 rpm for 5 min at RT. Meanwhile, ES cell medium containing 10% DMSO as the freezing medium was prepared and stored at 4 °C. The cells were resuspended in the freezing medium. The aliquots of cell suspension were dispensed into CryoPure vials, transferred to a pre-cooled Mr. Frosty™ container containing 2-propanol and stored at -80°C for 24 h. The cells were then transferred to liquid nitrogen.

**ES cell targeting, selection and screening.** 1 x $10^7$ ES cells were suspended in 750 µl ice-cold PBS and mixed with 25 µg of the linearized targeting construct. The mixture was put into a pre-cooled electroporation cuvette. The Gene Pulser® II was used for electroporation in the condition of 250 V and 500 µF. Immediately after the electroporation, 50 mL of the prewarmed fresh ES cell medium was added to the cells. Then the cells and the medium were transferred to the dish with MEFs. The ES cells without electroporation were cultured in a 6-well plate with MEFs as control. 20 h later, the selective medium, which contains Geneticin® at the concentration of 250 µg/mL, was used to select the ES cell clones with the targeted construct which contains the neomycin cassette providing the resistant capability of Geneticin®. The selective ES medium was used for 7 days and changed daily. ES clones were picked and transferred to the wells in 24-well plates with MEFs for further culturing and 96-well plates for collecting cells for DNA extraction and identification of the positive clones. The procedure of passaging and cryopreservation of the positive ES clones is shown in Figure 1.

**PCR Testing for mycoplasma contamination.** The targeted ES cells with the targeting construct were cultured to 100% confluency in the medium without antibotics for the test of

mycoplasma contamination. The PCR test was performed according to the protocol of the Venor® GeM kit (Minerva biolabs).

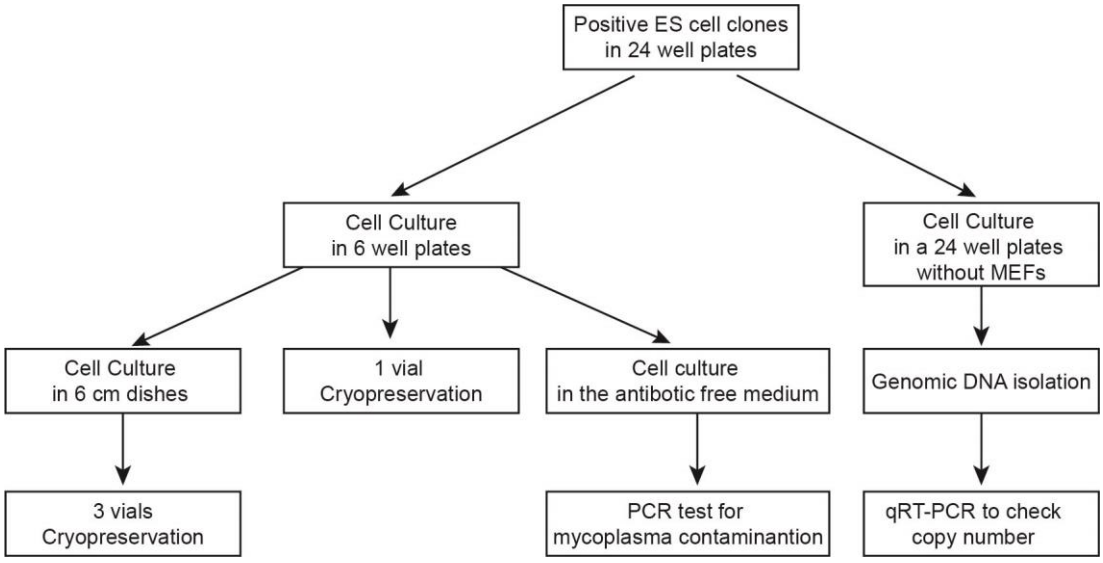


**Figure 1. The procedure of passaging and cryopreservation of ES positive clones**

## 5.4 Molecular biology

### 5.4.1 Genomic DNA isolation

50-150µL of Soriano lysis buffer was added to a tissue sample or a cell pellet for the isolation of genomic DNA. The mixture was incubated for lysis at 55 °C for 1.5 h. Proteinase K was inactivated at 95 °C for 15 min. Afterwards, the sample was vortexed and centrifuged to separate the supernatant at the speed of 14000 rpm for 10 min at 4 °C. The supernatant was stored at -20 °C.

### 5.4.2 Polymerase chain reaction (PCR)

**PCR.** Standard PCR is performed for screening and genotyping (Mullis et al., 1986). Table 19 shows the PCR reaction setup and condition. The amounts of the primers for each PCR reaction were optimized. The products of PCR reactions were stored at -20 °C further analysis.

**Table 19. Reaction components and conditions for standard PCR.**

| **Reaction Mix** | | **Reaction Conditions** | | |
|---|---|---|---|---|
| 12.5 µL | REDTaq® ReadyMix™ | 95 °C | 3 min | |
| 0.25–2 µL | forward primer (10 µM) | 95 °C | 45 s | 40x |
| 0.25–2 µL | reverse primer (10 µM) | 55 °C–72 °C | 60 s | |
| 1.5 µL | DNA | 72 °C | 90 s | |

| | | | | |
|---|---|---|---|---|
| ad 25 µL | distilled water | 25 °C | hold | |

**Genotyping and recombination PCR.** The isolated genomic DNA was used for PCR to determine the genotype of the animal. For each allele, specific primers were used as shown in Table 9. Table 20 indicates the temperatures of annealing and the sizes of PCR products. The genomic DNA was used as templates for the recombination PCR reactions to check the recombination of the *loxP* or *frt* flanked sequences.

**Table 20. Annealing temperatures and the sizes of PCR products of genotyping and recombination PCRs.**
WT: wild type allele; Mut: mutated allele; rec: mutated allele after the recombination of the two *loxP/frt* cassettes

| PCR name | Annealing temperature | PCR products (bp) |
|---|---|---|
| *Pdx1-Flp* | 55 °C | 620 (mut) / 300 (internal control) |
| *Pdx-cre* | 64°C | 674 (mut) / 202 (WT) |
| *FSF-Kras$^{G12D}$* | 55 °C | 350 (mut) / 270 (WT) |
| *FSF-Kras$^{G12D}$* recombination | 60 °C | 196 (rec) |
| *FSF* | 60 °C | 600 (mut) |
| *CreER$^{T2}$* | 55 °C | 190 (mut) |
| *R26-CAG* | 62 °C | 450 (mut) / 650 (WT) |
| *FSF* recombination | 60 °C | 490 (rec) |
| *Pdk1$^{lox}$* | 63 °C | 280 (mut) / 200 (WT) |
| *Pdk1$^{lox}$* recombination | 63 °C | 250 (rec) / 380 (mut) / 350 (WT) |
| *Pdk1$^{L155E}$* | 63 °C | 212 (mut) / 171 (WT) |
| *Trp53$^{frt}$* | 57 °C | 292 (mut) / 258 (WT) |
| *Trp53$^{lox}$* | 64 °C | 370 (mut) / 288 (WT) |
| *Ptf1a$^{Cre}$* | 60 °C | 400 (mut) / 600 (WT) |
| *LSL-Kras$^{G12D}$* | 55 °C | 170 (mut) / 270 (WT) |
| *R26-PIK3CA$^{H1047R}$* | 62 °C | 400 (mut) / 600 (WT) |
| *PIK3CA$^{H1047R}$* | 64 °C | 630 (mut) |
| *LSL-Trp53$^{R172H}$* | 60 °C | 270 (mut) / 570 (WT) |
| *Renilla* | 61 °C | 600 bp (mut) |
| *Rosa26$^{mT-mG}$* | 60 °C | 450 (mut) / 650(WT) |
| *Rosa26$^{mT-mG}$* recombination | 62 °C | 852 (mut) / 1023 (rec) |

**PCR for screening embryonic stem cell clones.** The genomic DNA isolated from the ES cells was used for screening PCR to find the clones with the correct homologous recombination of the targeting constructs. The ES clones with the targeted construct have a PCR product of 3933 bp. The genomic DNA was also used for the PCR to check the presence of the distal *loxP* site. The product of this PCR is 803 bp. The PCR setups and conditions of the two PCRs are shown in Tables 21 and 22.

**Table 21. PCR to identify the positive ES clones.**

| Reaction Mix | | Conditions | | |
|---|---|---|---|---|
| 11 µL | 5x Q-solution | 95 °C | 3 min | |
| 2 µL | Primer: pGL3-pA-pause-4645-UP (10 µM) | 95 °C | 40 s | 40x |
| 2 µL | Primer: ESkras-co-LP1 (10 µM) | 63 °C | 45 s | |
| 5 µL | 10x PCR buffer | 65 °C | 4min + 3 sec each cycle | |
| 2 µL | dNTP mix, 10 mM each | 65 °C | 10 min | |
| 0.35 µL | HotStar Taq polymerase | 25°C | hold | |
| 2 µl | DNA | | | |
| ad 50 µl | distilled water | | | |

**Table 22. PCR for the distal *loxP* in ES clones.**

| Reaction Mix | | Conditions | | |
|---|---|---|---|---|
| 12.5 µL | REDTaq® ReadyMix™ | 95 °C | 3 min | |
| 1 µL | Primer: lox-bgl-UP1 (10 µM) | 95 °C | 45 s | 40x |
| 1 µL | Primer: lox-bgl-LP1 (10 µM) | 58 °C | 60 s | |
| 1.5 µL | DNA | 72 °C | 90 s | |
| ad 25 µL | distilled water | 25 °C | hold | |

### 5.4.3 Agarose gel electrophoresis of PCR products

1x TAE buffer was used for the preparation of agarose gels and as well as for the preparation of the running buffer for the gel electrophoresis. 1%-2% agarose gels were prepared depending on the band sizes. The mixture of agarose and 1x TAE buffer was boiled, and the ethidium bromide was added to the gel before polymerization. The samples with DNA fragments were loaded into the gel wells and the gel was runed at 120 V. DNA fragments in the samples were visualized with UV light.

### 5.4.4 Quantitative real time PCR (qRT-PCR)

**The design of the primers.** The primers and the TaqMan probes with dye labels for qRT-PCR were generated by using the online Primer-Blast (www.ncbi.nlm.nih.gov/tools/primer-blast) with DNA sequence acquired at www.ensembl.org. The amplicons were about 150bp.

**qRT-PCR**. The StepOnePlus™ real time PCR system was used for qRT-PCR reactions. The ABsolute qPCR ROX Mix was used in the 25 µL reaction. β-actin was chosen as the internal reference. 400 nM of the primers of *neo* and *β-actin* was used. 200 nM of the TaqMan probes was added to the reaction mixture. 1 µL genomic DNA was added. $2^{-\Delta\Delta}$Ct method was employed for the subsequent analysis.

**$2^{-\Delta\Delta Ct}$ method.** The primers with the 1.8 to 2.2 efficiency were used for the qRT-PCR and the $2^{-\Delta\Delta Ct}$ method analysis (Pfaffl, 2001). The $2^{-\Delta\Delta Ct}$ calculation is shown below:

$$Ct\ [gene\ of\ interest] - Ct\ [control] = \Delta Ct$$

$$\Delta Ct\ [treated\ sample] - \Delta Ct\ [reference\ sample] = \Delta\Delta\ Ct$$

$2^{-\Delta\Delta Ct}$ was used for futher data analysis.

### 5.4.8 RNA sequencing

In collaboration with Prof. Roland Rad's lab (Klinikum rechts der Isar, Technical University of Munich, DE), RNA-Seq of the pancreatic tumor tissues from the tumor mice was performed to identify the molecular signatures and important signaling pathways. The tissue samples were harvested as described in 5.1.4. RNA isolation was performed by using QIAshredder columns and the RNeasy mini kit. The contamination of DNA was eliminated by DNase digestion. The concentration of RNA was determined by Qubit® 2.0 Fluorometer and the isolated RNA was immediately stored at -80 °C. A 1% agarose gel was used to check the quality of the isolated RNA. The samples with intact RNAs show two bands, which are the 28S and 18S ribosomal RNA (rRNA) respectively. 2 µg of the intact sample was processed for Illumina sequencing with the TruSeq® Stranded mRNA Sample Preparation Kit with Agencourt AMPure XP Beads and SuperScript II as reverse transcriptase. The strands of cDNA were synthesized before adaptor ligation. Afterwards, cDNAs with adaptors were enriched by PCR. The cDNA was loaded in a gel to check the integrity. Then the primers for the barcodes and the cDNA were put together. qRT-PCR and the Qubit® dsDNA BR Assay Kit on a Qubit® 2.0 fluorometer were used for the quantity. The samples with higher quality had bands with sizes between 200 to 500 bp and then were pooled in equimolar concentrations. Afterwards, the samples were used for sequencing with a single read of 50 bp on the Illumina HiSeq1500 platform. The bioinformatic analyses were carried out using R version 3.1.2 and Bioconductor version 3.0 (Gentleman et al., 2004) by Thomas Engleitner and Fabio Boniolo.

The mouse analogues of the molecular signature of the classical subtype (Moffitt et al., 2015) were used for the study of the correlation between the classical subtype and the tumor grades. The scores were calculated, ploted and compared in the bloxplot against the tumor grades. The DESeq2 package (Love et al., 2014) was applied on the variance stabilized transcriptomic profiling data to highlight the possible variation related to different tumor grades. For differential expression analysis, log-CPM (log counts per million) values from the multidimensional scaling (MDS) plot were used to calculate and visualize the expression patterns of the tumor tissue samples. $Log_2$ fold change >1 or < -1 was used for the cutoff value for the differential expression analysis. For gene set enrichment analysis (GSEA), a

gene set is significantly enriched when NOM *p*-value and FDR *q*-value are less than 0.05. The package for immune cell deconvolution (Sturm et al., 2020) was used to deconvolute the transcriptomic profiling data after normalization. The cibersort (absolute mode) method was employed to retrieve immune scores, which allows the comparison between samples.

## 5.5 Protein biochemistry

### 5.5.1 The extraction of proteins

The cancer cells were harvested when they were about 80% confluent in a 10 cm dish. The cancer cell medium was discarded, and cells were rinsed three times in PBS. 150 µL of pre-cooled IP lysis buffer containing inhibitors of protease and phosphatase was added to the 10-cm dish. A cell scraper was used to harvest the cells in a tube and the lysate was snap frozen in liquid nitrogen. The tube was transferred and stored at -80 °C. To measure the protein concentration, the lysate was spun down at the speed of 13200 rpm for 20 min at 4°C and the supernatant was used to determine the protein concentration.

### 5.5.2 Determination of protein concentration

The Bradford assay was used to measure the protein concentration (Bradford, 1976). The Bradford reagent was diluted 1:5 in water and 300 µL of the diluted reagent was transferred to one well in a 96-well plate. Afterwards, 1 µL of the sample was added and mixed with the diluted Bradford reagent. The solution was incubated for 10 min at RT and the microplate reader ClarioStar MARS was used to measure the absorbance values of the protein solutions. The concentration of the proteins in the sample was determined by using serial concentrations of BSA solutions as reference. All the samples were performed in triplicates. The protein loading buffer and IP buffer were used to adjust the protein concentrations of the samples to the same level. Then the laemmli buffer was added to the lysate by 1:5 (Laemmli, 1970). Proteins were denatured by the incubation of the sample at 95 °C for 5 min and, afterwards, stored at -20 °C.

### 5.5.3 SDS polyacrylamide gel electrophoresis (SDS-PAGE)

The SDS-PAGE (Laemmli, 1970) was performed to separate proteins based on their molecular weight. At first, the 10% or 12% separating gel was prepared by mixing the reagents as shown in Table 23. Afterwards, the gel was poured into a gel cassette and overlaid with 2-propanol to an additional height of 0.5 cm to prevent the air contact. The gel was left at RT for polymerization for 20 min. Afterwards, the stacking gel mixture was prepared and poured, and a comb was inserted. After the stacking gel polymerized, the comb was removed, and 80-120 µg protein of the samples and the molecular wight marker

was loaded in the well of the SDS polyacrylamide gel. First, electrophoresis was performed at 80 V for about 45 min in the stacking gel for protein concentration and then the gel was run at 120 V for about 1 h to separate the proteins.

### 5.5.4 Immunoblot

Following the SDS-PAGE, the proteins were transferred onto the NC blotting membrane. Then, the membrane was incubated in the blocking solution (5% BSA) at RT for 1 h to prevent unspecific antibody binding. Thereafter, the membrane was incubated in the solution containing the primary antibody against the protein of interest at 4 °C over night. The concentration of the primary antibody in the solution depends on the binding efficiency. The membrane was rinsed three times with the PBS-Tween solution and then incubated with the secondary antibody which was diluted in 5% BSA solution for 1 h at RT in the dark. Afterwards, the blotted membrane was rinsed three times with the PBS-Tween solution. The membrane was scanned at the wavelength of 700 nm or 800 nm in the Odyssey® Fc Imaging System from LI-COR Biosciences.

**Table 23. Recipe of SDS polyacrylamide gels.**

| Compounds | 10% separating gel | 12% separating gel | Stacking gel |
|---|---|---|---|
| $H_2O$ | 6150 µL | 5100 µL | 4500 µL |
| Separating gel buffer | 3900 µL | 3900 µL | - |
| Stacking gel buffer | - | - | 1950 µL |
| Rotiphorese® gel 30 | 4950 µL | 6000 µL | 1125 µL |
| 10% SDS | 150 µL | 150 µL | 75 µL |
| 10% APS | 75 µL | 75 µL | 37.5 µL |
| TEMED | 22.5 µL | 22.5 µL | 15 µL |

## 5.6 Statistical analysis

GraphPad Prism 8 was used for graphical depiction, data correlation and statistical analysis. Data was presented as mean values ± standard error of mean (SEM). Kaplan-Meier and Log rank test were used for statistical analysis of survival curves. Student's *t* test was used to calculate the statistical difference in the study of immune cell populations and the ADM and PanIN-1A lesions. A one-way analysis of variance (ANOVA) test was employed to analyze the statistical difference in the analysis of the mitotic activity, stromal content and lymphocytes in the tumors with different grades. The *p*-values are shown in the figures of the present study and $p < 0.05$ was considered to be statistically significant. Bonferroni-adjusted significance level was reported if more than one statistical test was performed on a single

data set. A nominal *p*-value was used for the analysis of the statistical significance for RNA sequencing analysis. Considering multiple testing affects the statistical significance, the probability of a false-positive result was estimated by the FDR. The significance level was set as $p < 0.05$ and FDR $q < 0.05$.

# 6 Results

Since the generation of *Kras*$^{G12D}$ mouse model, which allowed the mutant *Kras* expression from the endogenous locus, our group has established a variety of new GEMMs of PDAC by taking advantage of the *Cre/loxP* and *Flp/frt* systems. To provide basic insights into pancreatic cancer, we analyzed the tumor mice harboring modified alleles of genes which are associated with PDAC, such as *Cdkn2a*, *Trp53* and *Snail*. Figure 2 shows the representatives of the modified alleles used in this thesis.

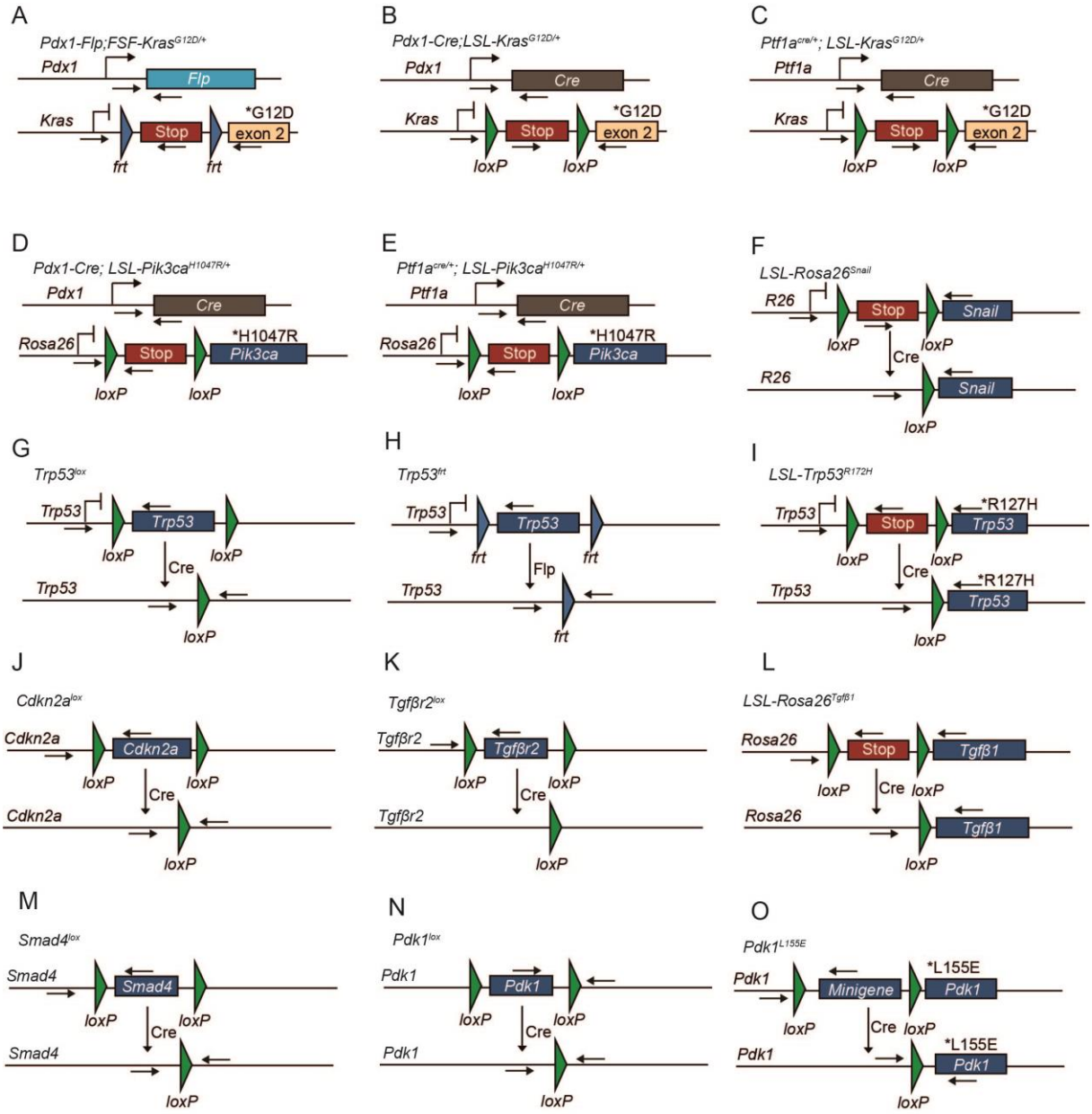


**Figure 2. Modified alleles of the genes in PDAC mouse models.**
(A) *Pdx1-Flp;FSF-Kras*$^{G12D/+}$*.Pdx1-Flp* removes the *frt-stop-frt* (*FSF*) cassette and activates the expression of *Kras*$^{G12D}$.

(B) *Pdx1-Cre;LSL-Kras$^{G12D/+}$*. *Pdx1-Cre* leads to the removal of the *loxP-stop-loxP* (*LSL*) cassette and activation of *Kras$^{G12D}$* expression.
(C) *Ptf1a$^{Cre/+}$;LSL-Kras$^{G12D/+}$*. *Ptf1a-Cre* deletes the *LSL* and activates the expression of *Kras$^{G12D}$*.
(D) *Pdx1-Cre;LSL-Pik3ca$^{H1047R/+}$*. *Pdx1-Cre* results in the removal of the *LSL* cassette and activates the expression of *Pik3ca$^{H1047R}$.*
(E) *Ptf1a$^{Cre/+}$;LSL-Pik3ca$^{H1047R/+}$*. *Ptf1a-Cre* removes the *LSL* cassette and activates the expression of *Pik3ca$^{H1047R}$*.
(F) *LSL-Rosa26$^{Snail}$*. The construct consisting of *LSL* cassette and the cDNA of mouse *Snail* gene is inserted into the *Rosa26* locus. The overexpression of *Snail* is mediated by *Cre* recombinase.
(G) *Trp53$^{lox}$*. The exons 2 to 10 of the endogenous *Trp53* are flanked by two *loxP* cassettes. The conditional inactivation of *Trp53* is mediated by Cre recombinase.
(H) *Trp53$^{frt}$*. The exons 2 to 6 of the endogenous *Trp53* are flanked by two *frt* cassettes. The expression of the *Flp* recombinase leads to the inactivation of *Trp53.*
(I) *LSL-Trp53$^{R172H}$*. *LSL-Trp53$^{R172H}$* introduces R127H mutation in the exon 5 at the endogenous *Trp53* locus. The removal of the *LSL* cassette results in the expression of mutated *Trp53.*
(J) *Cdkn2a$^{lox}$*. The exons 2 and 3 of *Cdkn2a* gene are flanked by two *loxP* sites. *Cre* expression leads to the deletion of both *p16$^{Ink4a}$* and *p19$^{Arf}$*.
(K) *Tgfβr2$^{lox}$*. The exon 2 at the endogenous *Tgfβr2* locus is flanked by two *loxP* sites. *Cre* expression results in the deletion of *Tgfβr2*.
(L) *LSL-Rosa26$^{Tgfβ1}$*. *LSL-Rosa26$^{Tgfβ1/+}$* is a knock-in construct at the Rosa26 locus. The *Tgfβ1* cDNA is silenced by the *LSL* cassette and can be activated by Cre recombinase.
(M) *Smad4$^{lox}$*. The exons 8 and 9 are flanked by two *loxP* sites in the endogenous *Smad4* locus. Cre recombinase leads to the deletion of *Smad4*.
(N) *Pdk1$^{lox}$*. The exons 3 and 4 of the endogenous *Pdk1* locus are flanked by two *loxP* sites. The expression of Cre recombinase leads to the inactivation of *Pdk1.*
(O) *Pdk1$^{L155E}$*. The L155E mutation is introduced in the exon 4 of the endogenous *Pdk1* locus. A minigene cassette consists of the exons 3 to 14 of *Pdk1* and it is in front of exon4, which is flanked by two *loxP* sites. The removal of the minigene by the Cre recombinase results in the *Pdk1$^{L155E}$* expression. Arrows indicate the annealing sites of the primers for genotyping. All these mouse models were generated, bred and analyzed by all the members in the lab of Prof. Dieter Saur.

## 6.1 The genotypes of these mouse models influence the life spans of the mice.

*Trp53* is known as tumor suppressor gene. In PDAC mouse models, the mice with a *Trp53* deletion have significantly shorter survival time compared with those PK mice, including *Pdx1-Flp;FSF-Kras$^{G12D/+}$*, *Pdx1-Cre;LSL-Kras$^{G12D/+}$* and *Ptf1a$^{Cre/+}$;LSL-Kras$^{G12D/+}$* mice (Figure 3A). The deletion of both *Trp53* alleles shortens the survivial time of the PK dramatically, with the median survival time of 67 days (Figure 3A). About 80% to 95% of sporadic PDAC patients harbor *CDKN2A* inactivation (Hustinx et al., 2005; Rozenblum et al., 1997). In addition to the *Kras* mutation, loss of *Cdkn2a* function leads to shorter life spans of PK mice. The survival time of the mice with homozygous deletion of *Cdkn2a* is significantly reduced (61.5 days vs 440 days, *Ptf1a$^{Cre/+}$;LSL-Kras$^{G12D/+}$;Cdkn2a$^{lox/lox}$* (PKC_HOM) vs PK, ****$p$<0.0001). It has been proved that *Snail* is a transcription factor involved in EMT and metabolic reprogramming (Liu et al., 2019). In PDAC mouse models, *Snail* overexpression accelerates PDAC progression (Figure 3C). Heterozygous *Trp53* deletion can shorten the survival time of *Ptf1a$^{Cre/+}$;LSL-Kras$^{G12D/+}$;LSL-Rosa26$^{Snail/+}$* (PKS) mice (91 days vs 190 days, *Ptf1a$^{Cre/+}$;LSL-Kras$^{G12D/+}$;LSL-Rosa26$^{Snail/+}$;Trp53$^{lox/+}$* (PKS_P_HET) vs PKS, ****$p$<0.0001), and loss of *Cdkn2a* function also makes the life span of PKS mice shorter (123 days vs 190

days, *Ptf1a*$^{Cre/+}$*;LSL-Kras*$^{G12D/+}$*;LSL-Rosa26*$^{Snail/+}$*; Cdkn2a*$^{lox/+}$ (PKS_C_HET) vs PKS, ****$p$<0.0001) (Figure 3C). The *TGF-β* signaling pathway is important for PDAC progression. *TGF-β* inactivation occurs to about 55% of PDAC patients and the type II *TGF-β* receptor (*TGFβR2*) gene has been shown to be altered in a smaller subset of patients. Pancreas-specific *Tgfbr2* knockout mice in the context of mutant *Kras*$^{G12D}$ expression show shorter survival time compared with those only with pancreas-specific *Kras*$^{G12D}$ mutation (Figure 3D). In the context of pancreas specific *Kras*$^{G12D}$ mutation expression and heterozygous *Trp53* deletion, *Snail* overexpression and *Tgfbr2* deletion result in rapid progression of PDAC with a median survival of 3 months and 1.5 months respectively (Figure 3E). A previous study has shown that *PI3K* and 3-phosphoinositide-dependent protein kinase 1 (*Pdk1*) are key effectors of oncogenic *Kras* in the progression of PDAC and *Pdk1* inactivation blocks PanIN formation and PDAC initiation (Eser et al., 2013). *Pdk1* deletion and *Pdk1*$^{L155E}$ mutation extend overall survival and the median survival of the mouse model is 496 days (Figure 3F). Aberrations in PI3K signaling pathway have a critical role in the progression of numerous cancers. *PIK3CA* mutations lead to an active PI3K and are present in about 3% to 5% of pancreatic cancer patients (Janku et al., 2013; Weiss et al., 2013). The mouse model with pancreas-specific *Pik3ca* mutation expression has shown the development of pancreatic tumor masses, which are often associated with large cystic structures (Payne et al., 2015). In this study, the mice with pancreas-specific *Pik3ca* mutation developed pancreatic tumors and the median survival time is 372 days (Figure 3G). *Trp53* deletion significantly reduces the survival time of the PDAC mice with *Pik3ca* mutation (Figure 3G). There is no significant difference of the survival time between oncogenic *Kras and Pik3ca* cohorts (Figure 3H).

## 6.2 Different mouse models present distinctive metastatic patterns of PDAC.

A high metastatic propensity is one of the challenges that underlie the high mortality of PDAC. Over 90% of the PDAC patients have developed metastatic disease (Siegel et al., 2020). Metastasis is an important parameter of the cancer staging system which is useful for prognosis and treatment options in clinical practice. The majority of PDAC metastases are detected in the liver, peritoneum, abdominal lymph nodes and lungs. Approximately 76% to 94% of the PDAC patients have liver metastasis. 41% to 56% of the patients develop peritoneum metastasis. The metastases in abdominal lymph nodes and lungs account for about 41% and 45% to 48% of the patients respectively (Haeno et al., 2012; Yachida et al., 2012). The peritoneal spread of disease of PDAC leads to ascites accumulation and

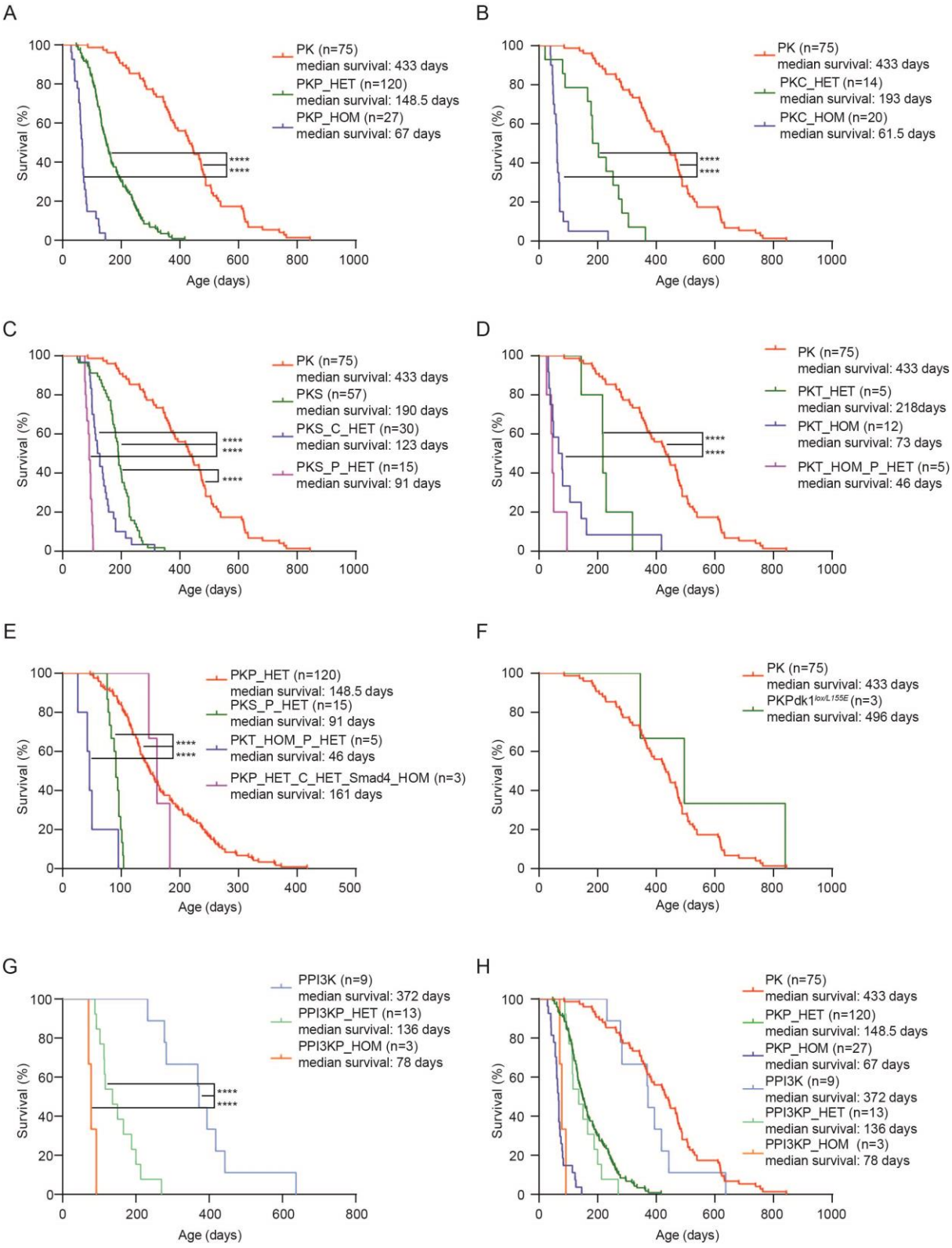


**Figure 3. Kaplan-Meier survival analysis of indicated genotypes.**
(A) Kaplan-Meier survival analysis of PK, PKP_HET and PKP_HOM. PK (n=75): *Pdx1-Flp;FSF-Kras$^{G12D/+}$*, *Pdx1-Cre;LSL-Kras$^{G12D/+}$*, *Ptf1a$^{Cre/+}$;LSL-Kras$^{G12D/+}$* mice. PKP_HET (n=120): *Pdx1-Flp;FSF-Kras$^{G12D/+}$;Trp53$^{frt/+}$*, *Pdx1-Cre;LSL-Kras$^{G12D/+}$;Trp53$^{lox/+}$*, *Ptf1a$^{Cre/+}$;LSL-Kras$^{G12D/+}$;Trp53$^{lox/+}$*, *Ptf1a$^{Cre/+}$;LSL-Kras$^{G12D/+}$;Trp53$^{R172H/+}$* mice. PKP_HOM (n=27): *Pdx1-Flp;FSF-Kras$^{G12D/+}$;Trp53$^{frt/frt}$*, *Pdx1-Cre;LSL-Kras$^{G12D/+}$;Trp53$^{lox/lox}$*, *Ptf1a$^{Cre/+}$;LSL-Kras$^{G12D/+}$;Trp53$^{lox/lox}$*, *Ptf1a$^{Cre/+}$;LSL-Kras$^{G12D/+}$;Trp53$^{R172H/R172H}$* mice.

(B) Kaplan-Meier survival analysis of PK, PKC_HET and PKC_HOM. PK (n=75): *Pdx1-Flp;FSF-Kras$^{G12D/+}$, Pdx1-Cre;LSL-Kras$^{G12D/+}$*, *Ptf1a$^{Cre/+}$;LSL-Kras$^{G12D/+}$* mice. PKC_HET (n=14): *Ptf1a$^{Cre/+}$;LSL-Kras$^{G12D/+}$;Cdkn2a$^{lox/+}$* mice. PKC_HOM (n=20): *Ptf1a$^{Cre/+}$;LSL-Kras$^{G12D/+}$;Cdkn2a$^{lox/lox}$* mice.
(C) Kaplan-Meier survival analysis of PK, PKS, PKS_C_HET and PKS_P_HET. PK (n=75): *Pdx1-Flp;FSF-Kras$^{G12D/+}$, Pdx1-Cre;LSL-Kras$^{G12D/+}$*, *Ptf1a$^{Cre/+}$;LSL-Kras$^{G12D/+}$* mice. PKS (n=57): *Ptf1a$^{Cre/+}$;LSL-Kras$^{G12D/+}$;LSL-Rosa26$^{Snail/+}$* mice. PKS_C_HET (n=30): *Ptf1a$^{Cre/+}$;LSL-Kras$^{G12D/+}$;LSL-Rosa26$^{Snail/+}$;Cdkn2a$^{lox/+}$* mice. PKS_P_HET (n=15): *Ptf1a$^{Cre/+}$;LSL-Kras$^{G12D/+}$;LSL-Rosa26$^{Snail/+}$;Trp53$^{lox/+}$* mice.
(D) Kaplan-Meier survival analysis of PK, PKT_HET, PKT_HOM and PKT_HOM_P_HET. PK (n=75): *Pdx1-Flp;FSF-Kras$^{G12D/+}$, Pdx1-Cre;LSL-Kras$^{G12D/+}$*, *Ptf1a$^{Cre/+}$;LSL-Kras$^{G12D/+}$* mice. PKT_HET (n=5): *Ptf1a$^{Cre/+}$;LSL-Kras$^{G12D/+}$;Tgfβr2$^{lox/+}$* mice. PKT_HOM (n=12): *Ptf1a$^{Cre/+;}$LSL-Kras$^{G12D/+}$;Tgfβr2$^{lox/lox}$* mice. PKT_HOM_P_HET (n=5): *Ptf1a$^{Cre/+}$;LSL-Kras$^{G12D/+}$;Tgfβr2$^{lox/lox}$; Trp53$^{lox/+}$* mice.
(E) Kaplan-Meier survival analysis of PKP_HET, PKS_P_HET, PKT_HOM_P_HET and PKP_HET_Smad4_HOM. PKP_HET (n=120): *Pdx1-Flp;FSF-Kras$^{G12D/+}$;Trp53$^{frt/+}$, Pdx1-Cre;LSL-Kras$^{G12D/+}$;Trp53$^{lox/+}$, Ptf1a$^{Cre/+}$;LSL-Kras$^{G12D/+}$;Trp53$^{lox/+}$, Ptf1a$^{Cre/+}$;LSL-Kras$^{G12D/+}$;Trp53$^{R172H/+}$* mice. PKS_P_HET (n=15): *Ptf1a$^{Cre/+}$;LSL-Kras$^{G12D/+}$;LSL-Rosa26$^{Snail/+}$;Trp53$^{lox/+}$* mice. PKT_HOM_P_HET (n=5): *Ptf1a$^{Cre/+;}$LSL-Kras$^{G12D/+}$;Tgfβr2$^{lox/lox}$; Trp53$^{lox/+}$* mice. PKP_HET_Smad4_HOM (n=3): *Pdx1-Flp;FSF-Kras$^{G12D/+}$; FSF-Rosa26$^{CAG-CreERT2/+}$;Ink4α$^{*/+}$;Smad4$^{lox/lox}$;Trp53$^{lox/+}$ mice.*
(F) Kaplan-Meier survival analysis of PK and PKPdk1$^{lox/L155E}$. PK (n=75): *Pdx1-Flp;FSF-Kras$^{G12D/+}$, Pdx1-Cre;LSL-Kras$^{G12D/+}$*, *Ptf1a$^{Cre/+}$;LSL-Kras$^{G12D/+}$* mice. PKPdk1$^{lox/L155E}$ (n=3): *Ptf1a$^{Cre/+}$;LSL-Kras$^{G12D/+}$; Pdk1$^{lox/+}$; Pdk1$^{L155E/+}$* mice.
(G) Kaplan-Meier survival analysis of PPI3K, PPI3KP_HET and PPI3KP_HOM. PPI3K (n=9): *Pdx1-Cre;LSL-Pik3ca$^{H1047R/+}$*, *Ptf1a$^{Cre/+}$;LSL-Pik3ca$^{H1047R/+}$* mice. PPI3KP_HET (n=13): *Ptf1a$^{Cre/+}$;LSL-Pik3ca$^{H1047R/+}$;Trp53$^{lox/+}$* mice. PPI3KP_HOM (n=3): *Ptf1a$^{Cre/+}$;LSL-Pik3ca$^{H1047R/+}$;Trp53$^{lox/lox}$* mice.
(H) Kaplan-Meier survival analysis of PK, PKP_HET, PKP_HOM, PPI3K, PPI3KP_HET and PPI3KP_HOM. PK (n=75): *Pdx1-Flp;FSF-Kras$^{G12D/+}$, Pdx1-Cre;LSL-Kras$^{G12D/+}$*, *Ptf1a$^{Cre/+}$;LSL-Kras$^{G12D/+}$* mice. PKP_HET (n=120): *Pdx1-Flp;FSF-Kras$^{G12D/+}$;Trp53$^{frt/+}$, Pdx1-Cre;LSL-Kras$^{G12D/+}$;Trp53$^{lox/+}$, Ptf1a$^{Cre/+}$;LSL-Kras$^{G12D/+}$;Trp53$^{lox/+}$, Ptf1a$^{Cre/+}$;LSL-Kras$^{G12D/+}$;Trp53$^{R172H/+}$* mice. PKP_HOM (n=27): *Pdx1-Flp;FSF-Kras$^{G12D/+}$;Trp53$^{frt/frt}$, Pdx1-Cre;LSL-Kras$^{G12D/+}$;Trp53$^{lox/lox}$, Ptf1a$^{Cre/+}$;LSL-Kras$^{G12D/+}$;Trp53$^{lox/lox}$, Ptf1a$^{Cre/+}$;LSL-Kras$^{G12D/+}$;Trp53$^{R172H/R172H}$* mice. PPI3K (n=9): *Pdx1-Cre;LSL-Pik3ca$^{H1047R/+}$*, *Ptf1a$^{Cre/+}$;LSL-Pik3ca$^{H1047R/+}$* mice. PPI3KP_HET (n=13): *Ptf1a$^{Cre/+}$;LSL-Pik3ca$^{H1047R/+}$;Trp53$^{lox/+}$* mice. PPI3KP_HOM (n=3): *Ptf1a$^{Cre/+}$;LSL-Pik3ca$^{H1047R/+}$;Trp53$^{lox/lox}$* mice.
*****p*<0.0001, log-rank test. All these mouse models were generated, bred and analyzed by all the members in the lab of Prof. Dieter Saur.

approximately 50% of patients have acites accumulation (Adam and Adam, 2004; Hicks et al., 2016).

The mice with *Trp53* deletion show a similar rate of overt macroscopic metastasis as the PK cohort (Figure 4A). The mice with loss of *Cdkn2a* function tend to have higher risk of metastasis formation. The PK mice with heterozygous and homozygous *Cdkn2a* show significantly higher percentages of metastasis than PK mice, 64.3% and 80% respectively (Figure 4B). It is worth mentioning that, compared with PK mice, the metastasis rate rises sharply, from 55% to 80%

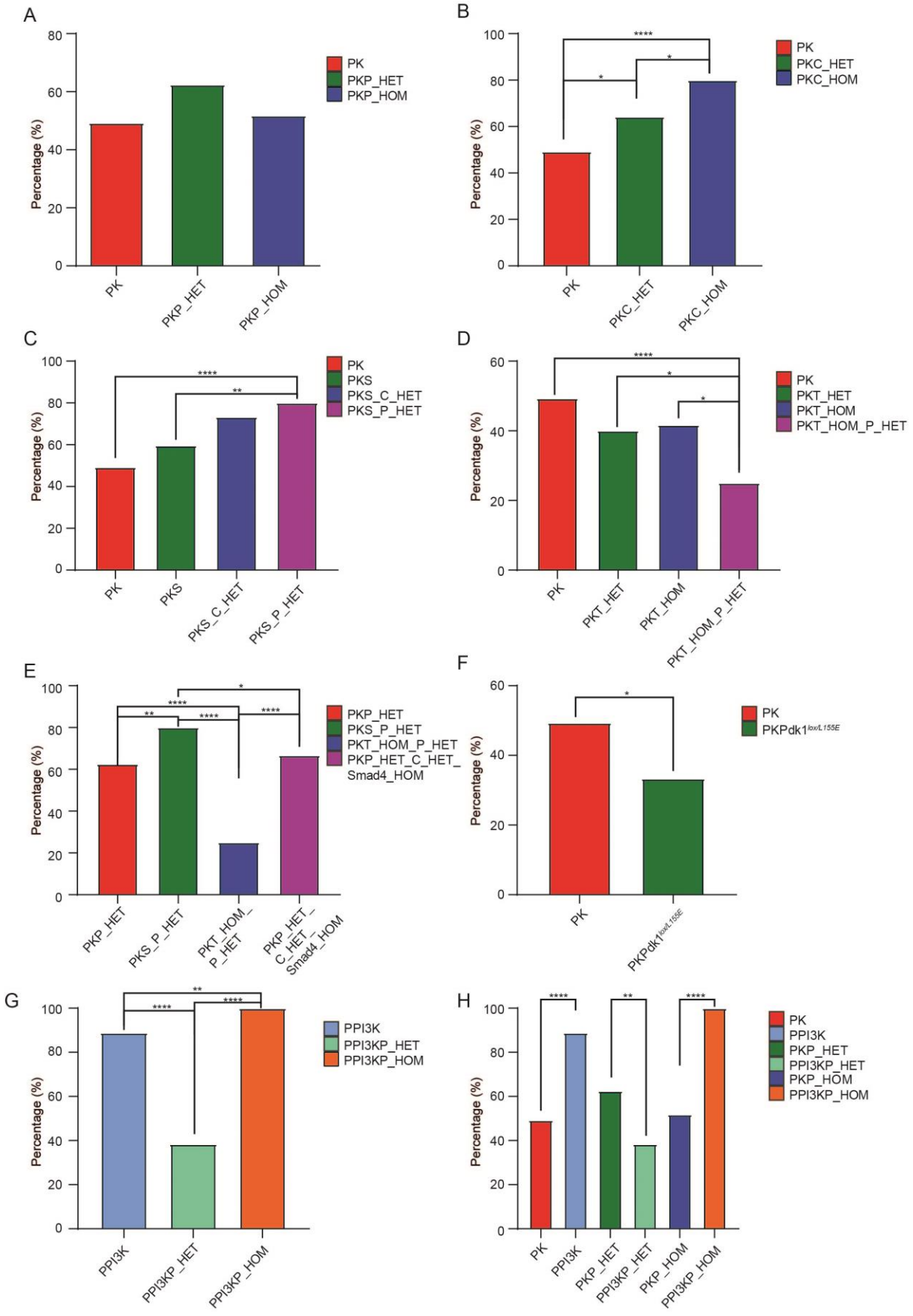


**Figure 4. The percentage of macroscopic metastases in the PDAC mouse models.**

(A) The percentages of macroscopic metastases of PK, PKP_HET and PKP_HOM. PK (n=75): *Pdx1-Flp;FSF-Kras$^{G12D/+}$, Pdx1-Cre;LSL-Kras$^{G12D/+}$, Ptf1a$^{Cre/+}$;LSL-Kras$^{G12D/+}$* mice. PKP_HET (n=120): *Pdx1-Flp;FSF-Kras$^{G12D/+}$;Trp53$^{frt/+}$, Pdx1-Cre;LSL-Kras$^{G12D/+}$;Trp53$^{lox/+}$, Ptf1a$^{Cre/+}$;LSL-Kras$^{G12D/+}$;Trp53$^{lox/+}$, Ptf1a$^{Cre/+}$;LSL-Kras$^{G12D/+}$;Trp53$^{R172H/+}$* mice. PKP_HOM (n=27): *Pdx1-Flp;FSF-Kras$^{G12D/+}$;Trp53$^{frt/frt}$, Pdx1-Cre;LSL-Kras$^{G12D/+}$;Trp53$^{lox/lox}$, Ptf1a$^{Cre/+}$;LSL-Kras$^{G12D/+}$;Trp53$^{lox/lox}$, Ptf1a$^{Cre/+}$;LSL-Kras$^{G12D/+}$; Trp53$^{R172H/R172H}$* mice.
(B) The percentages of macroscopic metastases of PK, PKC_HET and PKC_HOM. PK (n=75): *Pdx1-Flp;FSF-Kras$^{G12D/+}$, Pdx1-Cre;LSL-Kras$^{G12D/+}$, Ptf1a$^{Cre/+}$;LSL-Kras$^{G12D/+}$* mice. PKC_HET (n=14): *Ptf1a$^{Cre/+}$;LSL-Kras$^{G12D/+}$;Cdkn2a$^{lox/+}$* mice. PKC_HOM (n=20): *Ptf1a$^{Cre/+}$;LSL-Kras$^{G12D/+}$;Cdkn2a$^{lox/lox}$* mice.
(C) The percentages of macroscopic metastases of PK, PKS, PKS_C_HET and PKS_P_HET. PK (n=75): *Pdx1-Flp;FSF-Kras$^{G12D/+}$, Pdx1-Cre;LSL-Kras$^{G12D/+}$, Ptf1a$^{Cre/+}$;LSL-Kras$^{G12D/+}$* mice. PKS (n=57): *Ptf1a$^{Cre/+}$;LSL-Kras$^{G12D/+}$;LSL-Rosa26$^{Snail/+}$* mice. PKS_C_HET (n=30): *Ptf1a$^{Cre/+}$;LSL-Kras$^{G12D/+}$;LSL-Rosa26$^{Snail/+}$;Cdkn2a$^{lox/+}$* mice. PKS_P_HET (n=15): *Ptf1a$^{Cre/+}$;LSL-Kras$^{G12D/+}$;LSL-Rosa26$^{Snail/+}$;Trp53$^{lox/+}$* mice.
(D) The percentages of macroscopic metastases of PK, PKT_HET, PKT_HOM and PKT_HOM_P_HET. PK (n=75): *Pdx1-Flp;FSF-Kras$^{G12D/+}$, Pdx1-Cre;LSL-Kras$^{G12D/+}$, Ptf1a$^{Cre/+}$;LSL-Kras$^{G12D/+}$* mice. PKT_HET (n=5): *Ptf1a$^{Cre/+}$;LSL-Kras$^{G12D/+}$;Tgfβr2$^{lox/+}$* mice. PKT_HOM (n=12): *Ptf1a$^{Cre/+}$;LSL-Kras$^{G12D/+}$;Tgfβr2$^{lox/lox}$* mice. PKT_HOM_P_HET (n=5): *Ptf1a$^{Cre/+}$;LSL-Kras$^{G12D/+}$;Tgfβr2$^{lox/lox}$;Trp53$^{lox/+}$* mice.
(E) The percentages of macroscopic metastases of PKP_HET, PKS_P_HET, PKT_HOM_P_HET and PKP_HET_Smad4_HOM. PKP_HET (n=120): *Pdx1-Flp;FSF-Kras$^{G12D/+}$;Trp53$^{frt/+}$, Pdx1-Cre;LSL-Kras$^{G12D/+}$;Trp53$^{lox/+}$, Ptf1a$^{Cre/+}$;LSL-Kras$^{G12D/+}$;Trp53$^{lox/+}$, Ptf1a$^{Cre/+}$;LSL-Kras$^{G12D/+}$;Trp53$^{R172H/+}$* mice. PKS_P_HET (n=15): *Ptf1a$^{Cre/+}$;LSL-Kras$^{G12D/+}$;LSL-Rosa26$^{Snail/+}$;Trp53$^{lox/+}$* mice. PKT_HOM_P_HET (n=5): *Ptf1a$^{Cre/+}$;LSL-Kras$^{G12D/+}$;Tgfβr2$^{lox/lox}$;Trp53$^{lox/+}$* mice. PKP_HET_Smad4_HOM (n=3): *Pdx1-Flp;FSF-Kras$^{G12D/+}$;FSF-Rosa26$^{CAG-CreERT2/+}$; Ink4α$^{*/+}$;Smad4$^{lox/lox}$;Trp53$^{lox/+}$ mice.*
(F) The percentages of macroscopic metastases of PK and PKPdk1$^{lox/L155E}$. PK (n=75): *Pdx1-Flp;FSF-Kras$^{G12D/+}$, Pdx1-Cre;LSL-Kras$^{G12D/+}$, Ptf1a$^{Cre/+}$;LSL-Kras$^{G12D/+}$* mice. PKPdk1$^{lox/L155E}$ (n=3): *Ptf1a$^{Cre/+}$;LSL-Kras$^{G12D/+}$;Pdk1$^{lox/+}$;Pdk1$^{L155E/+}$* mice.
(G) The percentages of macroscopic metastases of PPI3K, PPI3KP_HET and PPI3KP_HOM. PPI3K (n=9): *Pdx1-Cre;LSL-Pik3ca$^{H1047R/+}$, Ptf1a$^{Cre/+}$;LSL-Pik3ca$^{H1047R/+}$* mice. PPI3KP_HET (n=13): *Ptf1a$^{Cre/+}$;LSL-Pik3ca$^{H1047R/+}$;Trp53$^{lox/+}$* mice. PPI3KP_HOM (n=3): *Ptf1a$^{Cre/+}$;LSL-Pik3ca$^{H1047R/+}$;Trp53$^{lox/lox}$* mice.
(H) The percentages of macroscopic metastases of PK, PKP_HET, PKP_HOM, PPI3K, PPI3KP_HET and PPI3KP_HOM. PK (n=75): *Pdx1-Flp;FSF-Kras$^{G12D/+}$, Pdx1-Cre;LSL-Kras$^{G12D/+}$, Ptf1a$^{Cre/+}$;LSL-Kras$^{G12D/+}$* mice. PKP_HET (n=120): *Pdx1-Flp;FSF-Kras$^{G12D/+}$;Trp53$^{frt/+}$, Pdx1-Cre;LSL-Kras$^{G12D/+}$;Trp53$^{lox/+}$, Ptf1a$^{Cre/+}$;LSL-Kras$^{G12D/+}$;Trp53$^{lox/+}$, Ptf1a$^{Cre/+}$;LSL-Kras$^{G12D/+}$;Trp53$^{R172H/+}$* mice. PKP_HOM (n=27): *Pdx1-Flp;FSF-Kras$^{G12D/+}$;Trp53$^{frt/frt}$, Pdx1-Cre;LSL-Kras$^{G12D/+}$;Trp53$^{lox/lox}$, Ptf1a$^{Cre/+}$;LSL-Kras$^{G12D/+}$;Trp53$^{lox/lox}$, Ptf1a$^{Cre/+}$;LSL-Kras$^{G12D/+}$; Trp53$^{R172H/R172H}$* mice. PPI3K (n=9): *Pdx1-Cre;LSL-Pik3ca$^{H1047R/+}$, Ptf1a$^{Cre/+}$;LSL-Pik3ca$^{H1047R/+}$* mice. PPI3KP_HET (n=13): *Ptf1a$^{Cre/+}$;LSL-Pik3ca$^{H1047R/+}$;Trp53$^{lox/+}$* mice. PPI3KP_HOM (n=3): *Ptf1a$^{Cre/+}$;LSL-Pik3ca$^{H1047R/+}$;Trp53$^{lox/lox}$* mice.
The percentage is calculated as follows: the number of mice with metastasis is divided by the total mouse number in the indicated cohort and multiplied by 100%. **p*<0.05, **p*<0.01, *****p*<0.0001, Fisher's exact test. All these mouse models were generated, bred and analyzed by all the members in the lab of Prof. Dieter Saur.

when both alleles of *Cdkn2a* are deleted, while the mice with the deletion of a single allele show a mild increase of the percentage of metastasis from 55% to 64.3% (Figure 4B). The metastasis rates of the PK and PKS mouse models are comparable (Figure 4C). PKS mice with one single allele *Cdkn2a* deletion have a slightly higher metastasis rate, compared with PKS, while deletion of one allele of *Trp53* significantly increases the rate (*p*<0.01) (Figure 4C). The metastasis rate gradually decreases when one or two alleles of *Tgfβr2* are deleted, but there is no sifinicant difference of the rate of overt macroscopic metastasis between the PK cohort and the PK mice with *Tgfβr2* deletion (Figure 4D). In the context of pancreas-

specific *Kras*$^{G12D}$ expression and homozygous *Tgfβr2* deletion, heterozygous *Trp53* deletion leads to a significant decrease of the metastatic rate ($p$<0.05) (Figure 4D). In the context of pancreas-specific *Kras*$^{G12D}$ expression and heterozygous *Trp53* deletion, the mice with *Snail* overexpression show a significantly higher metastatic rate ($p$<0.01), while heterozygous *Tgfβr2* knockout drastically decreases the metastasis rate ($p$<0.0001) (Figure 4E). In addition to the deletion of one allele of *Trp53,* the mice with both *Cdkn2a* and *Smad4* deletion have a slightly higher metastasis rate (66.7%) compared with *Pdx1-Flp;FSF-Kras*$^{G12D/+}$*;Trp53*$^{frt/+}$, *Pdx1-Cre;LSL-Kras*$^{G12D/+}$*;Trp53*$^{lox/+}$, *Ptf1a*$^{Cre/+}$*;LSL-Kras*$^{G12D/+}$*;Trp53*$^{lox/+}$ and *Ptf1a*$^{Cre/+}$*;LSL-Kras*$^{G12D/+}$*;Trp53*$^{R172H/+}$ (PKP_HET) mice (65.1%) (Figure 4E). *Pdk1* deletion and *Pdk1*$^{L155E}$ mutation result in a lower rate of metastasis ($p$<0.05) (Figure 4F). In the context of the PDAC mice driven by *Pik3ca*$^{H1047R}$ mutation, the mice with *Trp53* deletion show a lower metastasis rate and the mice with the homozygous deletion of *Trp53* exhibit a higher metastasis rate compared with those with deletion of a single allele of *Trp53* ($p$<0.0001) (Figure 4G). The metastasis rate of the tumor mice with *Pik3ca*$^{H1047R}$ is higher than that of those driven by *Kras*$^{G12D}$ mutation (Figure 4H). The deletion of one allele of *Trp53* leads to a significantly higher metastasis rate in mice with *Kras*$^{G12D}$ mutation than those with *Pik3ca*$^{H1047R}$ mutation ($p$<0.01), while, in the context of the deletion of both *Trp53* alleles, the mice with *Pik3ca*$^{H1047R}$ mutation exhibit a significantly higher metastasis rate than those with *Kras*$^{G12D}$ mutation ($p$<0.0001) (Figure 4H).

The metastatic sites are also analyzed in these mouse models. The majority of the PKP_HET mice have ascites (Figure 5A). PK mice have the highest rates of liver and lung metastases, when compared with the mice with the heterozygous and homozygous deletions of *Trp53* (Figure 5A). In the context of pancreas-specific *Kras*$^{G12D}$ mutation expression, complete loss of *Cdkn2a* function dramatically reduces the rate of the liver metastasis and these mice do not present peritoneal metastasis (Figure 5B). The rate of lung metastasis decreases sharply when one allele of *Cdkn2a* is deleted and further no lung metastasis is observed in the mice with homozygous deletion of *Cdkn2a* (Figure 5B). Ascites is predominant in PKS mice, while liver is the main metastastic site in PK mice (Figure 5C). The rates of liver, lymph nodes and lung in the PKS cohort are much lower than those of the PK cohort (Figure 5C). In the context of *Kras*$^{G12D}$ mutation expression and *Snail* overexpression, *Cdkn2a* deletion leads to an increase of the metastatic rates in all these five secondary organs (Figure 5C). Moreover, loss of *Trp53* function causes a higher rate of ascites (Figure 5C). *Tgfβr2* deletion results in a higher percentage of ascites, while the percentage of ascites slightly decreases when the mice have both the homozygous *Tgfβr2* deletion and the deletion of a single allele of *Trp53* (Figure 5D). *Ptf1a*$^{Cre/+}$*;LSL-Kras*$^{G12D/+}$*;Tgfβr2*$^{lox/+}$

(PKT_HET) and *Ptf1a*$^{Cre/+}$;*LSL-Kras*$^{G12D/+}$;*Tgfβr2*$^{lox/lox}$ (PKT_HOM) mice show lower

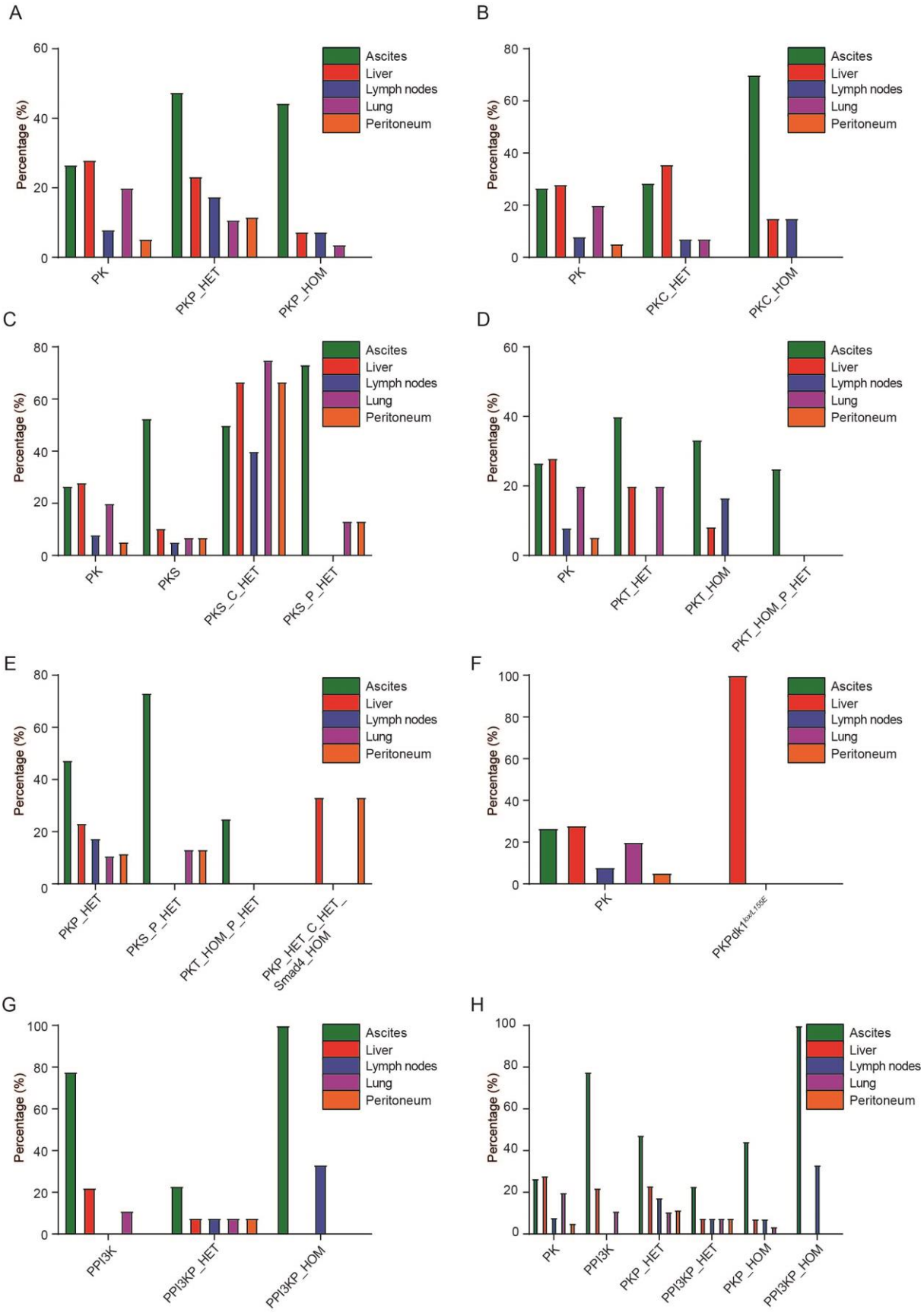

**Figure 5. The analysis of metastatic sites in the PDAC mouse models.**
(A) The analysis of metastatic sites in PK, PKP_HET and PKP_HOM mice. PK (n=75): *Pdx1-Flp;FSF-Kras$^{G12D/+}$, Pdx1-Cre;LSL-Kras$^{G12D/+}$*, *Ptf1a$^{Cre/+}$;LSL-Kras$^{G12D/+}$* mice. PKP_HET (n=120): *Pdx1-Flp;FSF-Kras$^{G12D/+}$;Trp53$^{frt/+}$*, *Pdx1-Cre;LSL-Kras$^{G12D/+}$;Trp53$^{lox/+}$*, *Ptf1a$^{Cre/+}$;LSL-Kras$^{G12D/+}$;Trp53$^{lox/+}$*, *Ptf1a$^{Cre/+}$;LSL-Kras$^{G12D/+}$;Trp53$^{R172H/+}$* mice. PKP_HOM (n=27): *Pdx1-Flp;FSF-Kras$^{G12D/+}$;Trp53$^{frt/frt}$*, *Pdx1-Cre;LSL-Kras$^{G12D/+}$;Trp53$^{lox/lox}$*, *Ptf1a$^{Cre/+}$;LSL-Kras$^{G12D/+}$;Trp53$^{lox/lox}$*, *Ptf1a$^{Cre/+}$;LSL-Kras$^{G12D/+}$; Trp53$^{R172H/R172H}$* mice.
(B) The analysis of metastatic sites in PK, PKC_HET and PKC_HOM mice. PK (n=75): *Pdx1-Flp;FSF-Kras$^{G12D/+}$, Pdx1-Cre;LSL-Kras$^{G12D/+}$*, *Ptf1a$^{Cre/+}$;LSL-Kras$^{G12D/+}$* mice. PKC_HET (n=14): *Ptf1a$^{Cre/+}$;LSL-Kras$^{G12D/+}$;Cdkn2a$^{lox/+}$* mice. PKC_HOM (n=20): *Ptf1a$^{Cre/+}$;LSL-Kras$^{G12D/+}$;Cdkn2a$^{lox/lox}$* mice.
(C) The analysis of metastatic sites in PK, PKS, PKS_C_HET and PKS_P_HET mice. PK (n=75): *Pdx1-Flp;FSF-Kras$^{G12D/+}$, Pdx1-Cre;LSL-Kras$^{G12D/+}$*, *Ptf1a$^{Cre/+}$;LSL-Kras$^{G12D/+}$* mice. PKS (n=57): *Ptf1a$^{Cre/+}$;LSL-Kras$^{G12D/+}$;LSL-Rosa26$^{Snail/+}$* mice. PKS_C_HET (n=30): *Ptf1a$^{Cre/+}$;LSL-Kras$^{G12D/+}$;LSL-Rosa26$^{Snail/+}$;Cdkn2a$^{lox/+}$* mice. PKS_P_HET (n=15): *Ptf1a$^{Cre/+}$;LSL-Kras$^{G12D/+}$;LSL-Rosa26$^{Snail/+}$;Trp53$^{lox/+}$* mice.
(D) The analysis of metastatic sites in PK, PKT_HET, PKT_HOM and PKT_HOM_P_HET mice. PK (n=75): *Pdx1-Flp;FSF-Kras$^{G12D/+}$, Pdx1-Cre;LSL-Kras$^{G12D/+}$*, *Ptf1a$^{Cre/+}$;LSL-Kras$^{G12D/+}$* mice. PKT_HET (n=5): *Ptf1a$^{Cre/+}$;LSL-Kras$^{G12D/+}$;Tgfβr2$^{lox/+}$* mice. PKT_HOM (n=12): *Ptf1a$^{Cre/+}$;LSL-Kras$^{G12D/+}$;Tgfβr2$^{lox/lox}$* mice. PKT_HOM_P_HET (n=5): *Ptf1a$^{Cre/+}$;LSL-Kras$^{G12D/+}$;Tgfβr2$^{lox/lox}$;Trp53$^{lox/+}$* mice.
(E) The analysis of metastatic sites in PKP_HET, PKS_P_HET, PKT_HOM_P_HET and PKP_HET_Smad4_HOM mice. PKP_HET (n=120): *Pdx1-Flp;FSF-Kras$^{G12D/+}$;Trp53$^{frt/+}$, Pdx1-Cre;LSL-Kras$^{G12D/+}$;Trp53$^{lox/+}$, Ptf1a$^{Cre/+}$;LSL-KrasG12D/+;Trp53$^{lox/+}$, Ptf1a$^{Cre/+}$;LSL-Kras$^{G12D/+}$;Trp53$^{R172H/+}$* mice. PKS_P_HET (n=15): *Ptf1a$^{Cre/+}$;LSL-Kras$^{G12D/+}$;LSL-Rosa26$^{Snail/+}$;Trp53$^{lox/+}$* mice. PKT_HOM_P_HET (n=5): *Ptf1a$^{Cre/+}$;LSL-Kras$^{G12D/+}$;Tgfβr2$^{lox/lox}$; Trp53$^{lox/+}$* mice. PKP_HET_Smad4_HOM (n=3): *Pdx1-Flp;FSF-Kras$^{G12D/+}$; FSF-Rosa26$^{CAG-CreERT2/+}$; Ink4α$^{*/+}$;Smad4$^{lox/lox}$;Trp53$^{lox/+}$ mice.*
(F) The analysis of metastatic sites in PK and PKPdk1$^{lox/L155E}$ mice. PK (n=75): *Pdx1-Flp;FSF-Kras$^{G12D/+}$, Pdx1-Cre;LSL-Kras$^{G12D/+}$*, *Ptf1a$^{Cre/+}$;LSL-Kras$^{G12D/+}$* mice. PKPdk1$^{lox/L155E}$ (n=3): *Ptf1a$^{Cre/+}$;LSL-Kras$^{G12D/+}$;Pdk1$^{lox/+}$;Pdk1$^{L155E/+}$* mice.
(G) The analysis of metastatic sites in PPI3K, PPI3KP_HET and PPI3KP_HOM mice. PPI3K (n=9): *Pdx1-Cre;LSL-Pik3ca$^{H1047R/+}$*, *Ptf1a$^{Cre/+}$;LSL-Pik3ca$^{H1047R/+}$* mice. PPI3KP_HET (n=13): *Ptf1a$^{Cre/+}$;LSL-Pik3ca$^{H1047R/+}$;Trp53$^{lox/+}$* mice. PPI3KP_HOM (n=3): *Ptf1a$^{Cre/+}$;LSL-Pik3ca$^{H1047R/+}$;Trp53$^{lox/lox}$* mice.
(H) The analysis of metastatic sites in PK, PKP_HET, PKP_HOM, PPI3K, PPI3KP_HET and PPI3KP_HOM mice. PK (n=75): *Pdx1-Flp;FSF-Kras$^{G12D/+}$, Pdx1-Cre;LSL-Kras$^{G12D/+}$*, *Ptf1a$^{Cre/+}$;LSL-Kras$^{G12D/+}$* mice. PKP_HET (n=120): *Pdx1-Flp;FSF-Kras$^{G12D/+}$;Trp53$^{frt/+}$, Pdx1-Cre;LSL-Kras$^{G12D/+}$;Trp53$^{lox/+}$, Ptf1a$^{Cre/+}$;LSL-KrasG12D/+;Trp53$^{lox/+}$, Ptf1a$^{Cre/+}$;LSL-Kras$^{G12D/+}$;Trp53$^{R172H/+}$* mice. PKP_HOM (n=27): *Pdx1-Flp;FSF-Kras$^{G12D/+}$;Trp53$^{frt/frt}$*, *Pdx1-Cre;LSL-Kras$^{G12D/+}$;Trp53$^{lox/lox}$, Ptf1a$^{Cre/+}$;LSL-Kras$^{G12D/+}$;Trp53$^{lox/lox}$, Ptf1a$^{Cre/+}$;LSL-Kras$^{G12D/+}$;Trp53$^{R172H/R172H}$* mice. PPI3K (n=9): *Pdx1-Cre;LSL-Pik3ca$^{H1047R/+}$*, *Ptf1a$^{Cre/+}$;LSL-Pik3ca$^{H1047R/+}$* mice. PPI3KP_HET (n=13): *Ptf1a$^{Cre/+}$;LSL-Pik3ca$^{H1047R/+}$;Trp53$^{lox/+}$* mice. PPI3KP_HOM (n=3): *Ptf1a$^{Cre/+}$;LSL-Pik3ca$^{H1047R/+}$;Trp53$^{lox/lox}$* mice.
The percentage is calculated as follows: the number of mice with the corresponding metastatic site is divided by the total mouse number in the indicated cohort and multiplied by 100%. All these mouse models were generated, bred and analyzed by all the members in the lab of Prof. Dieter Saur.

percentages of liver metastasis, 20% and 8.3%, respectively, compared with the PK cohort (28%) (Figure 5D). In the context of pancreas-specific *Kras$^{G12D}$* mutation expression and heterozygous *Trp53* deletion, *Snail* overexpression results in a higher percentage of ascites and a comparable rate of lung and peritoneal metastases, while the mice with *Tgfβr2* deletion present a lower percentage of ascites without any other metastatic sites (Figure 5E). The mice with *Cdkn2a* and *Smad4* deletions present higher percentages of liver and peritoneal metastases (Figure 5E). *Pdk1* deletion and *Pdk1$^{L155E}$* mutation lead to a higher percentage of liver metastasis (Figure 5F). The vast majority of the PDAC mice driven by *Pik3ca$^{H1047R}$* mutation have ascites and the mice with liver and lung metastases account for the 22.2%

and 11.1% of this cohort, respectively (Figure 5G). The mice with deletion of *Trp53* gene show a higher percentage of lymph node metastasis, but a lower percentage of liver metastasis compared with *Pdx1-Cre;LSL-Pik3ca*$^{H1047R/+}$ and *Ptf1a*$^{Cre/+}$*;LSL-Pik3ca*$^{H1047R/+}$ (PPI3K) mice (Figure 5G). PK mice have higher percentages of liver, lymph node, lung, and peritoneal metastases, but a lower percentage of ascites compared to the PPI3K cohort (Figure 5H). When one allele of *Trp53* is deleted, the PDAC mice driven by *Kras*$^{G12D}$ mutation have higher rates of metastases formation in all the metastatic sites than the mice driven by *Pik3ca*$^{H1047R}$ (Figure 5H).

21.3% of the PK mice with metastasis have 1 metastatic site (Figure 6A). The percentage of the mice with 1 metastatic site increases as the number of the deleted allele of *Trp53* increases (Figure 6A). The mice with heterozygous and homozygous *Trp53* deletions have lower percentages of 2 metastatic sites than the PK cohort (Figure 6A). 1.3% of the PK mice have 5 metastatic sites while the number of the metastatic sites of the mice with *Trp53* deletions is no more than 4 (Figure 6A). Most of the mice with heterozygous and homozygous deletion of *Cdkn2a* have 1 metastatic site, 50% and 65% respectively, which are drastically higher than that of the PK cohort (21.3%) (Figure 6B). Compared with PK mice, the PKS cohort has a higher percentage of metastasis in 1 metastatic site, but lower percentages of 2 and 3 sites (Figure 6C). In the context of *Kras*$^{G12D}$ mutation and *Snail* overexpression, the mice with the deletion of one allele *Cdkn2a* have a lower percentage of 1 metastatic site, but a higher percentage of 2 metastatic sites, than those with heterozygous *Trp53* deletion (Figure 6C). The mice with heterozygous *Tgfβr2* deletion have a higher percentage of 3 metastatic sites than PK mice (Figure 6D). In the context of *Kras*$^{G12D}$ mutation and homozygous *Tgfβr2* deletion, *Trp53* deletion leads to no more than 1 metastatic site (Figure 6D). When compared with PKP_HET cohort, *Snail* overexpression results in higher percentages of 1 and 2 metastatic sites in the context of *Kras*$^{G12D}$ mutation and heterozygous *Trp53* deletion (Figure 6E). In the same context, heterozygous *Cdkn2a* and homozygous *Smad4* deletion also result in a higher percentage of 1 metastatic site (Figure 6E). The mice with heterozygous *Trp53* deletion and heterozygous *Cdkn2a* and homozygous *Smad4* deletion do not present more than 1 metastatic site (Figure 6E). The mice with *Pdk1* deletion and *Pdk1*$^{L155E}$ mutation only have 1 metastatic site (Figure 6F). Most of the mice driven by *Pik3ca*$^{H1047R}$ have 1 metastatic site (Figure 6G). *Ptf1a*$^{Cre/+}$*;LSL-Pik3ca*$^{H1047R/+}$*;Trp53*$^{lox/+}$ (PPI3KP_HET) mice have a lower percentage of 1 metastatic site than PPI3K mice (Figure 6G). *Ptf1a*$^{Cre/+}$*;LSL-Pik3ca*$^{H1047R/+}$*;Trp53*$^{lox/lox}$ (PPI3KP_HOM) mice have a higher percentage of 2 metastatic sites than PPI3K cohort (Figure 6G). The mice driven by *Pik3ca*$^{H1047R}$ have no more than 3 metastatic sites while the mice driven by *Kras*$^{G12D}$ mutation can have up to 5 metastatic sites (Figure 6H). Heterozygous *Trp53* deletion leads to

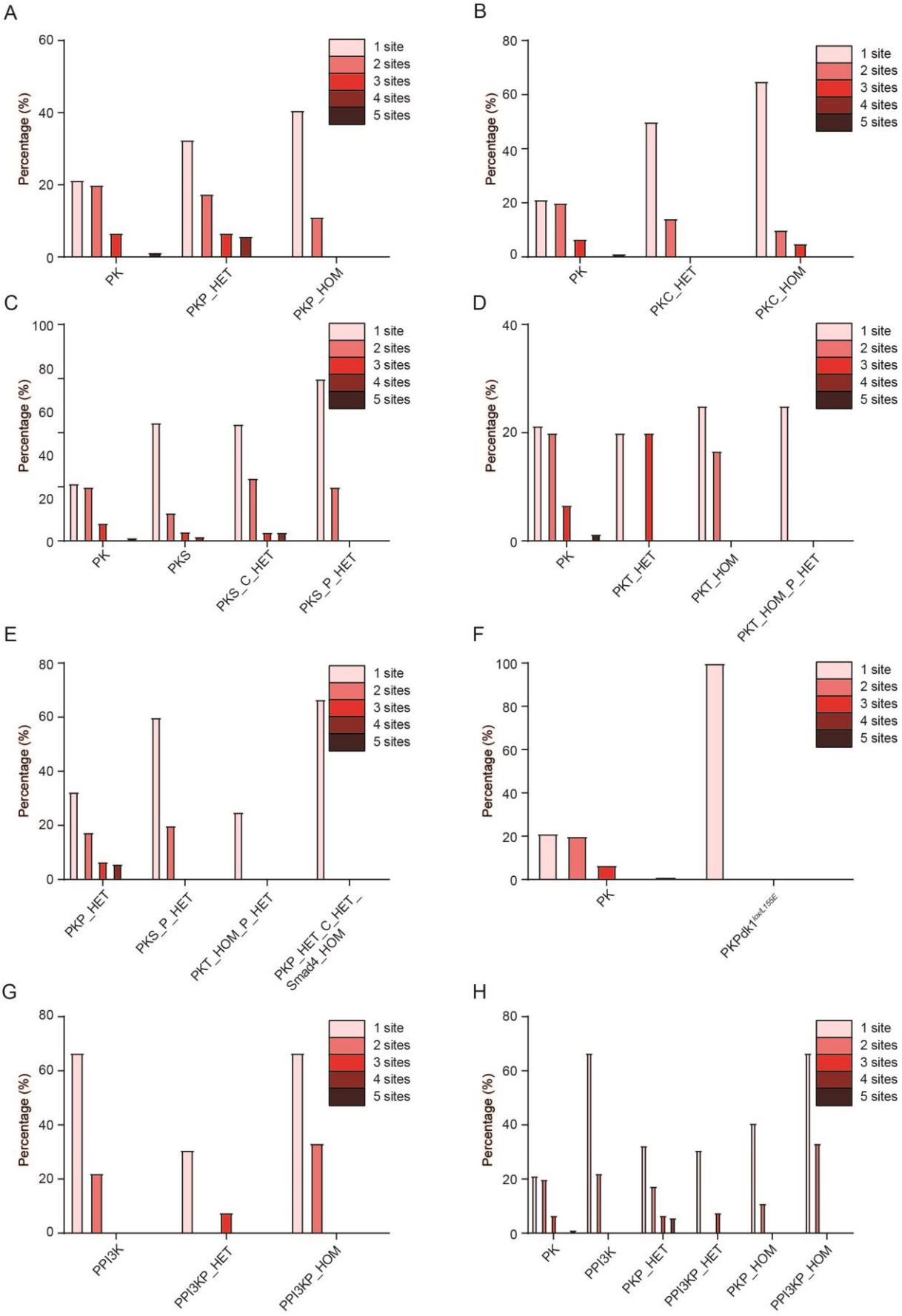


**Figure 6. The analysis of the number of metastatic sites in PDAC mouse models.**

(A) The analysis of the number of metastatic sites in PK, PKP_HET and PKP_HOM mice. PK (n=75): *Pdx1-Flp;FSF-Kras$^{G12D/+}$, Pdx1-Cre;LSL-Kras$^{G12D/+}$, Ptf1a$^{Cre/+}$;LSL-Kras$^{G12D/+}$* mice. PKP_HET (n=120): *Pdx1-Flp;FSF-Kras$^{G12D/+}$;Trp53$^{frt/+}$, Pdx1-Cre;LSL-Kras$^{G12D/+}$;Trp53$^{lox/+}$, Ptf1a$^{Cre/+}$;LSL-Kras$^{G12D/+}$;Trp53$^{lox/+}$, Ptf1a$^{Cre/+}$;LSL-Kras$^{G12D/+}$;Trp53$^{R172H/+}$* mice. PKP_HOM (n=27): *Pdx1-Flp;FSF-Kras$^{G12D/+}$;Trp53$^{frt/frt}$, Pdx1-Cre;LSL-Kras$^{G12D/+}$;Trp53$^{lox/lox}$, Ptf1a$^{Cre/+}$;LSL-Kras$^{G12D/+}$;Trp53$^{lox/lox}$, Ptf1a$^{Cre/+}$;LSL-Kras$^{G12D/+}$;Trp53$^{R172H/R172H}$* mice.
(B) The analysis of the number of metastatic sites in PK, PKC_HET and PKC_HOM mice. PK (n=75): *Pdx1-Flp;FSF-Kras$^{G12D/+}$, Pdx1-Cre;LSL-Kras$^{G12D/+}$, Ptf1a$^{cre/+}$;LSL-Kras$^{G12D/+}$* mice. PKC_HET (n=14): *Ptf1a$^{Cre/+}$;LSL-Kras$^{G12D/+}$;Cdkn2a$^{lox/+}$* mice. PKC_HOM (n=20): *Ptf1$^{Cre/+}$;LSL-Kras$^{G12D/+}$;Cdkn2a$^{lox/lox}$* mice.
(C) The analysis of the number of metastatic sites in PK, PKS, PKS_C_HET and PKS_P_HET mice. PK (n=75): *Pdx1-Flp;FSF-Kras$^{G12D/+}$, Pdx1-Cre;LSL-Kras$^{G12D/+}$, Ptf1a$^{Cre/+}$;LSL-Kras$^{G12D/+}$* mice. PKS (n=57): *Ptf1a$^{Cre/+}$;LSL-Kras$^{G12D/+}$;LSL-Rosa26$^{Snail/+}$* mice. PKS_C_HET (n=30): *Ptf1a$^{Cre/+}$;LSL-Kras$^{G12D/+}$;LSL-Rosa26$^{Snail/+}$;Cdkn2a$^{lox/+}$* mice. PKS_P_HET (n=15): *Ptf1a$^{Cre/+}$;LSL-Kras$^{G12D/+}$;LSL-Rosa26$^{Snail/+}$;Trp53$^{lox/+}$* mice.
(D) The analysis of the number of metastatic sites in PK, PKT_HET, PKT_HOM and PKT_HOM_P_HET mice. PK (n=75): *Pdx1-Flp;FSF-Kras$^{G12D/+}$, Pdx1-Cre;LSL-Kras$^{G12D/+}$, Ptf1a$^{Cre/+}$;LSL-Kras$^{G12D/+}$* mice. PKT_HET (n=5): *Ptf1a$^{Cre/+}$;LSL-Kras$^{G12D/+}$;Tgfβr2$^{lox/+}$* mice. PKT_HOM (n=12): *Ptf1a$^{Cre/+}$;LSL-Kras$^{G12D/+}$;Tgfβr2$^{lox/lox}$* mice. PKT_HOM_P_HET (n=5): *Ptf1a$^{Cre/+}$;LSL-Kras$^{G12D/+}$;Tgfβr2$^{lox/lox}$;Trp53$^{lox/+}$* mice.
(E) The analysis of the number of metastatic sites in PKP_HET, PKS_P_HET, PKT_HOM_P_HET and PKP_HET_Smad4_HOM mice. PKP_HET (n=120): *Pdx1-Flp;FSF-Kras$^{G12D/+}$;Trp53$^{frt/+}$, Pdx1-Cre;LSL-Kras$^{G12D/+}$;Trp53$^{lox/+}$, Ptf1a$^{Cre/+}$;LSL-Kras$^{G12D/+}$;Trp53$^{lox/+}$, Ptf1a$^{Cre/+}$;LSL-Kras$^{G12D/+}$;Trp53$^{R172H/+}$* mice. PKS_P_HET (n=15): *Ptf1a$^{Cre/+}$;LSL-Kras$^{G12D/+}$;LSL-Rosa26$^{Snail/+}$;Trp53$^{lox/+}$* mice. PKT_HOM_P_HET (n=5): *Ptf1a$^{Cre/+}$;LSL-Kras$^{G12D/+}$;Tgfβr2$^{lox/lox}$;Trp53$^{lox/+}$* mice. PKP_HET_Smad4_HOM (n=3): *Pdx1-Flp;FSF-Kras$^{G12D/+}$;FSF-Rosa26$^{CAG-CreERT2/+}$;Ink4α$^{*/+}$;Smad4$^{lox/lox}$;Trp53$^{lox/+}$ mice.*
(F) The analysis of the number of metastatic sites in PK and PKPdk1$^{lox/L155E}$ mice. PK (n=75): *Pdx1-Flp;FSF-Kras$^{G12D/+}$, Pdx1-Cre;LSL-Kras$^{G12D/+}$, Ptf1a$^{Cre/+}$;LSL-Kras$^{G12D/+}$* mice. PKPdk1$^{lox/L155E}$ (n=3): *Ptf1a$^{Cre/+}$;LSL-Kras$^{G12D/+}$;Pdk1$^{lox/+}$;Pdk1$^{L155E/+}$* mice.
(G) The analysis of the number of metastatic sites in PPI3K, PPI3KP_HET and PPI3KP_HOM mice. PPI3K (n=9): *Pdx1-Cre;LSL-Pik3ca$^{H1047R/+}$, Ptf1a$^{Cre/+}$;LSL-Pik3ca$^{H1047R/+}$* mice. PPI3KP_HET (n=13): *Ptf1a$^{Cre/+}$;LSL-Pik3ca$^{H1047R/+}$;Trp53$^{lox/+}$* mice. PPI3KP_HOM (n=3): *Ptf1a$^{Cre/+}$;LSL-Pik3ca$^{H1047R/+}$;Trp53$^{lox/lox}$* mice.
(H) The analysis of the number of metastatic sites in PK, PKP_HET, PKP_HOM, PPI3K, PPI3KP_HET and PPI3KP_HOM mice. PK (n=75): *Pdx1-Flp;FSF-Kras$^{G12D/+}$, Pdx1-Cre;LSL-Kras$^{G12D/+}$, Ptf1a$^{Cre/+}$;LSL-Kras$^{G12D/+}$* mice. PKP_HET (n=120): *Pdx1-Flp;FSF-Kras$^{G12D/+}$;Trp53$^{frt/+}$, Pdx1-Cre;LSL-Kras$^{G12D/+}$;Trp53$^{lox/+}$, Ptf1a$^{Cre/+}$;LSL-Kras$^{G12D/+}$;Trp53$^{lox/+}$, Ptf1a$^{Cre/+}$;LSL-Kras$^{G12D/+}$;Trp53$^{R172H/+}$* mice. PKP_HOM (n=27): *Pdx1-Flp;FSF-Kras$^{G12D/+}$;Trp53$^{frt/frt}$, Pdx1-Cre;LSL-Kras$^{G12D/+}$;Trp53$^{lox/lox}$, Ptf1a$^{Cre/+}$;LSL-Kras$^{G12D/+}$;Trp53$^{lox/lox}$, Ptf1a$^{Cre/+}$;LSL-Kras$^{G12D/+}$;Trp53$^{R172H/R172H}$* mice. PPI3K (n=9): *Pdx1-Cre;LSL-Pik3ca$^{H1047R/+}$, Ptf1a$^{Cre/+}$;LSL-Pik3ca$^{H1047R/+}$* mice. PPI3KP_HET (n=13): *Ptf1a$^{Cre/+}$;LSL-Pik3ca$^{H1047R/+}$;Trp53$^{lox/+}$* mice. PPI3KP_HOM (n=3): *Ptf1a$^{Cre/+}$;LSL-Pik3ca$^{H1047R/+}$;Trp53$^{lox/lox}$* mice.
The percentage is calculated as follows: the number of mice with the corresponding metastatic site is divided by the total mouse number in the indicated cohort and multiplied by 100%. All these mouse models were generated, bred and analyzed by all the members in the lab of Prof. Dieter Saur.

lower percentages of 2 metastatic sites in both oncogenic *Kras* and *Pik3ca* cohorts (Figure 6H).

## 6.3 Histological characterization of PDAC mouse models.

Tumor grade is used to describe how abnormal cells are under a microscope when compared to normal cells. In PDAC mouse models, Grade 1 (G1) is defined as well differentiated ductal carcinomas, G2 moderately differentiated, G3 as poorly differentiated

and G4 as undifferentiated. Figure 7 shows the hematoxylin and eosin (H&E) staining

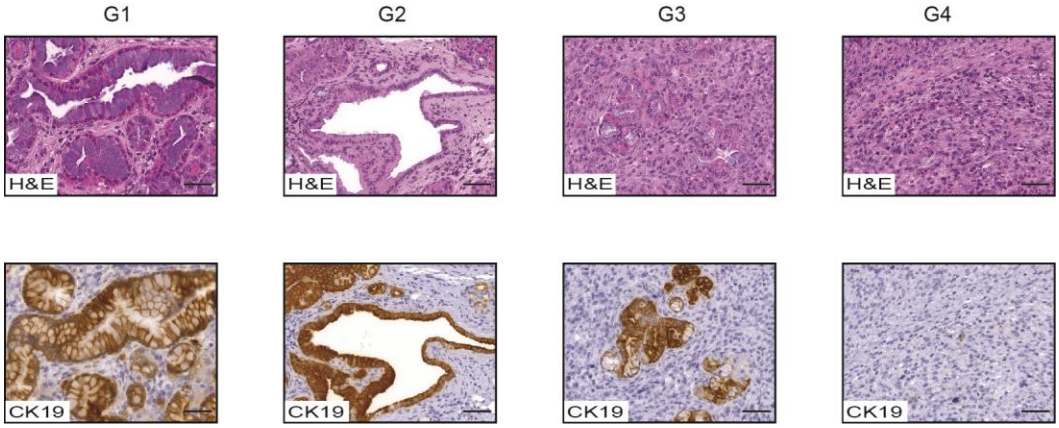


**Figure 7. The representative images of tumors in different grades with hematoxylin and eosin (H&E) staining and cytokeratin 19 (CK19) immunohistochemistry staining.** G1: Grade 1 tumors. G2: Grade 2 tumors. G3: Grade 3 tumors. G4: Grade 4 tumors. Scale bars indicate 50 μm.

images of these four grades, as well as the immunohistochemistry (IHC) staining for cytokeratin 19 (CK19), an epithelium marker used to detect the ductal structures of tumors.

Cell proliferation plays a critical role in cancer progression. The mitotic counts are positively related to the grading levels of the tumor. Figure 8A shows the mitotic activity on the H&E staining images of the four grades of PDAC tumors. As the grades increase, there is also an increase in the mitotic counts (Figure 8B).

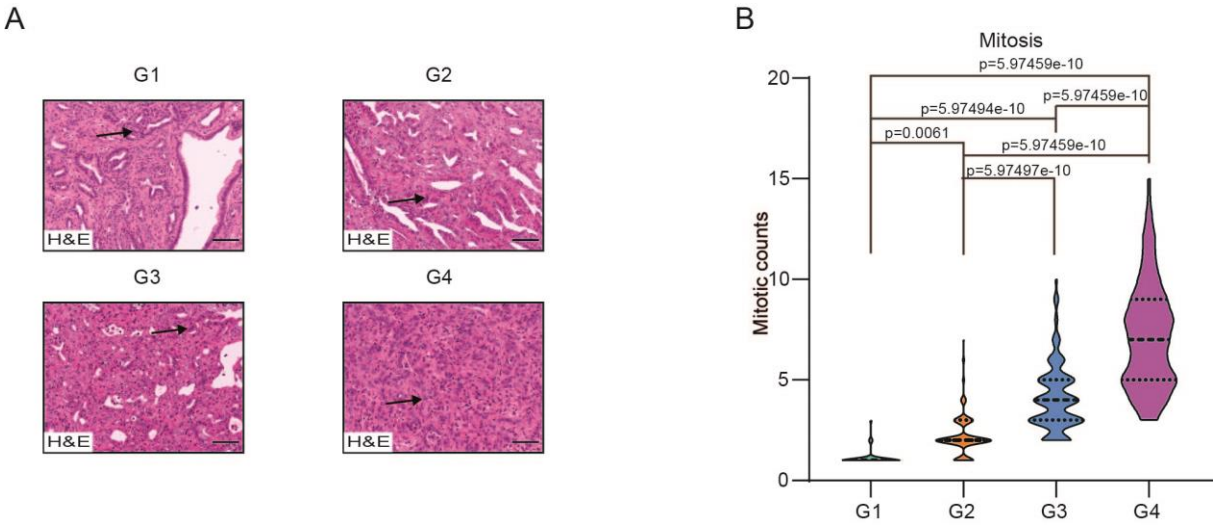


**Figure 8. The mitotic counts correlate with tumor grades.**

(A) The representative images of hematoxylin and eosin (H&E) staining of tumors with mitosis in different grades. The arrows indicate the cells undergoing mitosis. Scale bars indicate 50 µm.
(B) The mitotic counts in tumors in different grades. G1: n=33. G2: n=142. G3: n=229. G4: n=143. *p* values are indicated in the graph, one-way ANOVA. Pathologist PD Dr. med. Moritz Jesinghaus analyzed the slides.
G1: Grade 1 tumors. G2: Grade 2 tumors. G3: Grade 3 tumors. G4: Grade 4 tumors. All these mouse models were generated, bred and analyzed by all the members in the lab of Prof. Dieter Saur.

Most pancreatic cancer patients succumb from the illnesses caused by tumor cell spread and organ dysfunction. Metastasis is an important clinical parameter for diagnosis and prognosis. Figure 9A shows the typical H&E staining images of liver metastasis (Figure 9A.a), lung metastasis (Figure 9A.b), lymph nodes metastasis (Figure 9A.c) and the image of cancer cells isolated from ascites (Figure 9A.d) in PDAC mouse models. The correlation between the grades of the primary tumors and the metastatic patterns in the PDAC mouse models has also been investigated. The result shows that tumors with higher grades tend to have a higher percentage of metastasis (Figure 9B). As the grade goes from G1 to G3, the percentage of metastasis drastically increases from 38.2% to 67.9% ($p$<0.0001) (Figure 9B). The metastatic percentage of G4 cohort is 60.3%, higher than G1 and G2 mice (38.2% and 51.7% respectively) (Figure 9B). The mice with higher grades have a higher percentage of liver

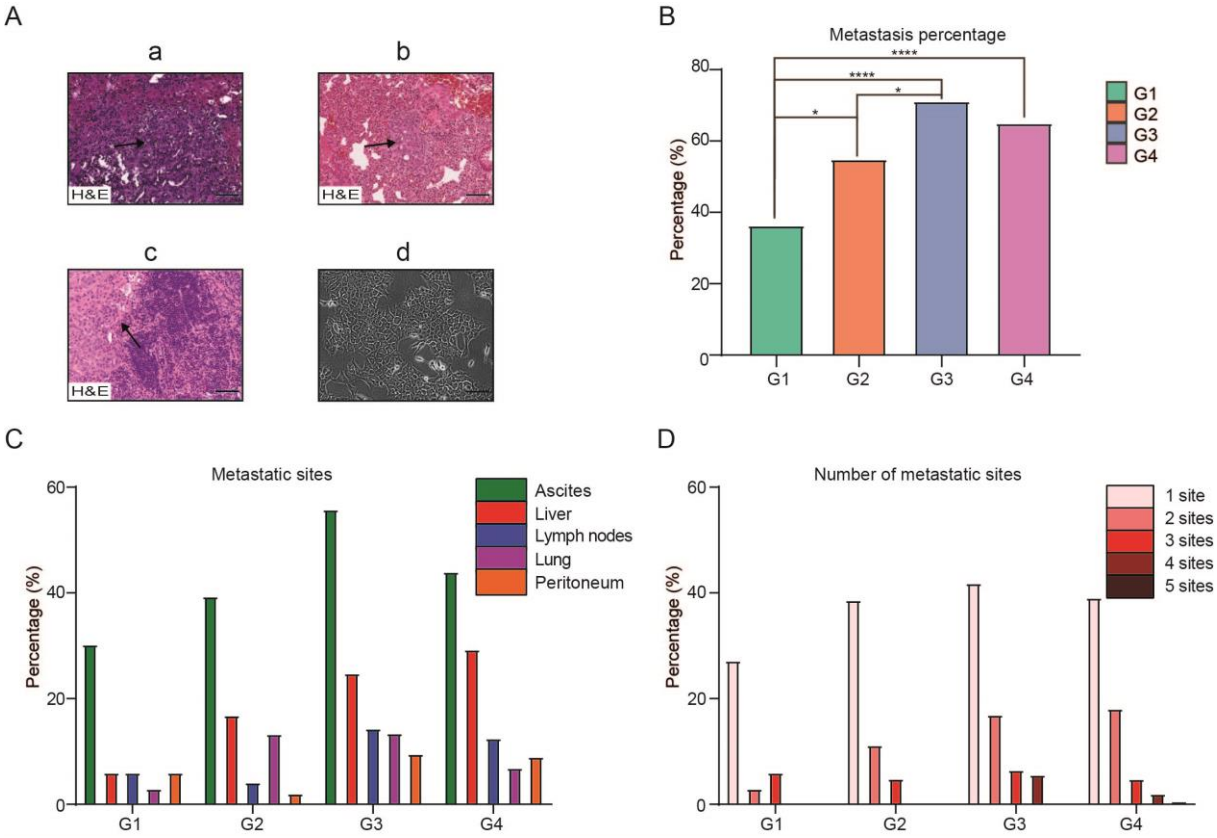


**Figure 9. Metastasis is associated with tumor grades.**
(A) The representative images of liver metastasis(a), lung metastasis(b), lymph nodes metastasis(c) and tumor cells isolated from ascites(d). Scale bars indicate 50 µm.
(B) The percentage of metastasis in different tumor grades. *$p$<0.05, ****$p$<0.0001, Fisher's exact test.

(C) The percentage of the metastatic sites in different tumor grades. The percentage is calculated as follows: the number of mice with the corresponding metastatic site is divided by the total mouse number in the indicated cohort and multiplied by 100%.
(D) The number of the metastatic sites in different tumor grades. The percentage is calculated as follows: the number of mice with the corresponding number of the metastatic sites is divided by the total mouse number in the indicated cohort and multiplied by 100%.
G1: n=33. G2: n=142. G3: n=229. G4: n=143. All these mouse models were generated, bred and analyzed by all the members in the lab of Prof. Dieter Saur.

metastasis (Figure 9C). Most of the mice in these four grades have 1 metastatic site (Figure 9D). The mice of G1 and G2 have no more than 3 metastatic sites, while the mice from G3 and G4 cohorts have at least 4 metastatic sites (Figure 9D). In G4 mice, metastases have been observed in 5 distinct metastatic sites, thought the percentage is low (Figure 9D).

One of the features of PDAC is the presence of a dense stroma. Stromal compartment consists of ECM proteins, fibroblasts, tumor vasculature and immune cells. Stroma has been proved to be a barrier to drug delivery and can increase intratumoral pressure (Provenzano et al., 2012). The infiltration of immune cells is involved in pancreatic tumor and previous studies demonstrated that these cells can be promising therapeutic targets (Ansell et al., 2015; Fan et al., 2020; Tsirigotis et al., 2016; Watt and Kocher, 2013). In the present study, pathologist PD Dr. med. Moritz Jesinghaus evaluated the percentages of the stromal compartment and lymphocytes of the tumors. Figure 10A shows the images of tumor grades with stroma. There is a significant difference in the percentage of stromal compartment between G1 and G4 cohorts (38.4% vs 18.0%, G1 vs G4) (Figure 10B). The percentage of stroma in G4 decreases sharply when compared to that of G1(Figure 10B). However, the percentage of stroma does not show significant difference between G1, G2 and G3 (Figure 10B). The image examples of tumor grades with lymphocytes are shown in Figure 10C. The percentage of lymphocytes in G4 decreases significantly compared with that of G1 (Figure 10D). The percentage of lymphocytes are comparable between G1 and G2 (Figure 10D). There is no significant difference in the percentage of lymphocytes between G1 and G3 (Figure 10D).

## 6.4 Transcriptional profiling and the link to histopathological features.

Pancreatic cancer is a molecularly heterogeneous disease. Its molecular features modulate PDAC progression, overall survival time and sensitivity to treatments. Understanding the molecular features has become a hallmark in the study of cancer entities (McGranahan and Swanton, 2017). Transcriptional profiling has been employed to identify cancer related

biomarkers, which can be used for diagnosis, treatment and prognosis of cancer patients (Amundson and Smilenov, 2010; Peng et al., 2007; Turashvili et al., 2011; Yousef et al., 2005). It has been widely acknowledged that a gene set can have more biological and clinical relevance than individual genes considering the need of genetic interactions for biological activities (Huang da et al., 2009a; Subramanian et al., 2005). Since cancer is a

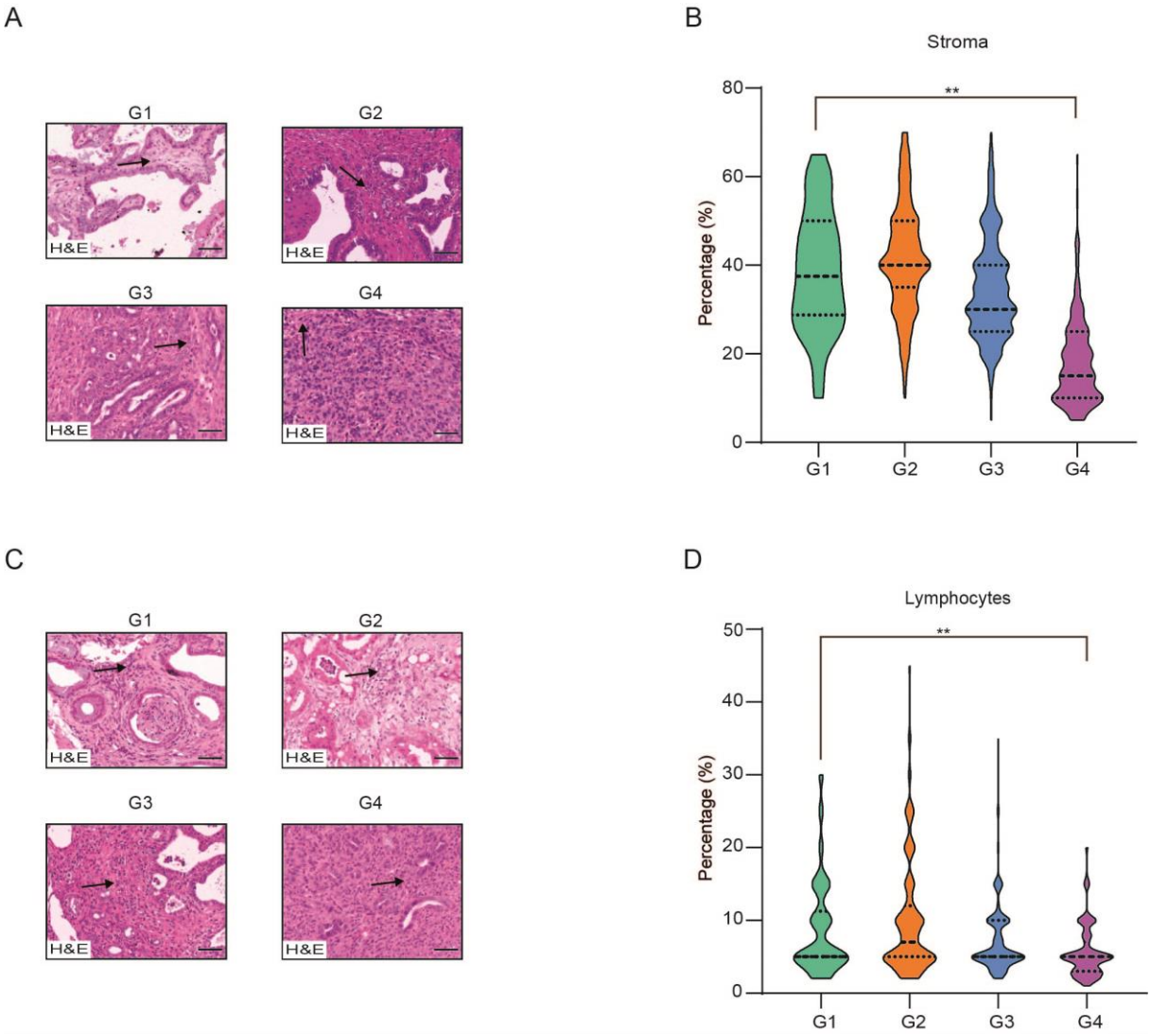


**Figure 10. The percentages of stroma and lymphocytes in different tumor grades.**
(A) The representative images of hematoxylin and eosin (H&E) staining of tumor grades with stroma. Arrows indicate stromal compartments. Scale bars indicate 50 µm.
(B) The percentage of stroma in tumor grades. ***p*<0.01, one-way ANOVA.
(C) The representative images of of hematoxylin and eosin (H&E) staining of tumor grades with lymphocytes. Arrows indicate lymphocytes. Scale bars indicate 50 µm.
(D) The percentage of lymphocytes in tumor grades. ***p*<0.01, one-way ANOVA.
G1: n=33. G2: n=142. G3: n=229. G4: n=143. Pathologist PD Dr. med. Moritz Jesinghaus analyzed the slides. All these mouse models were generated, bred and analyzed by all the members in the lab of Prof. Dieter Saur.

system biology disease, identification of tumor related molecular signatures could provide insights into the cancer biology (Hornberg et al., 2006; Huang da et al., 2009b; Wang et al., 2007). The molecular subtypes of PDAC have been identified based on the transcriptional profiles of PDAC patients (Bailey et al., 2016; Chan-Seng-Yue et al., 2020; Collisson et al., 2011; Moffitt et al., 2015). In this study, 547 PDAC mice are analyzed and the histopathology dataset is established on the basis of histopathology image analysis by pathologists. The transcriptional dataset is derived from the RNA-Seq profiles of the primary tumor samples from 267 mice out of the 547 PDAC mice. In combination with histopathological features of these mice, the transcriptional profiles are analyzed to investigate the correlation of molecular landscapes with histopathology phenotypes. The workflow is shown in Figure 11.

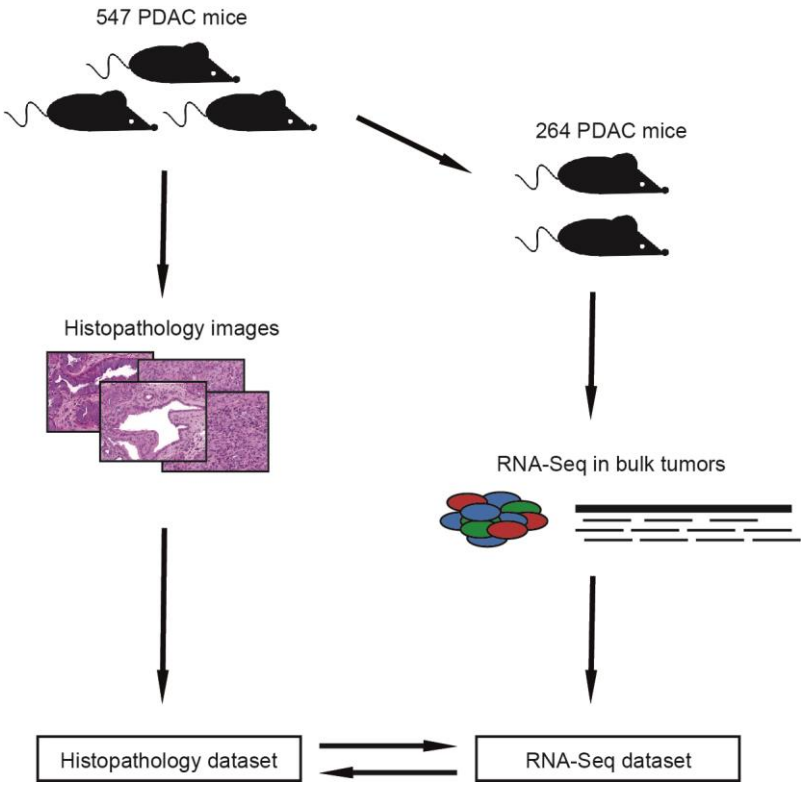


**Figure 11. The workflow to investigate the correlation of transcriptional profiling data with histopathological features.**

### 6.4.1 Identification of the molecular signature related to tumor grades.

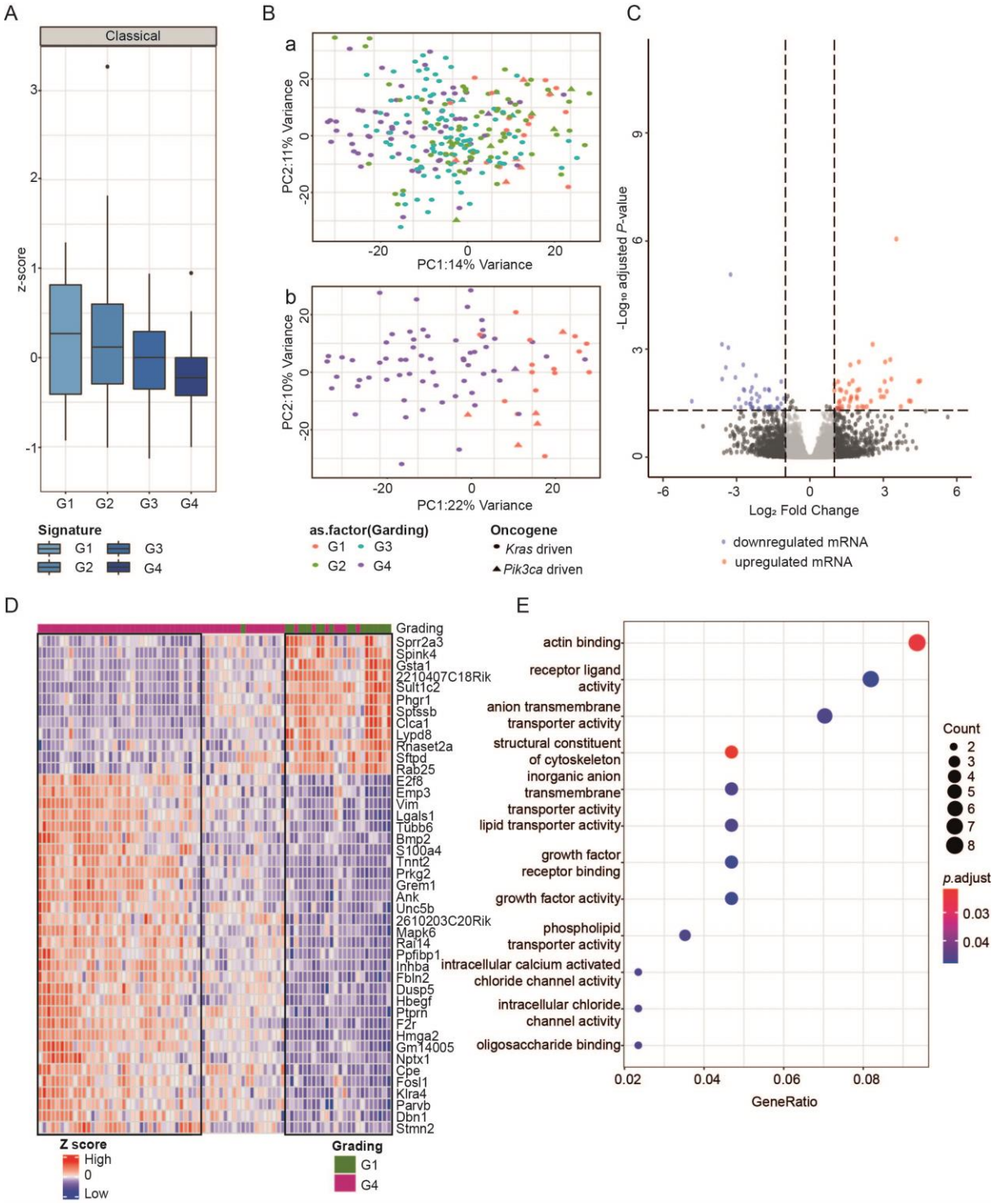


**Figure 12. Correlation between tumor grades and transcriptional profiling data in mouse PDAC tumors.**

(A) The correlation between the classical subtype of pancreatic ductal adenocarcinoma (PDAC) and tumor grades.

(B) Principal component analysis (PCA) of the RNA-Seq dataset based on tumor grades.

(C) The volcano plot of differential gene expression analysis between G1 and G4 cohorts (Log2 fold change >1 or < -1 and -$Log_{10}$ adjusted *p* value > 1.5).

(D) Heatmap of differential gene expression analysis between G1 and G4 cohorts.

(E) Signaling pathway enrichment based on the differential gene expression analysis of G1 and G4 cohorts.

G1: n=18. G2: n=80. G3: n=104. G4: n=62. Bioinformatician Fabio Boniolo performed the analysis for the correlation between tumor grades and the classical subtype (Figure 12A), the principal component analysis (PCA) (Figure 12B), the differential expression analysis (Figure 12C and 12D) and the enrichment of sigaling pathways (Figure 12E). All these mouse models were generated, bred and analysed by all the members in Prof. Dieter Saur. Mouse dissection, RNA preparation and RNA-seq were performed by all the members in the lab of Prof. Dieter Saur.

Previous studies have defined several transcriptomic subtypes which have shown the clinical relevance (Bailey et al., 2016; Chan-Seng-Yue et al., 2020; Collisson et al., 2011; Moffitt et al., 2015). In 2019, a study has demonstrated that morphological classification of PDAC can be used to predict molecular subtypes and these morphological patterns correlates with clinical outcomes (Kalimuthu et al., 2020). The present study finds the correlation between the classical subtype of PDAC and the tumor grades in mouse models, which provides the evidence to link the histopathological features to PDAC transcriptomic subtypes. Figure 12A shows the low grades (G1 and G2) are positively related to the classical subtype while the correlation between G4 and the classical subtype is negative. This finding is consistent and corroborates with previous study based on clinical data (Kalimuthu et al., 2020). The present study identifies the link between the histopathological characteristics and molecular subtypes in mouse models.

The principal component analysis (PCA) of the RNA-Seq dataset was performed by bioinformatician Fabio Boniolo. The analysis hows G2 and G3 are mixed, indicating the transcriptional profiles of the samples in these two groups are quite similar (Figure 12B.a). In contrast, G1 and G4 are separated in the PCA plot (Figure 12B.a and 12B.b). Most of G4 samples are clustered on the left side while the G1 samples are on the right side (Figure 12B.a and 12B.b). This indicates G1 and G4 mice have distinct gene expression patterns. The differential gene expression analysis shows that the expression of 74 genes is significantly downregulated and that of 83 genes is significantly upregulated in the G4 cohort, when compared to the G1 cohort (Figure 12C).

There are three clusters that can be defined in the heatmap of gene expression analysis (Figure 12D). The first cluster (on the left side of the heatmap) includes all the samples from G4 cohort while most of G1 samples are in the third cluster (on the right side of the heatmap) (Figure 12D). This study identifies a list of genes differently expressed between G1 and G4 tumors (Figure 12D). *Small proline-rich protein 2A3* (*Sprr2a3*) is an epithelial cell-specific gene and highly expressed in patients with bladder cancer (Haocheng et al., 2020). In this study, we find that *Sprr2a* is highly expressed in G1 mice, while its expression level is downregulated in G4 mice (Figure 12D). Presence of well-formed gland structures is the feature of G1 tumors and these gland structures are lined by pancreaticobiliary-type epithelium (Kalimuthu et al., 2020). This study shows the high expression level of *Sprr2a* is an indicator of the well-differentiated tumors. However, one previous study shows *Sprr2a*

induces EMT and promotes the local invasiveness in cholangiocarcinomas (Mizuguchi et al., 2014). These findings indicate the function of Sprr2a is dependent on tumor contexts. Serine peptidase inhibitor Kazal type 4 (Spink4) is a gastrointestinal peptide and highly expressed in human goblet cells. This study shows *Spink4* expression is downregulated in G4 tumors. In addition, it has been reported that poor prognosis of colorectal cancer patients is related to downregulated *Spink4* expression at both mRNA and protein levels (Wang et al., 2019d). High grade tumors

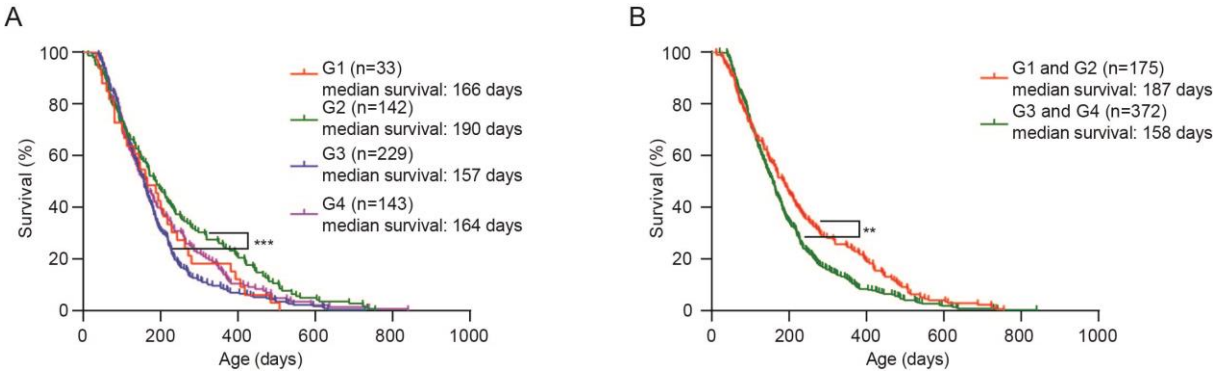


**Figure 13. Kaplan-Meier survival analysis of tumor mice with different grades.**
(A) Kaplan-Meier survival analysis of G1, G2, G3 and G4 mice. G1: n=33. G2: n=142. G3: n=229. G4: n=143.
(B) Kaplan-Meier survival analysis of low grades (G1 and G2) cohort and high grades (G3 and G4) cohort. G2, G3 and G4 mice. G1 and G2: n=175. G3 and G4: n=372.
The genotypes of the tumor mice *Pdx1-Flp;FSF-Kras$^{G12D/+}$*, *Pdx1-Cre;LSL-Kras$^{G12D/+}$*, *Ptf1a$^{Cre/+}$;LSL-Kras$^{G12D/+}$*, *Pdx1-Flp;FSF-Kras$^{G12D/+}$;Trp53$^{frt/+}$*, *Pdx1-Cre;LSL-Kras$^{G12D/+}$;Trp53$^{lox/+}$*, *Ptf1a$^{Cre/+}$;LSL Kras$^{G12D/+}$;Trp53$^{lox/+}$*, *Ptf1a$^{Cre/+}$;LSL-Kras$^{G12D/+}$;LSL-Trp53$^{R172H/+}$*, *Pdx1-Flp;FSF-Kras$^{G12D/+}$;Trp53$^{frt/frt}$*, *Pdx1-Cre;LSL-Kras$^{G12D/+}$;Trp53$^{lox/lox}$*, *Ptf1a$^{Cre/+}$;LSL-Kras$^{G12D/+}$;Trp53$^{lox/lox}$*, *Ptf1a$^{Cre/+}$;LSL-Kras$^{G12D/+}$;LSL-Trp53$^{R172H/R172H}$*, *Ptf1a$^{Cre/+}$;LSL-Kras$^{G12D/+}$;Cdkn2a$^{lox/+}$*, *Ptf1a$^{cre/+}$;LSL-Kras$^{G12D/+}$;Cdkn2a$^{lox/lox}$*, *Ptf1a$^{Cre/+}$;LSL-Kras$^{G12D/+}$;LSL-Rosa26$^{Snail/+}$*, *Ptf1a$^{Cre/+}$;LSL-Kras$^{G12D/+}$;LSL-Rosa26$^{Snail/+}$;Cdkn2a$^{lox/+}$*, *Ptf1a$^{Cre/+}$;LSL-Kras$^{G12D/+}$;LSL-Rosa26$^{Snail/+}$;Trp53$^{lox/+}$*, *Ptf1a$^{Cre/+}$;LSL-Kras$^{G12D/+}$;Tgfβr2$^{lox/+}$*, *Ptf1a$^{Cre/+}$;LSL-Kras$^{G12D/+}$;Tgfβr2$^{lox/lox}$*, *Ptf1a$^{Cre/+}$;LSL-Kras$^{G12D/+}$;Tgfβr2$^{lox/lox}$;Trp53$^{lox/+}$*, *Pdx1-Flp;FSF-Kras$^{G12D/+}$;FSF-Rosa26$^{CAG-CreERT2/+}$;Ink4α$^{*/+}$;Smad4$^{lox/lox}$;Trp53$^{lox/+}$*, *Ptf1a$^{Cre/+}$;LSL-Kras$^{G12D/+}$;Pdk1$^{lox/+}$;Pdk1$^{L155E/+}$*, *Pdx1-Cre;LSL-Pik3ca$^{H1047R/+}$*, *Ptf1a$^{Cre/+}$;LSL-Pik3ca$^{H1047R/+}$*, *Ptf1a$^{Cre/+}$;LSL-Pik3ca$^{H1047R/+}$;Trp53$^{lox/+}$*, *Ptf1a$^{Cre/+}$;LSL-Pik3ca$^{H1047R/+}$;Trp53$^{lox/lox}$*, *Ptf1a$^{Cre/+}$,LSL-Kras$^{G12D/+}$;Tnc$^{-/-}$*, *Ptf1a$^{Cre/+}$,LSL-Kras$^{G12D/+}$;Hnf4α$^{lox/lox}$*, *Ptf1a$^{Cre/+}$;LSL-Pik3ca$^{H1047R/+}$;Map2k1$^{lox/+}$*, *Ptf1a$^{Cre/+}$;LSL-Pik3ca$^{H1047R/+}$;Map2k1$^{lox/lox}$*, *Ptf1a$^{Cre/+}$;LSL-Pik3ca$^{H1047R/+}$;Pten$^{lox/+}$*, *Ptf1a$^{Cre/+}$;LSL-Kras$^{G12D/+}$;LSL-Rosa26$^{Snail/+}$;Tnc$^{-/-}$*, *Ptf1a$^{Cre/+}$;LSL-Kras$^{G12D/+}$;LSL-Rosa26$^{Snail/+}$;Hnf4a$^{lox/+}$*, *Ptf1a$^{Cre/+}$;LSL-Kras$^{G12D/+}$;LSL-Rosa26$^{Snail/+}$;Hnf4a$^{lox/lox}$*, *Pdx1-Flp;FSF-Kras$^{G12D/+}$;Rosa26$^{CAG-CreERT2/+}$;Cdh1$^{lox/+}$*, *Pdx1-Flp;FSF-Kras$^{G12D/+}$;Rosa26$^{CAG-CreERT2/+}$;Cdh1$^{lox/lox}$*, *Pdx1-Flp;FSF-Kras$^{G12D/+}$;Rosa26$^{CAG-CreERT2/+}$;Cdh1$^{lox/lox}$;LSL-Trp53$^{R172H/+}$*, *Pdx1-Flp;FSF-Kras$^{G12D/+}$;Rosa26$^{CAG-CreERT2/+}$;Cdh1$^{lox/+}$;LSL-Trp53$^{R172H/+}$*, *Pdx1-Flp;FSF-Kras$^{G12D/+}$;Rosa26$^{CAG-CreERT2/+}$;Cdh1$^{lox/+}$;LSL-Trp53$^{R172H/R172H}$*, *Pdx1-Flp;FSF-Kras$^{G12D/+}$;Rosa26$^{CAG-CreERT2/+}$;Cdh1$^{lox/lox}$;LSL-Trp53$^{R172H/R172H}$*, *Ptf1a$^{Cre/+}$;LSL-Pik3ca$^{H1047R/+}$;Erk1$^{lox/+}$*, *Ptf1a$^{Cre/+}$;LSL-Pik3ca$^{H1047R/+}$;Erk1$^{lox/lox}$*, *Ptf1a$^{Cre/+}$;LSL-Kras$^{G12D/+}$;Erk1$^{lox/lox}$*, *Pdx1-Flp;FSF-Kras$^{G12D/+}$;Rosa26$^{CAG-CreERT2/+}$;Map2k1$^{lox/+}$;Map2k2$^{lox/+}$*, *Pdx1-Flp;FSF-Kras$^{G12D/+}$;Rosa26$^{CAG-CreERT2/+}$;Map2k1$^{lox/lox}$;Map2k2$^{lox/+}$*, *Pdx1-Cre;LSL-Kras$^{G12D/+}$;LSL-Trp53$^{R172H/+}$;Raf1$^{lox/+}$*, *Ptf1a$^{Cre/+}$;LSL-Kras$^{G12D/+}$;LSL-Pcna$^{ATG-fLucl/+}$*, *Ptf1a$^{Cre/+}$;LSL-Kras$^{G12D/+}$;Trp53$^{lox/lox}$;LSL-Pcna$^{ATG-fLucl/+}$*, *Ptf1a$^{Cre/+}$;LSL-Kras$^{G12D/+}$;LSL-Trp53$^{R172H/+}$;LSL-Pcna$^{ATG-fLucl/+}$*, *Pdx1-Flp;FSF-Kras$^{G12D/+}$;Fgfr$^{frt/frt}$;Trp53$^{frt/frt}$*, *Pdx1-Flp;FSF-Kras$^{G12D/+}$;Fgfr$^{frt/+}$;Trp53$^{frt/+}$*, *Ptf1a$^{Cre/+}$;LSL-Kras$^{G12D/+}$;*Snail$^{lox/lox}$*, *Ptf1a$^{Cre/+}$;LSL-Kras$^{G12D/+}$;LSL-Rosa26$^{Snail/Snail}$*, *Ptf1a$^{Cre/+}$;LSL-Kras$^{G12D/+}$;LSL-Trp53$^{R172H/+}$;LSL-Rosa26$^{Snail/+}$*, *Pdx1-Flp;FSF-Kras$^{G12D/+}$;Rosa26$^{CAG-CreERT2/+}$;LSL-Trp53$^{wt/+}$*, *Pdx1-Flp;FSF-Kras$^{G12D/+}$;Rosa26$^{CAG-CreERT2/+}$;LSL-Trp53$^{wt/wt}$*, *Pdx1-Flp;FSF-Kras$^{G12D/+}$;Rosa26$^{CAG-CreERT2/+}$;Pdk1$^{lox/+}$*, *Pdx1-Cre;LSL-Kras$^{G12D/+}$;LSL-Trp53$^{R172H/+}$;Pdk1$^{lox/+}$;Raf1$^{lox/lox}$*, *Pdx1-Flp;FSF-Kras$^{G12D/+}$;Trp53$^{frt/+}$;Rosa26$^{CAG-CreERT2/+}$;Pdk$^{lox/lox}$*. Pathologist PD Dr. med. Moritz Jesinghaus analyzed

the slides. All these mouse models were generated, bred and analyzed by all the members in the lab of Prof. Dieter Saur.

are associated with poor differentiaton, high levels of invasiveness and poor overall survival (Figure 13A and 13B). This study indicates *Spink4* tends to be associated with poor prognosis in PDAC as it is observed in colorectal cancer. *Gsta1* gene encodes glutathione S-transferase A1, which adds glutathione to target electrophilic compounds and plays an important role in the detoxification of therapeutic drugs, carcinogenes and toxins. Down-regulated *GSTA1* expression inhibits cell survival and promotes apoptosis in human non-small lung cancer cell lines (Kumar et al., 2020). In the present study, we find that G1 tumors have a higher expression level of *Gsta1* than the G4 cohort (Figure 12D). Proline-, histidine-, glycine-rich 1 is encoded by *Phgr1* gene. *Phgr1* is specific expressed in epithelial cells of intestinal mucosa and is highly expressed in the most differentiated cells in colorectal cancer (Oltedal et al., 2018). It is observed that *Phgr1* is highly expressed in the well-differentiated form of PDAC (G1 tumors) in the present study (Figure 12D). *Clca1* gene encodes calcium-activated chloride channel regulator 1 and has been shown to participate in the progression of colorectal, pancreatic and ovarian cancers (Hu et al., 2018; Li et al., 2017). One study shows the pancreatic cancer patients with upregulated *CLCA1* expression have longer survival, indicating CLCA1 is a promising biomarker candidate for PDAC prognosis (Hu et al., 2018). In clinical practice, patients with G1 have better survival time than those with G4. Figure 12D shows the G1 mice have higher expression level of *Clca1* than the G4 cohort. This result is consistent with the findings observed in the patients. Ly6/Plaur domain-containing 8 (Lypd8) is a glycosylated glycosylphosphatidylinositol-anchored protein. It has been reported that Lypd8 plays a critical role in preserving intestinal homeostasis by taking part in the segregation of intestinal bacteria and epithelia in the colon (Okumura et al., 2016). In colorectal cancer, overexpression of *Lypd8* inhibits the secretion TNF-α and IL-6 and has an inhibiting effect on cancer cell proliferation and migration (Xu et al., 2019). The present study shows *Lypd8* has a higher expression level in G1 tumors than G4 tumors (Figure 12D). E2f transcriptional factor 8 (E2f8) is one member of E2f family which binds to the promoters of target genes and regulate their transcriptional activities. Previous studies reported that, together with E2f7, E2f8 is important for mouse embryonic development and angiogenesis (Weijts et al., 2012). Upregulated *E2f8* expression promotes the progression and proliferation of prostate, breast and hepatocellular cancers (Deng et al., 2010; Lee et al., 2016; Ye et al., 2016). Moreover, *E2f8* overexpression is related to more aggressive features of papillary thyroid cancer (Sun et al., 2017). E2f8 also plays an important role in regulating the tumor

growth and invasion via EMT in cervical cancer (Kim et al., 2020). The present study shows a higher expression level of *E2f8* is associated with more aggressive PDAC (Figure 12D). The epithelial membrane protein 3 (*Emp3*) is one member of the peripheral myelin protein gene family. Non-small cell lung tumors have a lower expression level of *Emp3* than healthy lung tissue (Xue et al., 2013). It is also highly associated with the TNM staging system of lung cancer in the terms of tumor size, reginal lymph nodes and distant metastasis. In contrast to lung cancer, in hepatocellular carcinoma, the expression of *Emp3* gene is considerably higher in the tumor tissue than in the healthy liver tissue and is negatively correlated with the differentiation of tumors (Hsieh et al., 2015). The present study shows that *Emp3* is upregulated in G4 tumors, which are more invasive than G1 tumors, and is negatively correlated with the differentiation of pancreatic tumors (Figure 12D). The similar expression pattern of *Emp3* is observed in hepatocellular carcinoma. Vimentin, encoded by *Vim*, is an EMT marker and associated with cell migration and motility. Previous studies show that *Vim* expression is associated with the increased risk of metastasis in numerous tumor entities (Dauphin et al., 2013; Tian et al., 2013). Loss of *Vim* function results in primary tumors with lower grade and *Vim* is required for cancer invasion and metastasis via the interactions between cancer cells and CAFs in lung adenocarcinoma (Richardson et al., 2018). In this study, downregulated *Vim* expression is found in low grade (G1) tumors when compared with G4 tumors (Figure 12D). Upregulation of *Vim* expression is related to the G4 tumors which have a high metastatic potential in PDAC (Figure 9B and 12D). S100a4 belongs to the S100 calcium binding protein family. It has been observed that the *S100a4* expression level is associated with invasion and metastasis of numerous human malignant cancers (de Silva Rudland et al., 2006; Ikenaga et al., 2009; Ling and Li, 2014; Sagara et al., 2010; Tsuna et al., 2009). *S100a4* promotes the migratory phenotype of cancer cells and downregulated *S100a4* expression reduces the migrating activity of tumor cells as well as inhibits EMT in colon cancer (Stein et al., 2006). *S100a4* overexpression is significantly related to high histological grade and promotes tumor metastasis in breast cancer (Bresnick et al., 2015; Pedersen et al., 2002). The present study also shows upregulated *S100a4* expression is associated with the high grade PDAC primary tumors, which is an aggressive phenotype of PDAC (Figure 12D). Gremlin 1 protein, encoded by *Grem1*, is a glycoprotein and is an antagonist of secreted bone morphogenetic proteins (BMPs) (Nolan et al., 2014). BMPs belong to Tgfβ family and are involved in the initiation and progression of breast cancer by triggering the phosphorylation of Smad proteins (Heldin et al., 1997). One recent study revealed that high expression of *GREM1* is associated with metastasis in breast cancer and correlates with the poor prognosis of patients who are estrogen receptor (ER) negative (Neckmann et al., 2019). Figure 12D shows that upregulated *Grem1* expression is

related to invasive and more malignant phenotype of PDAC. *Fbln2* encodes fibulin 2 protein, a secreted ECM component. Fibulin 2 is abundant in the ECM of lung cancer and lung tumor cells derived from mouse models with metastasis (Argraves et al., 2003; Timpl et al., 2003). Loss of *Fbln2* impairs the migrating and invading ability of lung tumor cells, indicating the critical role of this gene in driving the malignant progression of lung cancer (Baird et al., 2013). In the present study, the expression of *Fbln2* is upregulated in the invasive PDAC, while it has lower expression level in the low grade primary tumors (Figure 12D). Fos related antigen 1 (Fra1), encoded by *Fosl*, is a leucine zipper protein and, in combination with Jun family, forms the transcription factor complex AP1. One study unveiled that high expression of *Fosl1* promotes the progression and metastasis of prostate cancer (Luo et al., 2018). In lung and pancreatic cancers, a high *Fosl1* expression level is associated with the poor prognosis of the patients with *Kras* mutation (Vallejo et al., 2017). In PDAC mouse models, G4 tumors show a higher *Fosl1* expression than the G1 cohort (Figure 12D).

Signaling pathway enrichment analysis gives us an insight into the mechanistic interactions of the gene set generated from the RNA-Seq results. Gene Ontology (GO) pathway database is used for the pathway enrichment analysis in this study. Figure 12E illustrates the result of this analysis. Actin is a conserved critical component of the cytoskeleton. Over 100 actin-binding proteins consistently remodel the cytoskeleton, which is subverted in tumor cells, and make contribution to the alteration of cell growth, migration and invasiveness (Stevenson et al., 2012). Actin binding proteins facilitate metastatic cancer cells to break down the cell-to-cell juctions in primary tumors and invade other tissues. This study identifies the interactions of actin binding proteins in high grade tumors (Figure 12E). Growth factors are polypeptides which bind to transmembrane receptors to stimulate the intracellular signaling pathways, including the PI3K, the mitogen-activated protein kinase (MAPK) and Smad proteins. The interactions and stimulations caused by growth factors promote tumor progression. It has been observed that growth factors induce basement membrane disruption, cancer cells penetration into other tissues, the departure of tumor cells from the bloodstream/lymphatic stream and subsequent colonization of distant niches (Yilmaz and Christofori, 2009). In this study, growth factor binding and activity are highlighted in the more malignant and invasive PDAC (Figure 12E).

### 6.4.2 Molecular signature of mitosis and its high correlation with tumor grades.

Abnormal proliferation is one of the most prominent features of tumors. Normal cells have a stringent control of cell division through a tight regulation of the production of factors that promote or inhibit cell proliferation. Continuous autostimulation of the mitotic activities caused

by abnormal production of cell cycle factors leads to uncontrolled proliferation of tumor cells. Reduced growth factor requirement of cancer cells is another reason of abnormal proliferation. Several genes and signaling pathways have been proved to be related to the proliferation of pancreatic tumor cells. Oncogenic *Kras* mutation supports PDAC proliferation by changing the metabolic signaling pathways (Ying et al., 2012). It has been reported that miR-21 promotes epidermal growth factor (EGF) induced proliferation by targeting Mapk/Erk and Pi3k/Akt pathways (Zhao et al., 2018). Recent studies reveal that tumor microenviroment also plays a critical role in the proliferation of tumors (Beatty and Gladney, 2015; Carr and Fernandez-Zapico, 2016; Martinez-Bosch et al., 2018). These studies indicate that upregulated proliferation of cancer cells in PDAC is the result of the interactions of multiple factors. Bulk tumor RNA-Seq provides a good tool to investigate the genes promoting the proliferation of PDAC and their interactions. This study analyzes the murine PDAC tumor samples and, based on the mitotic counts of their histopathology images, divides these samples into two groups, the high mitotic count group which has $\geqslant$5/10 high power fields (HPF) and the group with low mitotic count (<5/10 HPF). In order to define the molecular signature which influences the mitosis, differential gene expression analysis is performed in the RNA-Seq datasets of these two groups.

The differential gene expression analysis shows the expression of 19 genes is upregulated and 16 genes present downregulated expression in the group with high mitotic counts, compared with the tumors with low mitotic counts (Figure 14A). Three clusters can be identified in the heatmap of the differential gene expression analysis (Figure 14B). Most of the mouse PDAC tumors in the first cluster (on the left side of the heatmap) have high mitotic counts, while the third cluster (on the right side of the heatmap) consists of the mice with low mitotic counts and only two tumors with high mitotic counts (Figure 14B). Cellular retinoic acid bing protein 1, encoded by *Crabp1*, binds to retinoid acid (RA) and is related to the transportation of RA. In breast cancer, the significantly upregulated CRABP1 level is associated with poor prognosis of patients, high Ki67 expression as well as high tumor grade (Liu et al., 2015). Crabp1 can attenuate cell growth arrest induced by RA (Liu et al., 2015). Figure 14B shows that the elevated expression of *Crabp1* gene correlates with the high mitotic activity and high tumor grade in PDAC. As metioned before, *S1004a* is related to invasion and metastasis of several cancers (de Silva Rudland et al., 2006; Ikenaga et al., 2009; Ling and Li, 2014; Sagara et al., 2010; Tsuna et al., 2009). *S1004a* also plays an important role in the proliferation of several cancers. Upregulated *S100a4* expression is associated with the higher proliferation activity and tumor grade in glioma (Jin et al., 2015). Downregulation of *S100a4* leads to the inhibition of cell growth and causes apoptosis in

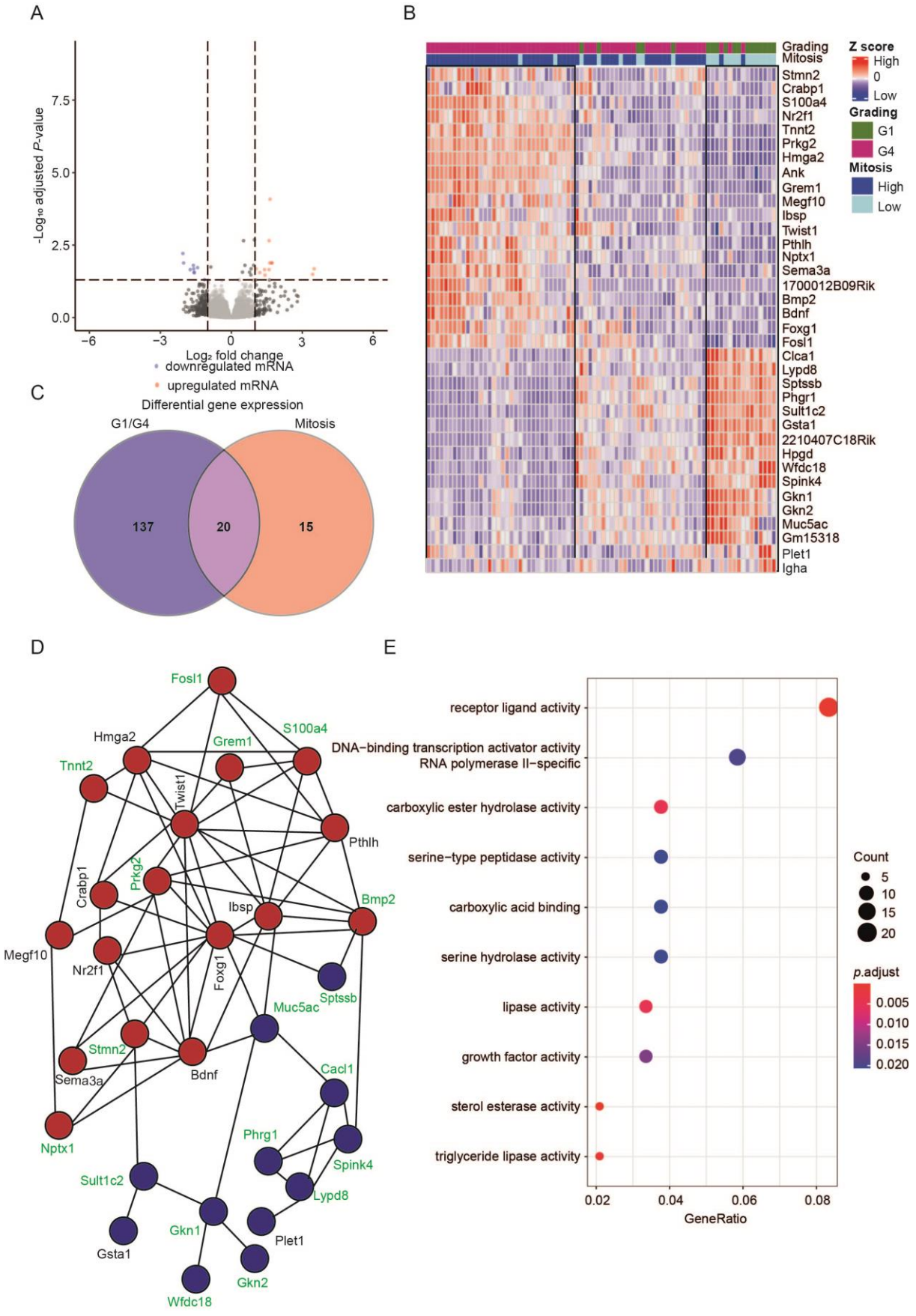


**Figure 14. Transcriptional features of mitosis in mouse PDAC tumors.**

(A) The volcano plot of differential gene expression analysis between the groups with high (⩾5/10 high-power fields, HPF) and low (<5/10 HPF) mitotic counts ($Log_2$ fold change >1 or < -1 and $-Log_{10}$ adjusted *p* value > 1.25). G1: n=18. G4: n=62. HPF: high power fields.
(B) Heatmap of differential gene expression analysis between the groups with high and low mitotic counts. G1: n=18. G4: n=62.
(C) The Venn diagram between the gene sets from differential gene expression analysis of G1/G4 and two mitotic count groups.
(D) Interaction network of the genes from differential gene expression analysis between the groups with high and low mitotic counts. Red dots indicate upregulated genes and blue dots indicate downregulated genes in tumors with high mitotic counts. The genes highlighted in green belong to the intersection part in Figure 14C.
(E) Signaling pathway enrichment based on the differential gene expression analysis between the groups with high and low mitotic counts.
Bioinformatician Fabio Boniolo did the differential expression analysis (Figure 14A and 14C) and the enrichment of signaling pathways (Figure 14E). All these mouse models were generated, bred and analyzed by all the members in the lab of Prof. Dieter Saur. Mouse dissection, RNA preparation and RNA-seq were performed by all the members in the lab of Prof. Dieter Saur.

thyroid cancer cells (Jia et al., 2013). The present study reveals that upregulated *S1004a* expression is related to highly active mitosis as well as high tumor grade in pancreatic cancer (Figure 14B). *Nr2f1* encodes nuclear receptor subfamily 2 group F member 1 protein. A recent study demonstrates that *Nr2f1* promotes cancer cell proliferation and invasion by activating Cxcl12/Cxcr4 signaling pathway in salivary adenoid cystic carcinoma (SACC) (Gao et al., 2019). The heatmap of the differential gene expression indicates upregulated *Nr2f1* expression is positively related to mitosis and high tumor grade in the mouse pancreatic tumors (Figure 14B). The high mobility group A2 protein, encoded by *Hmga2* gene is a transcription factor which binds to AT-rich sites in the minor groove of DNA to control transcription activity of numerous genes and influences the structures of chromatins. It has been observed that the *Hmga2* transcription is induced by Tgf-β which in turn activates EMT (Thuault et al., 2006). The *Hmga2* overexpression caused by non-random chromosomal translocations has been found in many mesenchymal tumors (Dreux et al., 2010; Schoenmakers et al., 1995). It is suggested that *Hmga2* influences the cell cycle of cancer cells. Ovarian cancer cells are arrested in G1 phase when the expression of *Hmga2* is downregulated (Malek et al., 2008). In addition, decreased *Hmga2* expression results in G2/M arrest through Pi3k/Akt/mTor pathway in acute myeloid leukemia (AML) cells (Tan et al., 2016). Moreover, it is reported that Hmga2 interacts directly with the E2f-responsive DNA elements and promotes the E2f1 activation, thereby leading to the progression of cell cycle in pituitary adenomas (Seville et al., 2005). In the present study, it is observed *Hmga2* expression is also upregulated in the tumors with high mitotic counts in PDAC (Figure 14B), indicating increased *Hmga2* expression also promotes the proliferation of cancer cells in pancreatic cancer. A recent study reveals that increased *Grem1* expression promotes proliferation and colony formation of gastric cancer (GC) cells *in vitro* (Sun et al., 2020). The

elevated *Grem1* expression is observed in mouse pancreatic tumors with a high mitotic activity (Figure 14B). This provides evidence that *Grem1* promotes the proliferation of cancer cells in PDAC. Multiple EGF-like domains 10 (Megf10) belongs to the multiple EGF-like domains protein family which is responsible for cell proliferation, adhesion and motility. High *Megf10* expression is associated with the active proliferation of glioma cells (Li et al., 2018). The finding of the present study suggests *Megf10* expression is upregulated in the PDAC tumors with high mitotic counts (Figure 14B). It is well-known that *Twist1* is one of the key inducers of EMT. It also influences the proliferation of numerous cancers. A previous study demonstrated that *Twist1* overexpression induces cell cycle progression through binding to the promoter of *Foxm1*, leading to the upregulation of *Foxm1* expression in GC (Qian et al., 2013). As a key downstream effector of p62, the presence of both Twist1 and p62 increases tumor growth (Qiang et al., 2014). In the present study, it is observed that the mitotic activity in PDAC samples is positively related to the expression level of *Twist1*.

Intriguingly, the differential gene expression analysis reveals that mitosis activity and tumor grades are closely correlated in the gene expression level. The gene sets identified by the differential gene expression analysis between tumors with a high and low mitotic activity also define the transcriptional signatures of G1 or G4 tumors in PDAC mouse models (Figure 14B). This study already shows that there is a strong correlation between tumor grades and mitotic counts based on the histopathology image analysis (Figure 8B). The close relationship between mitosis and tumor grades in the levels of both histopathology image analysis and transcriptional profiles suggests that the mitotic activity is one of the most important factors influencing the progression and malignancy of PDAC in mouse models. The gene set to identify G1 and G4 tumors has been defined (Figure 14C and 14D). This study finds the expression of 20 genes which can influence tumor grades and mitosis (Figure 14C). These genes are *Gkn1*, *Gkn2*, *Wfdc18*, *2210407C18Ri*, *Nptx1*, *Bmp2*, *Grem1*, *Lypd8*, *Sult1c2*, *S100a4*, *Fosl1*, *Tnnt2*, *1700012B09Rik*, *Spink4*, *Stmn2*, *Sptssb*, *Clca1*, *Prkg2*, *Phgr1* and *Muc5ac*. These genes have been proved to be associated with cancer cell proliferation and prognosis of cancer patients. For example, patients with advanced GC show lower *Gkn1* expression than those in the early stage (Yoon et al., 2019), indicating low *Gkn1* expression leads to poor prognosis. In line with the previous study, the present study inidicates downregulated *Gkn1* expression is associated with the higher tumor grade. Gastrokine 2, encoded by *Gkn2* shows a decreased expression level in GC (Dai et al., 2014). *Gkn2* overexpression results in cell cycle arrest in G1/S transition phase and therefore inhibits proliferation of gastric cancer cells (Dai et al., 2014). Decreased *GKN2* expression is associated with metastasis and poor patient prognosis (Dai et al., 2014; Moss et al., 2008). The differential gene expression analysis of this study shows that downregulated *Gkn2*

expression correlates with high mitotic counts and higher tumor grade in the mouse PDAC models. Neuronal pentraxin 1 (Nptx1) belongs to the long pentraxin protein family. High *NPTX1* expression has been shown to be associated with poor patient prognosis and tumor growth in hepatocellular carcinoma (Zhao et al., 2019). This study reveals upregulated *Nptx1* expression is associated with a high mitotic activity and a more malignant phenotype in mouse pancreatic tumors (Figure 14B). In line with previous studies, the present study demonstrates that downregulated expression of *Clca1* and upregulated expression of a *Grem1*, *S100a4* and *Fosl1* promote cancer cell proliferation and lead to higher tumor grade in PDAC (Figure 14B).

The interaction of these genes is investigated. This study employs the online database, STRING (https://string-db.org), to study the interaction network of the mentioned genes. Figure 14D shows the result of the analysis. The proteins which show upregulated expression are indicated with red dots and are at the top of the interaction network graph (Figure 14D). At the bottom, it shows the downregulated proteins which are indicated with blue dots (Figure 14D). Foxg1, Ibsp, Bdnf and Muc5ac play the essential roles in this network. Foxg1, Ibsp and Bdnf promote mitosis and progression of PDAC in this study. Overexpression of *Foxg1* facilitates the tumor proliferation in glioblastoma and mediates metastasis of the cancer cells through Wnt/β-catenin pathway in hepatolcellular carcinoma (Wang et al., 2018; Zheng et al., 2019). Increased *Ibsp* expression is associated with poor prognosis of esophageal squamous cell carcinoma (Wang et al., 2019a). High *BDNF* expression is correlated with shorter malignant pleural mesothelioma (MPM) patient survival (Smeele et al., 2018) and downregulated expression of this gene suppress proliferation of the cancer cells of lung squamous cell carcinoma (Ozono et al., 2017). Decreased *Muc5ac* expression is associated with more proliferative activities and a more malignant phenotype in mouse PDAC models (Figure 14B). In line with the present study, one previous study shows that high *MUC5AC* expression improves the prognosis of the advanced-stage PDAC patients (Higashi et al., 2015).

Furthermore, the signaling pathway enrichment analysis is performed to investigate the interactions of the gene set generated from differential gene expression analysis. Receptor ligand activity is highlighted in the analysis (Figure 14E). There are various predictive and confirmative receptor-ligand interactions within the genes with significantly different expression and between them and other genes. In GC, *Bmp2* encodes a secreted ligand which binds to Tgf-β receptors proteins and modulates cancer cell proliferation (Wen et al., 2004). The interactions between estrogen receptor-α and its ligands have been proved to make contribution to the induction of breast cancer cell proliferation (Nwachukwu et al., 2016). DNA-binding transcription activator activity also plays an important role in the

proliferation of PDAC (Figure 14E). For example, Fosl1 is a transcriptional factor and mediates the proliferation of cancer cells in pancreatic cancer (Yang et al., 2019).
The present study has identified the molecular signature influencing the mitosis of cancer cells in PDAC. Interestingly, the strong correlation between mitosis and tumor grades in both histopathology and transcriptional levels has been observed.

### 6.4.3 Molecular signature of liver metastasis and its high correlation with tumor grades.

A high metastatic propensity is one of the causes of PDAC lethality. More than 90% pancreatic cancer patients develop metastatic diseases. After surgical resection, recurrences are still developed in the majority of the PDAC patients (Conroy et al., 2018; Oettle et al., 2007; Sinn et al., 2017). Liver is the dominant metastatic site in the patients with advanced stages (Ryan et al., 2014). As little evidence has supported that liver metastasis resection can improve the prognosis of the patients, resection of liver metastasis in PDAC patients is not recommended in clinical practice (Tempero et al., 2017). The molecular mechanism of the liver metastasis in colorectal cancer has been investigated and the studies identify the potential therapeutic targets, such as *Cxcr4*, *Cxcr6* and *Ccl2* (Kawada et al., 2011). As opposed to liver metastasis of colorectal cancer, our understanding of this metastasis in PDAC is poor. The present study aims to identify the transcriptional features related to liver metastasis to provide the insight into metastasis in PDAC.
The differential gene expression analysis has been performed between the primary tumors from PDAC mice with or without liver metastasis. The expression of 3 genes is upregulated and the expression of 10 genes is downregulated in the cohort with liver metastasis (Figure 15A). Most of the tumor samples with liver metastasis are clustered on the right side of the heatmap of the differential gene expression analysis (Figure 15B). There is the correlation between histopathology grades and the transcription profiles of the primary tumors with liver metastasis in the PDAC mouse models (Figure 15B). *Gkn1* expression results in upregulated *Cdh1* expression and downregulated *β-catenin*, Vimentin and *Snail* expression, and suppresses EMT by inactivation of the Pi3k/Akt signaling pathway in GC (Yoon et al., 2011). However, one recent study reports that the expression of *Gkn1* enhances the metastasis of lung cancer in mouse models and results in poor survival (Yao et al., 2019). In our study, *Gkn1* is downregulated in most of the PDAC mice with liver metastasis and these mice have the most malignant tumors (G4) (Figure 15B). The *CLCA1*

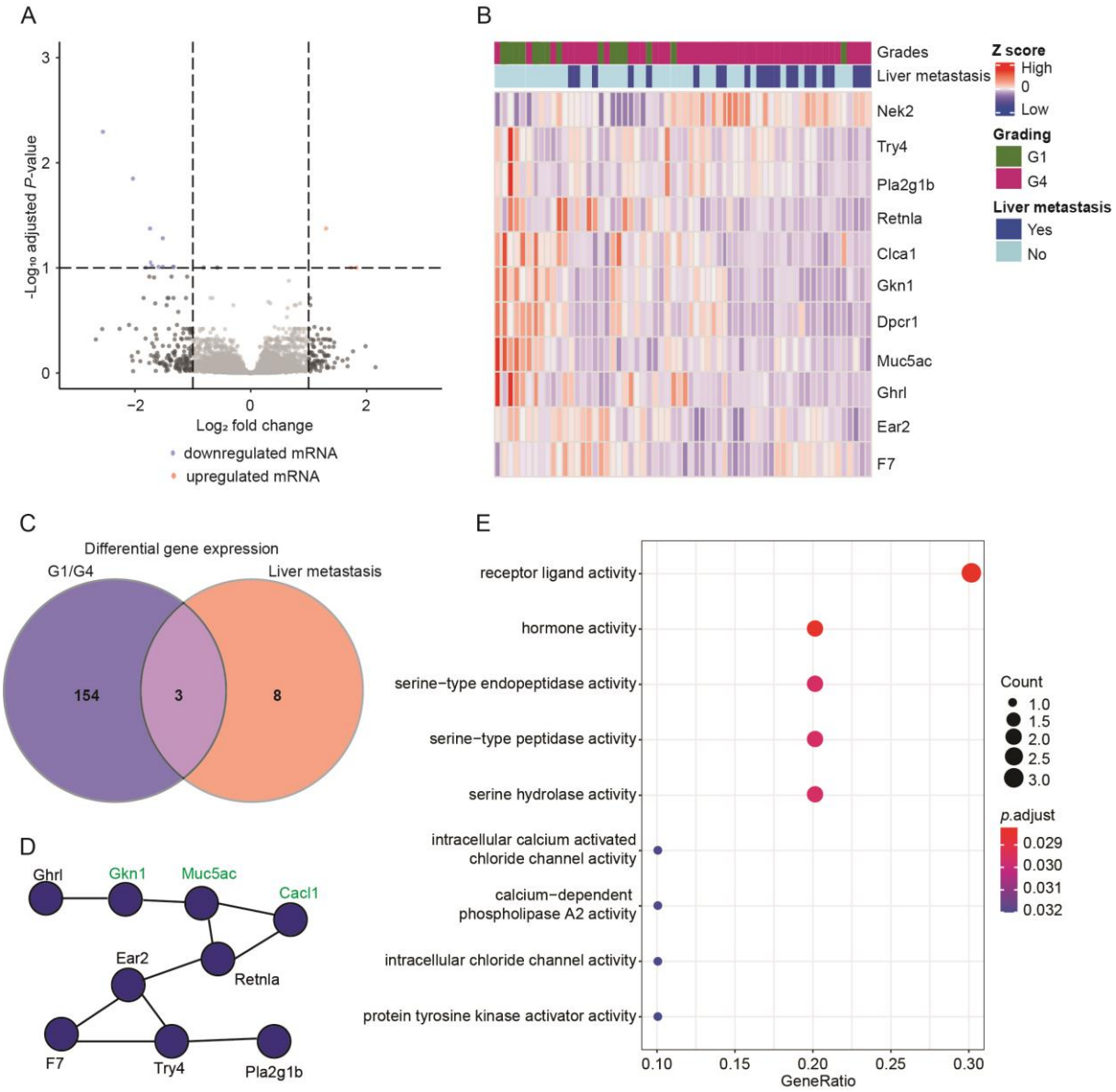


**Figure 15. Transcriptional features of liver metastasis in mouse PDAC tumors.**
(A) The volcano plot of differential gene expression analysis of primary mouse pancreatic ductal adenocarcinoma (PDAC) with or without liver mestasis ($Log_2$ fold change >1 or < -1 and $-Log_{10}$ adjusted *p* value > 1). G1: n=15. G4: n=48.
(B) Heatmap of differential gene expression analysis between the groups with or without liver metastasis. G1: n=15. G4: n=48.
(C) The Venn diagram between the gene sets from differential gene expression analysis of G1/G4 and two liver metastasis groups.
(D) Interaction network of the genes from differential gene expression analysis between the groups with or without liver metastasis. Blue dots indicate downregulated genes in tumors with metastasis. The genes highlighted in green belong to the intersection part in Figure 15C.
(E) Signaling pathway enrichment based on the differential gene expression analysis between the groups with or without liver metastasis.
Bioinformatician Fabio Boniolo performed the differential expression analysis (Figure 15A and 15C) and the enrichment of signaling pathways (Figure 15E). All these mouse models were generated, bred and analyzed by all the members in the lao of Prof. Dieter Saur. Mouse dissection, RNA preparation and RNA-seq were performed by all the members in the lab of Prof. Dieter Saur.

mRNA expression level inversely correlates with metastasis and patient stages of colorectal cancer through the suppression of the Wnt/β-catenin pathway (Li et al., 2017). Knockdown of *Clca1* leads to lower rate of metastasis in ovarian cancer (Musrap et al., 2015). A low *Clca1* expression level is significantly related to poor prognosis of PDAC (Hu et al., 2018). In line with the previous literature, this study reveals that downregulated *Clca1* expression is found in the tumor with the high grade and associated with liver metastasis in PDAC mouse models (Figure 15B). *Muc5ac* overexpression results in enhanced tumor progression and metastatic lesions in mouse models of colorectal cancer (Pothuraju et al., 2020). The expression level of *Muc5ac* deceases in the poorly differentiated gastric tumors and the decreased *Muc5ac* expression results in an increase in tumor invasion depth and number of metastatic lymph nodes in GC (Ilhan et al., 2010). This study shows that *Muc5ac* has a similar effect on PDAC as it does in GC and downregulated *Muc5ac* expression is associated with liver metastasis and the high tumor grade in PDAC (Figure 15B). NIMA-related expressed kinase 2, encoded by *Nek2*, has shown upregulated expression in numerous cancers, including ovarian, breast, lung, liver and colorectal cancers (Cappello et al., 2014; Chang et al., 2018; Liu et al., 2014; Neal et al., 2014; Zhong et al., 2014). Upregulated *Nek2* expression is associated with proliferation and metastasis of cancers. One previous study demonstrated that *Nek2* regulates the *Cdh1* and *MMP9* expression and therefore enhances metastasis of hepatocellular carcinoma (Chang et al., 2018). The present study shows that elevated *Nek2* expression correlates with liver metastasis in PDAC mouse models (Figure 15B).

The interactions of the proteins are shown in Figure 15D. Notably, Ear2 and Retnla serve the central roles in this interaction network. To investigate the signaling pathways that contribute to the liver metastasis of PDAC, signaling pathway enrichment is performed. Proteases can degrade the ECM and thus facilitate the invasion and migration of cancer cells. The overexpression of serine proteases is associated with high tumor grades, metastasis and poor prognosis in prostate cancer (Saleem et al., 2006). In colorectal cancer the presence of serine-type proteases results in tumor growth and metastasis (Tsai et al., 2007; Vogel et al., 2006). Moreover, the overexpression of serine proteases correlates with increasing tumor grades and the invasion and migration of cancer cells in breast cancer (Yamamoto et al., 2018; Zoratti et al., 2015). In the present study, serine-type peptidase activity is also observed in PDAC tumors with liver metastasis (Figure 15E). High tumor grade is also associated with serine-type peptidase activity (Figure 15E). Furthermore, ion channels have been proved to play a critical role in the progression of cancers. Chloride channels take a prominent place in tumorigenesis and are associated with the migration of cancer cells (Cuddapah and Sontheimer, 2011; Prevarskaya et al., 2010). Intracellular chloride channels are involved in the progression and invasion of cancers, and proteins from

this family have been identified in numerous cancers, including colorectal, lung, gastric, and ovarian cancers (Deng et al., 2014; Okudela et al., 2014; Tang et al., 2013; Wang et al., 2014). For example, one study demonstrated that chloride intracellular channel 1 regulates the metastasis of cancer cells through the reactive oxygen species (ROS)/ERK signaling pathway in the hypoxia-reoxygenation (H-R) process in colon cancer (Wang et al., 2014). Chloride intracellular channels are involved in liver metastasis and high tumor grade (Figure 15E). Phospholipase A2 ($PLA_2$) catalyses hydrolysis of fatty acids and has been proved to be involved in the migration of several cell types, including cancer cells. One clinical research reveals that $PLA_2$ is related to EGFR expression and results in poor patient diagnosis in breast cancer (Caiazza et al., 2011). The present study shows that calcium-dependent phospholipase A2 takes part in liver metastasis and is associated with the undifferentiated tumor phenotype (Figure 15E).

The analysis of the transcriptional profiles of the PDAC mice with and without liver metastasis is helpful to define the gene expression features related to the ability of tumor cells to metastasize to the liver and identify the gene set and signaling pathways that potentially contribute to the formation of liver metastasis. This study also provides the evidence for the link between the undifferentiated phenotype and metastasis.

### 6.4.4 Identification of immune cell subpopulations associated with tumor grades in PDAC.

PDAC has abundant stromal content with massive ECM deposition. Immune cells are one of the important components of the stroma in PDAC, accounting for about 50% of PDAC cellular components (Clark et al., 2007). The distribution and function of immune cells are influenced by their interactions with cancer cells and other components of the ECM (Feig et al., 2012). It has been revealed that immune cells, including tumor-associated macrophages and Treg cells, mediate immune evasion and promote the progression of PDAC (Zheng et al., 2013). Mutational burden influences anti-tumor immunity (Stone and Beatty, 2019). Oncogenic *Kras* mutations induce the secretion of growth factors, cytokines and chemokines to evade immune responses and promote inflammation, resulting in tumor progression and invasion (Dias Carvalho et al., 2018). Previous studies have demonstrated that oncogenic *Kras* mutations are involved in the regulation of myeloid and T cell populations (Liou et al., 2015; Tran et al., 2016; Zdanov et al., 2016). The roles of the immune cells in the progression and invasion of PDAC have been the focus of several studies. It has been reported that the expression of *CXCL1* and *VEGF* in tumor associated macrophages is

associated with vascular structure and depletion of this type of macrophages in PDAC mouse models remarkably suppresses metastasis and leads to impaired angiogenesis (Caiazza et al., 2011; Huang et al., 2018). To facilitate the elucidation of the roles played by infiltrating immune cells in cancers, computational methods for deconvolution of the transcriptional profiles of bulk tumor samples have been developed.

To characterize the immune contents within the TME of pancreatic cancer, the immune cells in the tumors from 80 PDAC mice are analyzed through deconvolution of the transcriptomic profiles by an experienced bioinformatician Fabio Boniolo. The composition of the immune microenvironment of the tumors in G1 and G4 cohorts varies, indicating the heterogeneity of immune cell infiltration related to the tumor grades in PDAC (Figure 16A).

There is significant difference in the composition of M2 macrophage, plasmacytoid dendritic cells, type 2 T helper (Th2) cells and memory B cells between G1 and G4 cohorts (Figure 16B, 16C, 16D and 16E). Macrophages are part of the innate immune system. Accumulating evidence reveals that tumor associated macrophages are an important cellular component of the TME of PDAC and play a critical role in the regulation of the initiation development and progression of pancreatic cancer. Clinical studies demonstrate that M2 macrophages are associated with metastasis and survival time of PDAC patients (Kurahara et al., 2011; Zheng et al., 2013). M2 macrophages are shown to promote immunosuppressive environment by inhibiting anti-tumor responses and supporting tumor escape (Kurahara et al., 2011; Movahedi et al., 2010). They are also involved in vascularization and degradation of ECM proteins and therefore promote angiogenesis and tumor invasiveness (Coffelt et al., 2009; Gocheva et al., 2010; Hagemann et al., 2004). The present study shows that there are more M2 macrophages in the well-differentiated PDAC tumors (Figure 16B), indicating these innate immune cells may support the development and progression of PDAC. One recent study revealed that the presence of M2 macrophages is associated with gemcitabine resistance in PDAC (Bulle et al., 2020). Considering TME components serve critical roles in drug resistance (Sharma et al., 2017) and G1 tumors have more stroma than the G4 cohort in pancreatic cancer (Figure 10B), the finding in the present study indicates that M2 macrophages might be an important stromal component which is involved in drug resistance in PDAC. Plasmacytoid dendritic cells are known as the producers of high levels of type I interferons. Clinical studies show that the presence of plasmacytoid dendritic cells is an indicator of poor prognosis in breast, oral and ovarian cancers (Han et al., 2017; Labidi-Galy et al., 2012; Treilleux et al., 2004). Plasmacytoid dendritic cells support the immunosuppressive environment by the induction of Tregs through the inducible costimulator (ICOS) and inducible costimulator ligand (ICOS-L) signaling pathways or the upregulated expression of indoleamine 2,3-dioxygenase (IDO) (Vermi et al., 2011). It is also observed

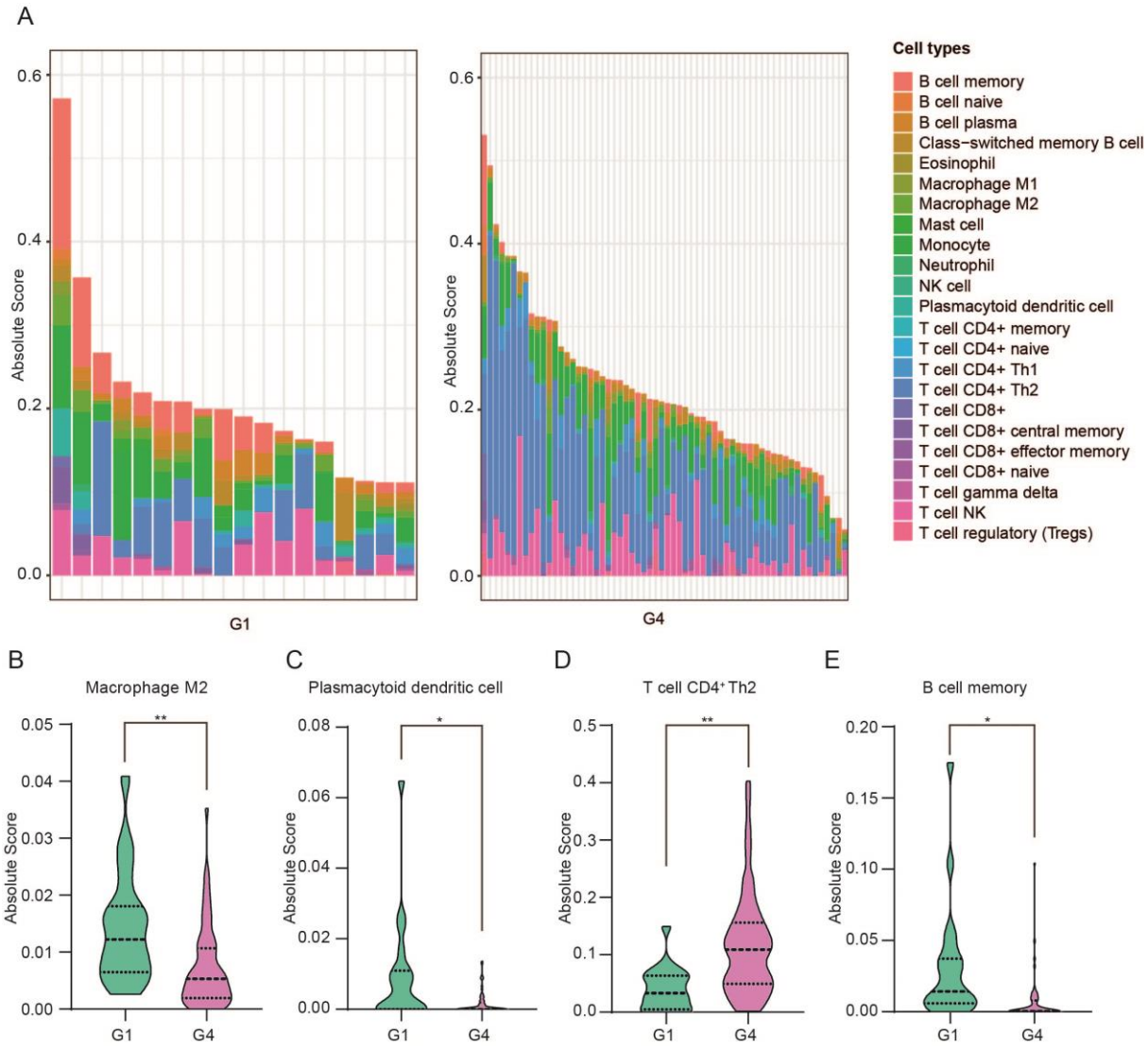


**Figure 16. Characterization of immune cell subpopulations using RNA-Seq data.**
(A) The absolute immune score of pancreatic ductal adenocarcinoma (PDAC) tumour samples based on RNA-Seq dataset.
(B) The absolute immune score of M2 macrophage in G1 and G4 cohorts. ***p*<0.01, Student's t test.
(C) The absolute immune score of plasmacytoid dendritic cells in G1 and G4 cohorts. **p*<0.05, Student's t test.
(D) The absolute immune score of $CD4^+$ T helper 2 (Th2) in G1 and G4 cohorts. ***p*<0.01, Student's t test.
(E) The absolute immune score of B cell memory in G1 and G4 cohorts. **p*<0.05, Student's t test.
G1: n=18. G4: n=62. Bioinformatician Fabio Boniolo performed the deconvolution of the transcriptomic profiles for immune cell subpopulations (Figure 16A). All these mouse models were generated, bred and analysed by all the members in the lab of Prof. Dieter Saur. Mouse dissection, RNA preparation and RNA-seq were performed by all the members in the lab of Prof. Dieter Saur.

that plasmacytoid dendritic cells produce the cytokine IL-1α to induce neoangiogenesis and invasion of human non-small cell lung cancer (Sorrentino et al., 2015). These studies reveal the pro-tumorigenic effect of plasmacytoid dendritic cells. In contrast to their immunosuppressive effect, plasmacytoid dendritic cells also show an anti-tumorigenic capacity. Previous studies demonstrated plasmacytoid dendritic cells can activate $CD8^+$ T

cells, myeloid dendritic cells (mDCs) and NK cells to initiate anti-tumor immunity in melanoma (Guery et al., 2014; Lelaidier et al., 2015; Liu et al., 2008). It is also reported that plasmacytoid dendritic cells kill cancer cells and inhibit tumor growth by activation of $CD8^+$ T cells and NK cells in breast cancer (Wu et al., 2017). High levels of plasmacytoid dendritic cells correlate with prolonged survival in breast cancer patients (Kini Bailur et al., 2016). This present study shows that the G4 cohort has a lower level of plasmacytoid dendritic cells compared with the mice with well differentiated tumors (Figure 16C). This finding reveals that plasmacytoid dendritic cells correlate with pancreatic malignancy, indicating these immune cells as a potential prognostic marker of PDAC. $CD4^+$ Th cells are classified into 3 subgroups, type 1 T helper (Th1) cells, Th2 cells and type 17 T helper (Th17) cells, and are mainly involved in tumor immunology (Zhou et al., 2009). IL-4, IL-5 and IL-10 are Th2-secreted cytokines and are associated with tumor growth and metastasis in hepatocellular carcinoma and melanoma (Budhu et al., 2006; Enninga et al., 2016). One study demonstrated that the presence of Th2 cell infiltration results in reduced overall survival of PDAC patients (De Monte et al., 2011). G4 tumor mice have a higher level of Th2 cells compared to the G1 cohort (Figure 16D). G4 is the most malignant phenotype of primary tumor in PDAC and is associated with poor prognosis. Therefore, the results of this study are in line with the previous study from De Monte and colleagues (De Monte et al., 2011), providing the evidence of the correlation between Th2 cells and PDAC pathology. Memory B cells is one long-lived subtype of B cells. They promote T cell expansion and initiate memory formation by presenting antigens. Memory B cells participate in the antitumor responses by producing interferon γ (IFN-γ), TNF-related apoptosis-inducing ligand (TRAIL) and granzyme B and cooperate with $CD8^+$ T cells in ovarian and liver cancers (Nielsen et al., 2012; Shi et al., 2013). Memory B cell infiltration is associated with favourable prognosis in hepatocellular carcinoma (Shi et al., 2013). The present study reveals G1 tumors, which are associated with better prognosis than G4 tumors, have a higher level of memory B cells (Figure 16E). This finding is consistent with the results in hepatocellular carcinoma patients.

This study characterizes the immune microenvironment of pancreatic tumors by employing the computational method of the deconvolution of the transcriptomic profiles from murine PDAC tumors. The composition of four immune subpopulations, namely M2 macrophages, plasmacytoid dendritic cells, Th2 cells and memory B cells, shows significant difference between G1 and G4 cohorts. This result indicates these subpopulations potentially influence the pathogenesis of PDAC.

## 6.5 Generation of a new mouse model allowing to inactivate endogenous *Kras$^{G12D}$*.

Oncogenic *Kras* mutation is the most remarkable genetic event in the PDAC initiation and progression. G12, G13 and Q61 are the main *Kras* mutation sites in human pancreatic cancer. The G12 mutation is the predominant mutation, accounting for approximately 98% of the *Kras* mutations. G12D, one of the most common mutations, makes up more than 51% of G12 mutations. To investigate the role of this oncogenic *Kras* mutation in the PDAC, a conditional *Kras$^{G12D}$* transgene mouse model was established. As reported by prevous studies, the expression of *Kras$^{G12D}$* is controlled by a *tet*-operator which is under the control of a *loxP-stop-loxP (LSL)* cassette (Ying et al., 2012). This mouse model is crossed with the mouse model with *LSL-Rosa26$^{rtTA\text{-}IRES\text{-}GFP/+}$*and with *Ptf1a$^{Cre/+}$* generated by Ying and colleagues (Ying et al., 2012). This generated GEMM harboring triple transgenes is designated as *iKras* strain (Ying et al., 2012). The expression of oncogenic *Kras* is induced by doxycycline (doxy). With the *iKras* strain, it has been proved that the *Kras* mutation is essential for the progression of PDAC and this mutation regulates the anabolic glucose metabolism to maintain PDAC tumors (Ying et al., 2012). However, subsequent studies reported that 70% of the *iKras* mice incur tumor relapse after the withdrawal of doxycyclin (Kapoor et al., 2014). The relapse tumors show a high expression level of oncogenic *Kras* while the endogenous WT *Kras* alleles remain intact (Kapoor et al., 2014). These findings indicate that the *iKras* mouse model has a leaky oncogenic *Kras* expression independent of the *tet* system. In order to overcome this drawback, this study develops a mouse model that introduces a *loxP* flanked *Kras$^{G12D}$* mutation in the endogenous *Kras* locus and allows the inactivation of endogenous oncogenic *Kras$^{G12D}$*.

Figure 17 shows the process of the development of this mouse model. Homologous recombination introduces the *FSF-Kras$^{lox\text{-}G12D\text{-}lox}$* to the genome of mouse embryonic stem (ES) cells. Microinjection of these ES cells with targeted *Kras* allele into blastocysts is performed to generate the mice with *FSF-Kras$^{lox\text{-}G12D\text{-}lox}$*. The mice with pancreatic specific *Flp* and those with *FSF-Rosa26$^{CAG\text{-}CreERT2}$* are crossed with the mice *FSF-Kras$^{lox\text{-}G12D\text{-}lox}$*. *Flp* induces the expression of the endogenous *Kras$^{G12D}$* by the recombination of two *frt* sites. TAM treatment allows CreER$^{T2}$ to remove the G12D mutation and therefore inactivates oncogenic *Kras* expression.

The targeting vector consists of a *frt* flanked stop cassette containing neomycin resistance (*neo*) cassette, a *loxP* flanked G12D mutation in *Kras* locus and DTA cassette. This targeting vector is linearized by PmlI and electroporated into 129 ES cells. The ES clones with targeted allele are identified by PCR. The PCR product of the targeted allele is 3933 bp and there are 9 clones with the targeted allele (Figure 18A and 18B). The presence of the distal

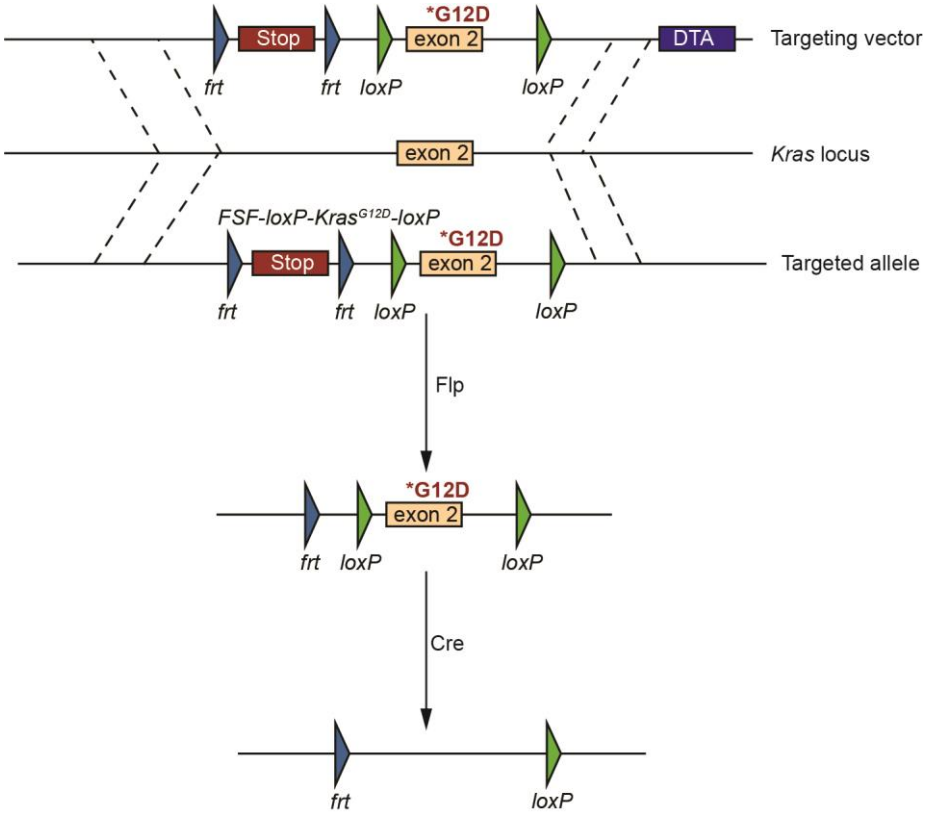


**Figure 17. The schematic design of a new mouse model with *FSF-Kras$^{lox\text{-}G12D\text{-}lox}$*.**
The targeting vector contains *FSF-Kras$^{lox\text{-}G12D\text{-}lox}$-DTA* and is transferred to embryonic stem (ES) cells with wild-type (WT) *Kras*. After homologous recombination, the targeted allele harbors the *FSF-Kras$^{lox\text{-}G12D\text{-}lox}$* cassette. The mice with *FSF-Kras$^{lox\text{-}G12D\text{-}lox}$* are generated by microinjection of gene targeted ES cells into blastocysts. The incorporation of targeted ES cells into the developing embryo of donor blastocyst results in chimeric offsprings. The positive mice, which are confirmed by polymerase chain reaction (PCR), is F0. A stable F1 generation mouse model was obtained by mating positive F0 generation mice. F1 mice with *FSF-Kras$^{lox\text{-}G12D\text{-}lox}$* are crossed with those with *Flp* and those with *Rosa26$^{CAG\text{-}CreERT2}$*. Flp removes the *FSF* cassette, allowing the expression of the endogenous *Kras$^{G12D}$*. Application of tamoxifen (TAM) activates Cre recombinase, removes the oncogenic *Kras$^{lox\text{-}G12D\text{-}lox}$* mutation therefore inactivating endogenous oncogenic *Kras$^{G12D}$* expression. *FSF*: *frt-stop-frt*. DTA: diphtheria toxin A. The targeting vector has been generated by Barbara Seidler and Andreas Arbeiter in the lab of Prof. Dieter Saur.

*loxP* is examined by PCR and BglII digestion. *Kras* WT allele has a BglII endonuclease digestion site while the BglII digestion site is disrupted by the distal *loxP* site. Therefore, PCR is used to amplify the fragment containing the BglII digestion site and the distal *loxP* site. If the PCR product can be cut completely, the distal *loxP* is lost. All the targeted clones except Clone 2 have the distal *loxP* site (Figure 18C). Quantitative real time PCR (qRT-PCR) of genomic DNA of the targeted ES cells is performed for the quantification of the copy number of the targeted allele. The result shows that all the clones have one copy of the targeted allele (Figure 18D). Two ES clones are sent for the microinjection. The founder mice (F0) are crossed to generate the *FSF-Kras$^{lox\text{-}G12D\text{-}lox}$* mice (F1). To examine if recombination of *loxP*

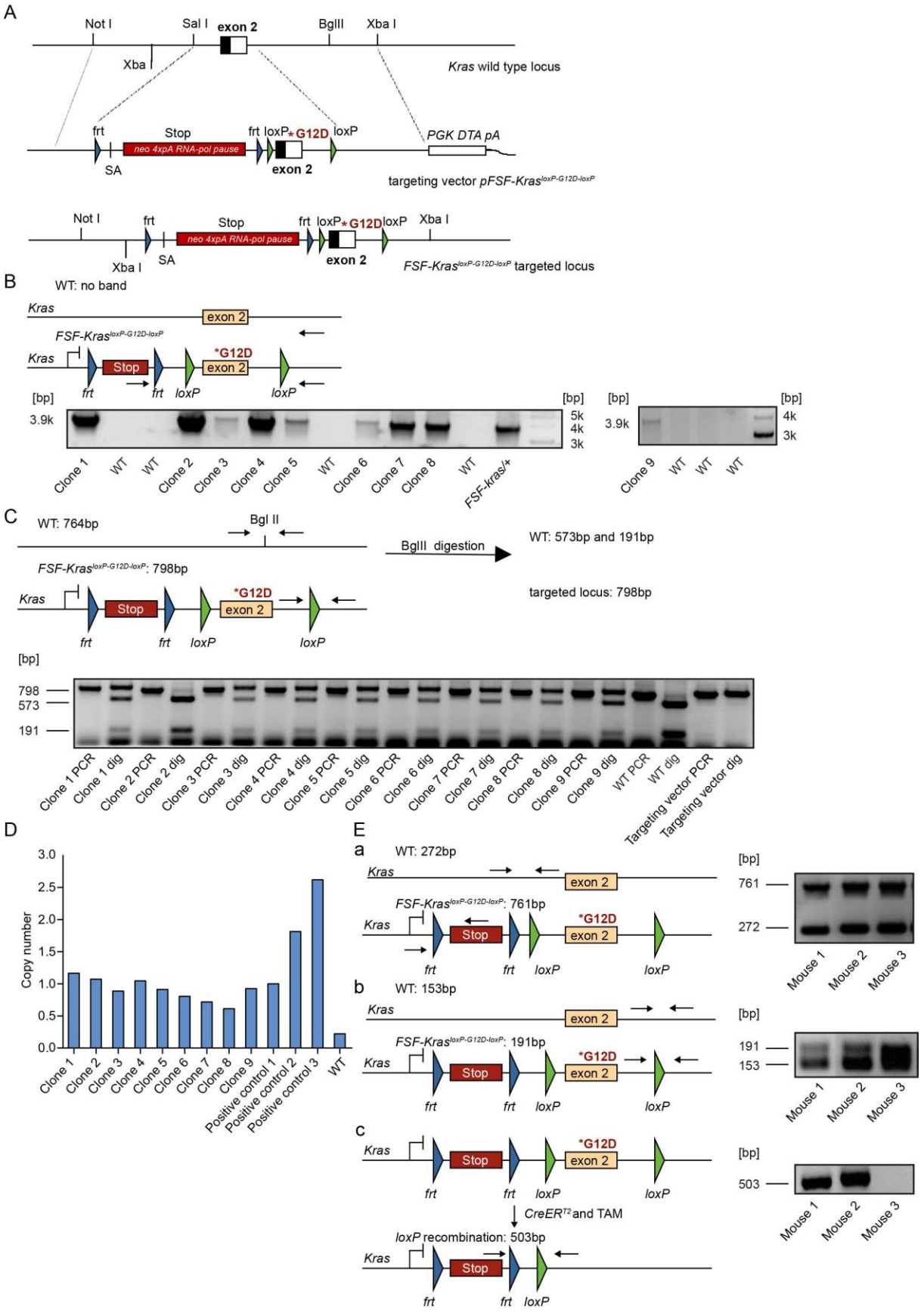


**Figure 18. Generation of a new mouse model allowing to inactivate endogenous *Kras$^{G12D}$*.**

(A) The targeting strategy of *Kras* locus. From top to bottom, diagrams of: *Kras* wild-type (WT) locus; the *pFSF-Kras$^{lox\text{-}G12D\text{-}lox}$* targeting vector with the promoterless *frt-stop-frt* (*FSF*) gene trapping cassette

5´ of *Kras* exon 2 containing *loxP-G12D-loxP*; the targeted *FSF-Kras*$^{lox\text{-}G12D\text{-}lox}$ locus. Restriction sites and the exon structure of the *Kras* locus are indicated. DTA: diphtheria toxin A. SA: splice acceptor. (B) Identification of the targeted embryonic stem (ES) clones by polymerase chain reaction (PCR). The forward primer binds to the stop cassette and the reverse primer binds to *Kras* locus after the second *loxP* site. The targeted ES clones have a 3.9 kb band while WT ES clones have no bands after PCR. DNA of *FSF-Kras*$^{G12D/+}$ mouse (Schönhuber et al., 2014) was used as positive control. The sizes of the PCR products and digestion products are indicated.
(C) Identification of the ES clones with the distal *loxP*. The PCR products of WT and the targeted allele are 764 bp and 798 bp, respectively. After BglII digestion, the products of WT band are 573 bp and 191bp. The PCR product of the targeted allele cannot be digested and remains 798 bp after the digestion. PCR indicates the PCR product. Dig indicates the digestion of the PCR product.
(D) The copy number of the targeted allele in the ES clones. The genomes of the corresponding ES cells were extracted and used as the templates of quantitative real time PCR (qRT-PCR). The primers of qRT-PCR and TaqMan probes targeting neomycin resistance (*neo*) cassette and β-actin are designed. β-actin was used as internal reference. $2^{-\Delta\Delta Ct}$ method was employed for the analysis of the copy number of the targeted allele in the ES clones as described in 5.4.4. The positive control 1 has 1 *neo* cassette. Positive control 2 has 2 *neo* cassettes. Positive control 3 has 3 *neo* cassettes.
(E) The identification of the mice with the targeted allele and the examination of the recombination of the two *loxP* sites. Mouse 1: *FSF-Kras*$^{lox\text{-}G12D\text{-}lox/+}$*;Rosa26*$^{CAG\text{-}CreERT2/+}$*.* Mouse 2: *FSF-Kras*$^{lox\text{-}G12D\text{-}lox/+}$*;Rosa26*$^{CAG\text{-}CreERT2/+}$*.* Mouse 3: *FSF-Kras*$^{lox\text{-}G12D\text{-}lox/+}$. Two PCRs (a and b) were performed for the identification of the mice with the targeted allele. a: WT, 272 bp; targeted allele, 761 bp. b: WT, 153 bp; targeted allele, 191 bp. c: Mice were fed with tamoxifen-containing chow (400 mg tamoxifen citrate per kilogram chow) for 1 week to activate CreER$^{T2}$. The recombination PCR was perfermed. After taxmoxifien treatment, the recombination of two *loxP* sites was detected in Mouse 1 and Mouse 2. Mouse 3 has no CreER$^{T2}$ and is the control. Recombination band: 503 bp. Magdalena Zukowska performed the PCRs in Figure 18E.
The targeting vector has been generated by Barbara Seidler and Andreas Arbeiter in the lab of Prof. Dieter Saur.

sites can be observed, F1 mice with the *FSF-Kras*$^{lox\text{-}G12D\text{-}lox/+}$ targeted allele are futher crossed with *Rosa26*$^{CAG\text{-}CreERT2/+}$ mice. Three mice, including Mouse 1, Mouse 2 and Mouse 3, are obtained. Their genotypes are *FSF-Kras*$^{lox\text{-}G12D\text{-}lox/+}$*;Rosa26*$^{CAG\text{-}CreERT2/+}$, *FSF-Kras*$^{lox\text{-}G12D\text{-}lox/+}$*;Rosa26*$^{CAG\text{-}CreERT2/+}$ and *FSF-Kras*$^{lox\text{-}G12D\text{-}lox/+}$, respectively. The targeted allele in these three mice is confirmed by the genotyping PCR (Figure 18E.a and Eb). Subsequently, these mice are fed with TAM-containing chow. After 1 week of the feeding, recombination PCR is performed. The result shows that the recombination is detected in Mouse 1 and Mouse 2 (Figure 18E.c). Mouse 3 does not have *CreER*$^{T2}$ expression and no recombination is observed in this animal (Figure 18E.c). These results indicate this new mouse model is successfully established. Further characterization of this mouse model will be performed in ongoing experiments.

## 6.6 Regulation of Cre expression via RNA interference (RNAi).

RNAi is a conserved endogenous mechanism that is exploited to suppress gene expression (Hemann et al., 2003). Gene silencing mediated by RNAi can be induced by short hairpin RNAs (shRNAs) embedded in the miRNA scaffold (Dickins et al., 2005).

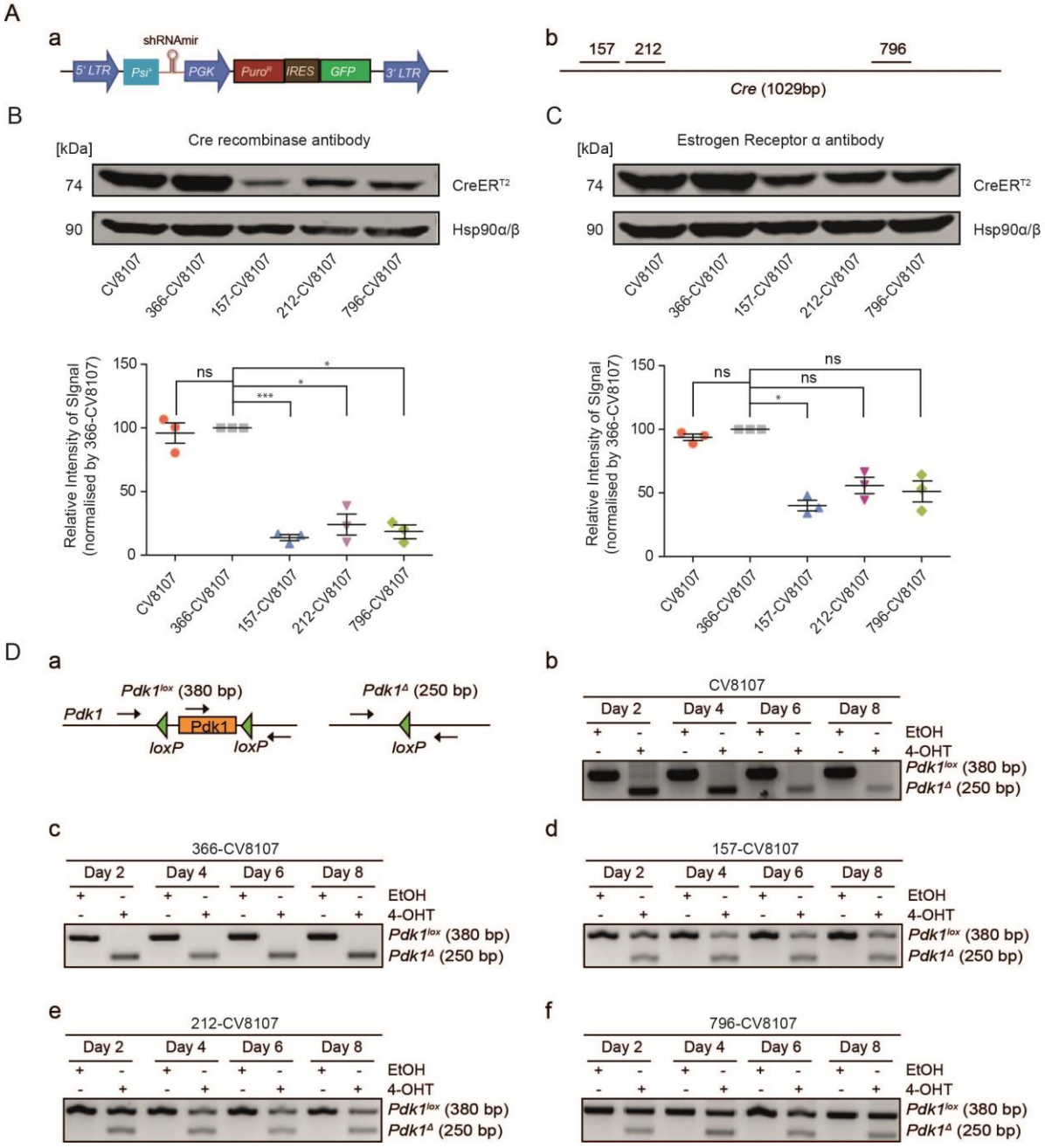


**Figure 19. The downregulation efficiencies of short hairpin RNAs (shRNAs) in CV8107 cell line.**
(A) The viral construct and the targeting sites of shRNAs. a, the viral construct, including 3' and 5' long terminal repeat (*LTR*) sequence, the RNA target site for packaging *Psi*$^{+}$, mouse phosphoglycerate kinase 1 (*PGK*) promoter, puromycin resistant (*Puro*$^{R}$) cassette, miRNA-based shRNA (shRNAmir), the internal ribosomal entry site (*IRES*) and green fluorescent protein (GFP). b shows the targeting sites of the three shRNAs in *Cre*.
(B) The western blot analysis of CreER$^{T2}$ using Cre recombinase antibody after transduction of CV8107 cell line with viral shRNAs constructs. The control group is 366-CV8107. The shRNA used for this group has no target site in *Cre*. Hsp90α/β is the endogenous reference protein. The band intensity of western blot is measured by Odyssey infrared imaging system. The Cre band intensity is normalised by Hsp90α/β band intensity for each group. The normalized band intensity values are then used for the quantitive comparison between the groups. The western blot image is on the top and the

quantification graph of relative signal intensity is at the bottom. Data represent mean ± SEM; n=3 per group. ns, not significant, *$p$<0.05, ***$p$<0.001, one-way ANOVA.
(C) The western blot analysis of CreER$^{T2}$ with estrogen receptor α antibody after transduction of CV8107 cell line with viral shRNAs constructs. The control group is 366-CV8107. The shRNA used for this group has no target site in *Cre*. Hsp90α/β is the endogenous reference protein. The band intensity of western blot is measured by Odyssey infrared imaging system. The Cre band intensity is normalised by Hsp90α/β band intensity for each group. The normalized band intensity values are then used for the quantitive comparison between the groups. The western blot image is on the top and the quantification graph of the relative signal is at the bottom. Data represent mean ± SEM; n=3 per group. ns, not significant, *$p$<0.05. one-way ANOVA.
(D) Recombination polymerase chain reaction (PCR) of *Pdk1*$^{lox/lox}$ is examined after 2, 4, 6 and 8 days of 4-hydroxytamoxifen (4-OHT) or ethanol (EtOH) treatment. The cells were harvested, and the respective DNA was extracted after 2, 4, 6 and 8 days of 4-OHT or EtOH treatment. Recombination PCR of *Pdk1*$^{lox/lox}$ was performed to examine the recombination of the two *loxP* sites induced by Cre recombinase. b, c, d, e and f show the PCR analysis of CV8107, 366-CV8107, 157-CV8107, 212-CV8107 and 796-CV8107, respectively.

This study tries to find if it is feasible to employ RNAi to control the expression of *Cre* and thus controls the expression of *loxP*-flanked genes in the process of tumor development in mice. To identify shRNAs that can induce potent suppression of *Cre*, we collaborated with Prof. Miething (Univ. Freiburg) who selected 3 potent shRNAs by bioinformatic approaches (shRNAs 157, 212 and 796, targeting *Cre* sequence) (Figure 19A). shRNA 366 does not target *Cre* sequence and is a negative control. CV8107 and V731 are two PDAC cell lines with *CreER*$^{T2}$ expression and their genotypes are *Pdx1-Flp*$^{+/-}$*,FSF-Kras*$^{G12D/+}$*;FSF-Rosa26*$^{CAG\text{-}CreERT2/+}$*;Pdk*$^{lox/lox}$*;Trp53*$^{frt/+}$ and *Pdx-Flp*$^{+/-}$*,FSF-Kras*$^{G12D/+}$*;FSF-Rosa26*$^{CAG\text{-}CreERT2/+}$*;Pdk*$^{lox/+}$*;Trp53*$^{frt/+}$*;Rosa26*$^{mT\text{-}mG/+}$, respectively. In CV8107 cell line, the western blot analysis shows shRNA construct 157 has the most efficient knockdown effect, although both shRNA 212 and 796 also lead to lower expression level of *CreER*$^{T2}$ compared with the 366 construct (Figure 19B and 19C). The PCR analysis of *PDK1*$^{loxP/loxP}$ recombination also shows that 157, 212 and 796 constructs inhibit the recombination while 366 construct does not influence the recombination (Figure 19D).

In V731 cell line, western blot analysis is performed to quantify the expression level of *CreER*$^{T2}$ in V731 cell line alone or V731 with the transduced shRNAs. The result shows that shRNA 796 can significantly suppress the expression of *CreER*$^{T2}$ compared with the 366 construct (Figure 20A and 20B). The expression level of *CreER*$^{T2}$ is comparable in the cells with 157 and 366 shRNAs (Figure 20A and 20B). The viral constructs have a GFP cassette and the GFP is cytoplasm targeted. The expression of cytoplasm targeted GPF indicates the successful transduction of shRNA constructs. V731 has *Rosa26*$^{CAG\text{-}CreERT2/+}$ and *Rosa26*$^{mT\text{-}mG/+}$ cassettes and, without 4-OHT treatment, the cells have the expression of membrane-targeted tdTomato. After 4-OHT treatment, CreER$^{T2}$ is activated and the tdTomato cassette is removed. This leads to the change of the reporter from tdTomato to EGFP and therefore, the cells have the expression of membrane targeted EGFP (Figure 20C). After 8 days of 4-OHT or EtOH treatment, the quantification of the cells with membrane-targeted EGFP is

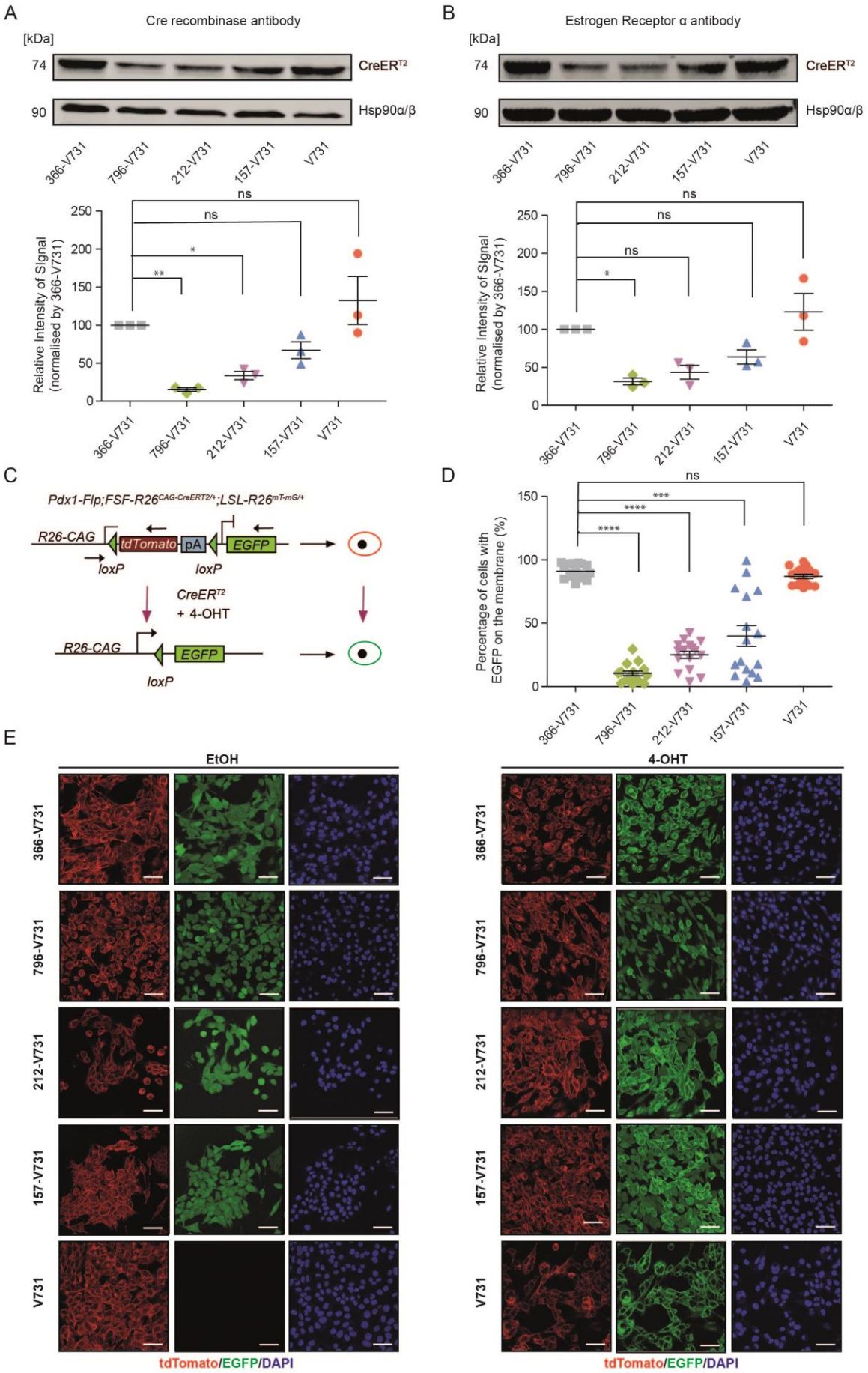
A
Cre recombinase antibody
[kDa]
74
CreER$^{T2}$
90
Hsp90α/β
366-V731
796-V731
212-V731
157-V731
V731
Relative Intensity of Signal (normalised by 366-V731)
ns
*
**
B
Estrogen Receptor α antibody
C
Pdx1-Flp;FSF-R26$^{CAG-CreERT2/+}$;LSL-R26$^{mT-mG/+}$
R26-CAG
tdTomato
pA
EGFP
loxP
CreER$^{T2}$
+ 4-OHT
D
Percentage of cells with EGFP on the membrane (%)
***
****
E
EtOH
4-OHT
tdTomato/EGFP/DAPI

**Figure 20. The downregulation efficiencies of short hairpin RNAs (shRNAs) in V731 cell line.**
(A) The western blot analysis of CreER$^{T2}$ using Cre recombinase antibody after transduction of V731 cell line with viral shRNAs constructs. The control group is 366-V731. The shRNA used for this group has no target site in Cre. Hsp90α/β is the endogenous reference protein. The band intensity of western blot is measured by Odyssey infrared imaging system. The Cre band intensity is normalised by Hsp90α/β band intensity for each group. The normalized band intensity values are then used for the quantitative comparison between the groups. The western blot image is on the top and the quantification graph of the relative signal intensity is at the bottom. Data represent mean ± SEM; n=3 per group. ns, not significant, *$p$<0.05, **$p$<0.01, one-way ANOVA.
(B) The western blot analysis of CreER$^{T2}$ using estrogen receptor α antibody after transduction of V731 cell line with viral shRNAs constructs. The control group is 366-V731. The shRNA used for this group has no target site in Cre. Hsp90α/β is the endogenous reference protein. The band intensity of western blot is measured by Odyssey infrared imaging system. The Cre band intensity is normalised by Hsp90α/β band intensity for each group. The normalized band intensity values are then used for the quantitative comparison between the groups. The western blot image is on the top and the quantification graph of the relative signal intensity is at the bottom. Data represent mean ± SEM; n=3 per group. ns, not significant, *$p$<0.05, one-way ANOVA.
(C) The schematic diagram of *Rosa26*$^{mT\text{-}mG}$ with CreER$^{T2}$ after 4-hydroxytamoxifen (4-OHT) treatment. When CreER$^{T2}$ is not activated, membrane-targeted tdTomato is expressed. After 4-OHT treatment, CreER$^{T2}$ is activated, leading to the removal of the tdTomato cassette flanked by two *loxP*s, and the membrane-targeted EGFP is expressed.
(D) The quantification of cells with EGFP on the membrane. Data represent mean ± SEM; n=16 microscopy fields per group. ns, not significant, ***$p$<0.001, ****$p$<0.0001, one-way ANOVA.
(E) The representative images of the cells after 8 days of 4-OHT or ethanol EtOH treatment. The GFP located in the cytoplasm is expressed from the viral construct (Figure 19A.a). Cytoplasm-targeted GFP indicates the cells with successful transduction. The membrane-targeted EGFP comes from the expression of *Rosa26*$^{mT\text{-}mG}$. When *CreER*$^{T2}$ is activated by 4-OHT, the tdTomato cassette is removed and the membrane-targeted EGFP is expressed. Scale bars indicate 50 µm.

performed. The result shows that 157, 212 and 796 shRNAs can significantly inhibit the recombination of *Rosa26*$^{mT\text{-}mG}$ (Figure 20D and 20E). It is observed that the downregulation efficiencies of these shRNAs are different in CV8107 and V731 cell lines (Figure 19B, 19C, 20A and 20B). This may be due to the different copy numbers of these constructs in the cell line.

This study tests 3 shRNA constructs and their suppressing efficiencies of *CreER*$^{T2}$ expression vary. To validate that the changes of *CreER*$^{T2}$ expression can influence the corresponding downstream gene cassettes, *Pdk1*$^{lox/lox}$ and the reporter gene *Rosa26*$^{mT\text{-}mG/+}$ are also examined and the results show it is feasible to regulate the genes under the control of Cre through RNAi. However, no complete downregulation/inactivation of Cre was achieved, making it impossible to switch Cre on and off as initially planned.

## 6.7 Loss of tenascin c (Tnc) function results in more ADM and PanIN-1A lesions.

Tenascin c (Tnc) is one of the ECM proteins. It is highly conserved and widely distributed in embryonic tissues (Chiquet, 1992). Adult tissues have restricted Tnc distribution (Fluck et al.,

2000). Tnc protein synthesis is an indicator of successful tissue repair and can be rapidly induced in many tissues under the pathological pressure. Stromal cells and inflammatory leukocytes are the main sources of Tnc (O'Connell et al., 2011). Tnc protein mediates numerous physiological and pathological cell responses, and its activity is cell-type dependent. The responses of cells to Tnc protein are context-specific and this protein often exerts the opposite effects in different cell types (Chiquet-Ehrismann and Tucker, 2011; Midwood and Orend, 2009). TME shows a high expression level of *Tnc*. Previous studies have shown that Tnc can promote and suppress proliferation of cancer cells and fibroblasts (Huang et al., 2001; Orend et al., 2003). Tnc is associated with the progression and metastasis of many types of human cancers, such as breast cancer and glioblastoma (Oskarsson et al., 2011; Song et al., 2017).

In this study, *Ptf1a*$^{Cre/+}$*,LSL-Kras*$^{G12D/+}$*;Tnc*$^{-/-}$ mice (Figure 21A) are used as the mouse model to investigate the effects of *Tnc* in PDAC. The survival time of *Ptf1a*$^{Cre/+}$*,LSL-Kras*$^{G12D/+}$*;Tnc*$^{-/-}$ mice is signicantly reduced, when compared with that of *Ptf1a*$^{Cre/+}$*,LSL-Kras*$^{G12D/+}$ mice (Figure 21B). Compared with that of *Ptf1a*$^{Cre/+}$*,LSL-Kras*$^{G12D/+}$ mice, the tumor incidence of *Ptf1a*$^{Cre/+}$*,LSL-Kras*$^{G12D/+}$*;Tnc*$^{-/-}$ mice is significantly lower ($p$<0.0001) (Figure 21C). The percentage of mice with macroscopic metastasis in *Ptf1a*$^{Cre/+}$*,LSL-Kras*$^{G12D/+}$*;Tnc*$^{-/-}$ cohort is significantly lower than that of the control group ($p$<0.0001) (Figure 21D). The deletion of *Tnc* results in lower percentages of ascites and liver metastasis (Figure 21E). The mice in *Ptf1a*$^{Cre/+}$*,LSL-Kras*$^{G12D/+}$*;Tnc*$^{-/-}$ cohort only have 1 metastatic site, while those in *Ptf1a*$^{Cre/+}$*,LSL-Kras*$^{G12D/+}$ cohort have up to 5 metastatic sites (Figure 21F). *Ptf1a*$^{Cre/+}$*,LSL-Kras*$^{G12D/+}$ mice display the 4 grades of invasive tumors while the tumors of PDAC mice with *Tnc* knockout are either G2 or G3 (Figure 21G and 20H). The different histopathological distribution of the grades in these two genotypes indicates the depletion of *Tnc* influences the tumor morphology. The *Tnc*-deleted mice show more ADM and PanIN-1A lesions than the control mice (Figure 21I and 21J), indicating *Tnc* ablation contributes to the formation of ADM and PanIN-1A.

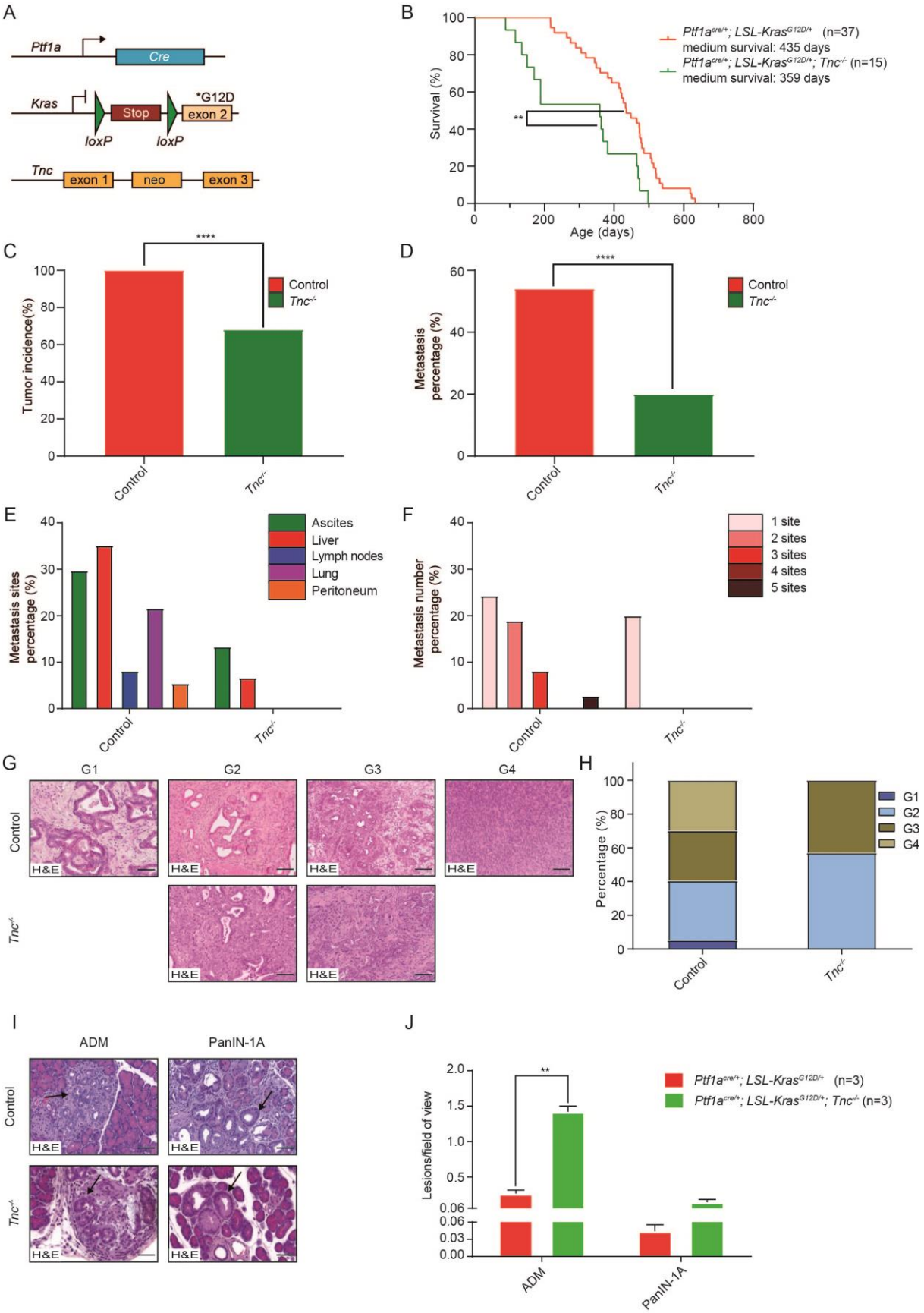


**Figure 21. Characterization of PDAC mice with *tenascin c (Tnc)* deletion.**
(A) The genetic strategy of *Tnc* knockout in PDAC tumor mice. Cre expression leads to the removal the *loxP-stop-loxP* (*LSL*) cassette and the expression of $Kras^{G12D}$. *Tnc* is silenced by the neomycin resistant (*neo*) cassette in exon2. *Tnc* is knocked out in the whole body of the mouse.

(B) Kaplan-Meier survival curves of *Ptf1a*$^{Cre/+}$*,LSL-Kras*$^{G12D/+}$ and *Ptf1a*$^{Cre/+}$*,LSL-Kras*$^{G12D/+}$*;Tnc*$^{-/-}$ mice. The median survival time of *Ptf1a*$^{Cre/+}$*,LSL-Kras*$^{G12D/+}$ (n=37) is 435 days. The median survival time of *Ptf1a*$^{Cre/+}$*,LSL-Kras*$^{G12D/+}$*;Tnc*$^{-/-}$ (n=15) is 359 days. ***p*<0.01, log-rank test.
(C) The incidence of invasive PDAC tumors in *Ptf1a*$^{Cre/+}$*,LSL-Kras*$^{G12D/+}$ and *Ptf1a*$^{Cre/+}$*,LSL-Kras*$^{G12D/+}$*; Tnc*$^{-/-}$ mice. Control (n=37): *Ptf1a*$^{Cre/+}$*,LSL-Kras*$^{G12D/+}$ mice. *Tnc*$^{-/-}$ (n=22): *Ptf1a*$^{Cre/+}$*,LSL-Kras*$^{G12D/+}$*;Tnc*$^{-/-}$ mice. *****p*<0.0001. Fisher's exact test.
(D) The percentages of macroscopic metastases of *Ptf1a*$^{Cre/+}$*,LSL-Kras*$^{G12D/+}$ and*Ptf1a*$^{Cre/+}$*,LSL-Kras*$^{G12D/+}$*;Tnc*$^{-/-}$ mice*.* Control (n=37): *Ptf1a*$^{Cre/+}$*,LSL-Kras*$^{G12D/+}$ mice. *Tnc*$^{-/-}$ (n=15): *Ptf1a*$^{Cre/+}$*,LSL-Kras*$^{G12D/+}$*;Tnc*$^{-/-}$ mice. *****p*<0.0001. Fisher's exact test.
(E) The analysis of metastatic sites in *Ptf1a*$^{Cre/+}$*,LSL-Kras*$^{G12D/+}$ and *Ptf1a*$^{Cre/+}$*,LSL-Kras*$^{G12D/+}$*;Tnc*$^{-/-}$ mice*.* Control (n=37): *Ptf1a*$^{Cre/+}$*,LSL-Kras*$^{G12D/+}$ mice. *Tnc*$^{-/-}$ (n=15): *Ptf1a*$^{Cre/+}$*,LSL-Kras*$^{G12D/+}$*;Tnc*$^{-/-}$ mice.
(F) The analysis of the number of metastatic sites in *Ptf1a*$^{Cre/+}$*,LSL-Kras*$^{G12D/+}$ and *Ptf1a*$^{Cre/+}$*,LSL-Kras*$^{G12D/+}$*;Tnc*$^{-/-}$ mice*.* Control (n=37): *Ptf1a*$^{Cre/+}$*,LSL-Kras*$^{G12D/+}$ mice. *Tnc*$^{-/-}$ (n=15): *Ptf1a*$^{Cre/+}$*,LSL-Kras*$^{G12D/+}$*;Tnc*$^{-/-}$ mice.
(G) Representative hematoxylin and eosin (H&E) stained tumor sections of different grades of *Ptf1a*$^{Cre/+}$*,LSL-Kras*$^{G12D/+}$ (top) and *Ptf1a*$^{Cre/+}$*, LSL-Kras*$^{G12D/+}$*; Tnc*$^{-/-}$ mice (bottom). Control (n=37): *Ptf1a*$^{Cre/+}$*,LSL-Kras*$^{G12D/+}$ mice. *Tnc*$^{-/-}$ (n=15): *Ptf1a*$^{Cre/+}$*,LSL-Kras*$^{G12D/+}$*;Tnc*$^{-/-}$ mice. Scale bars indicate 50 µm.
(H) The composition of different grades of tumors from *Ptf1a*$^{Cre/+}$*,LSL-Kras*$^{G12D/+}$ and *Ptf1a*$^{Cre/+}$*,LSL-Kras*$^{G12D/+}$*;Tnc*$^{-/-}$ mice. Control (n=37): *Ptf1a*$^{Cre/+}$*,LSL-Kras*$^{G12D/+}$ mice. *Tnc*$^{-/-}$ (n=14): *Ptf1a*$^{Cre/+}$*,LSL-Kras*$^{G12D/+}$*;Tnc*$^{-/-}$ mice.
(I) Representative H&E stained sections of acinar to ductal metasplasia (ADM) and pancreatic intraepithelial neoplasia 1A (PanIN-1A) of *Ptf1a*$^{Cre/+}$*,LSL-Kras*$^{G12D/+}$ (top) and *Ptf1a*$^{Cre/+}$*,LSL-Kras*$^{G12D/+}$*;Tnc*$^{-/-}$ mice (bottom). Arrows indicate ADM (left) or PanIN 1A (right). Control (n=3): *Ptf1a*$^{Cre/+}$*,LSL-Kras*$^{G12D/+}$ mice. *Tnc*$^{-/-}$ (n=3): *Ptf1a*$^{Cre/+}$*,LSL-Kras*$^{G12D/+}$*;Tnc*$^{-/-}$ mice. Scale bars indicate 50 µm.
(J) Quantification of ADM and PanIN-1A lesions in 1-month-old mice with genotypes as indicated (mean ± SEM). *Ptf1a*$^{Cre/+}$*,LSL-Kras*$^{G12D/+}$ mice: n=3. *Ptf1a*$^{Cre/+}$*,LSL-Kras*$^{G12D/+}$*;Tnc*$^{-/-}$ mice: n=3. ***p*<0.01, two-way ANOVA.

## 6.8 Hepatocyte nuclear factor 4α (Hnf4α) ablation prolongs the overall survival of PDAC mice.

Hepatocyte nuclear factor 4α, encoded by *Hnf4α*, is a highly conserved transcription factor. It involves in the regulation of the morphogenesis and function of epithelial cells in pancreas, kidney, liver, small intestine, and colon. The expression of *Hnf4α* is critical for hepatocyte function and the development of liver. Loss of *Hnf4α* function promotes the proliferation of cancer cells in hepatocellular carcinoma (Lazarevich et al., 2010). *HNF4A* exhibits a decreased expression pattern in numerous types of human cancer, including renal cell, hepatocellular and colorectal carcinomas (Oshima et al., 2007; Sel et al., 1996; Tanaka et al., 2006). One recent study revealed that prostate cancer patients show a reduced expression level of *HNF4A* and the downregulated expression of this gene promotes cancer cell proliferation and enhances the capacity of colony formation (Wang et al., 2020b). On the other hand, the expression of *Hnf4α* is also upregulated in ovarian mucinous carcinomas, lung mucinous adenocarcinomas and colorectal carcinomas (Darsigny et al., 2010; Sugai et al., 2008; Xiang et al., 2015) These studies suggest that *Hnf4α* may have distinct effects in different cancer entities or progression stages of cancers. The present study uses

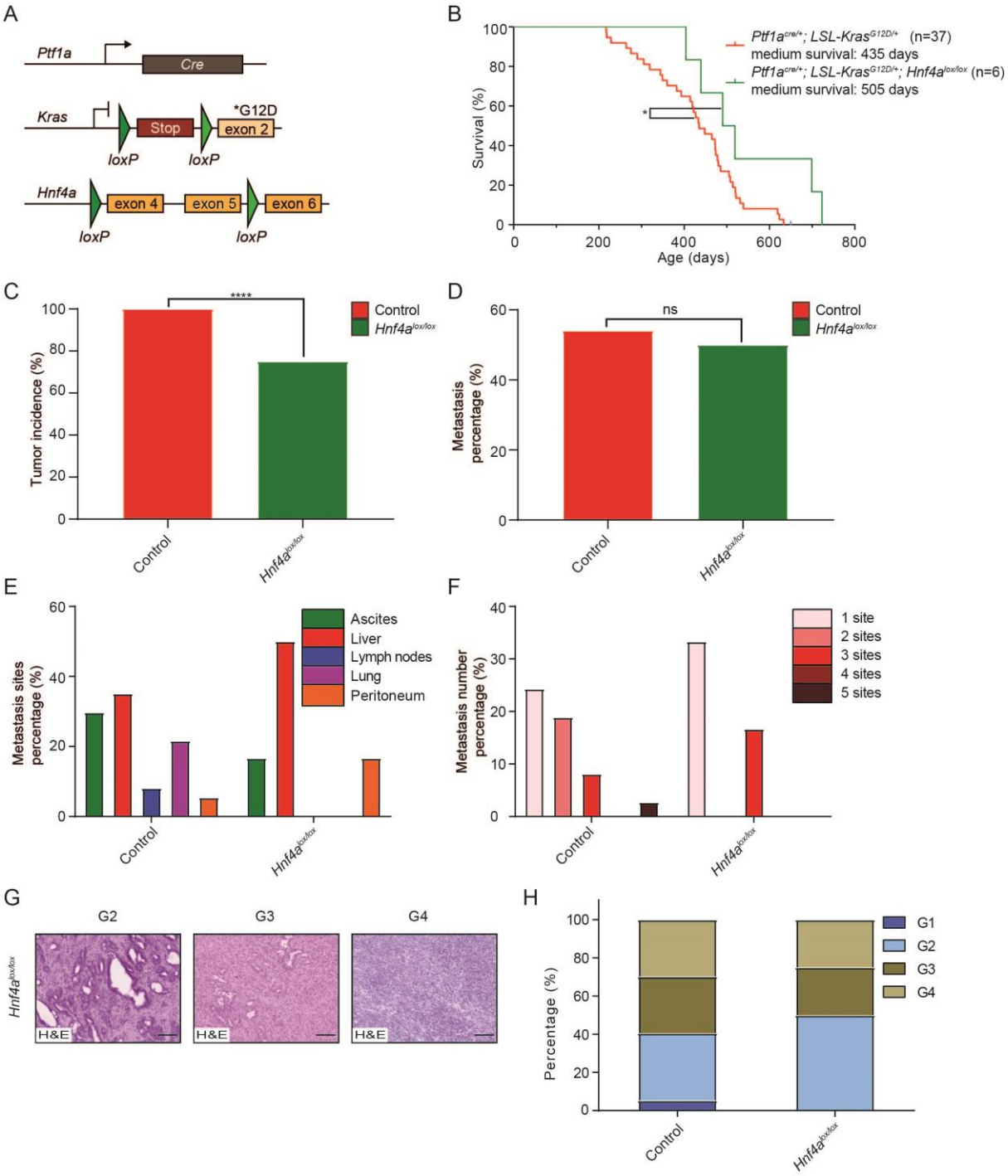


**Figure 22. Characterization of PDAC mice with *hepatocyte nuclear factor 4α (Hnf4α)* ablation.**
(A) The genetic strategy of *Hnf4a* knockout in pancreatic ductal adenocarcinoma (PDAC) tumor mice. *Cre* expression leads to the removal the *loxP-stop-loxP* (*LSL*) cassette and the expression of $Kras^{G12D}$. In the *Hnf4α* locus, exons 4 and 5 are removed by Cre recombinase.
(B) Kaplan-Meier survival curves of $Ptf1a^{Cre/+}$,$LSL\text{-}Kras^{G12D/+}$ and $Ptf1a^{Cre/+}$,$LSL\text{-}Kras^{G12D/+}$;$Hnf4α^{lox/lox}$ mice. The median survival time of $Ptf1a^{Cre/+}$,$LSL\text{-}Kras^{G12D/+}$ (n=37) is 435 days. The median survival time of $Ptf1a^{Cre/+}$,$LSL\text{-}Kras^{G12D/+}$;$Hnf4α^{lox/lox}$ (n=6) is 505 days. *$p$<0.05, log-rank test.
(C) The tumor incidence in $Ptf1a^{Cre/+}$,$LSL\text{-}Kras^{G12D/+}$ and $Ptf1a^{Cre/+}$,$LSL\text{-}Kras^{G12D/+}$;$Hnf4α^{lox/lox}$ mice. Control (n=37): $Ptf1a^{Cre/+}$,$LSL\text{-}Kras^{G12D/+}$ mice. $Hnf4α^{lox/lox}$ (n=8): $Ptf1a^{Cre/+}$,$LSL\text{-}Kras^{G12D/+}$;$Hnf4α^{lox/lox}$ mice. ****$p$<0.0001. Fisher's exact test.
(D) The percentages of macroscopic metastases of $Ptf1a^{Cre/+}$,$LSL\text{-}Kras^{G12D/+}$ and $Ptf1a^{Cre/+}$,$LSL\text{-}Kras^{G12D/+}$;$Hnf4α^{lox/lox}$ mice. Control (n=37): $Ptf1a^{Cre/+}$,$LSL\text{-}Kras^{G12D/+}$ mice. $Hnf4α^{lox/lox}$ (n=6): $Ptf1a^{Cre/+}$,$LSL\text{-}Kras^{G12D/+}$;$Hnf4α^{lox/lox}$ mice. ns, not significant. Fisher's exact test.

(E) The analysis of metastatic sites in *Ptf1a*$^{Cre/+}$,*LSL-Kras*$^{G12D/+}$ and *Ptf1a*$^{Cre/+}$,*LSL-Kras*$^{G12D/+}$;*Hnf4α*$^{lox/lox}$ mice. Control (n=37): *Ptf1a*$^{Cre/+}$,*LSL-Kras*$^{G12D/+}$ mice. *Hnf4α*$^{lox/lox}$ (n=6): *Ptf1a*$^{Cre/+}$,*LSL-Kras*$^{G12D/+}$;*Hnf4α*$^{lox/lox}$ mice.
(F) The analysis of the number of metastatic sites in *Ptf1a*$^{Cre/+}$,*LSL-Kras*$^{G12D/+}$ and *Ptf1a*$^{Cre/+}$,*LSL-Kras*$^{G12D/+}$;*Hnf4α*$^{lox/lox}$ mice. Control (n=37): *Ptf1a*$^{Cre/+}$,*LSL-Kras*$^{G12D/+}$ mice. *Hnf4α*$^{lox/lox}$ (n=6): *Ptf1a*$^{Cre/+}$,*LSL-Kras*$^{G12D/+}$; *Hnf4α*$^{lox/lox}$ mice.
(G) Representative hematoxylin and eosin (H&E) stained tumor sections of different grades of *Ptf1a*$^{Cre/+}$,*LSL-Kras*$^{G12D/+}$;*Hnf4α*$^{lox/lox}$ mice. Scale bars indicate 50 μm.
(H) The composition of different grades of tumors from *Ptf1a*$^{Cre/+}$,*LSL-Kras*$^{G12D/+}$ and *Ptf1a*$^{Cre/+}$,*LSL-Kras*$^{G12D/+}$;*Hnf4α*$^{lox/lox}$ mice. Control (n=37): *Ptf1a*$^{Cre/+}$,*LSL-Kras*$^{G12D/+}$ mice. *Hnf4α*$^{lox/lox}$ (n=4): *Ptf1a*$^{Cre/+}$,*LSL-Kras*$^{G12D/+}$;*Hnf4α*$^{lox/lox}$ mice.

*Ptf1a*$^{Cre/+}$,*LSL-Kras*$^{G12D/+}$;*Hnf4α*$^{lox/lox}$ mice (Figure 22A) to understand the effects of *Hnf4α* knockout in PDAC mice. Loss of *Hnf4α* can significantly improve the survival time of PDAC mice (Figure 22B), indicating its pro-tumoral effect in PDAC. The mice with homozygous *Hnf4α* deletion have significantly lower tumor incidence than *Ptf1a*$^{Cre/+}$,*LSL-Kras*$^{G12D/+}$ mice ($p$<0.0001) (Figure 22C). The metastasis percentage between *Ptf1a*$^{Cre/+}$,*LSL-Kras*$^{G12D/+}$ mice and *Ptf1a*$^{Cre/+}$,*LSL-Kras*$^{G12D/+}$;*Hnf4α*$^{lox/lox}$ mice are comparable (Figure 22D). The mice with homozygous *Hnf4α* deletion have higher percentages of liver and peritoneum metastasis but a lower percentage of ascites than those in *Ptf1a*$^{Cre/+}$,*LSL-Kras*$^{G12D/+}$ cohort (Figure 22E). Homozygous *Hnf4α* deletion leads to higher percentages of the mice with 1 and 3 metastatic sites (Figure 22F). Compared with tumors in *Ptf1a*$^{Cre/+}$,*LSL-Kras*$^{G12D/+}$ animals, the tumors with *Hnf4α* ablation do not exhibit G1 (Figure 22G and 22H).

# 7 Discussion and Outlook

Advances in the genetic engineering techniques have facilitated the development of GEMMs of pancreatic cancer. These mouse models recapitulate the recognized features that are observed in the progression of human pancreatic cancer, from PanIN precursor lesions to invasive adenocarcinoma. Clinical data shows that the progression of pancreatic cancer is a process of accumulating molecular changes, including the activation of oncogenes and the silencing of tumor suppressor genes. Multi-omics sequencing results reveal that PDAC has a high degree of intra-tumoral heterogeneity. To investigate the heterogeneous features of PDAC and dissect the complex mechanisms of pancreatic cancer progression, the generation and characterization of PDAC mouse models with genetic aberrations, including in *Trp53*, *Cdkn2a*, *Smad4*, *Tgfbr2*, *Tgfβ* and *Snail*, are required. The present study systematically characterizes the survival and metastatic features of the mouse models and identifies the molecular signatures related to tumor grades, mitosis and liver metastasis. Four immune subpopulations are revealed to be associated with histopathological phenotypes. Moreover, a new mouse model that facilitates the inactivation of the endogenous $Kras^{G12D}$ mutation is established and a new method to control gene expression mediated by the regulation of the expression of Cre recombinase using RNAi has been tested. Finally, this thesis demonstrates that *Tnc* deletion results in more ADM and PanIN-1A lesions and loss of *Hnf4α* function improves the survival of PDAC mice.

**Correlation between survival time and metastasis in PDAC mouse models**

Metastasis appears to correlate with the survival time in the PDAC mouse models. For example, PK mice with *Cdkn2a* alteration exhibit a shorter life span and more metastasis than PK mice (Figure 3B and 4B). Similar results have been also observed in numerous types of human cancer, including cervical cancer, nonsmall cell lung cancer, colon cancer and breast cancer (Oh et al., 2009; Wang et al., 2020a; Wang et al., 2019b; Yin et al., 2019b). Patients with colorectal cancer often have poorer survival outcomes as metastasis spreads to other organs (Wang et al., 2019b). PDAC mouse models also exhibit similar correlations between survival time and the number of metastatic sites. In the present study, mice with more metastatic sites tend to have poorer survival (Figure 3 and 6). This study provides evidence to correlate metastasis with poor prognosis in PDAC.

The relationship between survival time and metastasis has been discussed intensively in recent years (Wang et al., 2020a; Wang et al., 2019b; Yin et al., 2019b). Liver metastasis is related to the poor overall survival of cervical cancer patients (Yin et al., 2019b). A previous study revealed that it is necessary to adapt diverse treatment plans for colon cancer patients

with different metastatic patterns (Wang et al., 2020a). In breast cancer, patients with different metastatic sites show different clinicopathological features and survival outcomes (Wang et al., 2019b). Moreover, breast cancer patients with bone metastasis have favorable survival than those with brain metastasis (Wang et al., 2019b). These studies suggest the correlation exists between metastasis and survival time, which can provide critical information for studies of prognosis, pathology and treatment strategies for cancers. Therefore, to investigate the mechanisms underlining the relationship between metastasis and survival is critical. This study provides the clues for studying the molecular mechanisms of PDAC. *CDKN2A* mutations enhance tumorigenesis and metastasis and lead to poor OS in many types of human cancer. For example, *CDKN2A* alterations are involved in the lymph node metastasis in lung cancer (Marchetti et al., 1997). *CDKN2A* alterations also correlate with increased lymph node metastasis and the poor survival rates of patients with GC (Matsusaka et al., 2014). This study also finds *Cdkn2a* alterations lead to poor survival and more metastases in PDAC mouse models, which suggests that *Cdkn2a* plays an essential role in influencing the survival and metastasis in PDAC. Future studies should identify the genes that potentially influence the prognosis and metastasis of PDAC and elucidate the mechanisms of the correlation between metastasis and survival time.

**PDAC tumor grades and their association with other PDAC features**

Tumor grade is used to measure the degree of tumor differentiation and PDAC tumors are classified by their cytological and histopathological features into Grade 1 (G1, well-differentiated carcinomas); Grade 2 (G2, moderately-differentiated carcinomas); Grade 3 (G3, poorly-differentiated carcinomas) and Grade 4 (G4, undifferentiated carcinomas). Tumor grade is an indicator of prognosis in PDAC. A novel staging system for pancreatic cancer has incorporated tumor grades into the present TNM system to provide more accurate prognostications of survival for PDAC patients (Rochefort et al., 2013), which indicates the importance of taking tumor grades into consideration in clinical practice. Futhermore, this study reveals the correlation between tumor grades and other features of PDAC and identifies the features that shape the different histopathological phenotypes. Tumor grades are used to evaluate the differentiation of tumors and it has been observed that less differentiated tumors are more aggressive and associated with a poor prognosis. In addition, mitosis is a parameter for the evaluation of proliferative activities in cancer. Tumor grades are positively related to the mitotic activities of tumors in PDAC mouse models (Figure 8) and that cell proliferation is a predictive activity of tumor progression.

The present study also finds that as PDAC tumor grades increase, there are more metastases (Figure 9). It has been demonstrated that less differentiated tumors possess

more invasive features that result in local and distant metastasis (Rochefort et al., 2013). The results of this study reveal that the mice with higher tumor grades exhibit higher number of metastatic sites. Notably, the percentage of mice with liver metastasis is positively related to tumor grades (Figure 5C). Liver metastasis is often observed in PDAC patients in advanced stages. A previous study has observed that liver metastasis is associated with poorly differentiated tumor and poor survival (Sahin et al., 2018), which provides evidence that liver metastasis is associated with PDAC tumor grades. Altogether, these studies indicate that liver metastasis is a potential indicator of the malignancy and prognosis of PDAC tumors.

Pancreatic tumors contain an abundant stromal compartment. The PDAC TME consists of fibroblasts, infiltrating immune cells, PSCs, endothelial cells and ECM proteins. It has been shown that stromal components are involved in the pathogenesis of pancreatic cancer and associated with poor prognosis and drug resistance (Moffitt et al., 2015). According to a new TNMG (tumor, node, metastasis, grade) staging system, tumor grade is divided into two groups: a low-grade group including well- and moderately-differentiated tumors, and a high-grade group consisting of poorly-differentiated and undifferentiated tumors (Rochefort et al., 2013). The present study reveals that low-grade tumors have a higher percentage of stroma than high-grade tumors, which is consistent with previous studies (Neuzillet et al., 2019; Puleo et al., 2018). One recent study demonstrates that high-grade PDAC tumors are characterized by low stromal content and mesenchymal-like cancer cells mediate low stromal content via deactivation of PSCs and suppression of the proliferation of these cells in high-grade PDAC tumors (Steins et al., 2020). Thus, the interactions between tumor cells and PSCs modulate the histopathological features of PDAC. This thesis highlights the correlation between tumor grade and stromal contents. Further studies should focus on the mechanisms of this correlation and its clinical relevance.

**The molecular signatures of tumor grades**

Tumor grades are highly associated with the prognosis of PDAC patients. Thus, identifying the molecular signatures related to tumor grades is important to elucidate the mechanisms of PDAC pathogenesis. The transcriptional profiles of PDAC tumors have been used to define the molecular signatures of different subtypes (Bailey et al., 2016; Collisson et al., 2011; Moffitt et al., 2015; Puleo et al., 2018). These subtypes are defined by gene expression features from both PDAC cancer cells and the tumor microenvironment. It has been shown that they are related to the prognosis of PDAC patients and the options of treatment strategies. Undoubtedly, comprehensive molecular characterization of patients' tumors will facilitate precision medicine in human pancreatic cancer. However, multi-omics sequencing is time consuming, and the cost is unaffordable for most patients. The present study finds

that the transcription subtypes of PDAC correlate with tumor grades. One previous study also demonstrates that, according to the morphological features of tumors, PDAC patients can be classified into distinct categories that are associated with the molecular subtypes (Kalimuthu et al., 2020). These findings suggest the existence of a strong correlation between tumor histopathological features and molecular subtypes in PDAC and provide a basis for improving the taxonomy of pancreatic cancer, which will be useful for further treatment options.

Furthermore, this study identifies the molecular signatures of low-grade (G1) and high- grade (G4) PDAC tumors. PDAC heterogeneity is mirrored in the transcriptomic profiles of pancreatic tumors of different grades and the gene expression profiles of G1 and G4 tumors are grouped in three distinct clusters which are further analyzed to reveal their molecular features. The gene signatures that characterize the differentiation degree of PDAC tumors are associated with certain histopathological features, such as cancer cell proliferation, local invasion, and distant metastasis, which are also shown to be related to the tumor features of other cancer entities. For example, *Lypd8* and *E2f8* are associated with tumor cell proliferation in colorectal cancer and cervical cancer respectively (Kim et al., 2020; Xu et al., 2019). Additionally, *Sprr2a*, *Fbln2* and *Fosl1* are related to the metastasis of cholangiocarcinomas and lung cancer (Baird et al., 2013; Mizuguchi et al., 2014; Vallejo et al., 2017). The results of these studies indicate some genes have similar effects on the proliferation and metastasis in different cancer contexts. Moreover, these findings also suggest that tumor grades correlate with the proliferation and metastasis of PDAC tumors. Tumor morphology is a critical parameter of tumor grades and is related to the interaction of cancer cells and TME. The crosstalk between cancer cells and the TME modulates tumor features. The roles of the gene signatures in the crosstalk between cancer cells and the TME must be investigated to obtain a better understanding of the mechanisms of proliferation and metastasis in PDAC. The results of signaling pathway enrichment analysis indicate that actin-binding activity, structural constituents of the cytoskeleton and growth factor activities are involved in the differentiation of PDAC tumors. A previous study reveals that actin-binding proteins are involved in the proliferation and invasiveness of cancer cells through changes of the cytoskeleton (Stevenson et al., 2012). The interactions between growth factors and their receptors mediate cancer cell migration and tumor metastasis (Yilmaz and Christofori, 2009). The involvement of these activities suggests that the histopathological features of tumors are the result of intensive molecular interactions in PDAC. Since these activities have been proved to be related to tumor growth and metastasis, this finding confirms that PDAC tumor grades are associated with the proliferation and metastasis of

PDAC. Confirmative experiments are required to validate the involvement of these activities which can influence the differentiation grade of PDAC.

**The strong correlation between tumor grades and mitosis in histopathology and transcriptomic profiles in PDAC.**

Tumor grades correlate with mitotic activities in PDAC tumor (Figure 8B and 14B). Notably, similar results have been observed in other types of human cancer. For example, a study of patients with lung adenocarcinoma shows that the cancer cell proliferation activity becomes more active as the tumor grades increase (Kalogeraki et al., 2010). Furthermore, tumor grades are associated with the mitotic index in patients with oral mucosal melanoma (Ma et al., 2017). The differential gene expression analysis of murine PDAC tumors in this thesis demonstrates that tumor grades are strongly associated with mitosis (Figure 8B, 14B and 14C). Compared with those in G1 tumors, most mice from the G4 cohort have a more active mitotic activity in PDAC tumor (Figure 14B). Altogether, these results suggest that the different degrees of histopathological differentiation in PDAC tumors have a molecular basis and that the changes of the gene expression pattern underlie tumor grades in pancreatic cancer.

The strong correlation between tumor grades and mitosis in PDAC indicates that both tumor differentiation and mitotic activities can be affected by the overlapping gene set (Figure 14C). These genes have been shown to be associated with the proliferation and progression of other cancer entites. For example, a high expression level of *Gkn1* and *Gkn2* suppresses the proliferation of cancer cells, and downregulated expression of these two genes promotes metastasis and is associated with the invasive phenotype and an advanced stage of GC patients (Dai et al., 2014; Moss et al., 2008; Yoon et al., 2019). Moreover, overexpression of *S100a4* promotes the proliferation of cancer cells via the inhibition of starvation-induced autophagy in lung cancer (Hou et al., 2018). Additionally, upregulated *S100a4* expression is associated with high tumor grades and results in tumor metastasis in breast cancer (Bresnick et al., 2015; Pedersen et al., 2002). Notably, *Fosl1* regulates cancer cell proliferation in lung cancer patients with *Kras* mutations (Vallejo et al., 2017). A high level of *Fosl1* expression leads to reduced *Cdh1* expression and increased expression levels of *N-cadherin* and *Snail* and drives the malignant progression through the activation of EMT in prostate cancer (Luo et al., 2018). The functional similarities of these genes in different cancer contexts provide evidence that the overlapping genes have effects on tumor grades and mitosis of cancer.

The balance between cell proliferation and differentiation serves an important role in the development of cancers. This balance might be mirrored by the correlation between mitosis and tumor grades. Thus, understanding the interaction network of the overlapping genes

affecting both mitosis and tumor grades could be important to elucidate the mechanisms of PDAC progression. This study shows that *Prkg2*, *Bmp2*, *Muc5ac* and *Clca1* are of critical importance in the predicted interaction network (Figure 14D). Notably, the expression patterns of these genes have been studied in other human cancers. For example, *Bmp2* overexpression results in the invasive property of cancer cells, a feature associated with high-grade tumor, in melanoma (Rothhammer et al., 2005). The results of the present study indicate that these genes and the interaction network between them are associated with tumor growth and malignancy of PDAC and that they are potential targets for the treatment of pancreatic cancer. Further studies should focus on the functions of these genes in PDAC.

**The presence of liver metastasis is associated with tumor grades.**

PDAC patients are characterized by a high risk of metastasis. Approximately, 91% of pancreatic cancer patients incur metastasis and suffer from metastatic diseases. Lymph node metastasis and other distant metastases, including liver and lung metastases, are incorporated into the TNM staging system of pancreatic cancer, highlighting that metastasis is an important parameter for the prognosis of PDAC patients. Clinical studies have revealed that the majority, approximately 76-94%, of PDAC metastases are in the liver (Haeno et al., 2012; Yachida et al., 2012), while 41-56% of PDAC patients bear peritoneum metastasis. Metastasis in the lymph nodes is found in approximately 41% of PDAC patients, while patients with lung metastasis account for 45-48% of PDAC patients (Haeno et al., 2012; Yachida et al., 2012).

PDAC patients with different metastatic sites exhibit distinct clinical outcomes. PDAC patients with lung metastasis have a better prognosis than those with liver metastasis. Patients with poor tumor differentiation are preferably associated with liver metastasis (Sahin et al., 2018), indicating that liver metastasis is related to more malignant PDAC tumors. Consistent with the previous study, this thesis indicates that there is a higher risk of liver metastasis in murine PDAC tumors as tumor grades increase (Figure 9C). The correlation between tumor grades and liver metastasis has also been observed in the transcriptomic profiles of murine PDAC primary tumors. Differential gene expression analysis reveals that the expression of *Gkn1*, *Muc5ac* and *Clca1* potentially underlies the correlation between tumor grades and liver metastasis in PDAC. *Gkn1* mediates EMT and the migration of cancer cells by regulating the ROS and the Pi3k/Akt signaling pathway in GC (Dokhaee et al., 2018). A recent study reveals that *Muc5ac* is associated with the invasion and migration of cancer cells in colorectal cancer through its interactions with CD44 (Pothuraju et al., 2020). Downregulated *Clca1* expression is related to a high risk of metastasis by regulating EMT process and results in a higher tumor stage in colorectal cancer (Li et al., 2017). Therefore,

the roles of these genes in PDAC must be investigated. The relationship between PDAC tumor grades and liver metastasis suggests liver metastasis may be an important prognostic indicator in PDAC.

Moreover, several studies have demonstrated that liver pre-metastatic niche formation is critical for the successful engraftment and survival of metastatic cancer cells (Costa-Silva et al., 2015; Peinado et al., 2011; Sceneay et al., 2013). The formation of the pre-metastatic niches in the liver involves interactions between specific molecules and hepatic stellate cells. A previous study shows that PDAC-derived exosomes with a high level of migration inhibitory factor (MIF) induce the secretion of Tgfβ and elevated expression of fibronectin in hepatic stellate cells, which engage in the formation of liver pre-metastatic niches and, thus foster the development of liver metastasis (Costa-Silva et al., 2015). Furthermore, the interaction between the tissue inhibitor of metalloproteinase-1 (Timp1) and CD63 activates hepatic stellate cells to form liver pre-metastatic niches (Grunwald et al., 2016). These studies indicate the liver pre-metastatic niche is a key player in the formation of liver metastasis. While the primary PDAC tumor samples are analyzed, secondary liver tumor samples are not included in this thesis. Considering the critical roles of pre-metastatic niches in the liver metastasis of PDAC, integrating the secondary liver tumor sample in the analysis could be extremely helpful for improving our understanding of the mechanisms of liver metastasis in PDAC.

**Tumors of different grades exhibit distinct subpopulations of immune cells.**

The analysis of immune cell infiltration in histological sections of murine PDAC tumors reveals that well-differentiated tumors have a higher percentage of infiltrated immune cells than undifferentiated tumors (Figure 10D). Several studies have shown that the interactions between immune cells and other cellular components in PDAC tumors influence the distribution and function of immune cells and that the crosstalk between cancer cells and the surrounding microenvironment leads to a complex immunosuppressive microenvironment (Feig et al., 2012; Stone and Beatty, 2019). The results of this study highlight the association of infiltrated immune cells with tumor grades in pancreatic cancer and, thus provides the evidence of immune cell infiltration modulating the tumor microenvironment, which has prognostic relevance in PDAC.

Immune cells account for approximately 50% of the cellular components in PDAC tumors. Many immune cell subpopulations have been identified in PDAC, including tumor-associated macrophages, dendritic cells, natural NK cells, B cells and T cells. Flow cytometry and immunofluorescence have been widely used for the identification and characterization of the immune cell subset in cancer research. However, certain factors are hampering the

application of these two methods, including the specific binding ability of antibodies, the antibodies' quality and concentration, the quality of biopsies, the quality of the fluorescent probes and the spillover effects of the fluorescence (Finak et al., 2016; Nguyen et al., 2013; Odell and Cook, 2013). Apart from flow cytometry and immunofluorescence, computational methods for the deconvolution of transcriptomic profiles of tumor tissues have been developed and are used to quantify the composition of infiltrated immune cells in the studies of tumor immunity (Finotello and Trajanoski, 2018). Various studies have successfully recovered the fractions of different cell types by employing these approaches (Newman et al., 2015; Zhong et al., 2013). This present study employs this method and identifies the 23 subpopulations of immune cells in the PDAC tumors (Figure 16A). Further confirmative experiments should be performed to validate these results.

Immune cell subpopulations play distinct roles in the TME. For example, high density of M2 macrophages is associated with pro-tumoral activities and the poor prognosis of PDAC patients, while M1 macrophages engage in pro-inflammatory activities and exhibit antitumor functions (Lankadasari et al., 2019). Therefore, the functional study of immune cell subsets is essential to elucidate the pathology of tumors. This study has identified the distribution patterns of four immune cell subpopulations, including M2 macrophages, plasmacytoid dendritic cells, Th2 cells and memory B cells, which show significant differences between high- and low- grade PDAC tumors (Figure 16). These results indicate that these immune cells potentially contribute to the malignancy of pancreatic cancer.

The interactions of immune cells modulate immune responses and are related to the pathology of various diseases. For example, a recent study reveals that dendritic cells and M2 macrophages engage in the regulation of inflammation mediated by Th2 cells (Cho et al., 2019). Moreover, the extensive interactions between Treg cells and antigen-presenting-like cells have been shown to be associated with the immunosuppression in the TME and drive the progression of PDAC (Jang et al., 2017; Thornton and Shevach, 2000). Investigating the interactions of the immune cell subsets identified in this study with other cell types, such as cancer cells, may provide insight into the network of immune cells in the TME and the mechanisms of immune cell infiltration.

In recent years, immunotherapies, such as adoptive cell therapy and immune checkpoint inhibitory (ICI) therapy, have made notable progress in improving the clinical outcomes of cancer patients. However, current immunotherapeutic approaches have not produced any promising results in pancreatic cancer to date (O' Reilly et al., 2019). The immunosuppressive microenvironment in PDAC tumors influences the efficacy of immune therapies and results in a resistance to immunotherapies. The infiltrated immune cells and their interactions with other cellular components have been shown to be associated with the

establishment of the immunosuppressive microenvironment in PDAC. For example, macrophages can inhibit the antitumor effects of $CD8^+$ T cells by secreting immunosuppressive factors, such as IL-10 and arginase-1 (Arg1), to prompt the progression of pancreatic cancer (Kaneda et al., 2016). It has also been reported that MDSCs mediate the suppression of IFN-γ and thus, allow the tumor to escape immunosurveillance (Nagaraj et al., 2012). The immune cell subpopulations contributing to the immunosuppressive microenvironment could be potential targets for immunotherapies in PDAC. Moreover, dendritic cells and macrophages have been shown to affect the accumulation of T cell receptor (TCR)-engineered T cells, thus associated with the therapeutic efficacy of TCR gene therapy (Hotblack et al., 2018). Therefore, the study of tumor immunity can provide insight into the function of infiltrated immune cells and improve the current immunotherapies for PDAC patients by reversing immunodeficiencies or enhancing their antitumor effects.

**Generation of new GEMMs of PDAC.**

The development of gene editing techniques and the great needs to study pancreatic cancer have driven an explosion of PDAC GEMMs. GEMMs have recapitulated morphological changes and genetic alterations in the progression of PDAC and provide a powerful tool for researchers to study tumor pathogenesis and the efficacy of relevant therapies. Using these mouse models, researchers have made great advances in improving our understanding of pancreatic cancer. New GEMMs generated by introducing genetic modifications have facilitated the functional study of genes involved in pancreatic cancer. For example, the present study establishes a new mouse model, *Ptf1a*$^{cre/+}$*, LSL-Kras*$^{G12D/+}$*; Tnc*$^{-/-}$ by introducing *Tnc* deletion. Notably, the present study reveals that *Tnc* deletion is involved in the formation of ADM and PanIN-1A lesions (Figure 21I and 21J). However, certain weaknesses have been identified in mouse models, such as the *iKras* mouse model, which also highlight the needs for the generation of new and improved mouse models. The advantage of the *iKras* mouse model is that oncogenic *Kras*$^{G12D}$ expression is temporally regulated and reversible. However, it has been shown that 70% of *iKras* mice incur tumor relapse due to the doxy-independent expression of *Kras*$^{G12D}$ (Kapoor et al., 2014). In this study, a new mouse model is generated to overcome the leaky expression of *iKras* mice, which allows the inactivation of the endogenous oncogenic *Kras* mutation.

The progression of PDAC involves the process of accumulating genetic alterations. Multi-omics analysis has revealed a complex molecular landscape of PDAC tumors. Whole-genome sequencing has identified the recurrent mutations in pancreatic cancer patients, such as *KRAS*, *CDKN2A* and *SMAD4,* and other oncogenic drivers (Cancer Genome Atlas Research Network, 2017). Several studies have also defined the consensus transcriptomic

subtypes of PDAC which have clinical relevance (Bailey et al., 2016; Chan-Seng-Yue et al., 2020; Collisson et al., 2011; Moffitt et al., 2015). Proteomic profiling data shows that the proteomic subtypes are associated with prognosis and therapy options (Cancer Genome Atlas Research Network, 2017; Law et al., 2020). The findings of this thesis demonstrate that several genes and cell subpopulations are involved in tumor grades, mitosis, metastasis and immune cell infiltration. An inducible dual-recombinase system was developed in 2014 and combines the flippase-FRT (Flp-*FRT*) and Cre-*loxP* recombination technologies, providing a good strategy for studying the network of these genes and immune cell subsets in PDAC (Schönhuber et al., 2014). The dual-recombinase system allows researchers to generate new mouse models to investigate the multiple stages of PDAC progression, tumor subpopulations and cell components in the TME. The combination of this system and the multi-omics analysis will provide further insight into pancreatic cancer.

**Conclusion**

In summary, this study has characterized the histopathology and transcriptomic profiles of PDAC tumors and generated a new mouse model. The correlation between survival time and metastasis has been identified. Mitosis, metastasis, stromal content and lymphocyte infiltration have been proved to be associated with tumor grades in the PDAC mouse models. The correlation between the classical PDAC subtype and tumor grades and the transcriptomic signatures of high- and low-grade tumors are identified. In pancreatic cancer, a strong correlation exists between mitotic activity and tumor grades at the histopathological and transcriptomic levels. Liver metastasis has been shown to be related to tumor grades and the molecular signatures of primary pancreatic tumors from the mice with liver metastasis have been identified. Four immune cell subsets, including M2 macrophages, plasmacytoid dendritic cells, Th2 cells and memory B cells, exhibit distinct distributions between high- and low-grade tumors, which indicates that they could engage in the progression of PDAC. A new mouse model has been developed to facilitate the inactivation of the endogenous oncogenic *Kras* mutation and three shRNAs are tested to regulate gene expression by targeting Cre recombinase through RNAi. This thesis reveals that *Tnc* deletion leads to more ADM and PanIN-1A lesions and that loss of *Hnf4α* function prolongs the survival time of mice with tumors.

## Acknowledgements

Hereby, I would like to thank everyone who contributed to the success of this PhD thesis.

First, I thank Prof. Dr. Dieter Saur for giving me the chance to work on this interesting project, for his advice, help, valuable comments on the project and revision of the thesis.

I owe my gratitude to PD Dr. Günter Schneider and Prof. Dr. Marc Schmidt-Supprian for their kindness being members of my PhD committee.

I also thank PD Dr. med. Moritz Jesinghaus for evalution of the pancreatic tumor tissues. I really appreciate the advice and help of Olga Seelbach and Dr. med. vet. Katja Steiger.

I am grateful to Fabio Boniolo for his work in the analysis of the correlation between the classical subtype of PDAC and tumor grades, principal component analysis, differential expression analysis, signalling pathway enrichment, and deconvolution of the sequencing data for immune cell subpopulations.

I thank all the members in the lab of Prof. Dieter Saur. They generated the mouse models which were used in this thesis. The study of this thesis was performed on the basis of the information and samples they collected and the analysis they performed. Their work makes this study possible.

Furthermore, I owe my gratitude to…

… Barbara Seidler and Dr. Nina Schönhuber for her advice and help in the generation of the new mouse model.
… Dr. Rupert Öllinger for his help in the ES cell culture.
… Dr. Chuan Shan for his advice and work on the *Tnc* and *Hnf4a* mouse models.
… Tânia Custódio Santos for teaching me how to use the confocal system.
… Magdalena Zukowska and Markus Raspe for excellent technical support.
… all animal caretakers for caring for the mice.
… all other colleagues for discussion and the nice atmosphere in the lab.

Last but not least, I thank my family and my friends who always support me.

## References

Adam, R. A., and Adam, Y. G. (2004). Malignant ascites: past, present, and future. J Am Coll Surg *198*, 999-1011.
Aguirre, A. J., Bardeesy, N., Sinha, M., Lopez, L., Tuveson, D. A., Horner, J., Redston, M. S., and DePinho, R. A. (2003). Activated Kras and Ink4a/Arf deficiency cooperate to produce metastatic pancreatic ductal adenocarcinoma. Genes Dev *17*, 3112-3126.
Aichler, M., Seiler, C., Tost, M., Siveke, J., Mazur, P. K., Da Silva-Buttkus, P., Bartsch, D. K., Langer, P., Chiblak, S., Durr, A., *et al.* (2012). Origin of pancreatic ductal adenocarcinoma from atypical flat lesions: a comparative study in transgenic mice and human tissues. J Pathol *226*, 723-734.
Alizadeh, A. A., Eisen, M. B., Davis, R. E., Ma, C., Lossos, I. S., Rosenwald, A., Boldrick, J. C., Sabet, H., Tran, T., Yu, X., *et al.* (2000). Distinct types of diffuse large B-cell lymphoma identified by gene expression profiling. Nature *403*, 503-511.
Amedei, A., Niccolai, E., and Prisco, D. (2014). Pancreatic cancer: role of the immune system in cancer progression and vaccine-based immunotherapy. Hum Vaccin Immunother *10*, 3354-3368.
Amundson, S. A., and Smilenov, L. B. (2010). Integration of biological knowledge and gene expression data for biomarker selection: FN1 as a potential predictor of radiation resistance in head and neck cancer. Cancer Biol Ther *10*, 1252-1255.
Ansell, S. M., Lesokhin, A. M., Borrello, I., Halwani, A., Scott, E. C., Gutierrez, M., Schuster, S. J., Millenson, M. M., Cattry, D., Freeman, G. J., *et al.* (2015). PD-1 blockade with nivolumab in relapsed or refractory Hodgkin's lymphoma. N Engl J Med *372*, 311-319.
Argraves, W. S., Greene, L. M., Cooley, M. A., and Gallagher, W. M. (2003). Fibulins: physiological and disease perspectives. EMBO Rep *4*, 1127-1131.
Bailey, P., Chang, D. K., Nones, K., Johns, A. L., Patch, A. M., Gingras, M. C., Miller, D. K., Christ, A. N., Bruxner, T. J., Quinn, M. C., *et al.* (2016). Genomic analyses identify molecular subtypes of pancreatic cancer. Nature *531*, 47-52.
Baird, B. N., Schliekelman, M. J., Ahn, Y. H., Chen, Y., Roybal, J. D., Gill, B. J., Mishra, D. K., Erez, B., O'Reilly, M., Yang, Y., *et al.* (2013). Fibulin-2 is a driver of malignant progression in lung adenocarcinoma. PLoS One *8*, e67054.
Bardeesy, N., Cheng, K. H., Berger, J. H., Chu, G. C., Pahler, J., Olson, P., Hezel, A. F., Horner, J., Lauwers, G. Y., Hanahan, D., and DePinho, R. A. (2006). Smad4 is dispensable for normal pancreas development yet critical in progression and tumor biology of pancreas cancer. Genes Dev *20*, 3130-3146.
Basso, D., Fogar, P., Falconi, M., Fadi, E., Sperti, C., Frasson, C., Greco, E., Tamburrino, D., Teolato, S., Moz, S., *et al.* (2013). Pancreatic tumors and immature immunosuppressive myeloid cells in blood and spleen: role of inhibitory co-stimulatory molecules PDL1 and CTLA4. An in vivo and in vitro study. PLoS One *8*, e54824.
Basso, D., Gnatta, E., Padoan, A., Fogar, P., Furlanello, S., Aita, A., Bozzato, D., Zambon, C. F., Arrigoni, G., Frasson, C., *et al.* (2017). PDAC-derived exosomes enrich the microenvironment in MDSCs in a SMAD4-dependent manner through a new calcium related axis. Oncotarget *8*, 84928-84944.
Bausch, D., Pausch, T., Krauss, T., Hopt, U. T., Fernandez-del-Castillo, C., Warshaw, A. L., Thayer, S. P., and Keck, T. (2011). Neutrophil granulocyte derived MMP-9 is a VEGF independent functional component of the angiogenic switch in pancreatic ductal adenocarcinoma. Angiogenesis *14*, 235-243.

Bayascas, J. R., Wullschleger, S., Sakamoto, K., Garcia-Martinez, J. M., Clacher, C., Komander, D., van Aalten, D. M., Boini, K. M., Lang, F., Lipina, C., *et al.* (2008). Mutation of the PDK1 PH domain inhibits protein kinase B/Akt, leading to small size and insulin resistance. Mol Cell Biol *28*, 3258-3272.

Beatty, G. L., and Gladney, W. L. (2015). Immune escape mechanisms as a guide for cancer immunotherapy. Clin Cancer Res *21*, 687-692.

Bengsch, F., Knoblock, D. M., Liu, A., McAllister, F., and Beatty, G. L. (2017). CTLA-4/CD80 pathway regulates T cell infiltration into pancreatic cancer. Cancer Immunol Immunother *66*, 1609-1617.

Biankin, A. V., Waddell, N., Kassahn, K. S., Gingras, M. C., Muthuswamy, L. B., Johns, A. L., Miller, D. K., Wilson, P. J., Patch, A. M., Wu, J., *et al.* (2012). Pancreatic cancer genomes reveal aberrations in axon guidance pathway genes. Nature *491*, 399-405.

Biffi, G., Oni, T. E., Spielman, B., Hao, Y., Elyada, E., Park, Y., Preall, J., and Tuveson, D. A. (2019). IL1-Induced JAK/STAT Signaling Is Antagonized by TGFbeta to Shape CAF Heterogeneity in Pancreatic Ductal Adenocarcinoma. Cancer Discov *9*, 282-301.

Bradford, M. M. (1976). A rapid and sensitive method for the quantitation of microgram quantities of protein utilizing the principle of protein-dye binding. Anal Biochem *72*, 248-254.

Brat, D. J., Lillemoe, K. D., Yeo, C. J., Warfield, P. B., and Hruban, R. H. (1998). Progression of pancreatic intraductal neoplasias to infiltrating adenocarcinoma of the pancreas. Am J Surg Pathol *22*, 163-169.

Bresnick, A. R., Weber, D. J., and Zimmer, D. B. (2015). S100 proteins in cancer. Nat Rev Cancer *15*, 96-109.

Bryant, K. L., Mancias, J. D., Kimmelman, A. C., and Der, C. J. (2014). KRAS: feeding pancreatic cancer proliferation. Trends Biochem Sci *39*, 91-100.

Budhu, A., Forgues, M., Ye, Q. H., Jia, H. L., He, P., Zanetti, K. A., Kammula, U. S., Chen, Y., Qin, L. X., Tang, Z. Y., and Wang, X. W. (2006). Prediction of venous metastases, recurrence, and prognosis in hepatocellular carcinoma based on a unique immune response signature of the liver microenvironment. Cancer Cell *10*, 99-111.

Bulle, A., Dekervel, J., Deschuttere, L., Nittner, D., Libbrecht, L., Janky, R., Plaisance, S., Topal, B., Coosemans, A., Lambrechts, D., *et al.* (2020). Gemcitabine Recruits M2-Type Tumor-Associated Macrophages into the Stroma of Pancreatic Cancer. Transl Oncol *13*, 100743.

Caiazza, F., McCarthy, N. S., Young, L., Hill, A. D., Harvey, B. J., and Thomas, W. (2011). Cytosolic phospholipase A2-alpha expression in breast cancer is associated with EGFR expression and correlates with an adverse prognosis in luminal tumours. Br J Cancer *104*, 338-344.

Calhoun, E. S., Jones, J. B., Ashfaq, R., Adsay, V., Baker, S. J., Valentine, V., Hempen, P. M., Hilgers, W., Yeo, C. J., Hruban, R. H., and Kern, S. E. (2003). BRAF and FBXW7 (CDC4, FBW7, AGO, SEL10) mutations in distinct subsets of pancreatic cancer: potential therapeutic targets. Am J Pathol *163*, 1255-1260.

Cancer Genome Atlas Research Network (2017). Integrated Genomic Characterization of Pancreatic Ductal Adenocarcinoma. Cancer Cell *32*, 185-203 e113.

Candido, J. B., Morton, J. P., Bailey, P., Campbell, A. D., Karim, S. A., Jamieson, T., Lapienyte, L., Gopinathan, A., Clark, W., McGhee, E. J., *et al.* (2018). CSF1R(+) Macrophages Sustain Pancreatic Tumor Growth through T Cell Suppression and Maintenance of Key Gene Programs that Define the Squamous Subtype. Cell Rep *23*, 1448-1460.

Cappello, P., Blaser, H., Gorrini, C., Lin, D. C., Elia, A. J., Wakeham, A., Haider, S., Boutros, P. C., Mason, J. M., Miller, N. A., *et al.* (2014). Role of Nek2 on centrosome duplication and aneuploidy in breast cancer cells. Oncogene *33*, 2375-2384.

Carr, R. M., and Fernandez-Zapico, M. E. (2016). Pancreatic cancer microenvironment, to target or not to target? EMBO Mol Med *8*, 80-82.
Cascinu, S., Falconi, M., Valentini, V., Jelic, S., and Group, E. G. W. (2010). Pancreatic cancer: ESMO Clinical Practice Guidelines for diagnosis, treatment and follow-up. Ann Oncol *21 Suppl 5*, v55-58.
Casimiro, M. C., Velasco-Velazquez, M., Aguirre-Alvarado, C., and Pestell, R. G. (2014). Overview of cyclins D1 function in cancer and the CDK inhibitor landscape: past and present. Expert Opin Investig Drugs *23*, 295-304.
Chan-Seng-Yue, M., Kim, J. C., Wilson, G. W., Ng, K., Figueroa, E. F., O'Kane, G. M., Connor, A. A., Denroche, R. E., Grant, R. C., McLeod, J., *et al.* (2020). Transcription phenotypes of pancreatic cancer are driven by genomic events during tumor evolution. Nat Genet *52*, 231-240.
Chang, D. K., Grimmond, S. M., and Biankin, A. V. (2014). Pancreatic cancer genomics. Curr Opin Genet Dev *24*, 74-81.
Chang, Y. Y., Yen, C. J., Chan, S. H., Chou, Y. W., Lee, Y. P., Bao, C. Y., Huang, C. J., and Huang, W. (2018). NEK2 Promotes Hepatoma Metastasis and Serves as Biomarker for High Recurrence Risk after Hepatic Resection. Ann Hepatol *17*, 843-856.
Chen, L., and Flies, D. B. (2013). Molecular mechanisms of T cell co-stimulation and co-inhibition. Nat Rev Immunol *13*, 227-242.
Chiquet-Ehrismann, R., and Tucker, R. P. (2011). Tenascins and the importance of adhesion modulation. Cold Spring Harb Perspect Biol *3*.
Chiquet, M. (1992). Tenascin: an extracellular matrix protein involved in morphogenesis of epithelial organs. Kidney Int *41*, 629-631.
Cho, K. S., Kang, S. A., Kim, S. D., Mun, S. J., Yu, H. S., and Roh, H. J. (2019). Dendritic cells and M2 macrophage play an important role in suppression of Th2-mediated inflammation by adipose stem cells-derived extracellular vesicles. Stem Cell Res *39*, 101500.
Chu, G. C., Kimmelman, A. C., Hezel, A. F., and DePinho, R. A. (2007). Stromal biology of pancreatic cancer. J Cell Biochem *101*, 887-907.
Chytil, A., Magnuson, M. A., Wright, C. V., and Moses, H. L. (2002). Conditional inactivation of the TGF-beta type II receptor using Cre:Lox. Genesis *32*, 73-75.
Clark, C. E., Hingorani, S. R., Mick, R., Combs, C., Tuveson, D. A., and Vonderheide, R. H. (2007). Dynamics of the immune reaction to pancreatic cancer from inception to invasion. Cancer Res *67*, 9518-9527.
Coffelt, S. B., Hughes, R., and Lewis, C. E. (2009). Tumor-associated macrophages: effectors of angiogenesis and tumor progression. Biochim Biophys Acta *1796*, 11-18.
Collado, M., Blasco, M. A., and Serrano, M. (2007). Cellular senescence in cancer and aging. Cell *130*, 223-233.
Collisson, E. A., Sadanandam, A., Olson, P., Gibb, W. J., Truitt, M., Gu, S., Cooc, J., Weinkle, J., Kim, G. E., Jakkula, L., *et al.* (2011). Subtypes of pancreatic ductal adenocarcinoma and their differing responses to therapy. Nat Med *17*, 500-503.
Connor, A. A., Denroche, R. E., Jang, G. H., Timms, L., Kalimuthu, S. N., Selander, I., McPherson, T., Wilson, G. W., Chan-Seng-Yue, M. A., Borozan, I., *et al.* (2017). Association of Distinct Mutational Signatures With Correlates of Increased Immune Activity in Pancreatic Ductal Adenocarcinoma. JAMA Oncol *3*, 774-783.
Conroy, T., Hammel, P., Hebbar, M., Ben Abdelghani, M., Wei, A. C., Raoul, J. L., Chone, L., Francois, E., Artru, P., Biagi, J. J., *et al.* (2018). FOLFIRINOX or Gemcitabine as Adjuvant Therapy for Pancreatic Cancer. N Engl J Med *379*, 2395-2406.
Costa-Silva, B., Aiello, N. M., Ocean, A. J., Singh, S., Zhang, H., Thakur, B. K., Becker, A., Hoshino, A., Mark, M. T., Molina, H., *et al.* (2015). Pancreatic cancer exosomes initiate pre-metastatic niche formation in the liver. Nat Cell Biol *17*, 816-826.

Cuddapah, V. A., and Sontheimer, H. (2011). Ion channels and transporters [corrected] in cancer. 2. Ion channels and the control of cancer cell migration. Am J Physiol Cell Physiol *301*, C541-549.
Dai, J., Zhang, N., Wang, J., Chen, M., and Chen, J. (2014). Gastrokine-2 is downregulated in gastric cancer and its restoration suppresses gastric tumorigenesis and cancer metastasis. Tumour Biol *35*, 4199-4207.
Darsigny, M., Babeu, J. P., Seidman, E. G., Gendron, F. P., Levy, E., Carrier, J., Perreault, N., and Boudreau, F. (2010). Hepatocyte nuclear factor-4alpha promotes gut neoplasia in mice and protects against the production of reactive oxygen species. Cancer Res *70*, 9423-9433.
Dauphin, M., Barbe, C., Lemaire, S., Nawrocki-Raby, B., Lagonotte, E., Delepine, G., Birembaut, P., Gilles, C., and Polette, M. (2013). Vimentin expression predicts the occurrence of metastases in non small cell lung carcinomas. Lung Cancer *81*, 117-122.
De Monte, L., Reni, M., Tassi, E., Clavenna, D., Papa, I., Recalde, H., Braga, M., Di Carlo, V., Doglioni, C., and Protti, M. P. (2011). Intratumor T helper type 2 cell infiltrate correlates with cancer-associated fibroblast thymic stromal lymphopoietin production and reduced survival in pancreatic cancer. J Exp Med *208*, 469-478.
de Silva Rudland, S., Martin, L., Roshanlall, C., Winstanley, J., Leinster, S., Platt-Higgins, A., Carroll, J., West, C., Barraclough, R., and Rudland, P. (2006). Association of S100A4 and osteopontin with specific prognostic factors and survival of patients with minimally invasive breast cancer. Clin Cancer Res *12*, 1192-1200.
De Sousa, E. M. F., Wang, X., Jansen, M., Fessler, E., Trinh, A., de Rooij, L. P., de Jong, J. H., de Boer, O. J., van Leersum, R., Bijlsma, M. F., *et al.* (2013). Poor-prognosis colon cancer is defined by a molecularly distinct subtype and develops from serrated precursor lesions. Nat Med *19*, 614-618.
de Vries, A., Flores, E. R., Miranda, B., Hsieh, H. M., van Oostrom, C. T., Sage, J., and Jacks, T. (2002). Targeted point mutations of p53 lead to dominant-negative inhibition of wild-type p53 function. Proc Natl Acad Sci U S A *99*, 2948-2953.
Decker, K., Goldman, D. C., Grasch, C. L., and Sussel, L. (2006). Gata6 is an important regulator of mouse pancreas development. Dev Biol *298*, 415-429.
Deng, Q., Wang, Q., Zong, W. Y., Zheng, D. L., Wen, Y. X., Wang, K. S., Teng, X. M., Zhang, X., Huang, J., and Han, Z. G. (2010). E2F8 contributes to human hepatocellular carcinoma via regulating cell proliferation. Cancer Res *70*, 782-791.
Deng, Y. J., Tang, N., Liu, C., Zhang, J. Y., An, S. L., Peng, Y. L., Ma, L. L., Li, G. Q., Jiang, Q., Hu, C. T., *et al.* (2014). CLIC4, ERp29, and Smac/DIABLO derived from metastatic cancer stem-like cells stratify prognostic risks of colorectal cancer. Clin Cancer Res *20*, 3809-3817.
Dewan, M. Z., Ahmed, S., Iwasaki, Y., Ohba, K., Toi, M., and Yamamoto, N. (2006). Stromal cell-derived factor-1 and CXCR4 receptor interaction in tumor growth and metastasis of breast cancer. Biomed Pharmacother *60*, 273-276.
Dias Carvalho, P., Guimaraes, C. F., Cardoso, A. P., Mendonca, S., Costa, A. M., Oliveira, M. J., and Velho, S. (2018). KRAS Oncogenic Signaling Extends beyond Cancer Cells to Orchestrate the Microenvironment. Cancer Res *78*, 7-14.
Dickins, R. A., Hemann, M. T., Zilfou, J. T., Simpson, D. R., Ibarra, I., Hannon, G. J., and Lowe, S. W. (2005). Probing tumor phenotypes using stable and regulated synthetic microRNA precursors. Nat Genet *37*, 1289-1295.
Dokhaee, F., Mazhari, S., Galehdari, M., Bahadori Monfared, A., and Baghaei, K. (2018). Evaluation of GKN1 and GKN2 gene expression as a biomarker of gastric cancer. Gastroenterol Hepatol Bed Bench *11*, S140-S145.

Domanska, U. M., Kruizinga, R. C., Nagengast, W. B., Timmer-Bosscha, H., Huls, G., de Vries, E. G., and Walenkamp, A. M. (2013). A review on CXCR4/CXCL12 axis in oncology: no place to hide. Eur J Cancer *49*, 219-230.

Dreux, N., Marty, M., Chibon, F., Velasco, V., Hostein, I., Ranchere-Vince, D., Terrier, P., and Coindre, J. M. (2010). Value and limitation of immunohistochemical expression of HMGA2 in mesenchymal tumors: about a series of 1052 cases. Mod Pathol *23*, 1657-1666.

Elyada, E., Bolisetty, M., Laise, P., Flynn, W. F., Courtois, E. T., Burkhart, R. A., Teinor, J. A., Belleau, P., Biffi, G., Lucito, M. S., *et al.* (2019). Cross-Species Single-Cell Analysis of Pancreatic Ductal Adenocarcinoma Reveals Antigen-Presenting Cancer-Associated Fibroblasts. Cancer Discov *9*, 1102-1123.

Ene-Obong, A., Clear, A. J., Watt, J., Wang, J., Fatah, R., Riches, J. C., Marshall, J. F., Chin-Aleong, J., Chelala, C., Gribben, J. G., *et al.* (2013). Activated pancreatic stellate cells sequester CD8+ T cells to reduce their infiltration of the juxtatumoral compartment of pancreatic ductal adenocarcinoma. Gastroenterology *145*, 1121-1132.

Enninga, E. A., Nevala, W. K., Holtan, S. G., Leontovich, A. A., and Markovic, S. N. (2016). Galectin-9 modulates immunity by promoting Th2/M2 differentiation and impacts survival in patients with metastatic melanoma. Melanoma Res *26*, 429-441.

Erkan, M., Hausmann, S., Michalski, C. W., Fingerle, A. A., Dobritz, M., Kleeff, J., and Friess, H. (2012). The role of stroma in pancreatic cancer: diagnostic and therapeutic implications. Nat Rev Gastroenterol Hepatol *9*, 454-467.

Eser, S., Reiff, N., Messer, M., Seidler, B., Gottschalk, K., Dobler, M., Hieber, M., Arbeiter, A., Klein, S., Kong, B., *et al.* (2013). Selective requirement of PI3K/PDK1 signaling for Kras oncogene-driven pancreatic cell plasticity and cancer. Cancer Cell *23*, 406-420.

Facciabene, A., Motz, G. T., and Coukos, G. (2012). T-regulatory cells: key players in tumor immune escape and angiogenesis. Cancer Res *72*, 2162-2171.

Fan, J. Q., Wang, M. F., Chen, H. L., Shang, D., Das, J. K., and Song, J. (2020). Current advances and outlooks in immunotherapy for pancreatic ductal adenocarcinoma. Mol Cancer *19*, 32.

Feig, C., Gopinathan, A., Neesse, A., Chan, D. S., Cook, N., and Tuveson, D. A. (2012). The pancreas cancer microenvironment. Clin Cancer Res *18*, 4266-4276.

Feldmann, G., Beaty, R., Hruban, R. H., and Maitra, A. (2007). Molecular genetics of pancreatic intraepithelial neoplasia. J Hepatobiliary Pancreat Surg *14*, 224-232.

Finak, G., Langweiler, M., Jaimes, M., Malek, M., Taghiyar, J., Korin, Y., Raddassi, K., Devine, L., Obermoser, G., Pekalski, M. L., *et al.* (2016). Standardizing Flow Cytometry Immunophenotyping Analysis from the Human ImmunoPhenotyping Consortium. Sci Rep *6*, 20686.

Finotello, F., and Trajanoski, Z. (2018). Quantifying tumor-infiltrating immune cells from transcriptomics data. Cancer Immunol Immunother *67*, 1031-1040.

Fluck, M., Tunc-Civelek, V., and Chiquet, M. (2000). Rapid and reciprocal regulation of tenascin-C and tenascin-Y expression by loading of skeletal muscle. J Cell Sci *113 ( Pt 20)*, 3583-3591.

Forsberg, E., Hirsch, E., Frohlich, L., Meyer, M., Ekblom, P., Aszodi, A., Werner, S., and Fassler, R. (1996). Skin wounds and severed nerves heal normally in mice lacking tenascin-C. Proc Natl Acad Sci U S A *93*, 6594-6599.

Franklin, O., Oman, M., and Wanders, A. (2020). A Case of Pancreatic Ductal Adenocarcinoma Arising From Atypical Flat Lesions. Pancreas *49*, e60-e61.

Gaida, M. M., Steffen, T. G., Gunther, F., Tschaharganeh, D. F., Felix, K., Bergmann, F., Schirmacher, P., and Hansch, G. M. (2012). Polymorphonuclear neutrophils promote dyshesion of tumor cells and elastase-mediated degradation of E-cadherin in pancreatic tumors. Eur J Immunol *42*, 3369-3380.

Gao, X. L., Zheng, M., Wang, H. F., Dai, L. L., Yu, X. H., Yang, X., Pang, X., Li, L., Zhang, M., Wang, S. S., *et al.* (2019). NR2F1 contributes to cancer cell dormancy, invasion and metastasis of salivary adenoid cystic carcinoma by activating CXCL12/CXCR4 pathway. BMC Cancer *19*, 743.
Gao, Y., Zhu, Y. Y., and Yuan, Z. (2015). Colloid (mucinous non-cystic) carcinoma of the pancreas: A case report. Oncol Lett *10*, 3195-3198.
Gentleman, R. C., Carey, V. J., Bates, D. M., Bolstad, B., Dettling, M., Dudoit, S., Ellis, B., Gautier, L., Ge, Y., Gentry, J., *et al.* (2004). Bioconductor: open software development for computational biology and bioinformatics. Genome Biol *5*, R80.
Gil, J., and Peters, G. (2006). Regulation of the INK4b-ARF-INK4a tumour suppressor locus: all for one or one for all. Nat Rev Mol Cell Biol *7*, 667-677.
Gocheva, V., Wang, H. W., Gadea, B. B., Shree, T., Hunter, K. E., Garfall, A. L., Berman, T., and Joyce, J. A. (2010). IL-4 induces cathepsin protease activity in tumor-associated macrophages to promote cancer growth and invasion. Genes Dev *24*, 241-255.
Goggins, M. (2007). Identifying molecular markers for the early detection of pancreatic neoplasia. Semin Oncol *34*, 303-310.
Goicoechea, S. M., Garcia-Mata, R., Staub, J., Valdivia, A., Sharek, L., McCulloch, C. G., Hwang, R. F., Urrutia, R., Yeh, J. J., Kim, H. J., and Otey, C. A. (2014). Palladin promotes invasion of pancreatic cancer cells by enhancing invadopodia formation in cancer-associated fibroblasts. Oncogene *33*, 1265-1273.
Golan, T., Kanji, Z. S., Epelbaum, R., Devaud, N., Dagan, E., Holter, S., Aderka, D., Paluch-Shimon, S., Kaufman, B., Gershoni-Baruch, R., *et al.* (2014). Overall survival and clinical characteristics of pancreatic cancer in BRCA mutation carriers. Br J Cancer *111*, 1132-1138.
Grosse-Steffen, T., Giese, T., Giese, N., Longerich, T., Schirmacher, P., Hansch, G. M., and Gaida, M. M. (2012). Epithelial-to-mesenchymal transition in pancreatic ductal adenocarcinoma and pancreatic tumor cell lines: the role of neutrophils and neutrophil-derived elastase. Clin Dev Immunol *2012*, 720768.
Grunwald, B., Harant, V., Schaten, S., Fruhschutz, M., Spallek, R., Hochst, B., Stutzer, K., Berchtold, S., Erkan, M., Prokopchuk, O., *et al.* (2016). Pancreatic Premalignant Lesions Secrete Tissue Inhibitor of Metalloproteinases-1, Which Activates Hepatic Stellate Cells Via CD63 Signaling to Create a Premetastatic Niche in the Liver. Gastroenterology *151*, 1011-1024 e1017.
Guery, L., Dubrot, J., Lippens, C., Brighouse, D., Malinge, P., Irla, M., Pot, C., Reith, W., Waldburger, J. M., and Hugues, S. (2014). Ag-presenting CpG-activated pDCs prime Th17 cells that induce tumor regression. Cancer Res *74*, 6430-6440.
Guinney, J., Dienstmann, R., Wang, X., de Reynies, A., Schlicker, A., Soneson, C., Marisa, L., Roepman, P., Nyamundanda, G., Angelino, P., *et al.* (2015). The consensus molecular subtypes of colorectal cancer. Nat Med *21*, 1350-1356.
Haeberle, L., and Esposito, I. (2019). Pathology of pancreatic cancer. Transl Gastroenterol Hepatol *4*, 50.
Haeno, H., Gonen, M., Davis, M. B., Herman, J. M., Iacobuzio-Donahue, C. A., and Michor, F. (2012). Computational modeling of pancreatic cancer reveals kinetics of metastasis suggesting optimum treatment strategies. Cell *148*, 362-375.
Hagemann, T., Robinson, S. C., Schulz, M., Trumper, L., Balkwill, F. R., and Binder, C. (2004). Enhanced invasiveness of breast cancer cell lines upon co-cultivation with macrophages is due to TNF-alpha dependent up-regulation of matrix metalloproteases. Carcinogenesis *25*, 1543-1549.
Hahn, S. A., Schutte, M., Hoque, A. T., Moskaluk, C. A., da Costa, L. T., Rozenblum, E., Weinstein, C. L., Fischer, A., Yeo, C. J., Hruban, R. H., and Kern, S. E. (1996). DPC4, a candidate tumor suppressor gene at human chromosome 18q21.1. Science *271*, 350-353.

Han, N., Zhang, Z., Liu, S., Ow, A., Ruan, M., Yang, W., and Zhang, C. (2017). Increased tumor-infiltrating plasmacytoid dendritic cells predicts poor prognosis in oral squamous cell carcinoma. Arch Oral Biol *78*, 129-134.
Hartwig, W., Hackert, T., Hinz, U., Gluth, A., Bergmann, F., Strobel, O., Buchler, M. W., and Werner, J. (2011). Pancreatic cancer surgery in the new millennium: better prediction of outcome. Ann Surg *254*, 311-319.
Hasebe, T., Tsuda, H., Tsubono, Y., Imoto, S., and Mukai, K. (1997). Fibrotic focus in invasive ductal carcinoma of the breast: a histopathological prognostic parameter for tumor recurrence and tumor death within three years after the initial operation. Jpn J Cancer Res *88*, 590-599.
Hayhurst, G. P., Lee, Y. H., Lambert, G., Ward, J. M., and Gonzalez, F. J. (2001). Hepatocyte nuclear factor 4alpha (nuclear receptor 2A1) is essential for maintenance of hepatic gene expression and lipid homeostasis. Mol Cell Biol *21*, 1393-1403.
Heldin, C. H., Miyazono, K., and ten Dijke, P. (1997). TGF-beta signalling from cell membrane to nucleus through SMAD proteins. Nature *390*, 465-471.
Helm, O., Mennrich, R., Petrick, D., Goebel, L., Freitag-Wolf, S., Roder, C., Kalthoff, H., Rocken, C., Sipos, B., Kabelitz, D., *et al.* (2014). Comparative characterization of stroma cells and ductal epithelium in chronic pancreatitis and pancreatic ductal adenocarcinoma. PLoS One *9*, e94357.
Hemann, M. T., Fridman, J. S., Zilfou, J. T., Hernando, E., Paddison, P. J., Cordon-Cardo, C., Hannon, G. J., and Lowe, S. W. (2003). An epi-allelic series of p53 hypomorphs created by stable RNAi produces distinct tumor phenotypes in vivo. Nat Genet *33*, 396-400.
Hicks, A. M., Chou, J., Capanu, M., Lowery, M. A., Yu, K. H., and O'Reilly, E. M. (2016). Pancreas Adenocarcinoma: Ascites, Clinical Manifestations, and Management Implications. Clin Colorectal Cancer *15*, 360-368.
Higashi, M., Yokoyama, S., Yamamoto, T., Goto, Y., Kitazono, I., Hiraki, T., Taguchi, H., Hashimoto, S., Fukukura, Y., Koriyama, C., *et al.* (2015). Mucin expression in endoscopic ultrasound-guided fine-needle aspiration specimens is a useful prognostic factor in pancreatic ductal adenocarcinoma. Pancreas *44*, 728-734.
Hingorani, S. R., Petricoin, E. F., Maitra, A., Rajapakse, V., King, C., Jacobetz, M. A., Ross, S., Conrads, T. P., Veenstra, T. D., Hitt, B. A., *et al.* (2003). Preinvasive and invasive ductal pancreatic cancer and its early detection in the mouse. Cancer Cell *4*, 437-450.
Hingorani, S. R., Wang, L., Multani, A. S., Combs, C., Deramaudt, T. B., Hruban, R. H., Rustgi, A. K., Chang, S., and Tuveson, D. A. (2005). Trp53R172H and KrasG12D cooperate to promote chromosomal instability and widely metastatic pancreatic ductal adenocarcinoma in mice. Cancer Cell *7*, 469-483.
Hoadley, K. A., Yau, C., Wolf, D. M., Cherniack, A. D., Tamborero, D., Ng, S., Leiserson, M. D. M., Niu, B., McLellan, M. D., Uzunangelov, V., *et al.* (2014). Multiplatform analysis of 12 cancer types reveals molecular classification within and across tissues of origin. Cell *158*, 929-944.
Hornberg, J. J., Bruggeman, F. J., Westerhoff, H. V., and Lankelma, J. (2006). Cancer: a Systems Biology disease. Biosystems *83*, 81-90.
Horstmann, S., Ferrari, S., and Klempnauer, K. H. (2000). Regulation of B-Myb activity by cyclin D1. Oncogene *19*, 298-306.
Hotblack, A., Holler, A., Piapi, A., Ward, S., Stauss, H. J., and Bennett, C. L. (2018). Tumor-Resident Dendritic Cells and Macrophages Modulate the Accumulation of TCR-Engineered T Cells in Melanoma. Mol Ther *26*, 1471-1481.
Hou, S., Tian, T., Qi, D., Sun, K., Yuan, Q., Wang, Z., Qin, Z., Wu, Z., Chen, Z., and Zhang, J. (2018). S100A4 promotes lung tumor development through beta-catenin pathway-mediated autophagy inhibition. Cell Death Dis *9*, 277.

Hruban, R. H., Adsay, N. V., Albores-Saavedra, J., Compton, C., Garrett, E. S., Goodman, S. N., Kern, S. E., Klimstra, D. S., Kloppel, G., Longnecker, D. S., *et al.* (2001). Pancreatic intraepithelial neoplasia: a new nomenclature and classification system for pancreatic duct lesions. Am J Surg Pathol *25*, 579-586.

Hsieh, Y. H., Hsieh, S. C., Lee, C. H., Yang, S. F., Cheng, C. W., Tang, M. J., Lin, C. L., Lin, C. L., and Chou, R. H. (2015). Targeting EMP3 suppresses proliferation and invasion of hepatocellular carcinoma cells through inactivation of PI3K/Akt pathway. Oncotarget *6*, 34859-34874.

Hu, D., Ansari, D., Pawlowski, K., Zhou, Q., Sasor, A., Welinder, C., Kristl, T., Bauden, M., Rezeli, M., Jiang, Y., *et al.* (2018). Proteomic analyses identify prognostic biomarkers for pancreatic ductal adenocarcinoma. Oncotarget *9*, 9789-9807.

Huang, C., Li, Z., Li, N., Li, Y., Chang, A., Zhao, T., Wang, X., Wang, H., Gao, S., Yang, S., *et al.* (2018). Interleukin 35 Expression Correlates With Microvessel Density in Pancreatic Ductal Adenocarcinoma, Recruits Monocytes, and Promotes Growth and Angiogenesis of Xenograft Tumors in Mice. Gastroenterology *154*, 675-688.

Huang da, W., Sherman, B. T., and Lempicki, R. A. (2009a). Bioinformatics enrichment tools: paths toward the comprehensive functional analysis of large gene lists. Nucleic Acids Res *37*, 1-13.

Huang da, W., Sherman, B. T., and Lempicki, R. A. (2009b). Systematic and integrative analysis of large gene lists using DAVID bioinformatics resources. Nat Protoc *4*, 44-57.

Huang, W., Chiquet-Ehrismann, R., Moyano, J. V., Garcia-Pardo, A., and Orend, G. (2001). Interference of tenascin-C with syndecan-4 binding to fibronectin blocks cell adhesion and stimulates tumor cell proliferation. Cancer Res *61*, 8586-8594.

Hustinx, S. R., Leoni, L. M., Yeo, C. J., Brown, P. N., Goggins, M., Kern, S. E., Hruban, R. H., and Maitra, A. (2005). Concordant loss of MTAP and p16/CDKN2A expression in pancreatic intraepithelial neoplasia: evidence of homozygous deletion in a noninvasive precursor lesion. Mod Pathol *18*, 959-963.

Ideno, N., Yamaguchi, H., Ghosh, B., Gupta, S., Okumura, T., Steffen, D. J., Fisher, C. G., Wood, L. D., Singhi, A. D., Nakamura, M., *et al.* (2018). GNAS(R201C) Induces Pancreatic Cystic Neoplasms in Mice That Express Activated KRAS by Inhibiting YAP1 Signaling. Gastroenterology *155*, 1593-1607 e1512.

Ikenaga, N., Ohuchida, K., Mizumoto, K., Yu, J., Fujita, H., Nakata, K., Ueda, J., Sato, N., Nagai, E., and Tanaka, M. (2009). S100A4 mRNA is a diagnostic and prognostic marker in pancreatic carcinoma. J Gastrointest Surg *13*, 1852-1858.

Ilhan, O., Han, U., Onal, B., and Celik, S. Y. (2010). Prognostic significance of MUC1, MUC2 and MUC5AC expressions in gastric carcinoma. Turk J Gastroenterol *21*, 345-352.

Imaoka, H., Shimizu, Y., Mizuno, N., Hara, K., Hijioka, S., Tajika, M., Kondo, S., Tanaka, T., Ogura, T., Obayashi, T., *et al.* (2014). Clinical characteristics of adenosquamous carcinoma of the pancreas: a matched case-control study. Pancreas *43*, 287-290.

Jackson, E. L., Willis, N., Mercer, K., Bronson, R. T., Crowley, D., Montoya, R., Jacks, T., and Tuveson, D. A. (2001). Analysis of lung tumor initiation and progression using conditional expression of oncogenic K-ras. Genes Dev *15*, 3243-3248.

Jang, J. E., Hajdu, C. H., Liot, C., Miller, G., Dustin, M. L., and Bar-Sagi, D. (2017). Crosstalk between Regulatory T Cells and Tumor-Associated Dendritic Cells Negates Anti-tumor Immunity in Pancreatic Cancer. Cell Rep *20*, 558-571.

Janku, F., Wheler, J. J., Naing, A., Falchook, G. S., Hong, D. S., Stepanek, V. M., Fu, S., Piha-Paul, S. A., Lee, J. J., Luthra, R., *et al.* (2013). PIK3CA mutation H1047R is associated with response to PI3K/AKT/mTOR signaling pathway inhibitors in early-phase clinical trials. Cancer Res *73*, 276-284.

Jares, P., Colomer, D., and Campo, E. (2007). Genetic and molecular pathogenesis of mantle cell lymphoma: perspectives for new targeted therapeutics. Nat Rev Cancer *7*, 750-762.
Javle, M., Li, Y., Tan, D., Dong, X., Chang, P., Kar, S., and Li, D. (2014). Biomarkers of TGF-beta signaling pathway and prognosis of pancreatic cancer. PLoS One *9*, e85942.
Jia, W., Gao, X. J., Zhang, Z. D., Yang, Z. X., and Zhang, G. (2013). S100A4 silencing suppresses proliferation, angiogenesis and invasion of thyroid cancer cells through downregulation of MMP-9 and VEGF. Eur Rev Med Pharmacol Sci *17*, 1495-1508.
Jiang, H., He, C., Geng, S., Sheng, H., Shen, X., Zhang, X., Li, H., Zhu, S., Chen, X., Yang, C., and Gao, H. (2012). RhoT1 and Smad4 are correlated with lymph node metastasis and overall survival in pancreatic cancer. PLoS One *7*, e42234.
Jiang, X., Hao, H. X., Growney, J. D., Woolfenden, S., Bottiglio, C., Ng, N., Lu, B., Hsieh, M. H., Bagdasarian, L., Meyer, R., *et al.* (2013). Inactivating mutations of RNF43 confer Wnt dependency in pancreatic ductal adenocarcinoma. Proc Natl Acad Sci U S A *110*, 12649-12654.
Jimeno, A., and Hidalgo, M. (2006). Molecular biomarkers: their increasing role in the diagnosis, characterization, and therapy guidance in pancreatic cancer. Mol Cancer Ther *5*, 787-796.
Jin, T., Zhang, Z., Yang, X. F., and Luo, J. S. (2015). S100A4 expression is closely linked to genesis and progression of glioma by regulating proliferation, apoptosis, migration and invasion. Asian Pac J Cancer Prev *16*, 2883-2887.
Jones, S., Zhang, X., Parsons, D. W., Lin, J. C., Leary, R. J., Angenendt, P., Mankoo, P., Carter, H., Kamiyama, H., Jimeno, A., *et al.* (2008). Core signaling pathways in human pancreatic cancers revealed by global genomic analyses. Science *321*, 1801-1806.
Kadaba, R., Birke, H., Wang, J., Hooper, S., Andl, C. D., Di Maggio, F., Soylu, E., Ghallab, M., Bor, D., Froeling, F. E., *et al.* (2013). Imbalance of desmoplastic stromal cell numbers drives aggressive cancer processes. J Pathol *230*, 107-117.
Kalimuthu, S. N., Wilson, G. W., Grant, R. C., Seto, M., O'Kane, G., Vajpeyi, R., Notta, F., Gallinger, S., and Chetty, R. (2020). Morphological classification of pancreatic ductal adenocarcinoma that predicts molecular subtypes and correlates with clinical outcome. Gut *69*, 317-328.
Kalogeraki, A., Tzardi, M., Zoras, O., Giannikaki, E., Papadakis, M., Tamiolakis, D., Petraki, P. E., Diamantis, A., Siafakas, N., and Stathopoulos, E. (2010). Apoptosis and cell proliferation correlated with tumor grade in patients with lung adenocarcinoma. In Vivo *24*, 667-670.
Kanda, M., Matthaei, H., Wu, J., Hong, S. M., Yu, J., Borges, M., Hruban, R. H., Maitra, A., Kinzler, K., Vogelstein, B., and Goggins, M. (2012). Presence of somatic mutations in most early-stage pancreatic intraepithelial neoplasia. Gastroenterology *142*, 730-733 e739.
Kapoor, A., Yao, W., Ying, H., Hua, S., Liewen, A., Wang, Q., Zhong, Y., Wu, C. J., Sadanandam, A., Hu, B., *et al.* (2014). Yap1 activation enables bypass of oncogenic Kras addiction in pancreatic cancer. Cell *158*, 185-197.
Kawada, K., Hasegawa, S., Murakami, T., Itatani, Y., Hosogi, H., Sonoshita, M., Kitamura, T., Fujishita, T., Iwamoto, M., Matsumoto, T., *et al.* (2011). Molecular mechanisms of liver metastasis. Int J Clin Oncol *16*, 464-472.
Kenkel, J. A., Tseng, W. W., Davidson, M. G., Tolentino, L. L., Choi, O., Bhattacharya, N., Seeley, E. S., Winer, D. A., Reticker-Flynn, N. E., and Engleman, E. G. (2017). An Immunosuppressive Dendritic Cell Subset Accumulates at Secondary Sites and Promotes Metastasis in Pancreatic Cancer. Cancer Res *77*, 4158-4170.
Kikuta, K., Masamune, A., Watanabe, T., Ariga, H., Itoh, H., Hamada, S., Satoh, K., Egawa, S., Unno, M., and Shimosegawa, T. (2010). Pancreatic stellate cells promote epithelial-

mesenchymal transition in pancreatic cancer cells. Biochem Biophys Res Commun *403*, 380-384.
Kim, L. K., Park, S. A., Eoh, K. J., Heo, T. H., Kim, Y. T., and Kim, H. J. (2020). E2F8 regulates the proliferation and invasion through epithelial-mesenchymal transition in cervical cancer. Int J Biol Sci *16*, 320-329.
Kimura, Y., Fukuda, A., Ogawa, S., Maruno, T., Takada, Y., Tsuda, M., Hiramatsu, Y., Araki, O., Nagao, M., Yoshikawa, T., *et al.* (2018). ARID1A Maintains Differentiation of Pancreatic Ductal Cells and Inhibits Development of Pancreatic Ductal Adenocarcinoma in Mice. Gastroenterology *155*, 194-209 e192.
Kini Bailur, J., Gueckel, B., and Pawelec, G. (2016). Prognostic impact of high levels of circulating plasmacytoid dendritic cells in breast cancer. J Transl Med *14*, 151.
Kleeff, J., Korc, M., Apte, M., La Vecchia, C., Johnson, C. D., Biankin, A. V., Neale, R. E., Tempero, M., Tuveson, D. A., Hruban, R. H., and Neoptolemos, J. P. (2016). Pancreatic cancer. Nat Rev Dis Primers *2*, 16022.
Kleeff, J., Kusama, T., Rossi, D. L., Ishiwata, T., Maruyama, H., Friess, H., Buchler, M. W., Zlotnik, A., and Korc, M. (1999). Detection and localization of Mip-3alpha/LARC/Exodus, a macrophage proinflammatory chemokine, and its CCR6 receptor in human pancreatic cancer. Int J Cancer *81*, 650-657.
Kloppel, G., Lingenthal, G., von Bulow, M., and Kern, H. F. (1985). Histological and fine structural features of pancreatic ductal adenocarcinomas in relation to growth and prognosis: studies in xenografted tumours and clinico-histopathological correlation in a series of 75 cases. Histopathology *9*, 841-856.
Knudsen, E. S., Vail, P., Balaji, U., Ngo, H., Botros, I. W., Makarov, V., Riaz, N., Balachandran, V., Leach, S., Thompson, D. M., *et al.* (2017). Stratification of Pancreatic Ductal Adenocarcinoma: Combinatorial Genetic, Stromal, and Immunologic Markers. Clin Cancer Res *23*, 4429-4440.
Komura, T., Sakai, Y., Harada, K., Kawaguchi, K., Takabatake, H., Kitagawa, H., Wada, T., Honda, M., Ohta, T., Nakanuma, Y., and Kaneko, S. (2015). Inflammatory features of pancreatic cancer highlighted by monocytes/macrophages and CD4+ T cells with clinical impact. Cancer Sci *106*, 672-686.
Kondo, E., Furukawa, T., Yoshinaga, K., Kijima, H., Semba, S., Yatsuoka, T., Yokoyama, T., Fukushige, S., and Horii, A. (2000). Not hMSH2 but hMLH1 is frequently silenced by hypermethylation in endometrial cancer but rarely silenced in pancreatic cancer with microsatellite instability. Int J Oncol *17*, 535-541.
Koorstra, J. B., Hustinx, S. R., Offerhaus, G. J., and Maitra, A. (2008). Pancreatic carcinogenesis. Pancreatology *8*, 110-125.
Kouros-Mehr, H., Slorach, E. M., Sternlicht, M. D., and Werb, Z. (2006). GATA-3 maintains the differentiation of the luminal cell fate in the mammary gland. Cell *127*, 1041-1055.
Krimpenfort, P., Quon, K. C., Mooi, W. J., Loonstra, A., and Berns, A. (2001). Loss of p16Ink4a confers susceptibility to metastatic melanoma in mice. Nature *413*, 83-86.
Kumar, M., Martin, A., Nirgude, S., Chaudhary, B., Mondal, S., and Sarkar, A. (2020). Quinacrine inhibits GSTA1 activity and induces apoptosis through G1/S arrest and generation of ROS in human non-small cell lung cancer cell lines. Oncotarget *11*, 1603-1617.
Kurahara, H., Shinchi, H., Mataki, Y., Maemura, K., Noma, H., Kubo, F., Sakoda, M., Ueno, S., Natsugoe, S., and Takao, S. (2011). Significance of M2-polarized tumor-associated macrophage in pancreatic cancer. J Surg Res *167*, e211-219.
Kurahara, H., Takao, S., Maemura, K., Mataki, Y., Kuwahata, T., Maeda, K., Sakoda, M., Iino, S., Ishigami, S., Ueno, S., *et al.* (2013). M2-polarized tumor-associated macrophage infiltration of regional lymph nodes is associated with nodal lymphangiogenesis and occult nodal involvement in pN0 pancreatic cancer. Pancreas *42*, 155-159.

Kwei, K. A., Bashyam, M. D., Kao, J., Ratheesh, R., Reddy, E. C., Kim, Y. H., Montgomery, K., Giacomini, C. P., Choi, Y. L., Chatterjee, S., *et al.* (2008). Genomic profiling identifies GATA6 as a candidate oncogene amplified in pancreatobiliary cancer. PLoS Genet *4*, e1000081.
Labidi-Galy, S. I., Treilleux, I., Goddard-Leon, S., Combes, J. D., Blay, J. Y., Ray-Coquard, I., Caux, C., and Bendriss-Vermare, N. (2012). Plasmacytoid dendritic cells infiltrating ovarian cancer are associated with poor prognosis. Oncoimmunology *1*, 380-382.
Laemmli, U. K. (1970). Cleavage of structural proteins during the assembly of the head of bacteriophage T4. Nature *227*, 680-685.
Lankadasari, M. B., Mukhopadhyay, P., Mohammed, S., and Harikumar, K. B. (2019). TAMing pancreatic cancer: combat with a double edged sword. Mol Cancer *18*, 48.
LaPak, K. M., and Burd, C. E. (2014). The molecular balancing act of p16(INK4a) in cancer and aging. Mol Cancer Res *12*, 167-183.
Law, H. C., Lagundzin, D., Clement, E. J., Qiao, F., Wagner, Z. S., Krieger, K. L., Costanzo-Garvey, D., Caffrey, T. C., Grem, J. L., DiMaio, D. J., *et al.* (2020). The Proteomic Landscape of Pancreatic Ductal Adenocarcinoma Liver Metastases Identifies Molecular Subtypes and Associations with Clinical Response. Clin Cancer Res *26*, 1065-1076.
Lawlor, M. A., Mora, A., Ashby, P. R., Williams, M. R., Murray-Tait, V., Malone, L., Prescott, A. R., Lucocq, J. M., and Alessi, D. R. (2002). Essential role of PDK1 in regulating cell size and development in mice. EMBO J *21*, 3728-3738.
Lazarevich, N. L., Shavochkina, D. A., Fleishman, D. I., Kustova, I. F., Morozova, O. V., Chuchuev, E. S., and Patyutko, Y. I. (2010). Deregulation of hepatocyte nuclear factor 4 (HNF4)as a marker of epithelial tumors progression. Exp Oncol *32*, 167-171.
Lee, C. L., Moding, E. J., Huang, X., Li, Y., Woodlief, L. Z., Rodrigues, R. C., Ma, Y., and Kirsch, D. G. (2012). Generation of primary tumors with Flp recombinase in FRT-flanked p53 mice. Dis Model Mech *5*, 397-402.
Lee, S., Park, Y. R., Kim, S. H., Park, E. J., Kang, M. J., So, I., Chun, J. N., and Jeon, J. H. (2016). Geraniol suppresses prostate cancer growth through down-regulation of E2F8. Cancer Med *5*, 2899-2908.
Lelaidier, M., Diaz-Rodriguez, Y., Cordeau, M., Cordeiro, P., Haddad, E., Herblot, S., and Duval, M. (2015). TRAIL-mediated killing of acute lymphoblastic leukemia by plasmacytoid dendritic cell-activated natural killer cells. Oncotarget *6*, 29440-29455.
Li, G., Wang, Z., Zhang, C., Liu, X., Yang, F., Sun, L., Liang, J., Hu, H., Liu, Y., You, G., *et al.* (2018). MEGF10, a Glioma Survival-Associated Molecular Signature, Predicts IDH Mutation Status. Dis Markers *2018*, 5975216.
Li, X., Hu, W., Zhou, J., Huang, Y., Peng, J., Yuan, Y., Yu, J., and Zheng, S. (2017). CLCA1 suppresses colorectal cancer aggressiveness via inhibition of the Wnt/beta-catenin signaling pathway. Cell Commun Signal *15*, 38.
Ligorio, M., Sil, S., Malagon-Lopez, J., Nieman, L. T., Misale, S., Di Pilato, M., Ebright, R. Y., Karabacak, M. N., Kulkarni, A. S., Liu, A., *et al.* (2019). Stromal Microenvironment Shapes the Intratumoral Architecture of Pancreatic Cancer. Cell *178*, 160-175 e127.
Lim, S. A., Kim, J., Jeon, S., Shin, M. H., Kwon, J., Kim, T. J., Im, K., Han, Y., Kwon, W., Kim, S. W., *et al.* (2019). Defective Localization With Impaired Tumor Cytotoxicity Contributes to the Immune Escape of NK Cells in Pancreatic Cancer Patients. Front Immunol *10*, 496.
Ling, Z., and Li, R. (2014). Clinicopathological and prognostic value of S100A4 expression in gastric cancer: a meta-analysis. Int J Biol Markers *29*, e99-e111.
Liou, G. Y., Doppler, H., Necela, B., Edenfield, B., Zhang, L., Dawson, D. W., and Storz, P. (2015). Mutant KRAS-induced expression of ICAM-1 in pancreatic acinar cells causes

attraction of macrophages to expedite the formation of precancerous lesions. Cancer Discov *5*, 52-63.
Liou, G. Y., Doppler, H., Necela, B., Krishna, M., Crawford, H. C., Raimondo, M., and Storz, P. (2013). Macrophage-secreted cytokines drive pancreatic acinar-to-ductal metaplasia through NF-kappaB and MMPs. J Cell Biol *202*, 563-577.
Liu, C., Lou, Y., Lizee, G., Qin, H., Liu, S., Rabinovich, B., Kim, G. J., Wang, Y. H., Ye, Y., Sikora, A. G., *et al.* (2008). Plasmacytoid dendritic cells induce NK cell-dependent, tumor antigen-specific T cell cross-priming and tumor regression in mice. J Clin Invest *118*, 1165-1175.
Liu, C. Y., Xu, J. Y., Shi, X. Y., Huang, W., Ruan, T. Y., Xie, P., and Ding, J. L. (2013). M2-polarized tumor-associated macrophages promoted epithelial-mesenchymal transition in pancreatic cancer cells, partially through TLR4/IL-10 signaling pathway. Lab Invest *93*, 844-854.
Liu, G., McDonnell, T. J., Montes de Oca Luna, R., Kapoor, M., Mims, B., El-Naggar, A. K., and Lozano, G. (2000). High metastatic potential in mice inheriting a targeted p53 missense mutation. Proc Natl Acad Sci U S A *97*, 4174-4179.
Liu, M., Hancock, S. E., Sultani, G., Wilkins, B. P., Ding, E., Osborne, B., Quek, L. E., and Turner, N. (2019). Snail-Overexpression Induces Epithelial-mesenchymal Transition and Metabolic Reprogramming in Human Pancreatic Ductal Adenocarcinoma and Non-tumorigenic Ductal Cells. J Clin Med *8*.
Liu, R. Z., Garcia, E., Glubrecht, D. D., Poon, H. Y., Mackey, J. R., and Godbout, R. (2015). CRABP1 is associated with a poor prognosis in breast cancer: adding to the complexity of breast cancer cell response to retinoic acid. Mol Cancer *14*, 129.
Liu, X., Gao, Y., Lu, Y., Zhang, J., Li, L., and Yin, F. (2014). Upregulation of NEK2 is associated with drug resistance in ovarian cancer. Oncol Rep *31*, 745-754.
Love, M. I., Huber, W., and Anders, S. (2014). Moderated estimation of fold change and dispersion for RNA-seq data with DESeq2. Genome Biol *15*, 550.
Luker, K. E., and Luker, G. D. (2006). Functions of CXCL12 and CXCR4 in breast cancer. Cancer Lett *238*, 30-41.
Luo, Y. Z., He, P., and Qiu, M. X. (2018). FOSL1 enhances growth and metastasis of human prostate cancer cells through epithelial mesenchymal transition pathway. Eur Rev Med Pharmacol Sci *22*, 8609-8615.
Luttges, J., Schemm, S., Vogel, I., Hedderich, J., Kremer, B., and Kloppel, G. (2000). The grade of pancreatic ductal carcinoma is an independent prognostic factor and is superior to the immunohistochemical assessment of proliferation. J Pathol *191*, 154-161.
Ma, X., Wu, Y., Zhang, T., Song, H., Jv, H., Guo, W., and Ren, G. (2017). Ki67 Proliferation Index as a Histopathological Predictive and Prognostic Parameter of Oral Mucosal Melanoma in Patients without Distant Metastases. J Cancer *8*, 3828-3837.
Mace, T. A., Shakya, R., Pitarresi, J. R., Swanson, B., McQuinn, C. W., Loftus, S., Nordquist, E., Cruz-Monserrate, Z., Yu, L., Young, G., *et al.* (2018). IL-6 and PD-L1 antibody blockade combination therapy reduces tumour progression in murine models of pancreatic cancer. Gut *67*, 320-332.
Malek, A., Bakhidze, E., Noske, A., Sers, C., Aigner, A., Schafer, R., and Tchernitsa, O. (2008). HMGA2 gene is a promising target for ovarian cancer silencing therapy. Int J Cancer *123*, 348-356.
Marchetti, A., Buttitta, F., Pellegrini, S., Bertacca, G., Chella, A., Carnicelli, V., Tognoni, V., Filardo, A., Angeletti, C. A., and Bevilacqua, G. (1997). Alterations of P16 (MTS1) in node-positive non-small cell lung carcinomas. J Pathol *181*, 178-182.
Marisa, L., de Reynies, A., Duval, A., Selves, J., Gaub, M. P., Vescovo, L., Etienne-Grimaldi, M. C., Schiappa, R., Guenot, D., Ayadi, M., *et al.* (2013). Gene expression classification of

colon cancer into molecular subtypes: characterization, validation, and prognostic value. PLoS Med *10*, e1001453.
Martinez-Bosch, N., Vinaixa, J., and Navarro, P. (2018). Immune Evasion in Pancreatic Cancer: From Mechanisms to Therapy. Cancers (Basel) *10*.
Matsusaka, K., Funata, S., Fukayama, M., and Kaneda, A. (2014). DNA methylation in gastric cancer, related to Helicobacter pylori and Epstein-Barr virus. World J Gastroenterol *20*, 3916-3926.
Matthaei, H., Wu, J., Dal Molin, M., Shi, C., Perner, S., Kristiansen, G., Lingohr, P., Kalff, J. C., Wolfgang, C. L., Kinzler, K. W., *et al.* (2014). GNAS sequencing identifies IPMN-specific mutations in a subgroup of diminutive pancreatic cysts referred to as "incipient IPMNs". Am J Surg Pathol *38*, 360-363.
Matzinger, P., and Kamala, T. (2011). Tissue-based class control: the other side of tolerance. Nat Rev Immunol *11*, 221-230.
McGranahan, N., and Swanton, C. (2017). Clonal Heterogeneity and Tumor Evolution: Past, Present, and the Future. Cell *168*, 613-628.
Mehra, R., Varambally, S., Ding, L., Shen, R., Sabel, M. S., Ghosh, D., Chinnaiyan, A. M., and Kleer, C. G. (2005). Identification of GATA3 as a breast cancer prognostic marker by global gene expression meta-analysis. Cancer Res *65*, 11259-11264.
Midwood, K. S., and Orend, G. (2009). The role of tenascin-C in tissue injury and tumorigenesis. J Cell Commun Signal *3*, 287-310.
Mizuguchi, Y., Isse, K., Specht, S., Lunz, J. G., 3rd, Corbitt, N., Takizawa, T., and Demetris, A. J. (2014). Small proline rich protein 2a in benign and malignant liver disease. Hepatology *59*, 1130-1143.
Mlecnik, B., Bindea, G., Angell, H. K., Maby, P., Angelova, M., Tougeron, D., Church, S. E., Lafontaine, L., Fischer, M., Fredriksen, T., *et al.* (2016). Integrative Analyses of Colorectal Cancer Show Immunoscore Is a Stronger Predictor of Patient Survival Than Microsatellite Instability. Immunity *44*, 698-711.
Moffitt, R. A., Marayati, R., Flate, E. L., Volmar, K. E., Loeza, S. G., Hoadley, K. A., Rashid, N. U., Williams, L. A., Eaton, S. C., Chung, A. H., *et al.* (2015). Virtual microdissection identifies distinct tumor- and stroma-specific subtypes of pancreatic ductal adenocarcinoma. Nat Genet *47*, 1168-1178.
Morita, K., Mito, K., Niki, T., and Fukushima, N. (2018). Is an atypical flat lesion (AFL) a precursor lesion of the pancreatic ductal adenocarcinoma in human? Pathol Int.
Morris, J. P. t., Cano, D. A., Sekine, S., Wang, S. C., and Hebrok, M. (2010). Beta-catenin blocks Kras-dependent reprogramming of acini into pancreatic cancer precursor lesions in mice. J Clin Invest *120*, 508-520.
Moss, S. F., Lee, J. W., Sabo, E., Rubin, A. K., Rommel, J., Westley, B. R., May, F. E., Gao, J., Meitner, P. A., Tavares, R., and Resnick, M. B. (2008). Decreased expression of gastrokine 1 and the trefoil factor interacting protein TFIZ1/GKN2 in gastric cancer: influence of tumor histology and relationship to prognosis. Clin Cancer Res *14*, 4161-4167.
Movahedi, K., Laoui, D., Gysemans, C., Baeten, M., Stange, G., Van den Bossche, J., Mack, M., Pipeleers, D., In't Veld, P., De Baetselier, P., and Van Ginderachter, J. A. (2010). Different tumor microenvironments contain functionally distinct subsets of macrophages derived from Ly6C(high) monocytes. Cancer Res *70*, 5728-5739.
Mueller, S., Engleitner, T., Maresch, R., Zukowska, M., Lange, S., Kaltenbacher, T., Konukiewitz, B., Ollinger, R., Zwiebel, M., Strong, A., *et al.* (2018). Evolutionary routes and KRAS dosage define pancreatic cancer phenotypes. Nature *554*, 62-68.
Mullis, K., Faloona, F., Scharf, S., Saiki, R., Horn, G., and Erlich, H. (1986). Specific enzymatic amplification of DNA in vitro: the polymerase chain reaction. Cold Spring Harb Symp Quant Biol *51 Pt 1*, 263-273.

Musrap, N., Tuccitto, A., Karagiannis, G. S., Saraon, P., Batruch, I., and Diamandis, E. P. (2015). Comparative Proteomics of Ovarian Cancer Aggregate Formation Reveals an Increased Expression of Calcium-activated Chloride Channel Regulator 1 (CLCA1). J Biol Chem *290*, 17218-17227.
Nagata, K., Horinouchi, M., Saitou, M., Higashi, M., Nomoto, M., Goto, M., and Yonezawa, S. (2007). Mucin expression profile in pancreatic cancer and the precursor lesions. J Hepatobiliary Pancreat Surg *14*, 243-254.
Nagathihalli, N. S., Castellanos, J. A., VanSaun, M. N., Dai, X., Ambrose, M., Guo, Q., Xiong, Y., and Merchant, N. B. (2016). Pancreatic stellate cell secreted IL-6 stimulates STAT3 dependent invasiveness of pancreatic intraepithelial neoplasia and cancer cells. Oncotarget *7*, 65982-65992.
Nagtegaal, I. D., Odze, R. D., Klimstra, D., Paradis, V., Rugge, M., Schirmacher, P., Washington, K. M., Carneiro, F., Cree, I. A., and Board, W. H. O. C. o. T. E. (2020). The 2019 WHO classification of tumours of the digestive system. Histopathology *76*, 182-188.
Nakhai, H., Sel, S., Favor, J., Mendoza-Torres, L., Paulsen, F., Duncker, G. I., and Schmid, R. M. (2007). Ptf1a is essential for the differentiation of GABAergic and glycinergic amacrine cells and horizontal cells in the mouse retina. Development *134*, 1151-1160.
Neal, C. P., Fry, A. M., Moreman, C., McGregor, A., Garcea, G., Berry, D. P., and Manson, M. M. (2014). Overexpression of the Nek2 kinase in colorectal cancer correlates with beta-catenin relocalization and shortened cancer-specific survival. J Surg Oncol *110*, 828-838.
Neckmann, U., Wolowczyk, C., Hall, M., Almaas, E., Ren, J., Zhao, S., Johannessen, B., Skotheim, R. I., Bjorkoy, G., Ten Dijke, P., and Holien, T. (2019). GREM1 is associated with metastasis and predicts poor prognosis in ER-negative breast cancer patients. Cell Commun Signal *17*, 140.
Neuzillet, C., Tijeras-Raballand, A., Ragulan, C., Cros, J., Patil, Y., Martinet, M., Erkan, M., Kleeff, J., Wilson, J., Apte, M., *et al.* (2019). Inter- and intra-tumoural heterogeneity in cancer-associated fibroblasts of human pancreatic ductal adenocarcinoma. J Pathol *248*, 51-65.
Newman, A. M., Liu, C. L., Green, M. R., Gentles, A. J., Feng, W., Xu, Y., Hoang, C. D., Diehn, M., and Alizadeh, A. A. (2015). Robust enumeration of cell subsets from tissue expression profiles. Nat Methods *12*, 453-457.
Nguyen, R., Perfetto, S., Mahnke, Y. D., Chattopadhyay, P., and Roederer, M. (2013). Quantifying spillover spreading for comparing instrument performance and aiding in multicolor panel design. Cytometry A *83*, 306-315.
Nielsen, J. S., Sahota, R. A., Milne, K., Kost, S. E., Nesslinger, N. J., Watson, P. H., and Nelson, B. H. (2012). CD20+ tumor-infiltrating lymphocytes have an atypical CD27- memory phenotype and together with CD8+ T cells promote favorable prognosis in ovarian cancer. Clin Cancer Res *18*, 3281-3292.
Nielsen, M. F., Mortensen, M. B., and Detlefsen, S. (2016). Key players in pancreatic cancer-stroma interaction: Cancer-associated fibroblasts, endothelial and inflammatory cells. World J Gastroenterol *22*, 2678-2700.
Notta, F., Chan-Seng-Yue, M., Lemire, M., Li, Y., Wilson, G. W., Connor, A. A., Denroche, R. E., Liang, S. B., Brown, A. M., Kim, J. C., *et al.* (2016). A renewed model of pancreatic cancer evolution based on genomic rearrangement patterns. Nature *538*, 378-382.
Numata, M., Morinaga, S., Watanabe, T., Tamagawa, H., Yamamoto, N., Shiozawa, M., Nakamura, Y., Kameda, Y., Okawa, S., Rino, Y., *et al.* (2013). The clinical significance of SWI/SNF complex in pancreatic cancer. Int J Oncol *42*, 403-410.
Nwachukwu, J. C., Srinivasan, S., Zheng, Y., Wang, S., Min, J., Dong, C., Liao, Z., Nowak, J., Wright, N. J., Houtman, R., *et al.* (2016). Predictive features of ligand-specific signaling through the estrogen receptor. Mol Syst Biol *12*, 864.

Nywening, T. M., Belt, B. A., Cullinan, D. R., Panni, R. Z., Han, B. J., Sanford, D. E., Jacobs, R. C., Ye, J., Patel, A. A., Gillanders, W. E., *et al.* (2018). Targeting both tumour-associated CXCR2(+) neutrophils and CCR2(+) macrophages disrupts myeloid recruitment and improves chemotherapeutic responses in pancreatic ductal adenocarcinoma. Gut *67*, 1112-1123.

O'Connell, J. T., Sugimoto, H., Cooke, V. G., MacDonald, B. A., Mehta, A. I., LeBleu, V. S., Dewar, R., Rocha, R. M., Brentani, R. R., Resnick, M. B., *et al.* (2011). VEGF-A and Tenascin-C produced by S100A4+ stromal cells are important for metastatic colonization. Proc Natl Acad Sci U S A *108*, 16002-16007.

Odell, I. D., and Cook, D. (2013). Immunofluorescence techniques. J Invest Dermatol *133*, e4.

Oettle, H., Post, S., Neuhaus, P., Gellert, K., Langrehr, J., Ridwelski, K., Schramm, H., Fahlke, J., Zuelke, C., Burkart, C., *et al.* (2007). Adjuvant chemotherapy with gemcitabine vs observation in patients undergoing curative-intent resection of pancreatic cancer: a randomized controlled trial. JAMA *297*, 267-277.

Oh, Y., Taylor, S., Bekele, B. N., Debnam, J. M., Allen, P. K., Suki, D., Sawaya, R., Komaki, R., Stewart, D. J., and Karp, D. D. (2009). Number of metastatic sites is a strong predictor of survival in patients with nonsmall cell lung cancer with or without brain metastases. Cancer *115*, 2930-2938.

Okudela, K., Katayama, A., Woo, T., Mitsui, H., Suzuki, T., Tateishi, Y., Umeda, S., Tajiri, M., Masuda, M., Nagahara, N., *et al.* (2014). Proteome analysis for downstream targets of oncogenic KRAS--the potential participation of CLIC4 in carcinogenesis in the lung. PLoS One *9*, e87193.

Okumura, R., Kurakawa, T., Nakano, T., Kayama, H., Kinoshita, M., Motooka, D., Gotoh, K., Kimura, T., Kamiyama, N., Kusu, T., *et al.* (2016). Lypd8 promotes the segregation of flagellated microbiota and colonic epithelia. Nature *532*, 117-121.

Olive, K. P., Tuveson, D. A., Ruhe, Z. C., Yin, B., Willis, N. A., Bronson, R. T., Crowley, D., and Jacks, T. (2004). Mutant p53 gain of function in two mouse models of Li-Fraumeni syndrome. Cell *119*, 847-860.

Oltedal, S., Skaland, I., Maple-Grodem, J., Tjensvoll, K., Janssen, E. A. M., Gilje, B., Smaaland, R., Heikkila, R., and Nordgard, O. (2018). Expression profiling and intracellular localization studies of the novel Proline-, Histidine-, and Glycine-rich protein 1 suggest an essential role in gastro-intestinal epithelium and a potential clinical application in colorectal cancer diagnostics. BMC Gastroenterol *18*, 26.

Orend, G., Huang, W., Olayioye, M. A., Hynes, N. E., and Chiquet-Ehrismann, R. (2003). Tenascin-C blocks cell-cycle progression of anchorage-dependent fibroblasts on fibronectin through inhibition of syndecan-4. Oncogene *22*, 3917-3926.

Oshima, T., Kawasaki, T., Ohashi, R., Hasegawa, G., Jiang, S., Umezu, H., Aoyagi, Y., Iwanari, H., Tanaka, T., Hamakubo, T., *et al.* (2007). Downregulated P1 promoter-driven hepatocyte nuclear factor-4alpha expression in human colorectal carcinoma is a new prognostic factor against liver metastasis. Pathol Int *57*, 82-90.

Oskarsson, T., Acharyya, S., Zhang, X. H., Vanharanta, S., Tavazoie, S. F., Morris, P. G., Downey, R. J., Manova-Todorova, K., Brogi, E., and Massague, J. (2011). Breast cancer cells produce tenascin C as a metastatic niche component to colonize the lungs. Nat Med *17*, 867-874.

Ozdemir, B. C., Pentcheva-Hoang, T., Carstens, J. L., Zheng, X., Wu, C. C., Simpson, T. R., Laklai, H., Sugimoto, H., Kahlert, C., Novitskiy, S. V., *et al.* (2014). Depletion of carcinoma-associated fibroblasts and fibrosis induces immunosuppression and accelerates pancreas cancer with reduced survival. Cancer Cell *25*, 719-734.

Ozono, K., Ohishi, Y., Onishi, H., Nakamura, K., Motoshita, J., Kato, M., Nakanishi, R., Nakamura, M., and Oda, Y. (2017). Brain-derived neurotrophic factor/tropomyosin-related kinase B signaling pathway contributes to the aggressive behavior of lung squamous cell carcinoma. Lab Invest *97*, 1332-1342.
Patel, M. B., Pothula, S. P., Xu, Z., Lee, A. K., Goldstein, D., Pirola, R. C., Apte, M. V., and Wilson, J. S. (2014). The role of the hepatocyte growth factor/c-MET pathway in pancreatic stellate cell-endothelial cell interactions: antiangiogenic implications in pancreatic cancer. Carcinogenesis *35*, 1891-1900.
Patra, K. C., Kato, Y., Mizukami, Y., Widholz, S., Boukhali, M., Revenco, I., Grossman, E. A., Ji, F., Sadreyev, R. I., Liss, A. S., *et al.* (2018). Mutant GNAS drives pancreatic tumourigenesis by inducing PKA-mediated SIK suppression and reprogramming lipid metabolism. Nat Cell Biol *20*, 811-822.
Payne, S. N., Maher, M. E., Tran, N. H., Van De Hey, D. R., Foley, T. M., Yueh, A. E., Leystra, A. A., Pasch, C. A., Jeffrey, J. J., Clipson, L., *et al.* (2015). PIK3CA mutations can initiate pancreatic tumorigenesis and are targetable with PI3K inhibitors. Oncogenesis *4*, e169.
Pedersen, K. B., Nesland, J. M., Fodstad, O., and Maelandsmo, G. M. (2002). Expression of S100A4, E-cadherin, alpha- and beta-catenin in breast cancer biopsies. Br J Cancer *87*, 1281-1286.
Peinado, H., Lavotshkin, S., and Lyden, D. (2011). The secreted factors responsible for pre-metastatic niche formation: old sayings and new thoughts. Semin Cancer Biol *21*, 139-146.
Peng, Y., Li, W., and Liu, Y. (2007). A hybrid approach for biomarker discovery from microarray gene expression data for cancer classification. Cancer Inform *2*, 301-311.
Penny, H. L., Sieow, J. L., Adriani, G., Yeap, W. H., See Chi Ee, P., San Luis, B., Lee, B., Lee, T., Mak, S. Y., Ho, Y. S., *et al.* (2016). Warburg metabolism in tumor-conditioned macrophages promotes metastasis in human pancreatic ductal adenocarcinoma. Oncoimmunology *5*, e1191731.
Perou, C. M., Sorlie, T., Eisen, M. B., van de Rijn, M., Jeffrey, S. S., Rees, C. A., Pollack, J. R., Ross, D. T., Johnsen, H., Akslen, L. A., *et al.* (2000). Molecular portraits of human breast tumours. Nature *406*, 747-752.
Pestell, R. G. (2013). New roles of cyclin D1. Am J Pathol *183*, 3-9.
Pfaffl, M. W. (2001). A new mathematical model for relative quantification in real-time RT-PCR. Nucleic Acids Res *29*, e45.
Pinho, A. V., Rooman, I., Reichert, M., De Medts, N., Bouwens, L., Rustgi, A. K., and Real, F. X. (2011). Adult pancreatic acinar cells dedifferentiate to an embryonic progenitor phenotype with concomitant activation of a senescence programme that is present in chronic pancreatitis. Gut *60*, 958-966.
Pomerantz, J., Schreiber-Agus, N., Liegeois, N. J., Silverman, A., Alland, L., Chin, L., Potes, J., Chen, K., Orlow, I., Lee, H. W., *et al.* (1998). The Ink4a tumor suppressor gene product, p19Arf, interacts with MDM2 and neutralizes MDM2's inhibition of p53. Cell *92*, 713-723.
Pothuraju, R., Rachagani, S., Krishn, S. R., Chaudhary, S., Nimmakayala, R. K., Siddiqui, J. A., Ganguly, K., Lakshmanan, I., Cox, J. L., Mallya, K., *et al.* (2020). Molecular implications of MUC5AC-CD44 axis in colorectal cancer progression and chemoresistance. Mol Cancer *19*, 37.
Prevarskaya, N., Skryma, R., and Shuba, Y. (2010). Ion channels and the hallmarks of cancer. Trends Mol Med *16*, 107-121.
Provenzano, P. P., Cuevas, C., Chang, A. E., Goel, V. K., Von Hoff, D. D., and Hingorani, S. R. (2012). Enzymatic targeting of the stroma ablates physical barriers to treatment of pancreatic ductal adenocarcinoma. Cancer Cell *21*, 418-429.

Pu, N., Zhao, G., Gao, S., Cui, Y., Xu, Y., Lv, Y., Nuerxiati, A., and Wu, W. (2018). Neutralizing TGF-beta promotes anti-tumor immunity of dendritic cells against pancreatic cancer by regulating T lymphocytes. Cent Eur J Immunol *43*, 123-131.
Puleo, F., Nicolle, R., Blum, Y., Cros, J., Marisa, L., Demetter, P., Quertinmont, E., Svrcek, M., Elarouci, N., Iovanna, J., *et al.* (2018). Stratification of Pancreatic Ductal Adenocarcinomas Based on Tumor and Microenvironment Features. Gastroenterology *155*, 1999-2013 e1993.
Qian, J., Luo, Y., Gu, X., Zhan, W., and Wang, X. (2013). Twist1 promotes gastric cancer cell proliferation through up-regulation of FoxM1. PLoS One *8*, e77625.
Qiang, L., Zhao, B., Ming, M., Wang, N., He, T. C., Hwang, S., Thorburn, A., and He, Y. Y. (2014). Regulation of cell proliferation and migration by p62 through stabilization of Twist1. Proc Natl Acad Sci U S A *111*, 9241-9246.
Quaranta, V., Rainer, C., Nielsen, S. R., Raymant, M. L., Ahmed, M. S., Engle, D. D., Taylor, A., Murray, T., Campbell, F., Palmer, D. H., *et al.* (2018). Macrophage-Derived Granulin Drives Resistance to Immune Checkpoint Inhibition in Metastatic Pancreatic Cancer. Cancer Res *78*, 4253-4269.
Redston, M. S., Caldas, C., Seymour, A. B., Hruban, R. H., da Costa, L., Yeo, C. J., and Kern, S. E. (1994). p53 mutations in pancreatic carcinoma and evidence of common involvement of homocopolymer tracts in DNA microdeletions. Cancer Res *54*, 3025-3033.
Ren, B., Cui, M., Yang, G., Wang, H., Feng, M., You, L., and Zhao, Y. (2018). Tumor microenvironment participates in metastasis of pancreatic cancer. Mol Cancer *17*, 108.
Reutens, A. T., Fu, M., Wang, C., Albanese, C., McPhaul, M. J., Sun, Z., Balk, S. P., Janne, O. A., Palvimo, J. J., and Pestell, R. G. (2001). Cyclin D1 binds the androgen receptor and regulates hormone-dependent signaling in a p300/CBP-associated factor (P/CAF)-dependent manner. Mol Endocrinol *15*, 797-811.
Richardson, A. M., Havel, L. S., Koyen, A. E., Konen, J. M., Shupe, J., Wiles, W. G. t., Martin, W. D., Grossniklaus, H. E., Sica, G., Gilbert-Ross, M., and Marcus, A. I. (2018). Vimentin Is Required for Lung Adenocarcinoma Metastasis via Heterotypic Tumor Cell-Cancer-Associated Fibroblast Interactions during Collective Invasion. Clin Cancer Res *24*, 420-432.
Roberts, N. J., Norris, A. L., Petersen, G. M., Bondy, M. L., Brand, R., Gallinger, S., Kurtz, R. C., Olson, S. H., Rustgi, A. K., Schwartz, A. G., *et al.* (2016). Whole Genome Sequencing Defines the Genetic Heterogeneity of Familial Pancreatic Cancer. Cancer Discov *6*, 166-175.
Rochefort, M. M., Ankeny, J. S., Kadera, B. E., Donald, G. W., Isacoff, W., Wainberg, Z. A., Hines, O. J., Donahue, T. R., Reber, H. A., and Tomlinson, J. S. (2013). Impact of tumor grade on pancreatic cancer prognosis: validation of a novel TNMG staging system. Ann Surg Oncol *20*, 4322-4329.
Rooman, I., and Real, F. X. (2012). Pancreatic ductal adenocarcinoma and acinar cells: a matter of differentiation and development? Gut *61*, 449-458.
Rothhammer, T., Poser, I., Soncin, F., Bataille, F., Moser, M., and Bosserhoff, A. K. (2005). Bone morphogenic proteins are overexpressed in malignant melanoma and promote cell invasion and migration. Cancer Res *65*, 448-456.
Rozenblum, E., Schutte, M., Goggins, M., Hahn, S. A., Panzer, S., Zahurak, M., Goodman, S. N., Sohn, T. A., Hruban, R. H., Yeo, C. J., and Kern, S. E. (1997). Tumor-suppressive pathways in pancreatic carcinoma. Cancer Res *57*, 1731-1734.
Rucki, A. A., Foley, K., Zhang, P., Xiao, Q., Kleponis, J., Wu, A. A., Sharma, R., Mo, G., Liu, A., Van Eyk, J., *et al.* (2017). Heterogeneous Stromal Signaling within the Tumor Microenvironment Controls the Metastasis of Pancreatic Cancer. Cancer Res *77*, 41-52.
Ryan, D. P., Hong, T. S., and Bardeesy, N. (2014). Pancreatic adenocarcinoma. N Engl J Med *371*, 2140-2141.

S, N. K., Wilson, G. W., Grant, R. C., Seto, M., O'Kane, G., Vajpeyi, R., Notta, F., Gallinger, S., and Chetty, R. (2020). Morphological classification of pancreatic ductal adenocarcinoma that predicts molecular subtypes and correlates with clinical outcome. Gut *69*, 317-328.
Sadanandam, A., Lyssiotis, C. A., Homicsko, K., Collisson, E. A., Gibb, W. J., Wullschleger, S., Ostos, L. C., Lannon, W. A., Grotzinger, C., Del Rio, M., *et al.* (2013). A colorectal cancer classification system that associates cellular phenotype and responses to therapy. Nat Med *19*, 619-625.
Sagara, Y., Miyata, Y., Iwata, T., Kanda, S., Hayashi, T., Sakai, H., and Kanetake, H. (2010). Clinical significance and prognostic value of S100A4 and matrix metalloproteinase-14 in patients with organ-confined bladder cancer. Exp Ther Med *1*, 27-31.
Sahin, I. H., Elias, H., Chou, J. F., Capanu, M., and O'Reilly, E. M. (2018). Pancreatic adenocarcinoma: insights into patterns of recurrence and disease behavior. BMC Cancer *18*, 769.
Sahin, I. H., Iacobuzio-Donahue, C. A., and O'Reilly, E. M. (2016). Molecular signature of pancreatic adenocarcinoma: an insight from genotype to phenotype and challenges for targeted therapy. Expert Opin Ther Targets *20*, 341-359.
Sakellariou-Thompson, D., Forget, M. A., Creasy, C., Bernard, V., Zhao, L., Kim, Y. U., Hurd, M. W., Uraoka, N., Parra, E. R., Kang, Y., *et al.* (2017). 4-1BB Agonist Focuses CD8(+) Tumor-Infiltrating T-Cell Growth into a Distinct Repertoire Capable of Tumor Recognition in Pancreatic Cancer. Clin Cancer Res *23*, 7263-7275.
Saleem, M., Adhami, V. M., Zhong, W., Longley, B. J., Lin, C. Y., Dickson, R. B., Reagan-Shaw, S., Jarrard, D. F., and Mukhtar, H. (2006). A novel biomarker for staging human prostate adenocarcinoma: overexpression of matriptase with concomitant loss of its inhibitor, hepatocyte growth factor activator inhibitor-1. Cancer Epidemiol Biomarkers Prev *15*, 217-227.
Sano, M., Ijichi, H., Takahashi, R., Miyabayashi, K., Fujiwara, H., Yamada, T., Kato, H., Nakatsuka, T., Tanaka, Y., Tateishi, K., *et al.* (2019). Blocking CXCLs-CXCR2 axis in tumor-stromal interactions contributes to survival in a mouse model of pancreatic ductal adenocarcinoma through reduced cell invasion/migration and a shift of immune-inflammatory microenvironment. Oncogenesis *8*, 8.
Sceneay, J., Smyth, M. J., and Moller, A. (2013). The pre-metastatic niche: finding common ground. Cancer Metastasis Rev *32*, 449-464.
Schneider, G., and Schmid, R. M. (2003). Genetic alterations in pancreatic carcinoma. Mol Cancer *2*, 15.
Schoenmakers, E. F., Wanschura, S., Mols, R., Bullerdiek, J., Van den Berghe, H., and Van de Ven, W. J. (1995). Recurrent rearrangements in the high mobility group protein gene, HMGI-C, in benign mesenchymal tumours. Nat Genet *10*, 436-444.
Schönhuber, N., Seidler, B., Schuck, K., Veltkamp, C., Schachtler, C., Zukowska, M., Eser, S., Feyerabend, T. B., Paul, M. C., Eser, P., *et al.* (2014). A next-generation dual-recombinase system for time- and host-specific targeting of pancreatic cancer. Nat Med *20*, 1340-1347.
Schreiber, R. D., Old, L. J., and Smyth, M. J. (2011). Cancer immunoediting: integrating immunity's roles in cancer suppression and promotion. Science *331*, 1565-1570.
Schutte, M., Hruban, R. H., Geradts, J., Maynard, R., Hilgers, W., Rabindran, S. K., Moskaluk, C. A., Hahn, S. A., Schwarte-Waldhoff, I., Schmiegel, W., *et al.* (1997). Abrogation of the Rb/p16 tumor-suppressive pathway in virtually all pancreatic carcinomas. Cancer Res *57*, 3126-3130.
Sel, S., Ebert, T., Ryffel, G. U., and Drewes, T. (1996). Human renal cell carcinogenesis is accompanied by a coordinate loss of the tissue specific transcription factors HNF4 alpha and HNF1 alpha. Cancer Lett *101*, 205-210.

Seville, L. L., Shah, N., Westwell, A. D., and Chan, W. C. (2005). Modulation of pRB/E2F functions in the regulation of cell cycle and in cancer. Curr Cancer Drug Targets *5*, 159-170.
Shapouri-Moghaddam, A., Mohammadian, S., Vazini, H., Taghadosi, M., Esmaeili, S. A., Mardani, F., Seifi, B., Mohammadi, A., Afshari, J. T., and Sahebkar, A. (2018). Macrophage plasticity, polarization, and function in health and disease. J Cell Physiol *233*, 6425-6440.
Sharma, P., Hu-Lieskovan, S., Wargo, J. A., and Ribas, A. (2017). Primary, Adaptive, and Acquired Resistance to Cancer Immunotherapy. Cell *168*, 707-723.
Shen, R., Wang, Q., Cheng, S., Liu, T., Jiang, H., Zhu, J., Wu, Y., and Wang, L. (2013). The biological features of PanIN initiated from oncogenic Kras mutation in genetically engineered mouse models. Cancer Lett *339*, 135-143.
Shevchenko, I., Karakhanova, S., Soltek, S., Link, J., Bayry, J., Werner, J., Umansky, V., and Bazhin, A. V. (2013). Low-dose gemcitabine depletes regulatory T cells and improves survival in the orthotopic Panc02 model of pancreatic cancer. Int J Cancer *133*, 98-107.
Shi, J. Y., Gao, Q., Wang, Z. C., Zhou, J., Wang, X. Y., Min, Z. H., Shi, Y. H., Shi, G. M., Ding, Z. B., Ke, A. W., *et al.* (2013). Margin-infiltrating CD20(+) B cells display an atypical memory phenotype and correlate with favorable prognosis in hepatocellular carcinoma. Clin Cancer Res *19*, 5994-6005.
Siegel, R. L., Miller, K. D., and Jemal, A. (2020). Cancer statistics, 2020. CA Cancer J Clin *70*, 7-30.
Singh, M., and Maitra, A. (2007). Precursor lesions of pancreatic cancer: molecular pathology and clinical implications. Pancreatology *7*, 9-19.
Sinn, M., Bahra, M., Liersch, T., Gellert, K., Messmann, H., Bechstein, W., Waldschmidt, D., Jacobasch, L., Wilhelm, M., Rau, B. M., *et al.* (2017). CONKO-005: Adjuvant Chemotherapy With Gemcitabine Plus Erlotinib Versus Gemcitabine Alone in Patients After R0 Resection of Pancreatic Cancer: A Multicenter Randomized Phase III Trial. J Clin Oncol *35*, 3330-3337.
Smeele, P., d'Almeida, S. M., Meiller, C., Chene, A. L., Liddell, C., Cellerin, L., Montagne, F., Deshayes, S., Benziane, S., Copin, M. C., *et al.* (2018). Brain-derived neurotrophic factor, a new soluble biomarker for malignant pleural mesothelioma involved in angiogenesis. Mol Cancer *17*, 148.
Song, Y. C., Lu, G. X., Zhang, H. W., Zhong, X. M., Cong, X. L., Xue, S. B., Kong, R., Li, D., Chang, Z. Y., Wang, X. F., *et al.* (2017). Proteogenomic characterization and integrative analysis of glioblastoma multiforme. Oncotarget *8*, 97304-97312.
Sorrentino, R., Terlizzi, M., Di Crescenzo, V. G., Popolo, A., Pecoraro, M., Perillo, G., Galderisi, A., and Pinto, A. (2015). Human lung cancer-derived immunosuppressive plasmacytoid dendritic cells release IL-1alpha in an AIM2 inflammasome-dependent manner. Am J Pathol *185*, 3115-3124.
Stanger, B. Z., and Hebrok, M. (2013). Control of cell identity in pancreas development and regeneration. Gastroenterology *144*, 1170-1179.
Stein, U., Arlt, F., Walther, W., Smith, J., Waldman, T., Harris, E. D., Mertins, S. D., Heizmann, C. W., Allard, D., Birchmeier, W., *et al.* (2006). The metastasis-associated gene S100A4 is a novel target of beta-catenin/T-cell factor signaling in colon cancer. Gastroenterology *131*, 1486-1500.
Steinhart, Z., Pavlovic, Z., Chandrashekhar, M., Hart, T., Wang, X., Zhang, X., Robitaille, M., Brown, K. R., Jaksani, S., Overmeer, R., *et al.* (2017). Genome-wide CRISPR screens reveal a Wnt-FZD5 signaling circuit as a druggable vulnerability of RNF43-mutant pancreatic tumors. Nat Med *23*, 60-68.
Steins, A., van Mackelenbergh, M. G., van der Zalm, A. P., Klaassen, R., Serrels, B., Goris, S. G., Kocher, H. M., Waasdorp, C., de Jong, J. H., Tekin, C., *et al.* (2020). High-grade mesenchymal pancreatic ductal adenocarcinoma drives stromal deactivation through CSF-1. EMBO Rep *21*, e48780.

Stevenson, R. P., Veltman, D., and Machesky, L. M. (2012). Actin-bundling proteins in cancer progression at a glance. J Cell Sci *125*, 1073-1079.
Stone, M. L., and Beatty, G. L. (2019). Cellular determinants and therapeutic implications of inflammation in pancreatic cancer. Pharmacol Ther *201*, 202-213.
Sturm, G., Finotello, F., and List, M. (2020). Immunedeconv: An R Package for Unified Access to Computational Methods for Estimating Immune Cell Fractions from Bulk RNA-Sequencing Data. Methods Mol Biol *2120*, 223-232.
Subramanian, A., Tamayo, P., Mootha, V. K., Mukherjee, S., Ebert, B. L., Gillette, M. A., Paulovich, A., Pomeroy, S. L., Golub, T. R., Lander, E. S., and Mesirov, J. P. (2005). Gene set enrichment analysis: a knowledge-based approach for interpreting genome-wide expression profiles. Proc Natl Acad Sci U S A *102*, 15545-15550.
Sugai, M., Umezu, H., Yamamoto, T., Jiang, S., Iwanari, H., Tanaka, T., Hamakubo, T., Kodama, T., and Naito, M. (2008). Expression of hepatocyte nuclear factor 4 alpha in primary ovarian mucinous tumors. Pathol Int *58*, 681-686.
Sun, J., Shi, R., Zhao, S., Li, X., Lu, S., Bu, H., Ma, X., and Su, C. (2017). E2F8, a direct target of miR-144, promotes papillary thyroid cancer progression via regulating cell cycle. J Exp Clin Cancer Res *36*, 40.
Sun, Q., Zhang, B., Hu, Q., Qin, Y., Xu, W., Liu, W., Yu, X., and Xu, J. (2018). The impact of cancer-associated fibroblasts on major hallmarks of pancreatic cancer. Theranostics *8*, 5072-5087.
Sun, Z., Cai, S., Liu, C., Cui, Y., Ji, J., Jiang, W. G., and Ye, L. (2020). Increased Expression of Gremlin1 Promotes Proliferation and Epithelial Mesenchymal Transition in Gastric Cancer Cells and Correlates With Poor Prognosis of Patients With Gastric Cancer. Cancer Genomics Proteomics *17*, 49-60.
Takeuchi, S., Baghdadi, M., Tsuchikawa, T., Wada, H., Nakamura, T., Abe, H., Nakanishi, S., Usui, Y., Higuchi, K., Takahashi, M., *et al.* (2015). Chemotherapy-Derived Inflammatory Responses Accelerate the Formation of Immunosuppressive Myeloid Cells in the Tissue Microenvironment of Human Pancreatic Cancer. Cancer Res *75*, 2629-2640.
Tamborero, D., Rubio-Perez, C., Muinos, F., Sabarinathan, R., Piulats, J. M., Muntasell, A., Dienstmann, R., Lopez-Bigas, N., and Gonzalez-Perez, A. (2018). A Pan-cancer Landscape of Interactions between Solid Tumors and Infiltrating Immune Cell Populations. Clin Cancer Res *24*, 3717-3728.
Tan, L., Wei, X., Zheng, L., Zeng, J., Liu, H., Yang, S., and Tan, H. (2016). Amplified HMGA2 promotes cell growth by regulating Akt pathway in AML. J Cancer Res Clin Oncol *142*, 389-399.
Tanaka, T., Jiang, S., Hotta, H., Takano, K., Iwanari, H., Sumi, K., Daigo, K., Ohashi, R., Sugai, M., Ikegame, C., *et al.* (2006). Dysregulated expression of P1 and P2 promoter-driven hepatocyte nuclear factor-4alpha in the pathogenesis of human cancer. J Pathol *208*, 662-672.
Tang, H. Y., Beer, L. A., Tanyi, J. L., Zhang, R., Liu, Q., and Speicher, D. W. (2013). Protein isoform-specific validation defines multiple chloride intracellular channel and tropomyosin isoforms as serological biomarkers of ovarian cancer. J Proteomics *89*, 165-178.
Tempero, M. A., Malafa, M. P., Al-Hawary, M., Asbun, H., Bain, A., Behrman, S. W., Benson, A. B., 3rd, Binder, E., Cardin, D. B., Cha, C., *et al.* (2017). Pancreatic Adenocarcinoma, Version 2.2017, NCCN Clinical Practice Guidelines in Oncology. J Natl Compr Canc Netw *15*, 1028-1061.
Thornton, A. M., and Shevach, E. M. (2000). Suppressor effector function of CD4+CD25+ immunoregulatory T cells is antigen nonspecific. J Immunol *164*, 183-190.
Thuault, S., Valcourt, U., Petersen, M., Manfioletti, G., Heldin, C. H., and Moustakas, A. (2006). Transforming growth factor-beta employs HMGA2 to elicit epithelial-mesenchymal transition. J Cell Biol *174*, 175-183.

Tian, W., Wang, G., Yang, J., Pan, Y., and Ma, Y. (2013). Prognostic role of E-cadherin and Vimentin expression in various subtypes of soft tissue leiomyosarcomas. Med Oncol *30*, 401.
Timpl, R., Sasaki, T., Kostka, G., and Chu, M. L. (2003). Fibulins: a versatile family of extracellular matrix proteins. Nat Rev Mol Cell Biol *4*, 479-489.
Tran, E., Robbins, P. F., Lu, Y. C., Prickett, T. D., Gartner, J. J., Jia, L., Pasetto, A., Zheng, Z., Ray, S., Groh, E. M., *et al.* (2016). T-Cell Transfer Therapy Targeting Mutant KRAS in Cancer. N Engl J Med *375*, 2255-2262.
Treilleux, I., Blay, J. Y., Bendriss-Vermare, N., Ray-Coquard, I., Bachelot, T., Guastalla, J. P., Bremond, A., Goddard, S., Pin, J. J., Barthelemy-Dubois, C., and Lebecque, S. (2004). Dendritic cell infiltration and prognosis of early stage breast cancer. Clin Cancer Res *10*, 7466-7474.
Trovato, R., Fiore, A., Sartori, S., Cane, S., Giugno, R., Cascione, L., Paiella, S., Salvia, R., De Sanctis, F., Poffe, O., *et al.* (2019). Immunosuppression by monocytic myeloid-derived suppressor cells in patients with pancreatic ductal carcinoma is orchestrated by STAT3. J Immunother Cancer *7*, 255.
Tsai, W. C., Sheu, L. F., Chao, Y. C., Chen, A., Chiang, H., and Jin, J. S. (2007). Decreased matriptase/HAI-1 ratio in advanced colorectal adenocarcinoma of Chinese patients. Chin J Physiol *50*, 225-231.
Tsirigotis, P., Savani, B. N., and Nagler, A. (2016). Programmed death-1 immune checkpoint blockade in the treatment of hematological malignancies. Ann Med *48*, 428-439.
Tsuna, M., Kageyama, S., Fukuoka, J., Kitano, H., Doki, Y., Tezuka, H., and Yasuda, H. (2009). Significance of S100A4 as a prognostic marker of lung squamous cell carcinoma. Anticancer Res *29*, 2547-2554.
Turashvili, G., McKinney, S. E., Goktepe, O., Leung, S. C., Huntsman, D. G., Gelmon, K. A., Los, G., Rejto, P. A., and Aparicio, S. A. (2011). P-cadherin expression as a prognostic biomarker in a 3992 case tissue microarray series of breast cancer. Mod Pathol *24*, 64-81.
Tutt, A., Tovey, H., Cheang, M. C. U., Kernaghan, S., Kilburn, L., Gazinska, P., Owen, J., Abraham, J., Barrett, S., Barrett-Lee, P., *et al.* (2018). Carboplatin in BRCA1/2-mutated and triple-negative breast cancer BRCAness subgroups: the TNT Trial. Nat Med *24*, 628-637.
Vallejo, A., Perurena, N., Guruceaga, E., Mazur, P. K., Martinez-Canarias, S., Zandueta, C., Valencia, K., Arricibita, A., Gwinn, D., Sayles, L. C., *et al.* (2017). An integrative approach unveils FOSL1 as an oncogene vulnerability in KRAS-driven lung and pancreatic cancer. Nat Commun *8*, 14294.
van Heek, T., Rader, A. E., Offerhaus, G. J., McCarthy, D. M., Goggins, M., Hruban, R. H., and Wilentz, R. E. (2002). K-ras, p53, and DPC4 (MAD4) alterations in fine-needle aspirates of the pancreas: a molecular panel correlates with and supplements cytologic diagnosis. Am J Clin Pathol *117*, 755-765.
Vermi, W., Soncini, M., Melocchi, L., Sozzani, S., and Facchetti, F. (2011). Plasmacytoid dendritic cells and cancer. J Leukoc Biol *90*, 681-690.
Vogel, L. K., Saebo, M., Skjelbred, C. F., Abell, K., Pedersen, E. D., Vogel, U., and Kure, E. H. (2006). The ratio of Matriptase/HAI-1 mRNA is higher in colorectal cancer adenomas and carcinomas than corresponding tissue from control individuals. BMC Cancer *6*, 176.
Waddell, N., Pajic, M., Patch, A. M., Chang, D. K., Kassahn, K. S., Bailey, P., Johns, A. L., Miller, D., Nones, K., Quek, K., *et al.* (2015). Whole genomes redefine the mutational landscape of pancreatic cancer. Nature *518*, 495-501.
Wang, E., Lenferink, A., and O'Connor-McCourt, M. (2007). Cancer systems biology: exploring cancer-associated genes on cellular networks. Cell Mol Life Sci *64*, 1752-1762.
Wang, J., Li, S., Liu, Y., Zhang, C., Li, H., and Lai, B. (2020a). Metastatic patterns and survival outcomes in patients with stage IV colon cancer: A population-based analysis. Cancer Med *9*, 361-373.

Wang, L., Wang, J., Jin, T., Zhou, Y., and Chen, Q. (2018). FoxG1 facilitates proliferation and inhibits differentiation by downregulating FoxO/Smad signaling in glioblastoma. Biochem Biophys Res Commun *504*, 46-53.
Wang, M., Liu, B., Li, D., Wu, Y., Wu, X., Jiao, S., Xu, C., Yu, S., Wang, S., Yang, J., *et al.* (2019a). Upregulation of IBSP Expression Predicts Poor Prognosis in Patients With Esophageal Squamous Cell Carcinoma. Front Oncol *9*, 1117.
Wang, P., Zeng, Y., Liu, T., Zhang, C., Yu, P. W., Hao, Y. X., Luo, H. X., and Liu, G. (2014). Chloride intracellular channel 1 regulates colon cancer cell migration and invasion through ROS/ERK pathway. World J Gastroenterol *20*, 2071-2078.
Wang, R., Zhu, Y., Liu, X., Liao, X., He, J., and Niu, L. (2019b). The Clinicopathological features and survival outcomes of patients with different metastatic sites in stage IV breast cancer. BMC Cancer *19*, 1091.
Wang, W. Q., Liu, L., Xu, H. X., Wu, C. T., Xiang, J. F., Xu, J., Liu, C., Long, J., Ni, Q. X., and Yu, X. J. (2016). Infiltrating immune cells and gene mutations in pancreatic ductal adenocarcinoma. Br J Surg *103*, 1189-1199.
Wang, X., Wang, S., Troisi, E. C., Howard, T. P., Haswell, J. R., Wolf, B. K., Hawk, W. H., Ramos, P., Oberlick, E. M., Tzvetkov, E. P., *et al.* (2019c). BRD9 defines a SWI/SNF sub-complex and constitutes a specific vulnerability in malignant rhabdoid tumors. Nat Commun *10*, 1881.
Wang, X., Yu, Q., Ghareeb, W. M., Zhang, Y., Lu, X., Huang, Y., Huang, S., Sun, Y., Lin, J., Liu, J., and Chi, P. (2019d). Downregulated SPINK4 is associated with poor survival in colorectal cancer. BMC Cancer *19*, 1258.
Wang, Z., Li, Y., Wu, D., Yu, S., Wang, Y., and Leung Chan, F. (2020b). Nuclear receptor HNF4alpha performs a tumor suppressor function in prostate cancer via its induction of p21-driven cellular senescence. Oncogene *39*, 1572-1589.
Wartenberg, M., Zlobec, I., Perren, A., Koelzer, V. H., Gloor, B., Lugli, A., and Karamitopoulou, E. (2015). Accumulation of FOXP3+T-cells in the tumor microenvironment is associated with an epithelial-mesenchymal-transition-type tumor budding phenotype and is an independent prognostic factor in surgically resected pancreatic ductal adenocarcinoma. Oncotarget *6*, 4190-4201.
Watanabe, R., Ui, A., Kanno, S., Ogiwara, H., Nagase, T., Kohno, T., and Yasui, A. (2014). SWI/SNF factors required for cellular resistance to DNA damage include ARID1A and ARID1B and show interdependent protein stability. Cancer Res *74*, 2465-2475.
Watt, J., and Kocher, H. M. (2013). The desmoplastic stroma of pancreatic cancer is a barrier to immune cell infiltration. Oncoimmunology *2*, e26788.
Wei, D., Le, X., Zheng, L., Wang, L., Frey, J. A., Gao, A. C., Peng, Z., Huang, S., Xiong, H. Q., Abbruzzese, J. L., and Xie, K. (2003). Stat3 activation regulates the expression of vascular endothelial growth factor and human pancreatic cancer angiogenesis and metastasis. Oncogene *22*, 319-329.
Weijts, B. G., Bakker, W. J., Cornelissen, P. W., Liang, K. H., Schaftenaar, F. H., Westendorp, B., de Wolf, C. A., Paciejewska, M., Scheele, C. L., Kent, L., *et al.* (2012). E2F7 and E2F8 promote angiogenesis through transcriptional activation of VEGFA in cooperation with HIF1. EMBO J *31*, 3871-3884.
Weiss, G. A., Rossi, M. R., Khushalani, N. I., Lo, K., Gibbs, J. F., Bharthuar, A., Cowell, J. K., and Iyer, R. (2013). Evaluation of phosphatidylinositol-3-kinase catalytic subunit (PIK3CA) and epidermal growth factor receptor (EGFR) gene mutations in pancreaticobiliary adenocarcinoma. J Gastrointest Oncol *4*, 20-29.
Wen, X. Z., Miyake, S., Akiyama, Y., and Yuasa, Y. (2004). BMP-2 modulates the proliferation and differentiation of normal and cancerous gastric cells. Biochem Biophys Res Commun *316*, 100-106.

Wilentz, R. E., Goggins, M., Redston, M., Marcus, V. A., Adsay, N. V., Sohn, T. A., Kadkol, S. S., Yeo, C. J., Choti, M., Zahurak, M., *et al.* (2000). Genetic, immunohistochemical, and clinical features of medullary carcinoma of the pancreas: A newly described and characterized entity. Am J Pathol *156*, 1641-1651.
Witkiewicz, A. K., McMillan, E. A., Balaji, U., Baek, G., Lin, W. C., Mansour, J., Mollaee, M., Wagner, K. U., Koduru, P., Yopp, A., *et al.* (2015). Whole-exome sequencing of pancreatic cancer defines genetic diversity and therapeutic targets. Nat Commun *6*, 6744.
Wu, J., Jiao, Y., Dal Molin, M., Maitra, A., de Wilde, R. F., Wood, L. D., Eshleman, J. R., Goggins, M. G., Wolfgang, C. L., Canto, M. I., *et al.* (2011a). Whole-exome sequencing of neoplastic cysts of the pancreas reveals recurrent mutations in components of ubiquitin-dependent pathways. Proc Natl Acad Sci U S A *108*, 21188-21193.
Wu, J., Li, S., Yang, Y., Zhu, S., Zhang, M., Qiao, Y., Liu, Y. J., and Chen, J. (2017). TLR-activated plasmacytoid dendritic cells inhibit breast cancer cell growth in vitro and in vivo. Oncotarget *8*, 11708-11718.
Wu, J., Matthaei, H., Maitra, A., Dal Molin, M., Wood, L. D., Eshleman, J. R., Goggins, M., Canto, M. I., Schulick, R. D., Edil, B. H., *et al.* (2011b). Recurrent GNAS mutations define an unexpected pathway for pancreatic cyst development. Sci Transl Med *3*, 92ra66.
Xiang, X., Zhao, X., Qu, H., Li, D., Yang, D., Pu, J., Mei, H., Zhao, J., Huang, K., Zheng, L., and Tong, Q. (2015). Hepatocyte nuclear factor 4 alpha promotes the invasion, metastasis and angiogenesis of neuroblastoma cells via targeting matrix metalloproteinase 14. Cancer Lett *359*, 187-197.
Xu, J., Qian, J., Zhang, W., Chen, E., Zhang, G., Cao, G., Wang, F., Shen, X., Zhou, W., and Song, Z. (2019). LYPD8 regulates the proliferation and migration of colorectal cancer cells through inhibiting the secretion of IL6 and TNFalpha. Oncol Rep *41*, 2389-2395.
Xu, Y. F., Lu, Y., Cheng, H., Shi, S., Xu, J., Long, J., Liu, L., Liu, C., and Yu, X. (2014). Abnormal distribution of peripheral lymphocyte subsets induced by PDAC modulates overall survival. Pancreatology *14*, 295-301.
Xue, Q., Zhou, Y., Wan, C., Lv, L., Chen, B., Cao, X., Ju, G., Huang, Y., Ni, R., and Mao, G. (2013). Epithelial membrane protein 3 is frequently shown as promoter methylation and functions as a tumor suppressor gene in non-small cell lung cancer. Exp Mol Pathol *95*, 313-318.
Yachida, S., White, C. M., Naito, Y., Zhong, Y., Brosnan, J. A., Macgregor-Das, A. M., Morgan, R. A., Saunders, T., Laheru, D. A., Herman, J. M., *et al.* (2012). Clinical significance of the genetic landscape of pancreatic cancer and implications for identification of potential long-term survivors. Clin Cancer Res *18*, 6339-6347.
Yamada, S., Fuchs, B. C., Fujii, T., Shimoyama, Y., Sugimoto, H., Nomoto, S., Takeda, S., Tanabe, K. K., Kodera, Y., and Nakao, A. (2013). Epithelial-to-mesenchymal transition predicts prognosis of pancreatic cancer. Surgery *154*, 946-954.
Yamamoto, H., Itoh, F., Nakamura, H., Fukushima, H., Sasaki, S., Perucho, M., and Imai, K. (2001). Genetic and clinical features of human pancreatic ductal adenocarcinomas with widespread microsatellite instability. Cancer Res *61*, 3139-3144.
Yamamoto, K., Kawaguchi, M., Shimomura, T., Izumi, A., Konari, K., Honda, A., Lin, C. Y., Johnson, M. D., Yamashita, Y., Fukushima, T., and Kataoka, H. (2018). Hepatocyte growth factor activator inhibitor type-2 (HAI-2)/SPINT2 contributes to invasive growth of oral squamous cell carcinoma cells. Oncotarget *9*, 11691-11706.
Yan, L., McFaul, C., Howes, N., Leslie, J., Lancaster, G., Wong, T., Threadgold, J., Evans, J., Gilmore, I., Smart, H., *et al.* (2005). Molecular analysis to detect pancreatic ductal adenocarcinoma in high-risk groups. Gastroenterology *128*, 2124-2130.
Yang, G., Yin, J., Ou, K., Du, Q., Ren, W., Jin, Y., Peng, L., and Yang, L. (2020). Undifferentiated carcinoma with osteoclast-like giant cells of the pancreas harboring KRAS

and BRCA mutations: case report and whole exome sequencing analysis. BMC Gastroenterol *20*, 202.
Yang, W., Meng, L., Chen, K., Tian, C., Peng, B., Zhong, L., Zhang, C., Yang, X., Zou, J., Yang, S., and Li, L. (2019). Preclinical pharmacodynamic evaluation of a new Src/FOSL1 inhibitor, LY-1816, in pancreatic ductal adenocarcinoma. Cancer Sci *110*, 1408-1419.
Yao, S., Huang, H. Y., Han, X., Ye, Y., Qin, Z., Zhao, G., Li, F., Hu, G., Hu, L., and Ji, H. (2019). Keratin 14-high subpopulation mediates lung cancer metastasis potentially through Gkn1 upregulation. Oncogene *38*, 6354-6369.
Ye, L., Guo, L., He, Z., Wang, X., Lin, C., Zhang, X., Wu, S., Bao, Y., Yang, Q., Song, L., and Lin, H. (2016). Upregulation of E2F8 promotes cell proliferation and tumorigenicity in breast cancer by modulating G1/S phase transition. Oncotarget *7*, 23757-23771.
Yilmaz, M., and Christofori, G. (2009). EMT, the cytoskeleton, and cancer cell invasion. Cancer Metastasis Rev *28*, 15-33.
Yin, Z., Ma, T., Huang, B., Lin, L., Zhou, Y., Yan, J., Zou, Y., and Chen, S. (2019a). Macrophage-derived exosomal microRNA-501-3p promotes progression of pancreatic ductal adenocarcinoma through the TGFBR3-mediated TGF-beta signaling pathway. J Exp Clin Cancer Res *38*, 310.
Yin, Z., Tang, H., Li, L., Ni, J., Yuan, S., Lou, H., and Chen, M. (2019b). Impact of sites versus number of metastases on survival of patients with organ metastasis from newly diagnosed cervical cancer. Cancer Manag Res *11*, 7759-7766.
Ying, H., Kimmelman, A. C., Lyssiotis, C. A., Hua, S., Chu, G. C., Fletcher-Sananikone, E., Locasale, J. W., Son, J., Zhang, H., Coloff, J. L., *et al.* (2012). Oncogenic Kras maintains pancreatic tumors through regulation of anabolic glucose metabolism. Cell *149*, 656-670.
Yoon, J. H., Kang, Y. H., Choi, Y. J., Park, I. S., Nam, S. W., Lee, J. Y., Lee, Y. S., and Park, W. S. (2011). Gastrokine 1 functions as a tumor suppressor by inhibition of epithelial-mesenchymal transition in gastric cancers. J Cancer Res Clin Oncol *137*, 1697-1704.
Yoon, J. H., Park, Y. G., Nam, S. W., and Park, W. S. (2019). The diagnostic value of serum gastrokine 1 (GKN1) protein in gastric cancer. Cancer Med *8*, 5507-5514.
Yousef, G. M., White, N. M., Michael, I. P., Cho, J. C., Robb, J. D., Kurlender, L., Khan, S., and Diamandis, E. P. (2005). Identification of new splice variants and differential expression of the human kallikrein 10 gene, a candidate cancer biomarker. Tumour Biol *26*, 227-235.
Zdanov, S., Mandapathil, M., Abu Eid, R., Adamson-Fadeyi, S., Wilson, W., Qian, J., Carnie, A., Tarasova, N., Mkrtichyan, M., Berzofsky, J. A., *et al.* (2016). Mutant KRAS Conversion of Conventional T Cells into Regulatory T Cells. Cancer Immunol Res *4*, 354-365.
Zhang, A., Qian, Y., Ye, Z., Chen, H., Xie, H., Zhou, L., Shen, Y., and Zheng, S. (2017). Cancer-associated fibroblasts promote M2 polarization of macrophages in pancreatic ductal adenocarcinoma. Cancer Med *6*, 463-470.
Zhao, Q., Chen, S., Zhu, Z., Yu, L., Ren, Y., Jiang, M., Weng, J., and Li, B. (2018). miR-21 promotes EGF-induced pancreatic cancer cell proliferation by targeting Spry2. Cell Death Dis *9*, 1157.
Zhao, Y., Yu, Y., Zhao, W., You, S., Feng, M., Xie, C., Chi, X., Zhang, Y., and Wang, X. (2019). As a downstream target of the AKT pathway, NPTX1 inhibits proliferation and promotes apoptosis in hepatocellular carcinoma. Biosci Rep *39*.
Zheng, L., Xue, J., Jaffee, E. M., and Habtezion, A. (2013). Role of immune cells and immune-based therapies in pancreatitis and pancreatic ductal adenocarcinoma. Gastroenterology *144*, 1230-1240.
Zheng, X., Lin, J., Wu, H., Mo, Z., Lian, Y., Wang, P., Hu, Z., Gao, Z., Peng, L., and Xie, C. (2019). Forkhead box (FOX) G1 promotes hepatocellular carcinoma epithelial-Mesenchymal transition by activating Wnt signal through forming T-cell factor-4/Beta-catenin/FOXG1 complex. J Exp Clin Cancer Res *38*, 475.

Zhong, X., Guan, X., Dong, Q., Yang, S., Liu, W., and Zhang, L. (2014). Examining Nek2 as a better proliferation marker in non-small cell lung cancer prognosis. Tumour Biol *35*, 7155-7162.
Zhong, Y., Wan, Y. W., Pang, K., Chow, L. M., and Liu, Z. (2013). Digital sorting of complex tissues for cell type-specific gene expression profiles. BMC Bioinformatics *14*, 89.
Zhou, L., Chong, M. M., and Littman, D. R. (2009). Plasticity of CD4+ T cell lineage differentiation. Immunity *30*, 646-655.
Zoratti, G. L., Tanabe, L. M., Varela, F. A., Murray, A. S., Bergum, C., Colombo, E., Lang, J. E., Molinolo, A. A., Leduc, R., Marsault, E., *et al.* (2015). Targeting matriptase in breast cancer abrogates tumour progression via impairment of stromal-epithelial growth factor signalling. Nat Commun *6*, 6776.